

APPENDIX

**Weathering products and geochemistry of waste residues
at the Brukunga Pyrite Mine, Adelaide Hills, S.A., in
relation to environmental impacts.**

by

Mandy Agnew

11th Nov. 1994.

Dept of Geology and Geophysics, University of Adelaide.

ENV 10312 V.2
MERFF

R2004/00419



02233907

APPENDIX A1:

HISTORY AND GENERAL OVERVIEW OF THE BRUKUNGA MINE SITE

EXPLORATION AND HISTORY OF MINE DEVELOPMENT

The Talisker Calcsiltstone of the Kanmantoo Group, formally known as the Nairne Pyrite Member, found at the base of the Brukunga Formation, has been known since the nineteenth century.

During the 1890's, a small quantity of sulphide ore was used as a flux in the Scott's Creek Copper Smelter, but no further mining took place at this time. During this period, the deposit was not of economic importance as ample supplies of elemental sulfur were available overseas.

The Brukunga pyrite mine was established in the early 1950's to provide a local source of sulfur for the manufacture of superphosphate. At the time, a world shortage, as well as the prospect of limited supplies in the future, had resulted in a high price for sulfur. This, together with a guarantee of the Commonwealth Government to pay a subsidy if the price of sulfur fell below a certain fixed price, the saving of foreign exchange and the opportunity to establish a local industry, led the South Australian government to encourage and sponsor the formation of Nairne Pyrites Pty. Ltd (Doherty, 1978).

Investigational work was commenced by Enterprise Exploration Co. Pty Ltd and later taken over by Nairne Pyrite Pty Ltd. The latter company was formed in August, 1951, at the instigation of the State Government and comprised Wallaroo-Mt Lyell Fertilisers Ltd, Adelaide Chemical and Fertilizer Co. Ltd., Cresco Fertilizer Ltd., with BHP Co. Ltd as quarry and treatment plant operators (Armstrong and Betheras, 1952).

By the early 70's, sulfur was being obtained at relatively low cost from Canada where the refinement of sour natural gas had resulted in large surplus stock piles. Consequently, when the sulfur bonus was abolished, the mine became uneconomical and production ceased in May 1972. Although the company maintained a caretaker staff, they were unable to check the gradual deterioration of the area and the resulting increase in pollution. Concern about this by the South Australian Department of Mines led them to commission the Australian Mineral Development Laboratories (AMDEL) to study and propose a solution to the problem (Doherty, 1978).

Responsibility for the "clean up" of the River Bremer into which Dawesley Creek discharges was accepted by the South Australian Government in May 1977.

Administration of the rehabilitation of the mine then became the responsibility of the South Australian Department of Mines.

Design, construction and subsequent maintenance of the rehabilitation works are being undertaken by the Engineering and Water Supply Department, in conjunction with the Department of Mines.

GEOLOGY

The orebody is a conformable pyritic meta-sedimentary layer enclosed within regionally metamorphosed Kanmantoo Group rocks. Armstrong and Betheras (1952) described the ore body as being divided into five parallel bodies, the sequence from the hanging wall being;

- No 1. ore body
- Waste bed A
- No 2. ore body
- Waste bed B
- No 3. ore body

See Fig A1₁-1, diagram of ore body, abstract from Armstrong and Betheras (1952).

The three major iron sulfide beds are approx. 15-30 m thick and the two waste beds are 5 m thick each. Ore zones consist of iron sulfide bearing-muscovite schists and gneisses with minor lenses of calc silicate and quartz plagioclase metasediments. The waste zones consist of quartz plagioclase granofels and minor calc silicate granofels, muscovite schists and gneisses. Thus, there is very little chemical difference in the silicate phase of ore and waste, the main difference being the iron sulphide content (Mason, G., 1968).

The pyrite horizon crops out widely throughout the region and shows prominent weathering. Armstrong and Betheras (1952), described the oxidation of sulfide minerals as rarely exceeding a few feet in depth and in some regions sulfides were outcropping. However, Skinner (1958) reported that weathering produces a resistant limonite-quartz-kaolinite gossan containing sporadic pyrite. Additionally, the more easily weathered pyrrhotite was not observed in outcrops. He suggested that these observations confirm that a natural slow rate of weathering is associated with the in-situ undisturbed rock. However, La Ganza (1959) reported gossans extending to depths of 18 m (EGI, Report 1993).

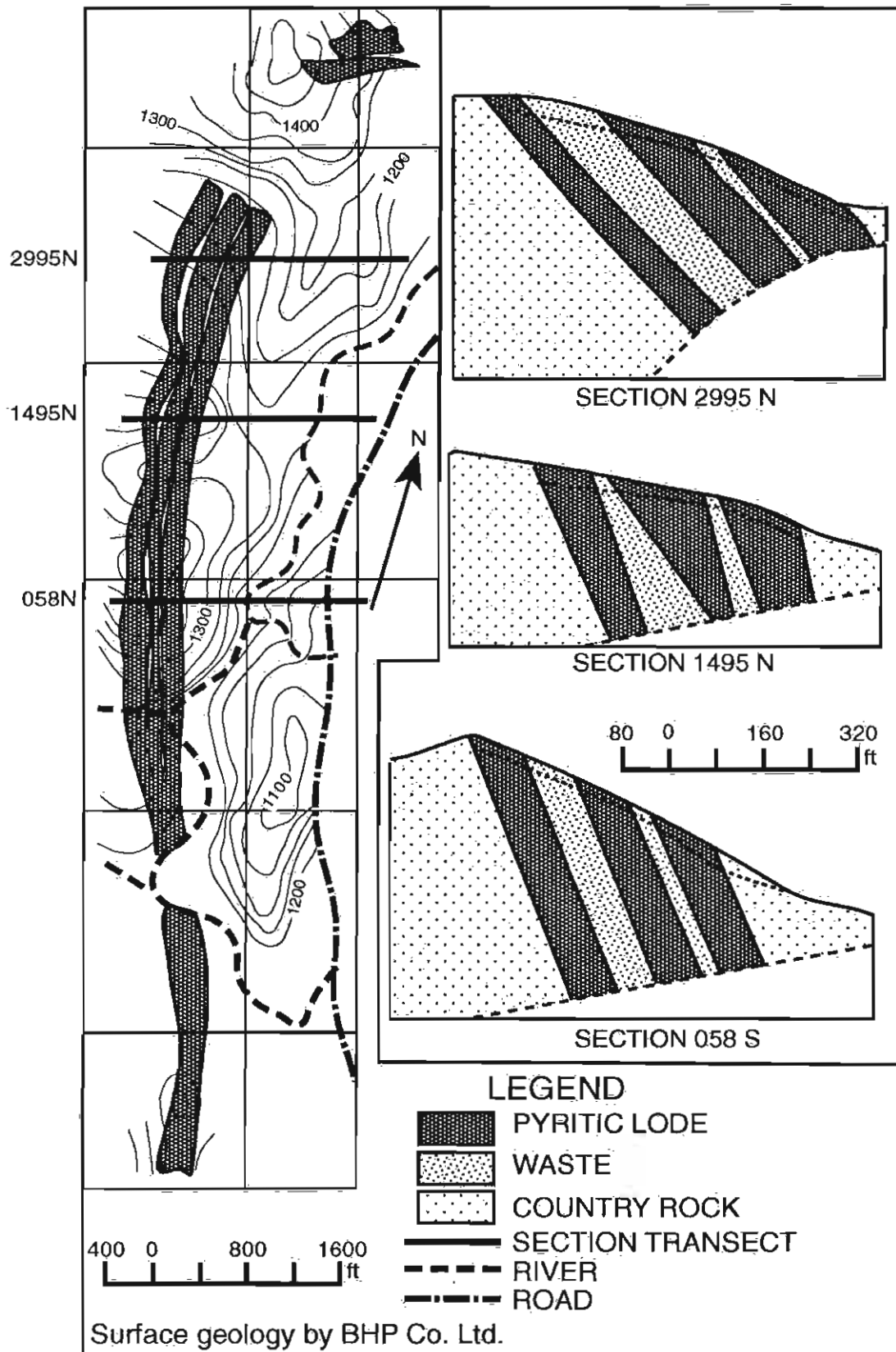


Fig1A₁.1:Orebody geology of Brukunga Pyrite Deposit. (after Armstrong & Betheras, 1952)

The heavy metals causing many of the pollution problems originate from the metasedimentary host rocks and the sulfide ore. Normally the silicates of the host rocks would weather to clays such as kaolinite. However, because of the low pH resulting from the sulfuric acid produced by sulfide oxidation, materials containing alunite and jarosite have also formed. Additionally, this low pH resulted in mobility of aluminium, iron and sodium which subsequently reprecipitated in Dawesley Creek when the flow contacts diluted water (Doherty 1978).

The origin of this deposit has long been a strong point of contention. According to Both (1990), Ridgway (1949) considered it to be a replacement deposit, with certain regions being completely replaced by pyrite, pyrrhotite and quartz. Edwards and Carlos (1954) suggested the deposit had a hydrothermal origin. A sedimentary origin for this deposit was proposed by Skinner (1958) on the basis of its conformable nature; the relationship between sulfides and sedimentary structures; and evidence that the sulfides had undergone metamorphism along with the host sedimentary rocks. Subsequent studies by La Ganza (1959) and George (1967, 1969a) supported Skinner's interpretation.

Sulfur isotope studies by Jensen and Whittle (1969) and Seccombe *et al* (1985) demonstrated that the sulfur is of biogenic origin. The isotope distribution pattern is in accordance with the model of Schwarcz and Burnie (1973) for H_2S produced in a euxenic environment with freely available sulfate, and a sulfate source from Cambrian sea water. Berner (1984) suggested an analogy with modern sediments indicating that the pyrite probably formed during early diagenesis by reaction of detrital iron minerals with the H_2S (Both, 1990).

MINING AND PROCESSING

The open cut operations commenced towards the northern end of the ore body, (Armstrong and Betheras, 1952). Material containing more than 5% sulfide was regarded as ore. This was processed by crushing, fine grinding and then separated using jigs and flotation. Following dewatering, the concentrates were forwarded to a plant at Port Adelaide for the production of sulfuric acid, the first delivery taking place in July 1955.

EGI (1993) reports that a total of approximately 5MT of ore was mined with final concentrate product accounting for about 25% of the ore, and therefore approximately 3.5MT of flotation tailings was produced and is stored in the tailings dam located to the east of Dawesley Creek. The separated fine waste slurry from the flotation process was pumped to a tailings settling pond in an adjacent broad valley. Settled water from this was piped back to the plant and so contamination of the creek was minimised. Approximately

10MT of waste rock was also produced and is stored in two main dumps, the Northern Waste Dump and Southern Waste Dump located on the west bank of Dawesley Creek.

Variable statistics have been recorded for the sulfur content of the ore, ranging from 8 to 13%S. Blesing et al. (1974) suggested that the waste rock contained on average about 2%S. Blesing et al. (1974) also reported 1.4 S% for the tailings dam occurring predominantly as pyrrhotite.

GENERAL OVERVIEW OF REHABILITATION AT BRUKUNGA MINE SITE

The very large and dense pyrite formation at Brukunga has been opened to chemical attack through mining. The pyrite present only requires oxygen and water to begin degrading, producing sulfuric acid, mobile heavy metals and sulfate in the process. Once started this process will not stop until all pyrite is converted to acid and iron sulphate, unless the oxygen itself (from both the atmosphere and dissolved water) can not gain access or can be removed completely by other processes. The EWS (1993) reports that in all the ore body has the potential to generate 300, 000 tonnes of sulfuric acid.

During the operation of the mine the company was forced to provide alternative water supplies to landholders adjacent to Dawesley Creek when acidic drainage contaminated their water source. During 1972 complaints were heard of dead fish in Lake Alexandrina (Dawesley Creek flows into the Bremer River which in turn discharges into the Lake) and concern was expressed over the long term effect on the important Angas-Bremer Irrigation Area (Smith and Hancock, 1992). It has been since this time that investigations have taken place into the rehabilitation of the Brukunga mine site.

The main limitation to rehabilitation at Brukunga has been financial, this is because of the large area the mine occupies and ultimately influences, and the nature of the waste rock dumps (SADME, 1989).

According to SADME (1989), the most effective rehabilitation of the Brukunga mine site is to produce an environment conducive to sustained and vigorous vegetation growth. Vigorous vegetation growth will lead to much reduced infiltration of rain water, thereby minimising the generation of acid water and the volume of polluted water discharged from the various seepage points around the site. Lowering water infiltration is not the only answer to the acidity problem, as the existing groundwater has the capacity to continue the pyrite oxidation process. The rock mass must be managed in such a manner that the chemical environment is changed from an oxidised to a reduced state, and as much as possible of the contaminated water is collected for treatment prior to being discharged from the site.

The measures proposed at Brukunga have followed these principles, and the rehabilitation includes:

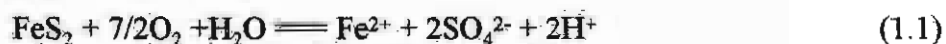
- a) Diversion of fresh water streams to minimise contact with sulfide-bearing areas, and the collection of acid seepages.
- b) Treatment of the collected acid seepages at a neutralisation plant and the safe disposal of them
- c) Prevention or minimisation of acid generation.

An extensive review of the rehabilitation at the Brukunga mine site is provided in Appendix A2. Rehabilitation schemes undertaken include:

- covering and revegetation of the tailings dam
- vegetation and sewage application trials on the mine bench
- sewage application trials and air seeding of the waste rock dumps
- diversion schemes to remove runoff from the mine benches
- collecting and treatment of acid water in the neutralisation plant
- research into the temperature and gas levels of both the waste rocks dumps and the tailings dam to determine their condition.

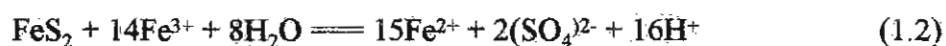
GENERATION OF ACIDIC WATERS

At the Brukunga mine the most abundant sulfide minerals are pyrite and lesser amounts of pyrrhotite, with minor sphalerite, galena and chalcopyrite. Acid mine drainage (AMD) forms when sulfide is oxidised. There are two important oxidising agents - dissolved oxygen and ferric iron. Oxidation by dissolved oxygen can be written



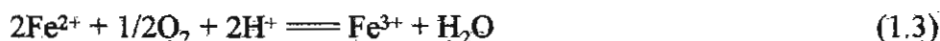
in which only the sulfur atoms of the pyrite are oxidised, from S^{2-} to SO_4^{2-} , and iron remains in the ferrous state. Two moles of H^+ are produced for each mole of FeS_2 .

Oxidation by ferric iron can be written



Again only the sulfide part of the pyrite is oxidised and Fe^{2+} is released. In this case, 16moles of H^+ are produced for each mole of FeS_2 . Oxidation by Fe^{3+} is rapid compared to that by dissolved oxygen.

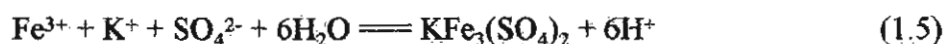
Reaction (1.2) can only proceed at a significant rate if sufficient Fe^{3+} is present. The amount of Fe^{3+} is dependant on the rate of oxidation of Fe^{2+} produced in reaction (1.1) and (1.2), and also on the pH of the system, which governs the solubility of ferric oxyhydroxides. Ferrous iron is oxidised according to the following equation:



Reaction (1.3) can occur abiotically, but is strongly catalysed (by factors of 10 to 10^5 , according to various authors) by acidophilic, aerobic bacteria, mainly thiobacilli. If the reaction occurs in acidic conditions, then the Fe^{3+} produced remains in solution and is available to degrade pyrite as in eq (1.2). However, if the pH is greater than about 4, then most of the Fe^{3+} is precipitated as, for example



In more acidic conditions and in the presence of high concentrations of sulfate, then jarosite-type compounds will be formed, eg.



Combining equations (1.1), (1.3) and (1.4), that is the stage of sulfide oxidation, of ferrous iron oxidation, and of ferric iron precipitation, gives the equation generally written to describe the generation of acidic mine drainage



EFFECT OF AMD ON THE ENVIRONMENT

The generation of acid water around the Brukunga mine site has had a dramatic effect on the local and downstream environment. Not only have toxic levels of heavy metals affected the soil and waters at the mine site itself, but also and more importantly, have resulted in the degradation in quality of downstream water. Discharge from the mine was blamed for the death of fish in Lake Alexandrina, which lies 65 km downstream, in 1972 (Blesing et al, 1974). The unsightly deposits of various precipitates on rocks, vegetation and in the creeks has resulted in considerable attention being applied to halt the release of polluted waters.

Downstream of the mine, evaporites and insoluble precipitates occur on the banks and rocks which form visual pollution for the first 3km. Just below the junction of the first two major tributaries, dilution and a change in pH has resulted in the precipitation of other deposits. The first type of deposits occur in the Nairne Creek where the deposits are highly

Appendix A1 History and general overview

ferruginous and coloured red. The second precipitates occur in the Mt Barker Creek, 16km downstream, where the deposits are high in aluminium and coloured grey (Doherty, 1978).

At times of low flow, a sulfate sludge and mud into which metals become absorbed collects in the bottom of the streams. During later high flow these sludges are washed further downstream. As a result of this it is estimated that most of the metals released from the mine, other than iron and aluminium, would enter Lake Alexandrina. Although these deposits are probably held in an inert condition in the bottom muds of the lake, there has been a fear expressed that they could be rendered soluble by organic processes and lead to fish poisoning (Doherty, 1978).

The acid neutralisation plant and stream diversion systems have been used in an attempt to minimise the chemical loading of water migrating to the local creeks and streams. Although the neutralisation plant has significantly reduced the levels of pollutants leaving the site (Walker, 1986; Read, 1986), they have not been reduced to levels regarded as environmentally safe. The costs necessary for operation and maintenance of these remediation methods exclude them being considered as a long-term solution, and this is one of the major problems facing mining companies and governments faced with rehabilitation of abandoned mines.

In its present state, the Brukunga Mine remains a significant hazard to the surrounding and downstream environment. Information to date suggests that the highly polluted acid water will drain from the site for many decades to come. The economics of maintaining the neutralisation plant to treat the acid drainage is clearly not a long-term practical solution (SADME, 1989).

APPENDIX A2

POLLUTION & REHABILITATION OF

BRUKUNGA PYRITE MINE

HISTORY & REHABILITATION OF THE TAILINGS DAM

The tailings dam is located to the east of Dawesley Creek and contains approximately 3.5MT of flotation tailings (EGI report, 1993). At present the tailings dam is free of any residue water from mining, has been covered and a large part of the area has been revegetated.

The starter dam for forming the initial tailings settling pond was built from earth and rock directly onto the natural valley floor. Two 150 mm steel draw-off pipes were laid through the lowest point of the dam. A concrete diversion pipe was also laid through the base of the dam, but it was later plugged with concrete at the downstream end (Doherty, 1978).

Raising of the dam was done by bulldozing the coarsest tailings from the "beach". This material was predominantly in the fine sand size as distinct from the bulk of the tailings which were mainly of the fine silt size and referred to as fine tailings or slimes. The downstream slope was built at an average slope of about 1 in 3.7 and was protected by a layer of rock fill about 3-3.5 m thick on the slope and about 0.6m thick on the berms (Doherty, 1978).

By 1967, a height of 35 m had been reached. A final height of about 65 m was proposed, but seepage over a major length of the downstream face, and the absence of any filters to control the seepage led to concern over the ultimate stability (Doherty, 1978).

Mr K.C. Pile of the South Australian Institute of Technology was commissioned to investigate the stability of the tailings dam. The stone dumped on the downstream face of the dam was found to contribute to safety by providing significant effective stress in the tailings. It also enhanced the safety by eliminating local sloughing failures which have been reported in tailings dams elsewhere around the world (Doherty, 1978).

In 1970, the high phreatic surface induced a series of "runs" to occur from the base of the dam, these amounted to over 300 tonnes of tailings. Also a sink hole approximately 6 m in diameter and 7.5 m deep occurred over the line of the old steel draw-off pipes and about 100 m from the toe. This problem was overcome by grouting the lower 15 m of these pipes and filling the sink hole (Doherty, 1978).

Following closure of the mine, the tailings dam became a major source of seepage. To prevent this, the seepage was pumped back into the pond, thus recycling and concentrating it. Although it would take many years to recycle all the acid water in the dam, leaching could eventually lead to piping and the loss of water in the pond. This has been referred to as "tailings dam suicide". (Doherty 1978)

Residue mining water was still covering part of the tailings dam in 1986. This water consisted of 90% mine water, with additional runoff from surrounding areas, and AMD collected at the base of the dam. Measurements of the water flow rate at the base of the dam have been undertaken regularly since Sept 1988. These have shown that 5 kilolitres/hr of liquid at a pH 2.3 with minimal variations continues to flow with very minor effects due to seasonal changes.

The lowest pH values from the mine have been recorded on leachates from the tailings dam. It is significant that the difficult-to-float "concentric" pyrrhotite was the main sulphide in the tailings. This type of sulfide is recognised as providing a very quick generation of acid and iron sulfates. It also contains a fifteen-fold higher proportion of nickel than the other iron sulfides in the main deposit (Dainis 1992). This, along with the fact that the dam acted as a collection/evaporation pond for acid seepages for many years, contribute to this low pH level.

Rehabilitation of the tailings dam has taken place over the last 18 years. The dam was covered in two sections, a small 150m² section of the southern region being covered in 1976. Low grade ore gravel used in conjunction with untreated sewage effluent was applied directly to the tailings (no soil). During this same year, AMDEL commenced a revegetation trial on the tailings dam (southern end). Nine small areas were dosed with various amounts of lime and fertilizer and were sown with grasses and clovers. Also 103 trees of 18 different species including S.A blue gum, golden wattle, weeping peppermint and native lilac were planted. After 7 months the area dosed with lime at the rate of 20 tonnes/hectare and fertilized with 1.2 tonnes/hectare of NPK (complete D) fertiliser was deemed to show the best results. Consequently the 15 ha dry surface on the southern region of the tailings dam was recommended for revegetation at an estimated cost of \$500 per hectare (Doherty 1978). Revegetation was not commenced until several years later.

The AMDEL vegetation plot tried in this region was not very successful with only a few trees surviving to the present day. It has been suggested that this may have been due to the fact that the trees were not watered and no top soil was used when planting (Grindley, 1994).

The northern region was not completely covered until 1990, the remaining water was removed just prior to that time. The lime sludge from the water treatment plant was initially deposited on this region. Covering initially started in the central area and then over the period 1989-1990, it was continued to the edge of the present lime sludge lagoons. (Grindley, 1994). Cover consisted of variations of gravel, top soil, sewage sludge, local waste and lime sludge in the regions where lime sludge deposition occurred in previous years (Grindley, 1994).

Revegetation of this area started in the central region with 5000 trees, and during the following years a similar number of trees were planted to the north and south of this initial site. At present the number of trees planted over the site is approximately 17,000 (Grindley, 1994). The dam wall is also being revegetated. A mixture of sewage effluent, lime sludge and E&WS waste material is initially smoothed down the face of the dam. Approximately 10,000 tonnes of lime treatment sludge is removed from the lagoons and dumped in the required areas each year. The wall is then covered by soil and sewage sludge prior to revegetation. This revegetation scheme, in conjunction with the covering, is utilized to seal the sulfide bearing rocks (of which this dam wall is made) from water and air access, in the hope of reducing the acid effluent formation (Grindley, 1994). It is estimated that this sealing of the tailings dam surface will reduce acid effluent load by 15-20% (Dainis, 1992).

The continued revegetation of the dam wall will take some time. Sludge that has been transported to the edge needs to dry out (1 yr) before being smoothed down the dam wall ie. the area covered with lime treatment sludge this year will not be revegetated until next year (Grindley, 1994).

Revegetation has involved the use of Australian native trees. Rows of trees are planted 4 m apart, with tree spacing of 3 m. The plants are individually watered for 3 years. A section of trees near the treatment lagoons was planted in 1990, and 1994 is the first year they have not been watered. They have survived through the summer, which suggests that they are established sufficiently to grow without further assistance (Grindley, 1994).

An area of 2 acres has been cleaned in the front of the dam ready for revegetation. A total of 6 acres are to be revegetated this year, this will comprise the planting of approximately 7-8000 trees. Three thousand trees will be placed on the central front surface of the

Appendix A2 Mine History & General Overview

tailings dam; 2-3000 - tailings wall; 2000 on a 2 acres plot between the AMD holding ponds at the base of the dam and the adjacent stream (Grindley, 1994).

SADME (1989) suggests that the seepage from the tailings dam continues, albeit at a diminishing rate, in response to the revegetation. However, Grindley explains that it is difficult to determine the effect of this revegetation on the tailings dam as measurements have only been undertaken since 1988, after the initial covering had taken place. Additionally these results have shown a constant flow rates with only slight seasonal variation (Grindley, 1994).

Several monitoring stations have recently been constructed by ANSTO. Temperature and oxygen probes have been placed at regular depths within capped drill holes, and peizometers installed for measurement of depth to water table. The data collected are put into a computer model to estimate the rate of AMD generation. Preliminary results suggest AMD will continue for about 200years (Grindley, 1994).

During May 1994, a French drain was constructed in front of the AMD holding ponds at the base of the dam as an additional rehabilitation exercise. The trench was filled with gravel so as to divert seepage occurring away from the seepage pond along this drain rather than into the adjacent stream area. A pump was installed to pump this seepage back to the pond where it will eventually get transported to the neutralisation plant and be treated (Grindley, 1994).

HISTORY & REHABILITATION **OF THE WASTE ROCK DUMPS**

The waste rock piles are largely composed of materials containing less than 5% sulfur. These include the leached and weathered rock which covered the small spur separating Day Creek from Dawesley Creek, along with the low grade waste beds. Rainfall infiltration into this rock mass is likely to be very high despite the steep slopes because of the rubbly surface and the coarse, angular, blocky nature of the material. Some fine grained matrix material would exist within the mass; however, it is insufficient to give the dumps much water shedding capacity. Minor discharges occur along the edges of the waste rock dumps, generally resulting in a progressive increase in creek acidity (SADME, 1989). Seepage ponds have been designed to trap low pH waters before they enter into the stream, and the stream itself has been diverted to reduce contact with the waste material. Unfortunately much of the seepage runs directly into the stream in localities where catchments cannot be utilized successfully.

Revegetation of the waste dumps is a difficult problem because of the ruggedness and steepness of the sides. Because of this, an experiment was undertaken in which a large quantity of seeds were sprayed over the area by helicopter. It was hoped a small proportion of these would germinate. From this trial *Pinus radiata* have been partly successful as they will tolerate soil pH as low as 4 but other species which exhibit higher levels of rainfall interception would have been preferable, since the slopes are steep and the impact of advective evaporation could be very high (SADME, 1989). Rehabilitation of this material can only be achieved to the extent that revegetation will reduce water accessions.

Sewage trials have been undertaken on the rubble regions. The southern mullock heap has had 250 tonnes of 10 yr old sewage sludge placed over a small area. The effect of this is difficult to assess, as the area covered is insignificant compared to the extent of the heaps (Grindley, 1994).

The recent drilling by ANSTO on the mullock heaps will allow determination of the oxygen and temperature environment, to determine the evolving geochemistry. This drilling has confirmed that the mullock heaps are quite porous. Results obtained will help in the understanding of the quantities and rates of AMD production occurring in the dump.

POLLUTION – HYDROLOGICAL SETTING

The mine is located in the upper reaches of the Bremer River catchment with ephemeral streams which drain into Lake Alexandrina. It is adjacent to Dawesley Creek, a tributary of which, Days Creek, drains between the north cut of the mine and the northern waste rock dump.

Even during the operation of the mine the company was forced to provide alternative water supplies to landholders adjacent to Dawesley Creek when acidic drainage contaminated their water source. During 1972 complaints were heard of dead fish in Lake Alexandrina (Dawesley Creek flows into the Bremer River which in turn discharges into the Lake) and concern was expressed over the long term effect on the important Angas-Bremer Irrigation Area (Smith and Hancock, 1992).

When acidic waters contaminated local water supplies its effect was detrimental. Such waters can cause fish and plant death in water ways mainly by heavy metal contamination, the process attacks clay minerals and feldspars and gives rise to geotechnical instability which commonly exposes fresh pyrite when failures occur. This reaction is self-sustaining and very detrimental to local and downstream environments.

Since Brukunga receives about 600 mm of rain per year, the 76 ha surface area of the quarry, spoil heaps, and tailings dam receives an estimated 450 megalitres of water per year. This is less than the annual Dawesley Creek flow of 820 megalitres. The creeks are dry in the summer months when surface water is only available from occasional storms and the seepages of acidic mine water. Figure 1A2.1 (SADME, 1989) presents the average rainfall and evaporation for Nairne and this generates considerable runoff from both the upper unaffected catchment (above and to the west of the mine) as well as from the mine catchment (SADME, 1989).

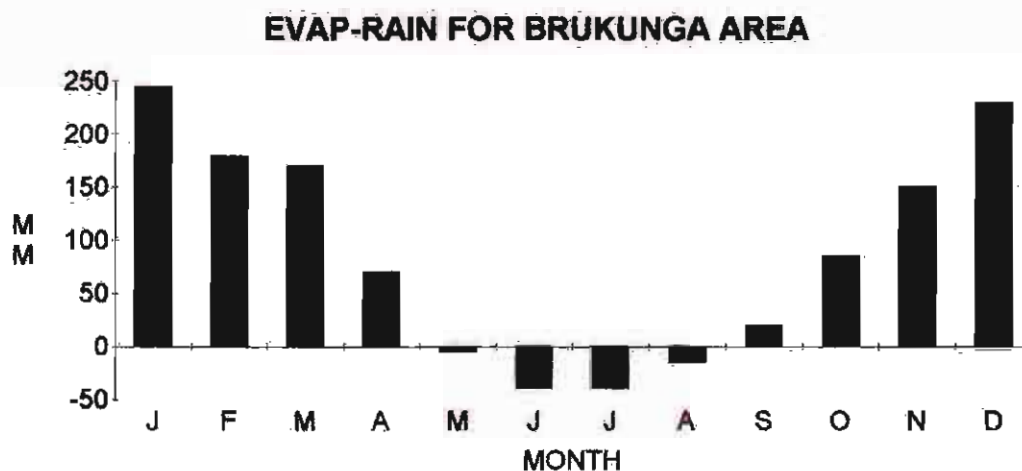


Fig 1A₂.1: Evaporation - Rainfall graph for the Brukunga area.

About 50% of the rainfall is lost through evaporation. Only a very small amount is lost through the chemical reactions that produce sulfates. About 70% of the remaining half quickly flushes the quarry areas, spoil heaps, and tailings dam (Dainis 1992). Attempts have been made to separate surface runoff by channels and pipes from the ponded acidic water which ultimately ends up in the seepage ponds unless these overflow. A small portion which flushes the surface of the tailings dam is largely channelled directly into the creek. A detailed review of the diversion techniques is explained later.

Sources of water contribute to individual seepages in different proportions. For example, it is likely that the seepages from the northern waste rock dump arise from infiltration of rainwater since the dump has been formed above the old land surface. In contrast, the seepages in the deepest source is a combination of rainfall recharge locally on the mine benches and recharge from outside the mine area.

Groundwater occurs in the mine area at shallow depths discharging in the lowest parts of the cuts and in places along the upper bench (Read, 1986). It can be assumed that ground water recharge occurs by local infiltration of winter rains. Groundwater discharge occurs naturally along the local drainage lines (SADME, 1989).

The ground water levels in the mine recorded by Read (1986) give an indication of a markedly anisotropic permeability. Ground water levels adjacent to the deepest northern cut are near the ground surface, this is measured to the east, across the strike of the regional foliation and layering. One bore sited along strike from this cut has a much deeper level of about 9m, inferring a much greater permeability along strike than across strike. Water level data from bores drilled in the mine (Read, 1986) are given in Table 1A_{2.1} (SADME, 1989).

TABLE 1A_{2.1}

Groundwater levels in Mine Area

SADME Unit No.	27/4/85	16/9/86
7454	1.41	0.16
7455	2.52	0.42
7456	10.40	9.83
7457	1.68	0.51
7458	1.60	1.21
7459	9.75*	0.95

Notes:

(1) Prefix for unite numbers is 6627WW

(2) 7456 is along strike from northern deep cut

(3) * this water level reportedly had not recovered

(SADME 1989)

This information suggests that the rocks have drained along strike from the deepest cuts, but there is insufficient information available to map the extent of this effect. Across strike to the west there is a steep hydraulic gradient of about 1, and few examples of significant drainage through the pit faces can be seen (SADME, 1989).

Before it reaches the orebody, the local ground water has salinity of 2,000 mg/L and near neutral pH (SADME, 1989). It is low in iron, aluminium, potassium, magnesium, and sulfates but is relatively high in calcium and especially high in sodium chloride. It may also contain varying amounts of phosphate and nitrate/nitrite. Unpolluted water reported by Read is shown in Table 1A2.2 - (SADME, 1989). When this water contains oxygen and contacts iron sulfides, it produces a very rapid oxidation of these sulfides. The process is actively promoted by certain specific bacteria, and very quickly, it produces a dilute solution of ferrous sulfate together with sulfuric acid. The sulfuric acid will attack other sulfides and also the carbonates, phosphates, and silicates present. It is this attack either alone or in combination with ferric sulfate that releases aluminium, manganese, zinc, copper and nickel and also produces some elemental sulfur (Dainis, 1992).

TABLE 1A2.2

Chemistry of Non-Polluted Groundwater

SADME Unit No.	Date	Ca ²⁺	Mg ²⁺	Na ⁺	HCO ³⁻	SO ₄ ²⁻	Cl ⁻	Location
5918	8/1/52	83	97	586	150	127	1062	Diamond drillhole at mine
5920	25/5/50	51	71	593	131	176	926	Well at mine site
5944	18/1/50	125	113	630	147	257	1154	Well south of mine

Note Prefix for unit numbers is 6627WW

(SADME 1989)

Although arsenic, silver, mercury, cadmium and lead compounds are also attacked, these metals themselves are not seen in effluents in relatively large amounts because of the poor solubility of their sulfates and/or further interaction with ferrous sulfate or ferrous/ferric hydroxysulfates. Similarly, although the attack of silicates by sulfuric acid is rapid and leads to high aluminium values, vanadium and chromium are not seen in large concentration in effluents, presumably because of secondary, subsequent reactions limiting the solubility of these elements (Dainis, 1992).

Doherty reported in 1978 that water quality leaving the mine is dependant on the fresh water flow in Dawesley Creek. In winter the flow was found to have a typical pH of about 3-4 and an acidity value about 1000mg/l. (Acidity value was arbitrarily chosen to be the amount of calcium carbonate required to neutralise the acid). With summer flows,

especially if "out of phase" release of acidic water occurred, acidity values as well as heavy metal concentrations of up to nine times the winter values were found. After the junction with Nairne Creek, 10 km downstream the water quality during winter became marginally suitable for livestock and most irrigation purposes. However, with summer flow, unacceptable levels of pollutants were found as far downstream as the junction with the Bremer River, 20 km downstream. Even 50 km downstream in the wine grape growing area of Langhorne Creek, excess concentration of aluminium, manganese and cadmium have been found (Doherty, 1978).

Since that time the river pollution has been markedly reduced, at least in the short term, by drainage works at the mine site and the construction and operation of a neutralisation plant (SADME 1989).

Stream conditions have become slightly better with pH 7.2 above the town, but by the old bridge area downstream a pH of 3.7 develops. This has been suggested to be due to groundwater movement through the mullock heaps recharging the AMD conditions. Along with this, the addition of effluent from surrounding towns to the river (Mt Barker Council area) may also be affecting the final product (Grindley, 1994).

During periods of high rainfall the AMD holding ponds can over-flow and spill into the river, causing increased acidic conditions. In 1989, the ponds were increased in size and the capacity of the lime treatment plant was also increased. Thus, overflow water would never have to be pumped on top of the tailings dam for storage again (Grindley, 1994).

QUARRY BENCH-WALL

To date, proposed rehabilitation strategies of the mine itself have involved bench sealing and revegetation, but these are prohibitively expensive because of the size of the mine. Seepage from this mine and waste rock dumps has not reduced over the years, although the worst of it is collected for neutralisation (SADME, 1989).

The SADME (1989) report explained the major seepages to be QSB - QSP inclusive. The main contributions of acid seepage are those from the two deepest cuts of the mine (QSB and QSE), with one other major source at the dam sited downstream from the southern waste rock dump. The seeps QSB and QSE emerge in part in the quarry face and from the floor, and flow across the extensive floor areas of the deepest cuts of the mine. Here, obvious precipitation of a variety of compounds has occurred and continues to occur today. These seepages are now collected for treatment at the neutralisation plant. Their locations are shown in Fig 1.2 (chapter 1) and estimates of their flows are given in Table 1A2.3 (SADME, 1989).

TABLE 1A2.3**Main Seepage Flows**

<u>Seepage</u>	<u>Flow (ML/a)</u>	<u>Notes</u>
QSB+QSE	58	Some additional seepage overflows into Dawesley Creek in wet weather
QSC	12	Deduced from water balance
QSF	3	Deduced from water balance
QSG	0.5	
QSH	2.5	
QSI	0.2	
TOTAL	76	

In addition, two minor water courses QSAs and QSBs have been dammed outside the mine, with pipes and channels through the mine designed to keep the surface runoff water isolated from sulfide bearing rocks (SADME, 1989).

In the mine area, the situation is more complex. The major seepages are being collected for treatment, but seepage into Dawesley Creek continues in a largely disseminated way from the waste rock dumps, which flank the creek (SADME, 1989).

The main measures recommended to date for long-term control of the problem can be briefly summarised as sealing the mine benches to exclude oxygen and minimise the infiltration of rainwater, and revegetation of the waste rock dumps (SADME, 1989).

During the history of the mine rehabilitation, three different experiments have been undertaken to determine the best method of sealing the bench, see Fig 1.2 (chapter 1) for placements of trials.

Trial 1

A small area of the main bench was covered with Woven polythene sheet (Sarlon Polyweave LX) and topped with 200 mm of soil and grassed. The area was graded at a shallow slope (about 1 in 100 to reduce the possibility of the top soil slipping over the membrane) to the drainage channels already installed and the surface was cleared of large stones. As a test, a sheet was laid out and a grader driven over it several times. When held up to the light no holes could be seen which indicated the toughness of the material. The test is still in progress and so far has been successful. An advantage of the plastic membrane over clay is that it avoids the cracking problem after a dry spell. Nevertheless, doubts about the very long term durability of plastic and the possibility of damage suggests that this may not be a suitable method of sealing. Also any natural tree growth would cause a problem due to the likelihood of the trees blowing over (Doherty, 1978).

However, the top soil applied to the plastic now grows a good crop of grass (Grindley, 1994).

Trial 2

During 1990-1991 a pond trial was set up on the main bench. Water was obtained from holes drilled into the quarry face at approx 10° for 100m. Monitoring has been undertaken to determine the effect of the two sub-horizontal drill holes constructed into an upper face of the mine in the vicinity of the Southern Cut. The intention of these wells, which are artesian (under pressure), is to lower the water table head thus minimising the quantity of groundwater flowing throughout the ore body. A meter was installed in September 1992, measurements in April (1994) indicate that a total of 39456 m³ has flowed through this since that time. The pond trial was developed to exclude oxygen from coming into contact with the unoxidised ore. The dam was filled with eight year old sewage sludge and in doing so formed an anaerobic lagoon. Three angled drill holes have been constructed on the eastern margin of the lagoon to monitor the effect of this experiment (Smith and Hancock 1992). Unfortunately the rock has been discovered to be very impervious, and as a result of this none of the anaerobic water has penetrated through the rock to date, and thus has had no immediate effect on the AMD production (Grindley 1994).

Trial 3

A similar test to trial 1 was undertaken on a area adjacent to that using the membrane in late 1992. In this experiment spent 8 year old treated sewage sludge was applied directly to the bench. Last year this area grew mainly weeds, but this year management are hoping for a crop of self sown grass (Grindley 1994).

The results achieved so far are encouraging as regards grass formation (for trials 1 and 3) on areas where sludge is on high drainable areas or sits on elevated soil cover. However it now appears that the sludge is either too microbially inactive and/or too devoid of the readily available nutrients which are required to generate the deeper reducing conditions that stop oxidation of the pyrites. Sewage sludge appears to be the lowest cost organic material available in bulk but it has two disadvantages. It eventually breaks down to release metals and metalloids such as lead, cadmium, mercury and arsenic; and it also needs to be mixed intimately with soil and bacteria-assisting fertilizers if it is to break down quickly for maximum effect. Although it forms some use as a soil conditioner in mixtures sold by fertilizer firms, essentially as a cheap source of eventual organic carbon, it has to be used with care in areas prone to high soil cadmium etc which may concentrate in animal kidneys, and also potatoes, carrots and other root crops (Dainis, 1992).

DIVERSION TECHNIQUES

Shallow ponding of water in sulfur bearing areas is undesirable because:

- a) It provides a continuing source of aerated water to lower areas.
- b) It will gradually become more acidic with time, and when flushed out by further inflows of water, will provide a ready source of acid.
- c) If the ponds evaporate to dryness, a dusty acidic residue is left.

It was for this reason that a scheme known as 'partial diversion' was undertaken and has been completed. Days Creek was cleaned out and the two minor creeks (QSAs and QSBs Fig 1.2, Chapter 1) which fed directly into the bench area were diverted by pipes and channels into it. A system of dams and channels was built for the collection of the major acidic seepages and pumps were installed for pumping the acid to the tailings dam. The pipes installed in the new works were laid so they could drain back to the collection ponds and completely empty to reduce incrustation (Doherty, 1978).

Channels were cut in two areas of the main bench where the worst ponding occurred. Although the flow in them will continue to be acidic until the benches are sealed, it was decided that the greatest benefit would result by diverting the water directly into the creek system. This would reduce the build-up of water in the holding ponds and leave storage for the collection of the more concentrated seepages, which is then pumped up to the neutralisation plant to be treated chemically.

In January of 1977 when the majority of the partial diversion works were in operation, a survey showed that the acid level downstream of the mine had reduced to between one third and one half of the previous value. This agrees well with calculations indicating that this figure will drop to one quarter when all the partial diversion works are in operation (Doherty, 1978).

NEUTRALISATION PLANT

In 1979, an acidic drainage treatment plant was costed at \$425,000, with a yearly operational cost of \$140,000 and a recommendation was made for the continuing rehabilitation and revegetation of waste dumps and tailings dam. By 1980 the cost of the treatment plant had increased to \$560, 000. In September 1980 the treatment plant was commissioned. The final construction cost of the treatment plant in 1981 had swelled out to \$640,000. Surface water monitoring continued and problems occurred with scaling (gypsum precipitation) in pipes from the treatment plant, and open drains were constructed in 1987 (Smith and Hancock, 1992).

In 1982, three acidic mine drainage collection ponds were installed on the advice of the monitoring agency. Questions were asked in Parliament on the cost to "the tax payers of SA to maintain the Brukunga Mine from the time the government took over control and maintenance of the mine. The capital cost was given as \$840,000 (Nairne Pyrites Pty Ltd contribution \$75,000), with operations and maintenance cost from 1977 -82 being \$470,000 (Smith and Hancock 1992).

Chemical neutralization was studied by the Australian Mineral Development Laboratories both in the laboratory and by the construction of a pilot plant on the tailings dam. The final process chosen incorporated a locally available waste lime slurry for the neutralizing agent. The process commences by mixing the lime slurry with the acidic water in predetermined proportions so as to raise the pH to between 9.5 and 10. This high alkalinity is required to ensure the removal of manganese which is the last toxic heavy metal to precipitate. Consumption of the lime slurry which contains about 25% solids (mainly $\text{Ca}(\text{OH})_2$) is between 20 and 34 litres per kilolitre of water treated depending on the source. Following mixing, the alkaline liquid is fed to a rake type thickener. The clear water overflow is discharged to Dawesley Creek while the underflow is pumped to lagoon holding ponds on the northern region of the tailings dam.

At present the operation treats water collected from the main seepage areas. The residue from the neutralization plant consists of mainly of hydroxides of the heavy metals which are insoluble. This stable sludge is deposited on the tailings dam in holding lagoons. The neutralisation plant represents a continuing cost until effective rehabilitation of the entire site can be undertaken.

The long term nature of the seepage from the tailings dam and mine area has been recognised. This means that the treatment plant will probably be maintained in some form for many years, and that there will be a relatively small incremental cost in treating other sources of acidic drainage, at least until the tailings (and mine site) seepage becomes small enough to release or to treat in some other way (SADME, 1989).

APPENDIX B

Preliminary Investigations of samples collected during the ANSTO drilling program in the Brukunga tailings dam, April 1994.

Table 2B.1: includes 5 tables of results from preliminary investigational work.

Hue/value/chroma values were obtained using the Munsell colour chart. A 1:5 tailings to liquid mixture was used for E.C and pH determination. Textures were classified according to:

- 1 Coarse sand
- 2 Medium - coarse sand
- 3 Medium sand
- 4 Fine to medium sand
- 5 Fine sand
- 6 Loamy medium sand
- 7 Loamy fine sand (-)
- 8 Loamy fine sand
- 9 Loamy fine sand (+)
- 10 Loamy very fine sand
- 11 Fine sandy loam (-)
- 12 Fine sandy loam
- 13 Fine sandy loam (+)
- 14 Silty loam

HOLE 31291							
DEPTH	DRY COLOUR	WET COLOUR	TEXTURE	TEXT CLAS	E.C	pH WATER	pH CaCl2
1	10YR 8/8 2.5YR 7/6	RANDOM	F-C S & OM	2	1.48	3.68	3.61
2	5Y 7/2-3 2.5YR 8/8	5Y 5/3	L F-SAND	8	0.7	3.99	3.93
3	5Y 5/1 2.5YR 7/2	5Y 3/1	M SAND	3	0.33	4.39	4.32
4	5Y 6/1 5Y 5/1	5Y 4/3	F-M SAND	4	1.05	3.46	3.42
5	5Y 6/3 2.5YR 7/2	5Y 4/2	M SAND	3	0.7	3.89	3.83
6	2.5YR 6/2	5Y 4/1-2	AA	3	0.47	4.11	4.02
7	5Y 6/1	5Y 3/1	AA	3	0.43	4.2	4.11
8	5Y 6/2	5Y 4/2	L F-SAND	8	0.9	3.43	3.4
9	2.5YR 6/3	AA	AA	8	0.74	3.57	3.54
10	5Y 6/4	AA	L F-SAND	7	0.56	3.8	3.74
11	5Y 6/3	AA	AA	7	0.5	3.9	3.84
12							
13							
14							
15							
16							
17							
18	5Y 6/4 2.5YR 5/2	5Y 3/2	F-L SAND	7	0.54	3.88	3.85
19	O. A. R.	O. A. R.	F-L SAND	8	0.8	3.66	3.53
20	O. A. R.	O. A. R.	AA	8	0.57	3.98	3.81

Appendix B Preliminary Tailings Investigations

Table 2B.1 Cont

HOLE 31292

DEPTH	DRY COLOUR	WET COLOUR	TEXTURE	TEXT CL	E.C	pH WATER	pH CaCl2
1	2.5YR 7/02.5YR7/6	RANDOM	F-C S & OM	2	0.56	3.47	3.44
2	2.5YR 8/0 5Y 6/6	5Y 5/3	L F-SAND	8	0.65	3.79	3.77
3	2.5 Y 7/4	5Y 4/3	AA	8	0.84	3.57	3.53
4	5Y 6/1	5Y 4/2	F-M SAND	4	0.32	4.38	4.19
5	AA	AA	AA	4	0.36	4.35	4.2
6	AA	AA	AA	4	0.29	4.42	4.25
7	AA	5Y 5/2	AA	4	0.38	4.42	4.27
8	AA	5Y 5/1	AA	4	0.49	4.31	4.18
9	5Y 5/3	5Y 4/2	M SAND	3	1.04	3.64	3.62
10	2.5YR 6/4	AA	AA	3	0.52	4.44	4.35
11	5Y 6/1	5Y 4/1	F-M SAND	4	0.41	4.44	4.33
12	AA	5Y 4/2	AA	4	0.49	4.34	4.24
13	O. A. R.	O. A. R.	F SAND	5	0.16	5.16	4.58

HOLE 31293

DEPTH	DRY COLOUR	WET COLOUR	TEXTURE	TEXT CL	E.C	pH WATER	pH CaCl2
1	RANDOM	RANDOM	M-C SAND	2	0.69	3.55	3.53
2	5Y 7/1 10YR/6/8	5Y 5/2	L F-SAND	8	0.45	4.04	4.02
3	5Y 7/2	5Y 5/3	AA	8	0.75	3.91	3.9
4	AA	AA	AA	8	0.9	3.95	3.94
5	5Y 6/1	5Y 5/2	L F-SAND+	9	0.71	4.14	4.12
6	AA	5Y 4/2	AA	9	0.8	4.2	4.15
7	5Y 7/2	AA	AA	9	0.82	4.07	3.99
8	AA	5Y 5/2	AA	9	0.66	4.17	4.06
9	AA	5Y 4/2	AA	9	0.6	4.14	4.06
10	5Y 7/1-2	5Y 5/2	SILT-LOAM	14	0.59	4.18	4.07
11	5Y7/2-1	AA	AA	14	0.95	3.88	3.83
12	5Y 7/1	AA	AA	14	0.94	4.08	3.99
13	AA	5Y 4/2	AA	14	0.56	4	3.93
14	5Y 6/1	5Y 4/1	AA	14	0.77	3.9	3.91
15	AA	5Y 5/2	AA	14	0.61	4.01	3.9
16	AA	5Y4/1-2	AA	14	0.6	3.82	3.79
17	AA	5Y 4/1	AA	14	0.71	3.77	3.76
18	AA	5Y 4/2	AA	14	0.82	3.61	3.6
19	AA	5Y 3/1	AA	14	0.88	3.68	3.67
20	AA	5Y 4/2	AA	14	0.65	3.96	3.88
21	5Y 6/2	AA	F-S LOAM	12	0.27	4.42	4.09

HOLE 31294

DEPTH	DRY COLOUR	WET COLOUR	TEXTURE	TEXT CL	E.C	pH WATER	pH CaCl2
1	10YR 7/85Y 8/6	10YR 5/6	F-C S & OM	2	1.74	4.42	4.34
2	5Y 6/1 2.5YR 7/6	10YR 5/65Y 7/8	5Y 4/1	3	1.19	4.01	3.99
3	5Y 6/1 2.5 YR 7/7	AA	AA	3	0.82	4	3.99
4	5Y 5/3	10YR 5/65Y 3/1	AA	3	0.88	3.83	3.83
5	5Y 6/1 10YR 7/8	10YR 5/65Y 6/1	5Y 3/1	3	0.97	3.7	3.69
6	5Y 7/3	5Y 4/3	AA	3	0.99	3.74	3.73
7	5Y 6/3	5Y 6/4	L F-SAND	8	0.99	3.64	3.61
8	AA	5Y 4/3	F-S LOAM	11	1.05	3.54	3.52
9	5Y 5/3	AA	M SAND	3	0.85	3.94	3.9
10	AA	AA	L F-SAND	8	0.85	3.65	3.6
11	AA	AA	F-M SAND	4	1.04	3.54	3.49
12	5Y 6/2	5Y 4/2	AA	4	0.96	3.63	3.58
13	5Y 6/1	5Y 4/1-2	AA	4	0.31	4.07	3.96
14	AA	AA	L F-SAND	8	0.32	4.07	3.96
15	5Y 6/2	5Y 3/2	AA	8	0.28	4.08	3.94
16	AA	AA	F-S LOAM	12	0.54	3.79	3.72
17	5Y 6/1	5Y 3/2	AA	12	0.59	3.97	3.87
18	5Y 5/3	7.5 YR 4/12	L F-SAND	8	0.4	4.23	4.05

Appendix B Preliminary Tailings Investigations

Table 2B.1 cont

HOLE 31295							
DEPTH	DRY COLOUR	WET COLOUR	TEXTURE	TEXT CL	E.C	pH WATER	pH CaCl2
1	10YR 6/6	10YR 5/6	M-C S & OM	2	2.02	3.6	3.56
2	5Y 6/1 2.5YR 8/3 & 7/8	5Y 5/3 5Y 4/1	M SAND	3	0.75	4.16	4.13
3	5Y 5/1 10YR 6/3	10YR 5/6 5Y 3/1	AA	3	0.5	4.36	4.33
4	5Y 6/3 2.5 7/0	5Y 4/3	L F-SAND	8	0.87	4.26	4.22
5	5Y 6/1 2.5 7/8	5Y 3/2	L M-SAND	6	0.48	4.24	4.19
6	AA	5Y 4/2	L F-SAND	8	0.43	4.15	4.06
7	5Y 5/1	AA	AA	8	0.41	4.29	4.17
8	5Y 6/2-3	AA	F-S LOAM	12	0.44	4.07	3.98
9	5Y 6/2	AA	F-M SAND	4	0.44	4.01	3.92
10	AA	5Y 5/2	L F-SAND	8	0.5	4.21	4.08
11	5Y 6/1	AA	AA	8	0.43	4.28	4.13
12	AA	5Y 4/2	AA	8	0.27	4.16	3.98
13	AA	AA	AA	8	0.55	3.69	3.64
14	5Y 6/2	AA	F-S LOAM	12	0.3	4.01	3.9
15	AA	AA	L F-SAND	8	0.4	3.79	3.72
16	AA	AA	AA	8	0.27	4.04	3.9
17	AA	5Y 3/2	AA	8	0.26	4.14	3.96
18	AA	5Y 4/2	AA	8	0.29	4.04	3.91
19	AA	5Y 5/2	AA	8	0.33	3.93	3.82
20	5Y 6/1	5Y 4/1-2	AA	8	0.32	3.92	3.84
21	AA	5Y 2.5/2	AA	8	0.53	3.98	3.9
22	AA	5Y 3/2	AA	8	0.5	3.93	3.87
23	AA	5Y 4/2	F-S LOAM	12	0.56	4.07	3.98
24	5Y 6/2	5Y 3/1	L F-SAND	8	0.46	3.85	3.78
25	5Y 5/2	5Y 4/2	AA	8	0.42	3.83	3.76
26	AA	5Y 3/1	AA	8	0.45	3.73	3.68
27	AA	AA	AA	8	0.71	3.44	3.44
28	5Y 5/1	5Y 4/2	AA	8	0.49	3.7	3.66
29	5Y 5/1-2	5Y 3/1	F-S LOAM	12	0.58	3.53	3.51
30	5Y 5/2	5Y 3/2	AA	12	0.56	3.69	3.65
31	5Y 5/1	AA	AA	12	0.55	3.74	3.67
32	5Y 5/1 5Y 5/3	AA	AA	12	0.46	4.25	4.06
33	5Y 5/2 5Y 6/6	2.5YR 3/2	L M-SAND	6	0.45	7	6.97

HOLE 31296							
DEPTH	DRY COLOUR	WET COLOUR	TEXTURE	TEXT CL	E.C	pH WATER	pH CaCl2
1	10YR 7/5 2.5 YR 8/0	10YR 5/4	L M-C SAND	6	2.33	3.93	3.89
2	AA	10YR 5/5	AA	6	2.34	3.96	3.96
3	2.5 YR 7/4	2.5YR 6/4	AA	6	2.18	4.06	4.02
4	5Y 6/2 10YR 7/8	5YR 4/2	F-S LOAM	11	1.04	4.11	4.03
5	5Y 6/2-3	AA	AA	11	1.14	3.87	3.83
6	5Y 6/2	AA	AA	11	1.17	4.02	3.94
7	2.5YR 6/2	AA	AA	11	0.89	3.67	3.63
8	5Y 6/3 10YR 8/1 2.5YR 6/6	AA	AA	11	1.06	3.64	3.6
9	5Y 6/2-3	AA	AA	11	0.73	3.94	3.88
10	5Y 6/2 5Y 5/1	AA	M SAND	3	0.78	4.08	4.02
11	5Y 6/3	5Y 4/3-4	F-M SAND	4	0.57	4.01	3.93
12	5Y 6/3 10YR 7/8	5Y 4/2	AA	4	0.6	4.05	3.97
13	5Y 6/2	5Y 4/1	F-M SAND+	4	0.41	4.17	4.05
14	5Y 6/1	5Y 4/1-2	AA	4	0.29	4.28	4.12
15	5Y 6/3	5Y 4/2	M SAND	3	0.32	4.3	4.17
16	2.5YR 5/4	5Y 5/4	F-C SAND	3	1.37	7.65	7.51

HOLE 31297							
DEPTH	DRY COLOUR	WET COLOUR	TEXTURE	TEXT CL	E.C	pH WATER	pH CaCl2
1	RANDOM	RANDOM	C S & OM	1	0.26	4.26	4.07
2	5Y 7/1 2.5YR 7/8 & 8/6	5Y 5/2	L F-SAND	8	0.31	4.39	4.3
3	5Y 7/1 2.5YR 7/8	AA	AA	8	0.23	4.31	4.18
4	AA	5Y 5/2-3	AA	8	0.24	4.49	4.3
5	5Y 7/1 5Y 6/1	5Y 4/2	F SAND	5	0.17	4.63	4.39
6	5Y 6/1	AA	F-M SAND	4	0.24	4.4	4.18
7	AA	AA	AA	4	0.24	4.3	4.12
8	AA	AA	AA	4	0.28	4.23	4.07
9	5Y 5/1	5Y 2.5/2	M-F SAND	4	0.23	4.41	4.22
10	5Y 6/1	5Y 4/2	F-M SAND	4	0.27	4.34	4.18
11	AA	AA	AA	4	0.32	4.33	4.15
12	2.5YR 6/2	AA	L M-SAND	6	0.24	4.45	4.23
13	5Y 6/1	AA	AA	6	0.18	4.54	4.31
14	5Y 6/2	AA	AA	6	0.28	4.42	4.24
15	5Y 6/1	5Y 4/1	AA	6	0.23	4.21	3.95
16	AA	AA	L F-SAND	8	0.47	4.14	3.98
17	5Y 6/2	5Y 4/2	AA	8	0.33	4.13	3.94
18	5Y 6/1	5Y 4/1	L VF-SAND	10	0.66	4.87	3.8
19	AA	AA	AA	10	0.79	3.85	3.8
20	AA	AA	AA	10	0.61	3.99	3.88
21	5Y 6/1-2	AA	AA	10	0.41	4.12	3.98
22	5Y 6/1	AA	L F-SAND	8	0.55	4.08	3.98
23	AA	5Y 3/1	L M-SAND	6	0.59	4.04	3.94
24	5Y 5/1	AA	L F-SAND	8	0.68	3.87	3.88
25	AA	AA	AA	8	0.37	3.97	3.91
26	AA	AA	AA	8	0.56	4.16	4.01

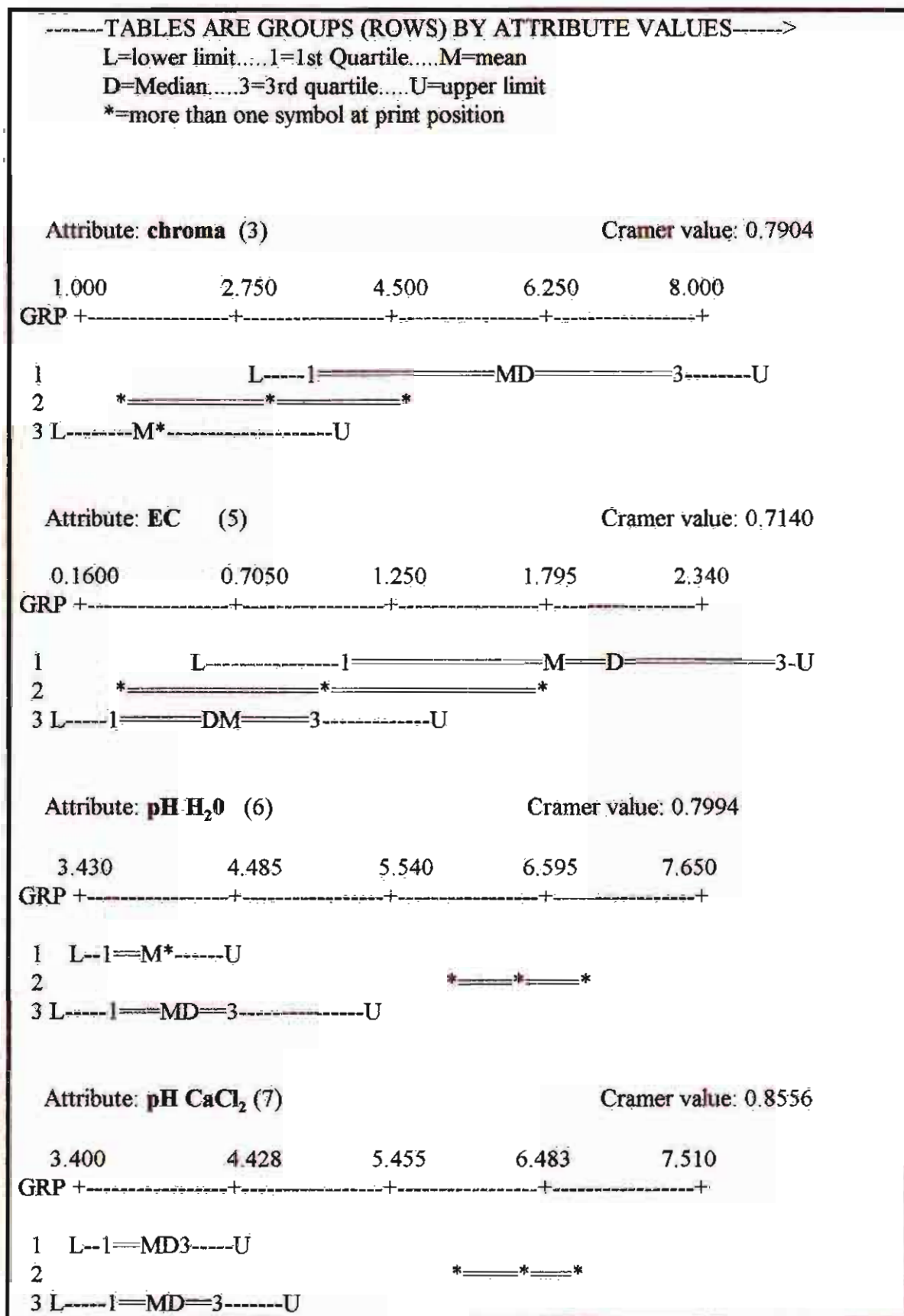
Appendix B Preliminary Tailings Investigations

Table 2B.2: The 3 groups of samples produced by the first run of the classification.

GROUP:	1	8 MEMBERS						
	1 1	(1)	5 1	(66)	4 1	(48)	6 1	(95)
	6 2	(96)	6 3	(97)	4 2	(49)	4 3	(50)
GROUP:	2	2 MEMBERS						
	5 33	(94)	6 16	(110)				
GROUP:	3	122	MEMBERS					
	1 2	(2)	3 3	(30)	3 4	(31)	2 2	(16)
	1 9	(9)	1 19	(13)	2 3	(17)	4 10	(57)
	4 7	(54)	1 10	(10)	1 11	(11)	5 13	(78)
	5 28	(89)	5 15	(80)	5 25	(86)	4 14	(61)
	5 20	(85)	5 6	(71)	5 7	(72)	5 12	(77)
	5 16	(81)	4 18	(65)	3 5	(32)	3 8	(35)
	3 6	(33)	3 7	(34)	3 9	(36)	5 4	(69)
	1 20	(14)	7 16	(126)	7 26	(132)	7 25	(131)
	3 2	(29)	5 10	(75)	5 11	(76)	5 17	(82)
	7 17	(127)	5 18	(83)	5 19	(84)	7 2	(112)
	7 4	(114)	7 3	(113)	7 18	(128)	7 19	(129)
	7 20	(130)	1 8	(8)	5 27	(88)	5 26	(87)
	1 18	(12)	4 15	(62)	5 5	(70)	4 16	(63)
	5 30	(91)	5 31	(92)	4 17	(64)	5 32	(93)
	5 29	(90)	5 8	(73)	5 14	(79)	3 10	(37)
	3 15	(42)	3 11	(38)	3 12	(39)	3 13	(40)
	3 20	(47)	3 18	(45)	3 14	(41)	3 16	(43)
	3 17	(44)	3 19	(46)	4 8	(55)	6 7	(101)
	6 8	(102)	6 4	(98)	6 5	(99)	6 6	(100)
	6 9	(103)	1 3	(3)	5 3	(68)	7 9	(119)
	7 1	(111)	1 5	(5)	5 9	(74)	6 12	(106)
	6 10	(104)	6 11	(105)	1 6	(6)	1 7	(7)
	2 11	(25)	4 13	(60)	6 13	(107)	6 14	(108)
	2 4	(18)	2 5	(19)	2 6	(20)	7 6	(116)
	7 7	(117)	7 8	(118)	6 15	(109)	2 10	(24)
	2 12	(26)	2 7	(21)	7 10	(120)	7 11	(121)
	2 8	(22)	7 12	(122)	7 14	(124)	7 13	(123)
	7 15	(125)	5 2	(67)	2 13	(27)	7 5	(115)
	1 4	(4)	4 11	(58)	2 9	(23)	4 12	(59)
	4 6	(53)	4 9	(56)	2 1	(15)	3 1	(28)
	4 4	(51)	4 5	(52)				

Appendix B Preliminary Tailings Investigations

Table 2B.3: Box and whisker plot showing the important attributes for delineating groups 1, 2 and 3.



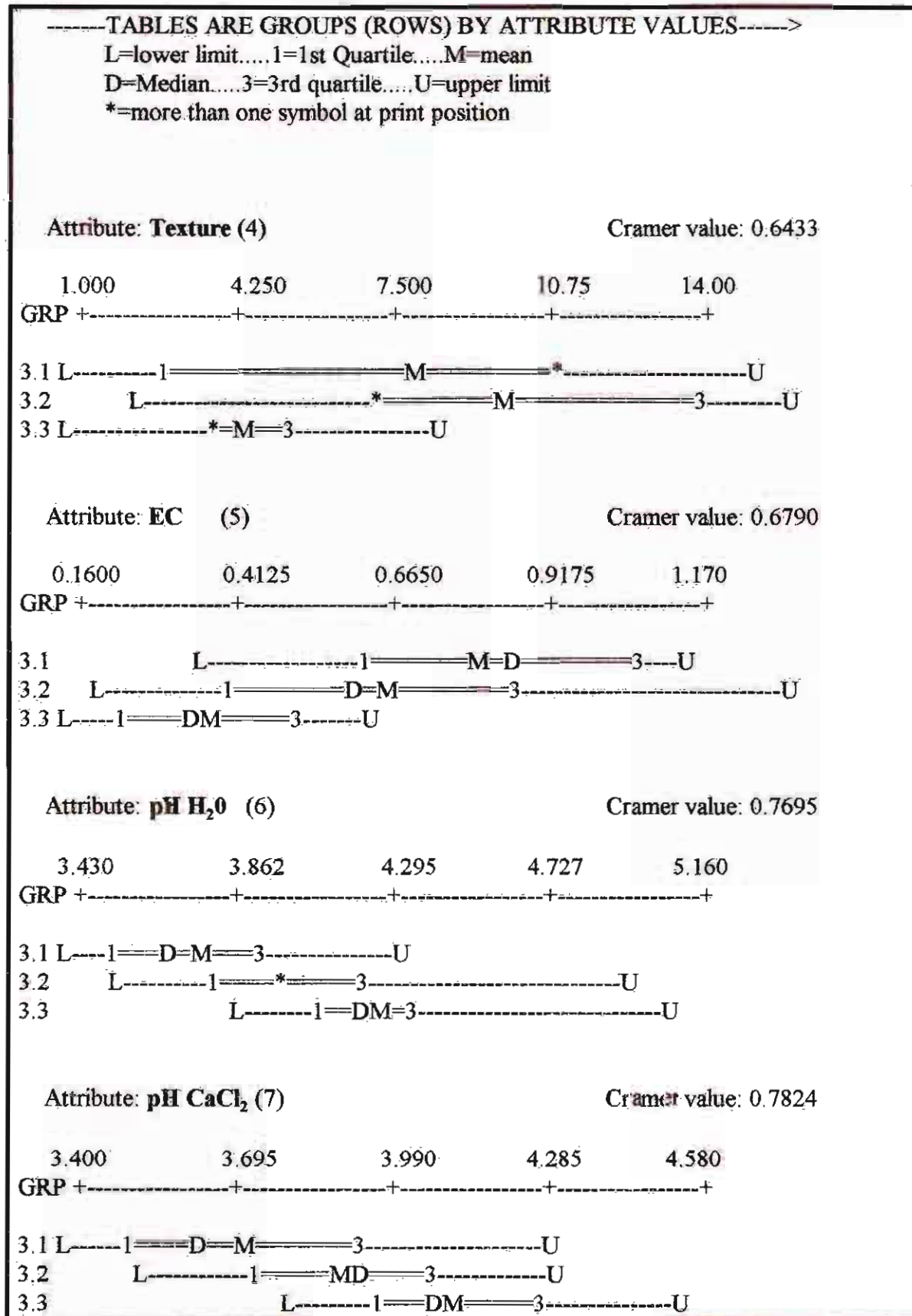
Appendix B Preliminary Tailings Investigations

Table 2B.4 Group membership for subgroups of group 3, ie., groups 3.1, 3.2, 3.3.

GROUP:	3.1	25 MEMBERS					
1 2	(1)	3 3	(2)	3 4	(3)	2 2	(4)
5 2	(110)	4 7	(9)	1 9	(5)	1 19	(6)
2 3	(7)	4 10	(8)	1 8	(46)	4 8	(71)
1 4	(113)	4 11	(114)	2 9	(115)	4 12	(116)
4 6	(117)	4 9	(118)	5 27	(47)	5 29	(57)
5 26	(48)	4 4	(121)	4 5	(122)	2 1	(119)
3 1	(120)						
GROUP:	3.2	65 MEMBERS					
1 10	(10)	1 11	(11)	5 13	(12)	5 28	(13)
5 15	(14)	5 25	(15)	1 20	(29)	1 18	(49)
5 5	(51)	5 32	(56)	4 16	(52)	5 30	(53)
5 31	(54)	4 17	(55)	3 6	(25)	3 7	(26)
3 9	(27)	5 4	(28)	1 5	(82)	5 9	(83)
6 12	(84)	6 10	(85)	6 11	(86)	4 14	(16)
5 20	(17)	7 16	(30)	7 26	(31)	7 25	(32)
7 15	(109)	7 18	(43)	7 19	(44)	7 20	(45)
5 6	(18)	5 7	(19)	5 12	(20)	5 16	(21)
4 15	(50)	3 5	(23)	3 8	(24)	3 2	(33)
5 10	(34)	5 11	(35)	5 17	(36)	7 17	(37)
5 18	(38)	5 19	(39)	5 8	(58)	5 14	(59)
3 13	(64)	3 20	(65)	6 9	(77)	3 10	(60)
3 15	(61)	3 11	(62)	3 12	(63)	3 18	(66)
6 7	(72)	6 8	(73)	6 4	(74)	6 5	(75)
6 6	(76)	3 14	(67)	3 16	(68)	3 17	(69)
3 19	(70)						
GROUP:	3.3	32 MEMBERS					
4 18	(22)	2 13	(111)	7 2	(40)	7 4	(41)
7 3	(42)	7 12	(106)	7 14	(107)	7 13	(108)
2 7	(102)	7 10	(103)	7 11	(104)	7 9	(80)
2 4	(93)	2 5	(94)	2 6	(95)	7 6	(96)
6 15	(99)	7 7	(97)	7 8	(98)	2 10	(100)
2 12	(101)	7 5	(112)	1 3	(78)	5 3	(79)
2 11	(89)	1 6	(87)	1 7	(88)	6 13	(91)
4 13	(90)	6 14	(92)	2 8	(105)	7 1	(81)

Appendix B Preliminary Tailings Investigations

Table 2B.5 Box and whisker plots of measured attributes for groups 3.1, 3.2 and 3.3, showing clear distinctions between subgroups on their EC and pH values.



Appendix B Preliminary Tailings Investigations

Table 2B.6 Group statistics for the classification of tailings materials.

	group	N	N*	MEAN	MEDIAN	STDEV	SEMEAN
depth	1	8	0	1.750	1.500	0.886	0.313
	2	2	0	24.50	24.50	12.02	8.50
	31	25	0	8.84	7.00	8.11	1.62
	32	65	0	13.938	14.000	6.953	0.862
	33	32	0	8.531	8.000	4.385	0.775
hue	1	7	1	7.50	10.00	3.23	1.22
	2	2	0	3.75	3.75	1.77	1.25
	31	22	3	5.0000	5.0000	0.0000	0.0000
	32	64	1	5.0000	5.0000	0.0000	0.0000
	33	30	2	5.0833	5.0000	0.4564	0.0833
value	1	7	1	5.571	5.000	0.976	0.369
	2	2	0	4.00	4.00	1.41	1.00
	31	22	3	4.045	4.000	0.844	0.180
	32	64	1	4.1719	4.0000	0.6560	0.0820
	33	30	2	4.217	4.000	0.665	0.121
chroma	1	7	1	5.857	6.000	1.676	0.634
	2	2	0	3.00	3.00	1.41	1.00
	31	22	3	2.409	3.000	0.908	0.194
	32	64	1	1.8281	2.0000	0.4562	0.0570
	33	30	2	1.7000	2.0000	0.4661	0.0851
texture	1	8	0	3.375	3.000	2.326	0.822
	2	2	0	3.50	3.50	3.54	2.50
	31	25	0	6.080	8.000	2.999	0.600
	32	65	0	9.462	8.000	2.905	0.360
	33	32	0	4.469	4.000	1.665	0.294
EC	1	8	0	1.763	1.880	0.560	0.198
	2	2	0	0.910	0.910	0.651	0.460
	31	25	0	0.8276	0.8500	0.1672	0.0334
	32	65	0	0.5875	0.5600	0.2249	0.0279
	33	32	0	0.3244	0.3100	0.1000	0.0177
pH(H ₂ O)	1	8	0	3.9575	3.9800	0.2492	0.0881
	2	2	0	7.325	7.325	0.460	0.325
	31	25	0	3.6824	3.6400	0.1918	0.0384
	32	65	0	4.0025	4.0100	0.2063	0.0256
	33	32	0	4.3709	4.3550	0.1857	0.0328
pH(CaCl ₂)	1	8	0	3.9200	3.9750	0.2462	0.0871
	2	2	0	7.240	7.240	0.382	0.270
	31	25	0	3.6504	3.6000	0.1941	0.0388
	32	65	0	3.9017	3.9100	0.1506	0.0187
	33	32	0	4.2084	4.1950	0.1254	0.0222

APPENDIX C1

Detailed Review of Brukunga Waste & Mine Rock Investigations

&

Presentation of data referred to in Chapter 3, Section A.

Figures referred to in Chapter 3 - Section A follow. These figures represent EDX spectra obtained during SEM investigations, and are presented for verification of the presence of specific minerals observed.

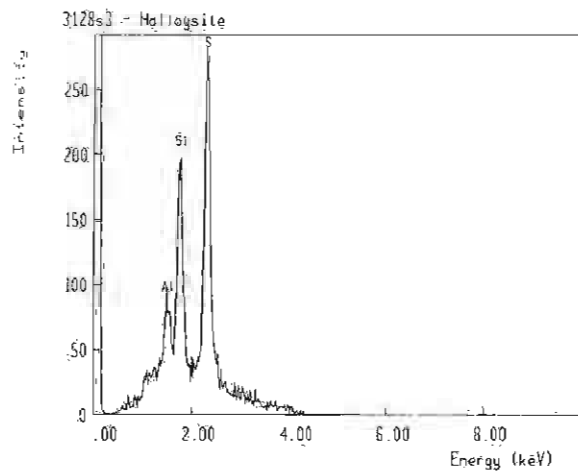


Fig 3.5a Halloysite present in rock 5.

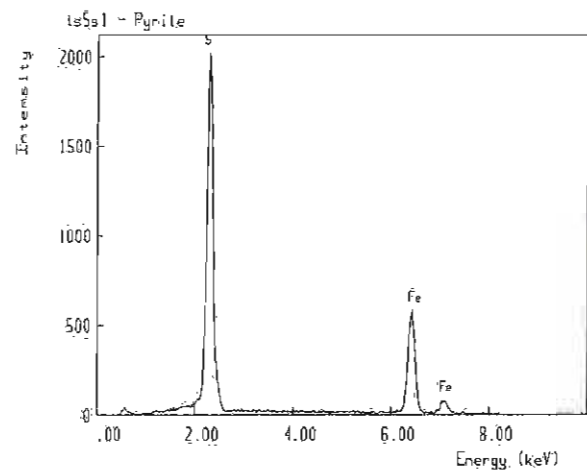


Fig 3.7a Pyrite present in rock 5

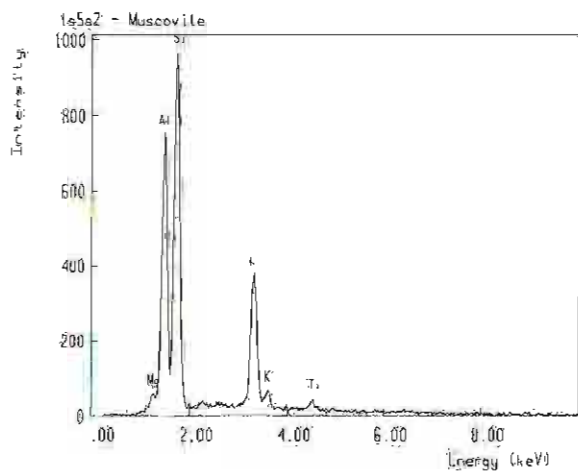


Fig 3.7b Muscovite present in rock 5

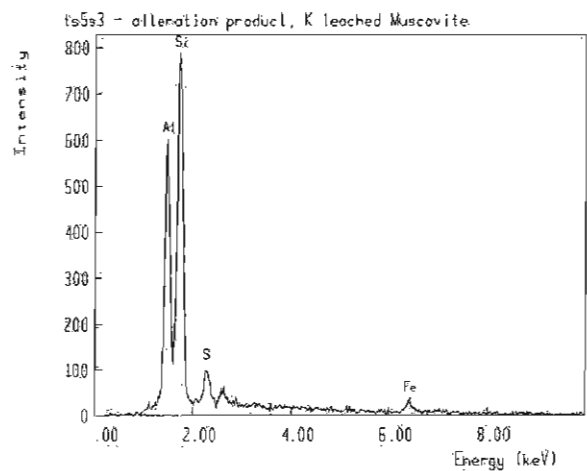


Fig 3.7c Alteration rims of kaolinite developed between pyrite and muscovite present in Rock 5.

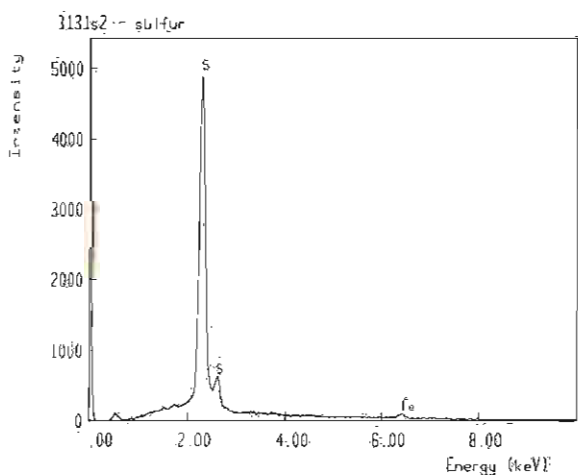


Fig 3.9a Alteration product sulfur developed within rock 11.

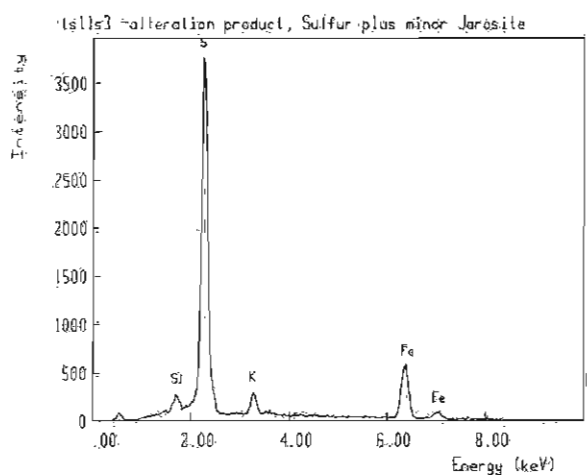


Fig 3.11a Alteration product sulfur and minor jarosite developed within rock 11.

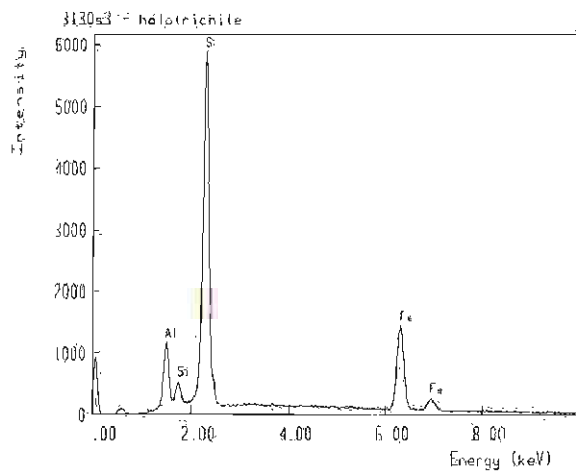


Fig 3.15a Halotrichite developed in rock 9.

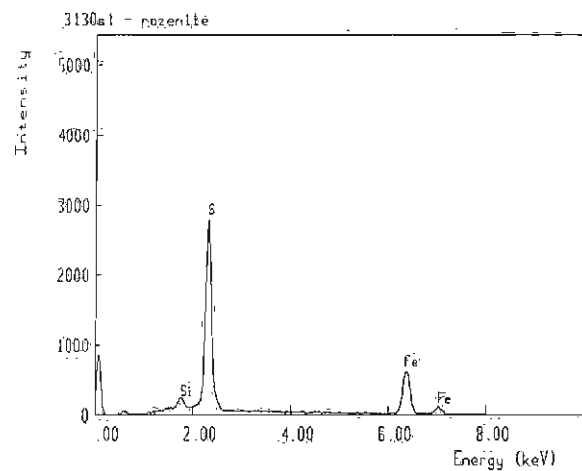


Fig 3.19a Iron sulfate developed in rock 9 probably rozenite.

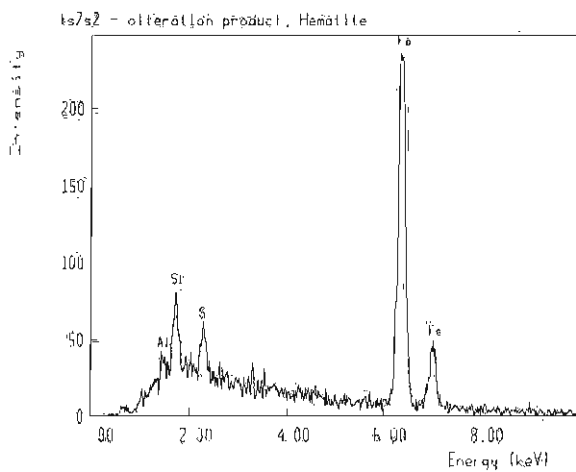


Fig 3.22a Hematite developed in rock 7.

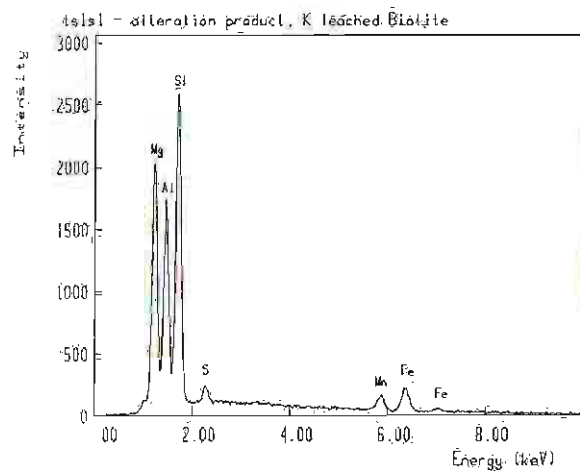


Fig 3.26a Alteration product in rock 1, K-leached biotite.

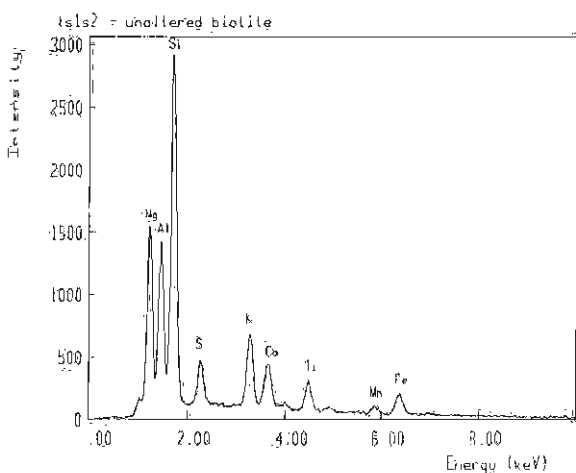


Fig 3.26b Unaltered biotite within rock 1.

Detailed Review of Brukunga Waste & Mine Rock Investigations

ROCK 5 Highly weathered pyritic schist.

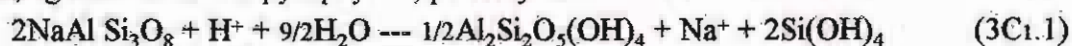
This sample is a weathered, friable pyritic schist with white matrix, and evenly distributed pyrite associated with a slight foliation. Main components determined via XRD and verified by optical microscopy and SEM/EDX are;

pyrite	30-40%
quartz	15-25%
muscovite	10-20%
kaolinite	5-10%
albite	<5%
rutile	<5%

XRF data (Table 3.4) reflects the high quantity of pyrite shown as increased amounts of iron and sulfur compared to other samples investigated. SEM/EDX and optical microscopy demonstrated that the pyrite crystals have conchoidal fracturing which produces subhedral forms, and are at varying states of weathering. Crystals ranged from only slightly weathered to moderately weathered in which dissolution of crystals had occurred, leaving depressions (Fig 3.1). Pyrophyllite ($\text{Al}_4(\text{Si}_8\text{O}_{20})(\text{OH})_4$) was observed during investigations using the SEM/EDX, as part of the host rock. The shape and context in which the pyrophyllite occurs suggests it is in fact part of the primary structure. Deer *et al* suggests that this material may occur as a weathering product of similar origin to kaolinite, but its morphology does not support this (Fig 3.6).

Kaolinite ($\text{Al}_2\text{Si}_2\text{O}_5(\text{OH})_4$) appears to be the main weathering product. SEM/EDX allowed identification of halloysite ($\text{Al}_2\text{Si}_2\text{O}_5(\text{OH})_4 \cdot 4\text{H}_2\text{O}$), a hydrated form of kaolinite, on both the pyrite and host rock (Fig 3.5 & 3.5a).

Kaolinite can be formed principally via the weathering of feldspars, feldspathoids and other silicates, eg muscovite and pyrophyllite, possibly as:



albite

kaolinite



anorthite

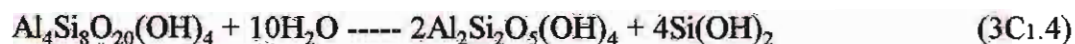
kaolinite

Appendix C1 Waste Rock Investigations



k-feldspar

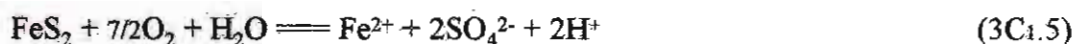
kaolinite



pyrophyllite

kaolinite

Kaolinite can be formed naturally through weathering, but the system is probably accelerated due to the presence of H^+ ions. The H^+ ions are supplied through the oxidation of FeS_2 :



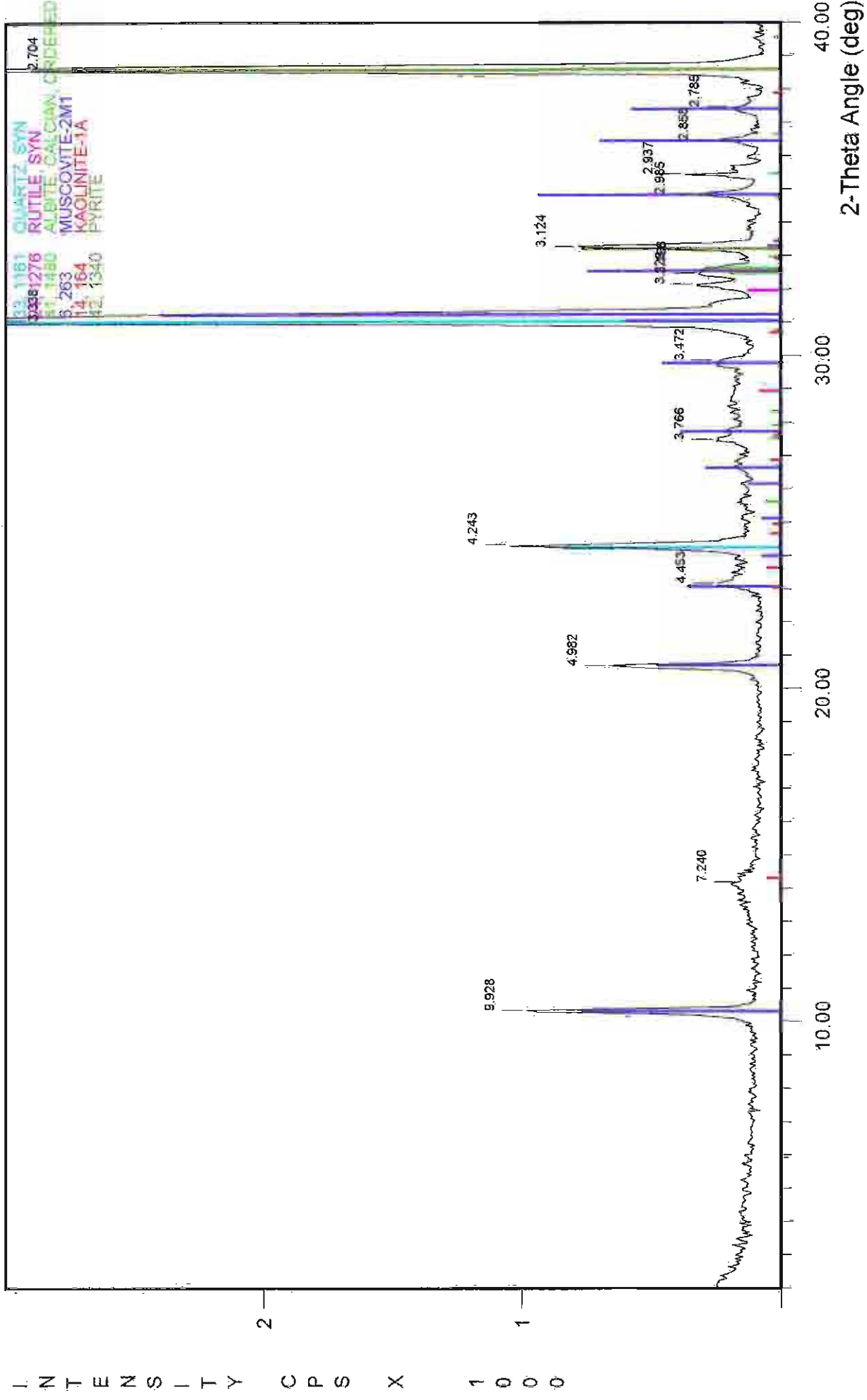
pyrite

The kaolinite forming in response to feldspar, mica and pyrophyllite weathering can be observed in Fig 3.6 where halloysite coats the particles. The main alteration forms observed microscopically occurs in the fine matrix of the rock, particularly along contact boundaries with pyrite crystals (Fig 3.7 (frame width 0.5mm), & 3.7a, 3.7b, 3.7c). In locations where muscovite is in direct contact with the pyrite crystals, reaction rims are present with muscovite altering to kaolinite. The altered pyrite crystals and gangue minerals show orange staining, which can be attributed to the presence of iron oxides. Fig 3.8 (frame width 0.5mm) shows iron oxide staining of muscovite along boundaries and the degradation of muscovite to kaolinite. Further into the interior of the specimen, sharp boundaries can be observed between pyrite and muscovite, indicating the lack of oxygen and water infiltration to these areas.

Potential Environmental Impact

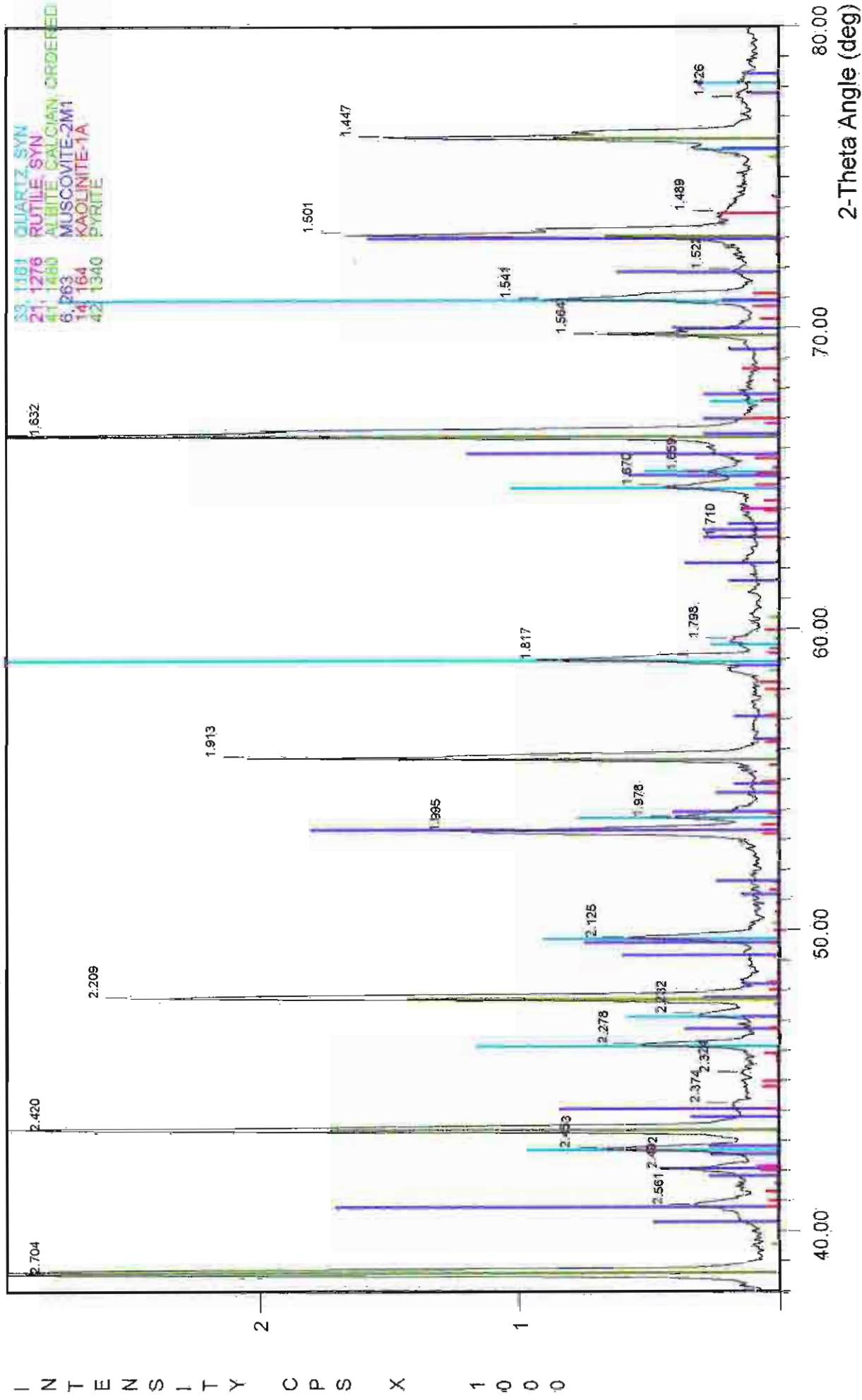
If this rock type is major component of the mine and waste rock dumps, then it would have a major detrimental effect of the surrounding environment. It is the sheer quantity of pyrite present within this specimen that produces the highest ranking Acid Mine Drainage (AMD) potential (NNP = -748 kg H_2SO_4 per tonne). The muscovite present has some neutralising capacity (Jambor & Blowes, 1994), but this is insignificant compared to the quantity of sulfide present. Thus this specimen would have a strong effect on the surrounding environment, where leaching would promote large quantities of acid to enter the water system, further polluting the already unstable system.

ROCK 5 : Highly weathered pyritic schist



File Name: A:\BRUKROCK.105

ROCK 5 : Highly weathered pyritic schist



File Name: A:\BRUKROCK.105

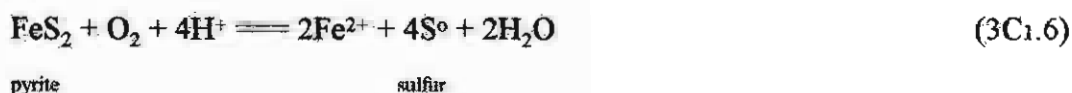
ROCK 11 Highly weathered Metasediment

The initial state of this rock before weathering is difficult to determine. It has degraded to a friable, pale grey, fine grained massive structureless material with agglomerations of pure sulfur formed in depressions. Main components determined via XRD and verified by optical microscopy and SEM/EDX are:

muscovite	20-30%
quartz	15-20%
pyrite	15-20%
jarosite	<5%
clinochlore	<5%
anorthite	<5%
marcasite	
sulfur	
alunite	

SEM/EDX and optical microscopy indicated the majority of the host rock is in fact covered with a coating of jarosite crystals (Fig 3.12). Many of the grains were too fine to be probed individually using the EDX analyser. The majority of the sections that were probed showed a jarosite signature (Fig 3.12a). XRD data suggests 15-20% pyrite exists within the host rock. XRF data (Table 3.4) confirms this, but pyrite was not detected during SEM/EDX investigations. This can be attributed to a combination of the fact that much of the pyrite was too small to probe, and the jarosite coating reduced the signal of any larger grains. Thin section microscopy investigations revealed coarse pyrite grains associated with veins or layering and they showed strong weathering, while the finer grained material showed only very minor alteration. In locations where pyrite previously existed, iron staining takes its place around the edge of voids. The muscovites surrounding these positions of degradation are also highly altered and covered with iron staining. SEM/EDX and optical microscopy indicated the presence of minor chalcopyrite, rutile and zircon within the host rock.

SEM/EDX investigations at high magnification allowed observation of the sulfur. It was shown to form amorphous homogeneous accumulations (Fig 3.9, 3.9a & 3.10). The formation of sulfur occurs from the oxidation of pyrite within the rock



Thin section microscopy showed sulfur formation is associated with the degradation of pyrite and develops in the voids left where pyrite crystals once existed, along with minor jarosite (Fig 3.11 (frame width 0.5mm) & 3.11a).

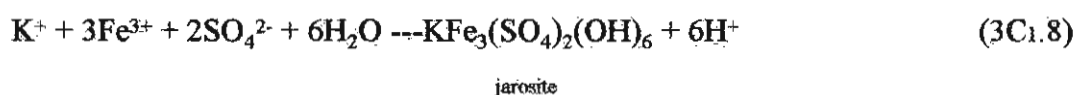
Nordstrom (1982) explains that at first the sulfur simply remains at the surface as part of the structure while ferrous ions leach out from the surrounding lattice sites. This sulfur rich surface would eventually become unstable finally disrupting and reorganising into elemental sulfur such as S₈ rings.

Both jarosite (KFe₃(SO₄)₂(OH)₆) and alunite (KAl₃(SO₄)₂(OH)₆) are by-products of this same weathering. SEM/EDX observations showed jarosite mainly as a coating on all minerals present except sulfur (Fig 3.12). Initially pyrite is oxidised sending Fe²⁺ into solution (eq 3C1.5) which is itself subsequently altered oxidised to produce Fe³⁺.

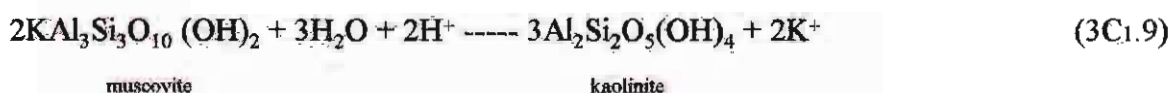
T.ferrioxidans are sulfur-oxidizing bacteria which act as catalysts in this reaction. They are reported to speed up the reaction by approximately one million times (Singer and Stumm, 1970).



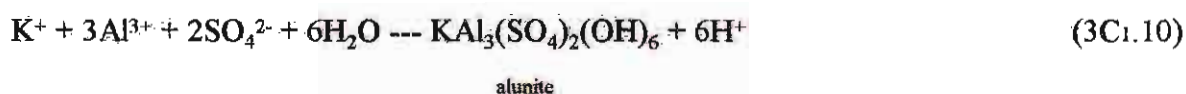
Then jarosite is precipitated out of solution



where K⁺ is present in solution due to the weathering of muscovite



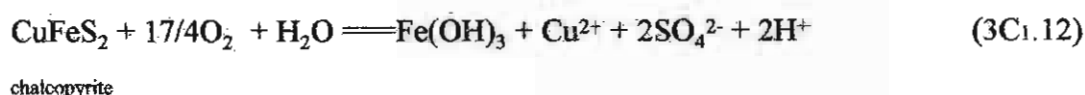
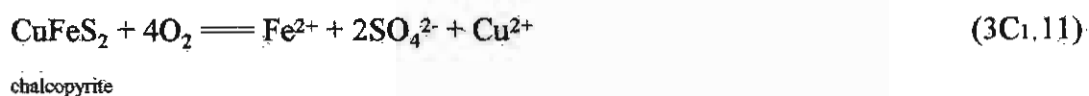
Alunite precipitates out through similar processes, where Al³⁺ is present in solution from the continued decomposition of aluminosilicate minerals.



Potential Environmental hazard

Thin section microscopy indicated the majority of pyrite in the rock is very fine grained, allowing greater surface area available for oxidation and thus acid formation. This and the fact that a substantial quantity of sulfides is present leads to the second highest ranking of AMD Potential (NNP = -461 kg H₂SO₄ per tonne). However, it should be noted also that thin section microscopy showed minerals with neutralising potential are also fine grained and make up the majority of the host rock. Nevertheless the quantity and potential for neutralisation of these minerals are obviously too low (A.C 1.4 kg H₂SO₄ per tonne) to have any major effect.

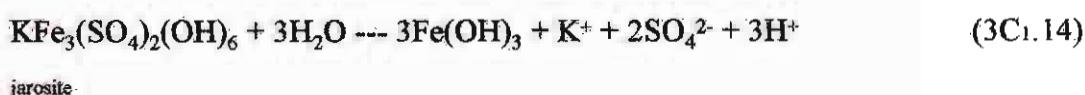
Additionally the minor quantity of chalcopryrite (FeCuS_2) present would also oxidise, thus adding Cu^{2+} to the system which has been subsequently leached from the surroundings probably precipitating elsewhere as a copper sulfate. The oxidation and precipitation of the Fe also present would then add acidity to the region.



The subsequent oxidation of sulfur again creates more acidity in the system



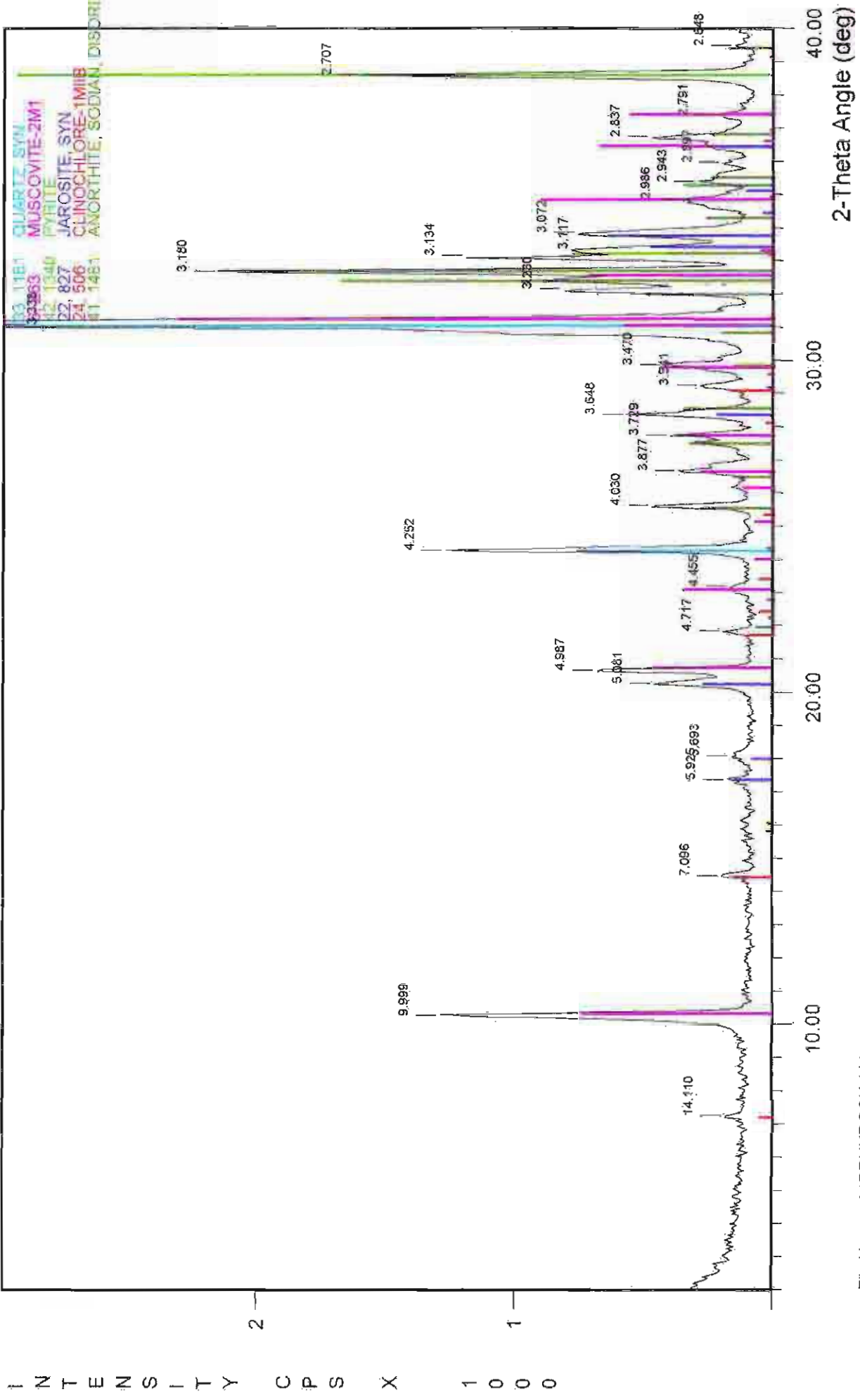
The jarosite present in the rocks has little effect on the system during the flush of AMD, however it can play a role after most of the pyrite has oxidised. If the system is then leached with rain so that soluble SO_4 is removed, then it changes slowly to $\text{Fe}(\text{OH})_3$ and releases acid



On the other hand, if there is any residual acid about (perhaps retained on the minerals), then it could have a neutralising effect by reaction of H^+ with its hydroxyl groups. However, this might only be temporary, since it would bring Fe^{3+} into solution only to reprecipitated as $\text{Fe}(\text{OH})_3$ and add acid, thus the effect of jarosite on the system is uncertain.

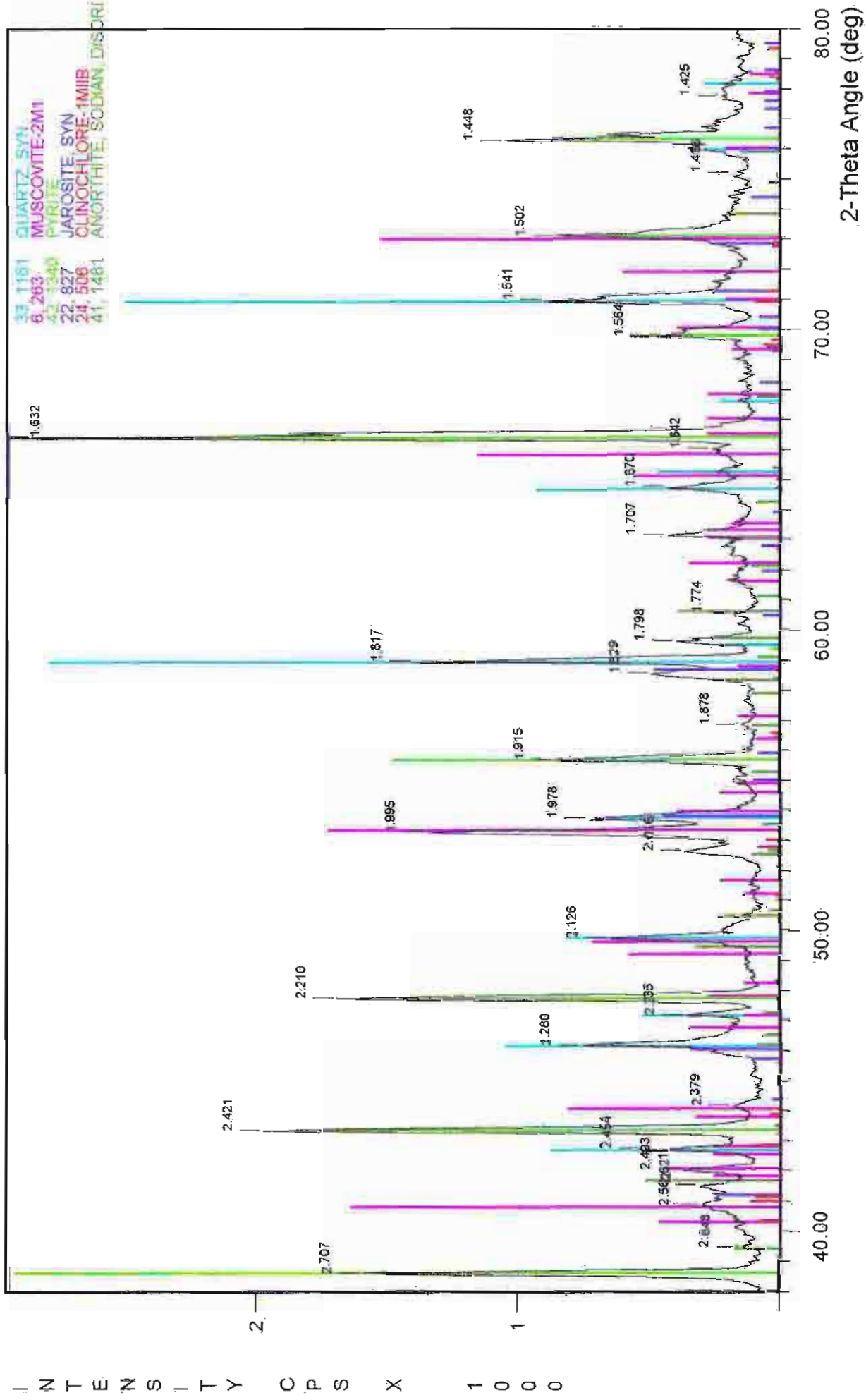
A combination of the fine grained nature of this sample; the sulfur and sulfides present; and the lack of major neutralising minerals, indicate that a rock type of this sort - a highly weathered metasediment, still has a large potential for producing an environmental hazard to the surrounding terrain.

ROCK 11 : Highly weathered metasediment



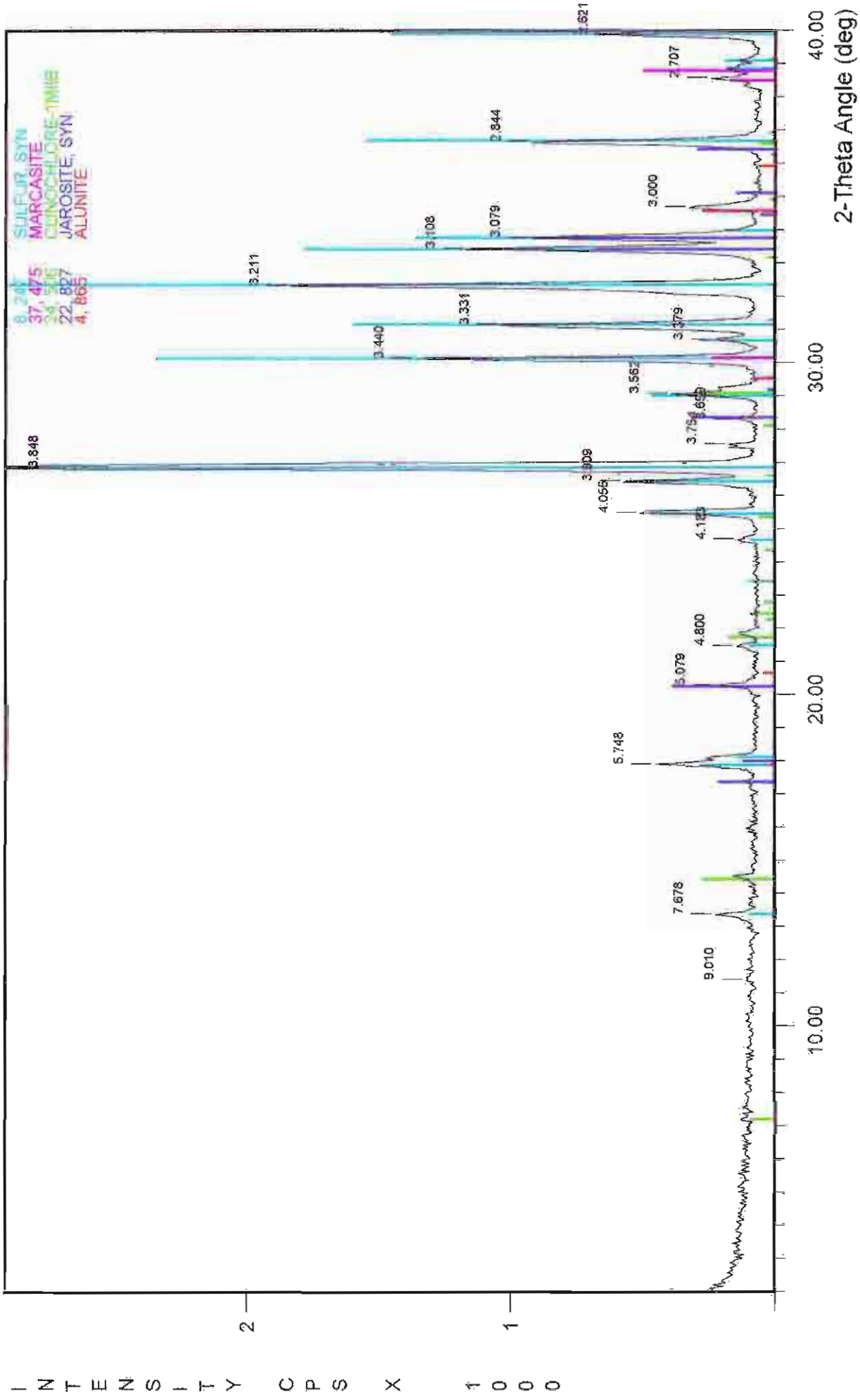
File Name: A:\BRUKROCK.111

ROCK 11 : Highly weathered metasediment



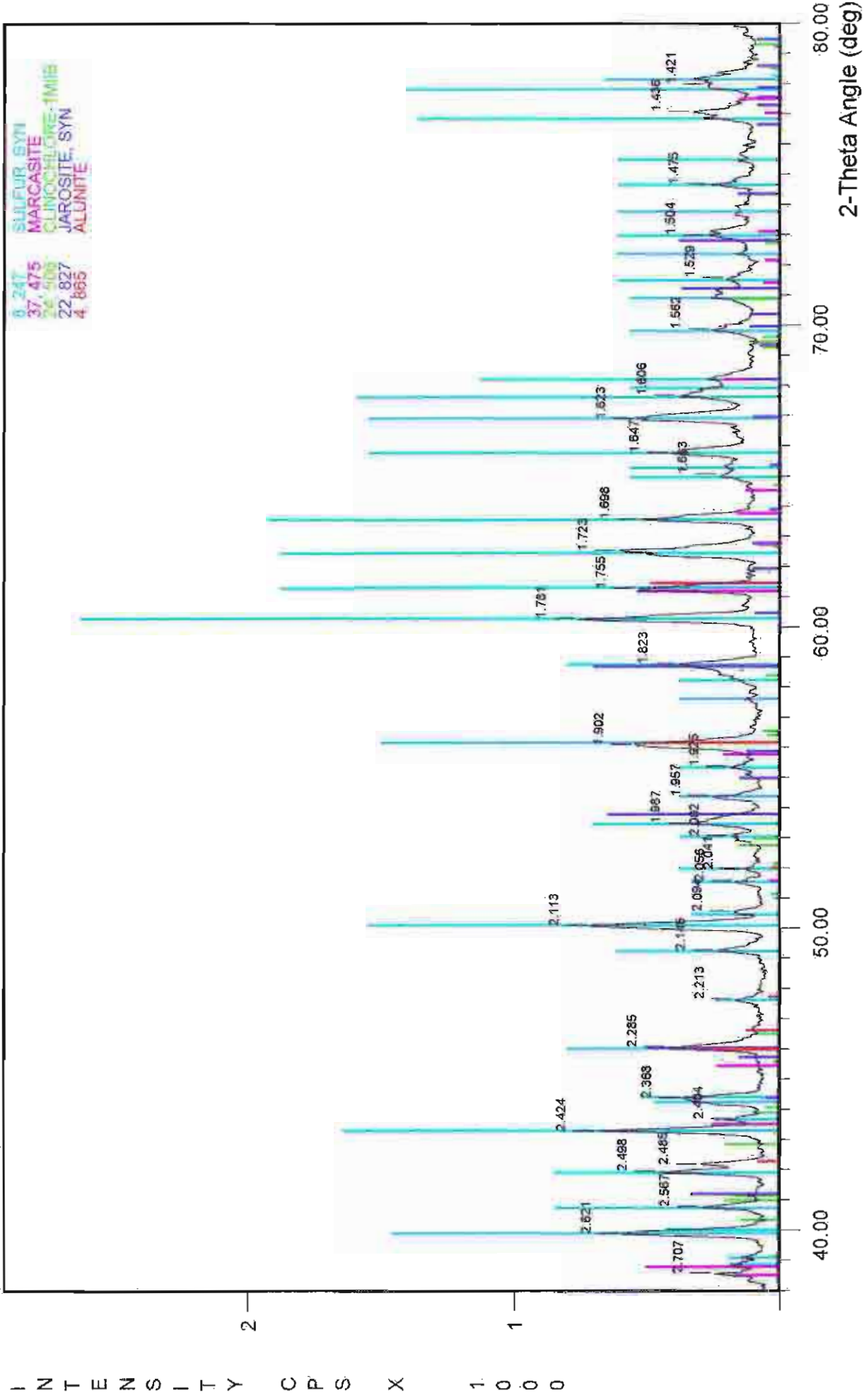
File Name: A:\BRUKROCK\111

ROCK 11 : Highly weathered metasediment (black material)



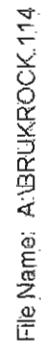
File Name: A:\BRUKROCK.113

ROCK 11 : Highly weathered metasediment (black material)

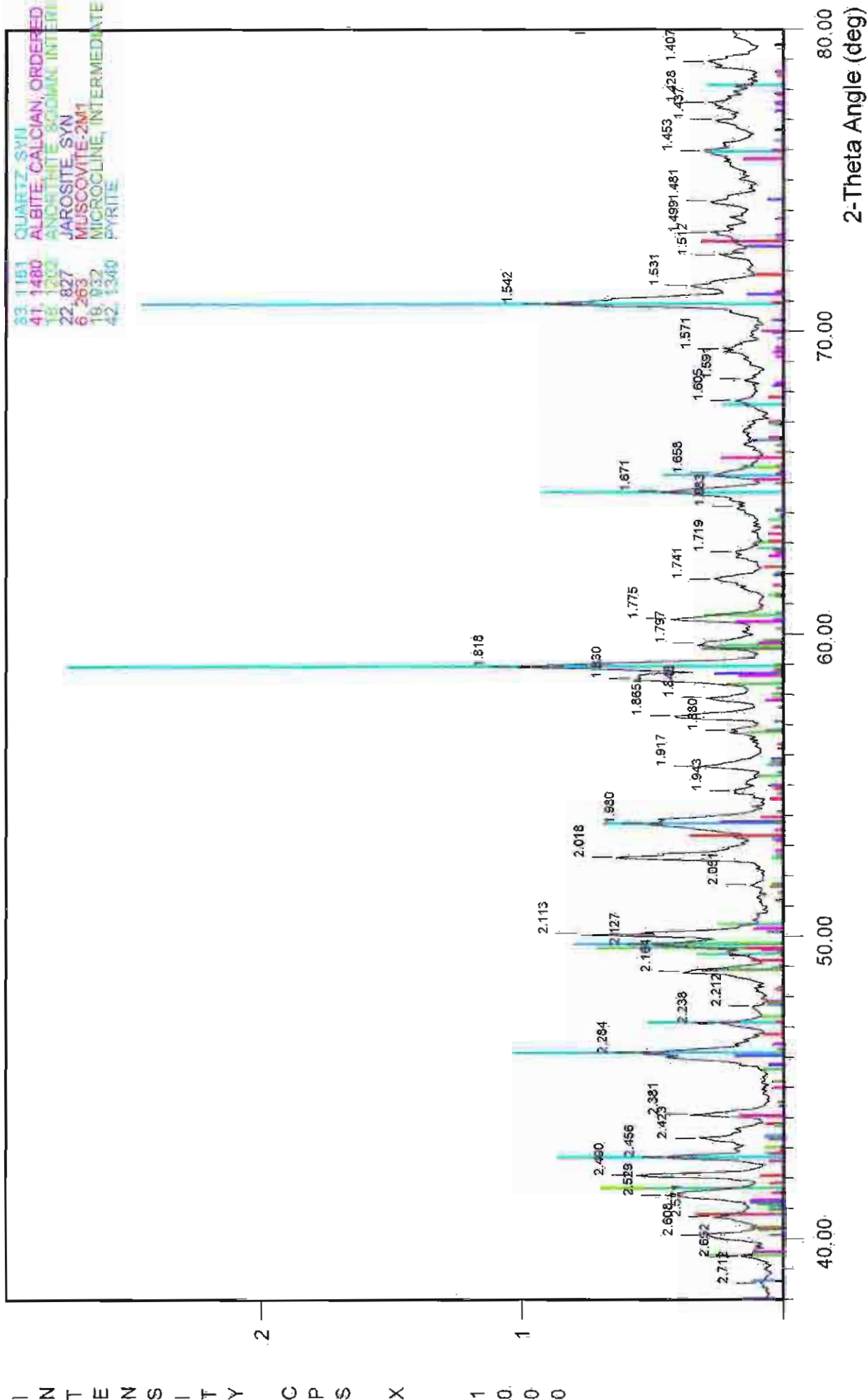


File Name: A:\BRUKROCK.113

= N T E N S - T Y O P S X 1 0 0 0



ROCK 11 : Highly weathered metasediment (host rock)



File Name: A:\BRUKROCK.114

ROCK 6 Highly weathered coarse pyritic gneiss

The friable, very fine grained green-cream matrix has well developed pyrite crystals along discrete layers. The main components determined via XRD and verified by optical microscopy and SEM/EDX are:

Muscovite	15-25%
quartz	15-20%
pyrite	5-10%
albite	<5%
hematite	<5%
jarosite	<5%

SEM/EDX and optical microscopy also identified biotite and intermediate anorthite-albite feldspar within the host rock (Fig 3.25). Pyrite crystals showed fracturing at low magnification (Fig 3C.1). At higher resolution the crystals actually have a covering of jarosite (Fig 3C.2) and strongly pitted surfaces, developing hexagon-shaped voids (Fig 3.2). The voids formed may indicate the removal of a less resistant iron sulfide eg. marcasite from these sites. In some voids small spherical jarosite accumulations are observable. These may have formed initially as a coating of these depressions and through further alteration of their structure, they have curled up into spherical shapes. It should however be pointed out that the jarosite observed with the depressions may have been transported to this position in their present form, but this seems an unlikely option.

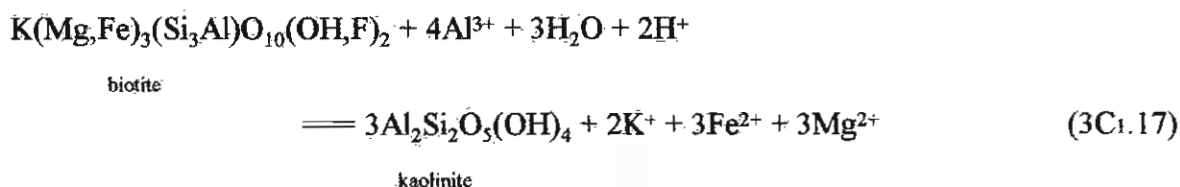
Jarosite (eq 3C1.8) and hematite are the main alteration products of pyrite in this highly weathered gneiss. They were observed through optical microscopy mainly as coatings on pyrite crystals associated with altered muscovite. Hematite is formed from pyrite weathering (eq 3C1.1) and subsequent oxidation, precipitation and dehydration of iron oxyhydroxides.



During a period when the moist rock was allowed to dry out, pale yellow fibrous crystals developed. XRD analysis indicated these crystals were a mixture of kalinite ($\text{KAl}(\text{SO}_4)_2 \cdot 11\text{H}_2\text{O}$ - a fibrous type of K-Al alum), halloysite, halotrichite and gypsum. The fact that these minerals are not observed on this rock in the field may be due to its exposed positioning, where soluble salts would be readily removed by leaching.

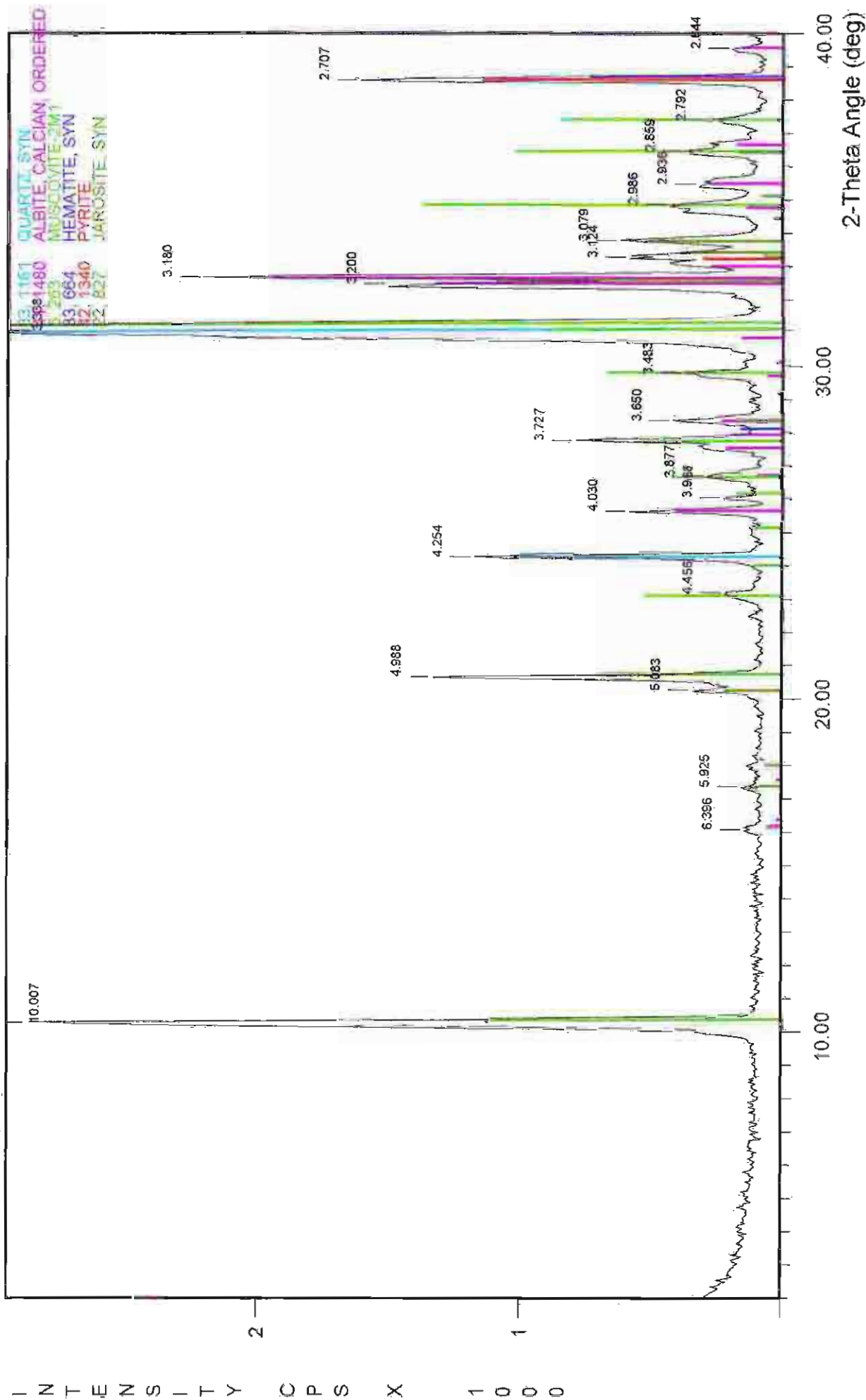
Potential Environmental Impact

The NNP of this sample was determined as -244 kg H₂SO₄ per tonne. This is quite substantial compared to many samples, and may be attributed to the moderate quantity of pyrite present, as determined by XRD and XRF. The potential neutralising minerals present are muscovite (eq 3C1.9) and biotite (Fig 3.25):



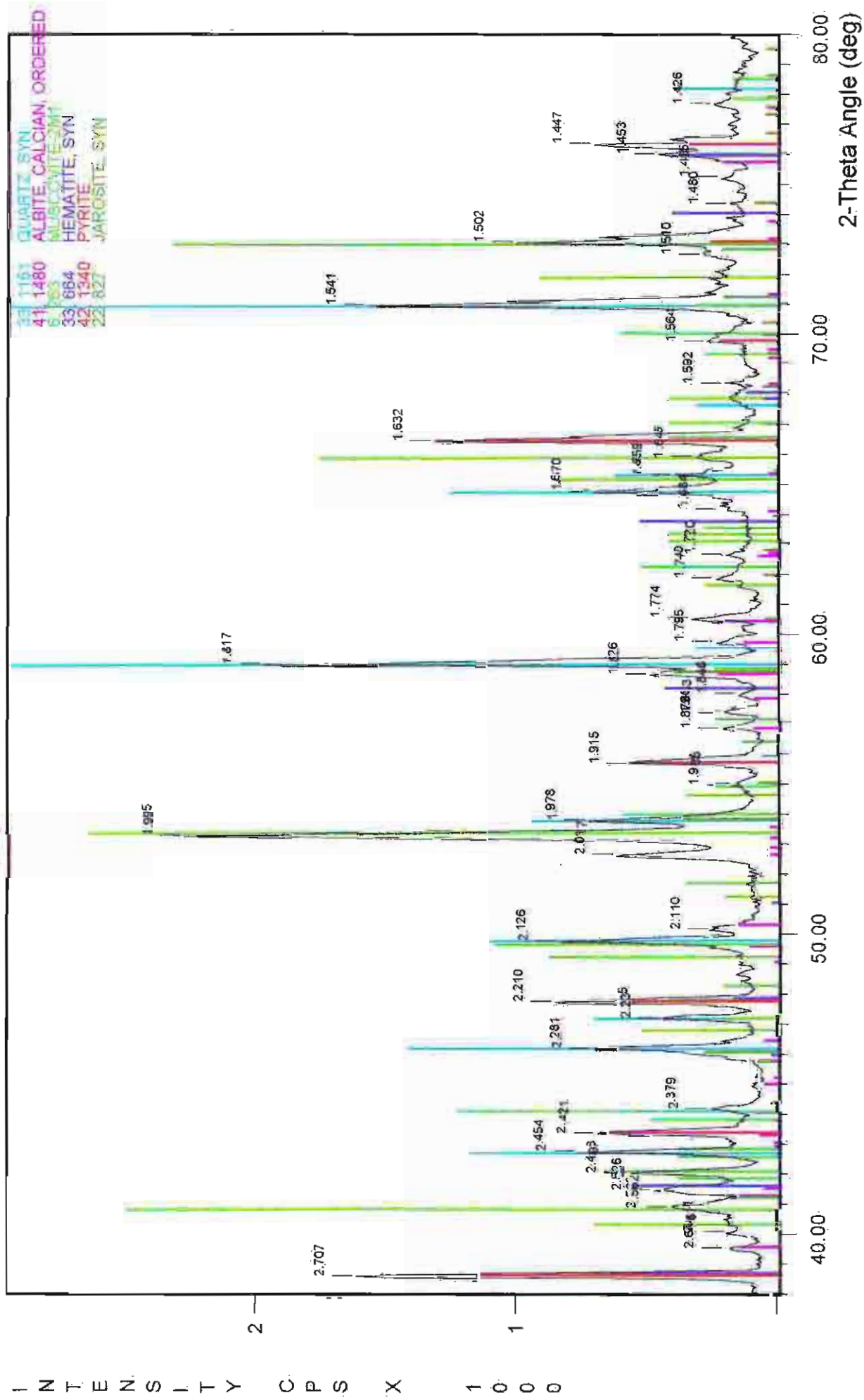
The neutralising potential minerals obviously are reacting to some extent, as shown by their degraded nature. Cleavages are expanding with alteration minerals precipitating between layers.

ROCK 6 : Highly weathered coarse pyritic gneiss



File Name: A:\BRUKROCK.106

ROCK 6 : Highly weathered coarse pyritic gneiss



File Name: A:\BRUKROCK.106

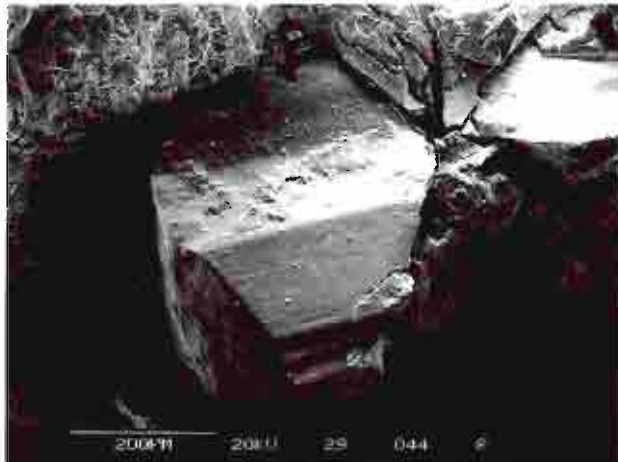


Fig 3C.1 Pyrite alteration with jarosite coating - rock 6.

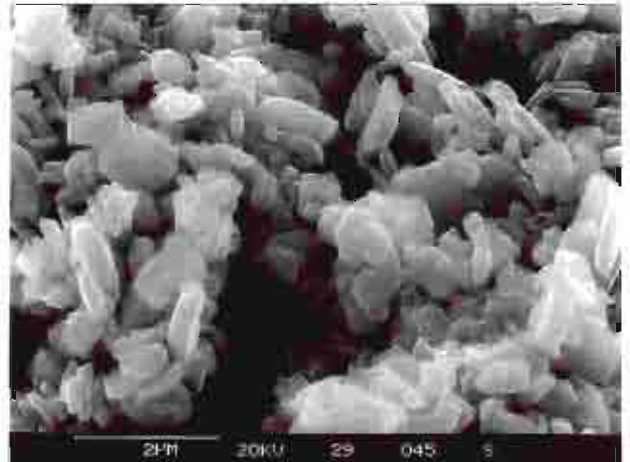


Fig 3C.2 Close up of jarosite coating on pyrite crystals - rock 6.

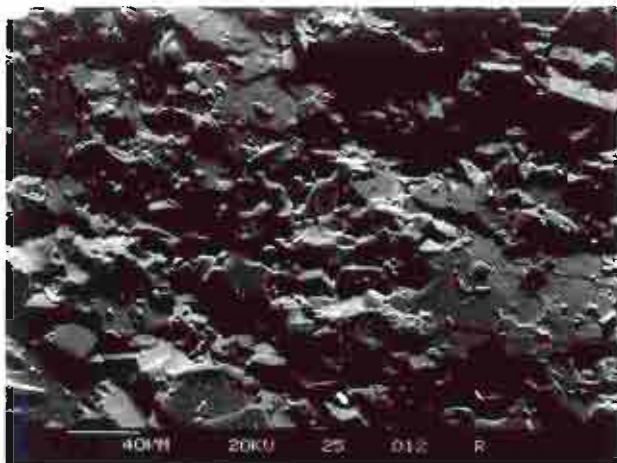


Fig 3C.3 Overview of ore and host rock minerals -rock 1.

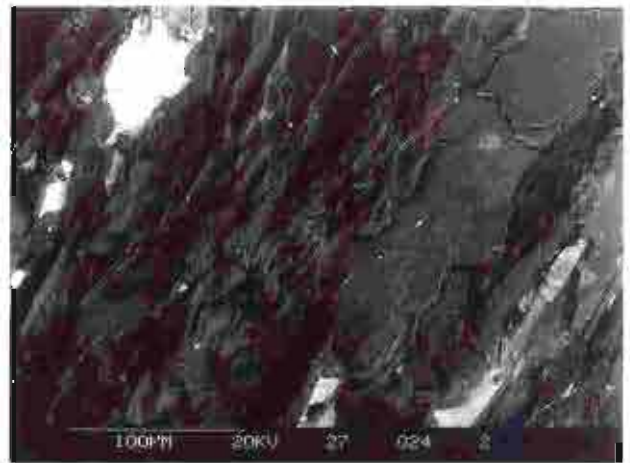


Fig 3C.4 Overview of ore and host rock minerals - rock 3.

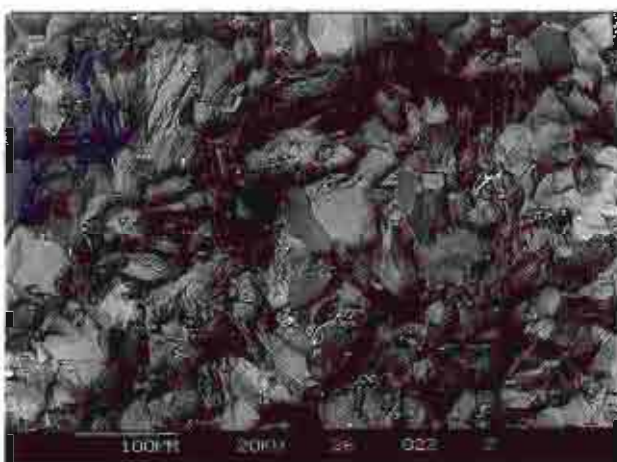


Fig 3C.5 Overview of tremolite rich metasediment - rock 2.

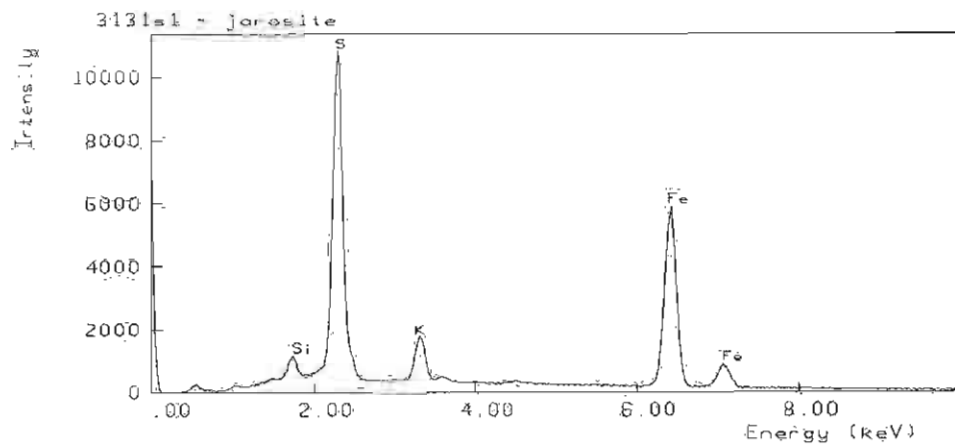


Fig 3.12a
Jarosite
developed
within rock 11.

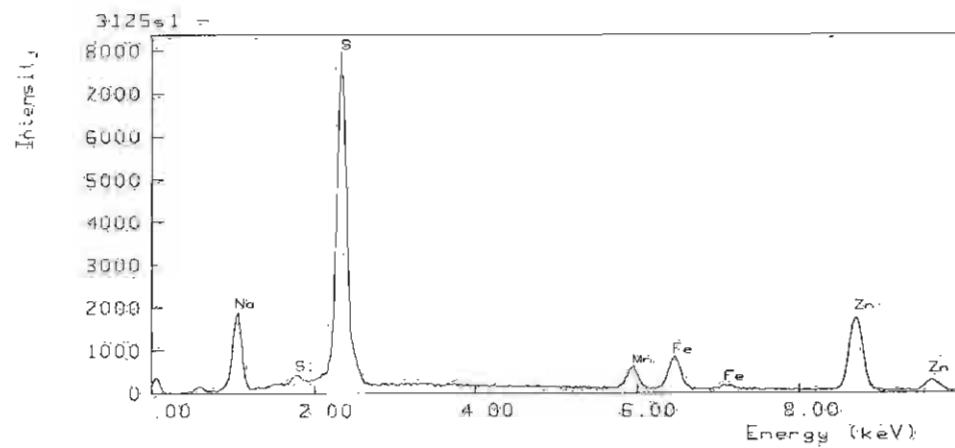


Fig 3C.3a
Sphalerite
present in
rock 6.

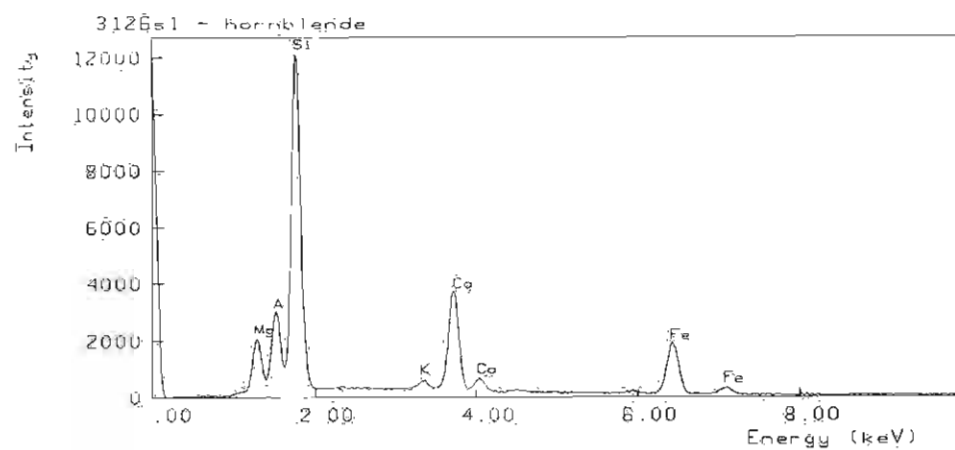


Fig 3C.5a
Hornblende
present in
rock 2.

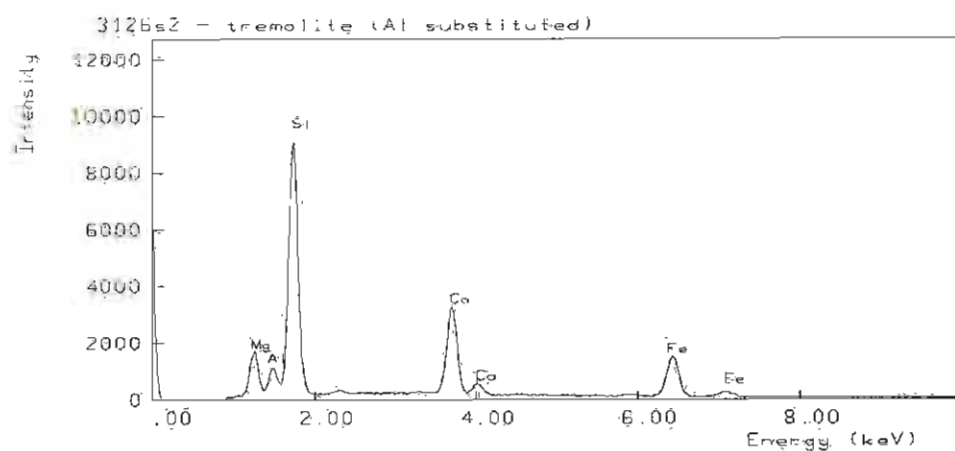


Fig 3C.5b
Tremolite (Al
substituted)
present in
rock 2.

ROCK 1 Massive pyritic quartzite

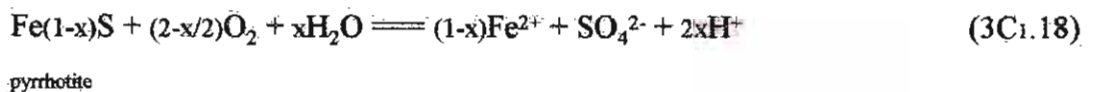
This massive pyritic quartzite contains layers of pyrite as well as pyrite distributed throughout the matrix. The main components determined via XRD and verified by optical microscopy and SEM/EDX are:

quartz	25-30%
muscovite	15-25%
pyrite & pyrrhotite	10-15%
clinochlore	5-10%
jarosite	<5%
albite	<5%
hematite	<5%
calcite	<5%
rutile	<1%

In addition, SEM/EDX and optical microscopy identified sphalerite (Fig 3C.3a), anorthite, apatite, manganite, galena and iron oxyhydroxides in trace amounts (Fig 3C.3).

At low magnification (optical microscopy) pyrite seemed to be well preserved, but depressions filled with iron oxides suggested weathering. At a much higher resolution using the SEM/EDX, individual pyrite faces could be seen to be decaying in planes of low resistance due to crystal weakness or to field exposure to prevailing weathering conditions (oxygen and water adulteration). This weathering has resulted in a finger-like structure of more resistant material remaining after the weaker sections have been removed (Fig 3.3 & 3.4).

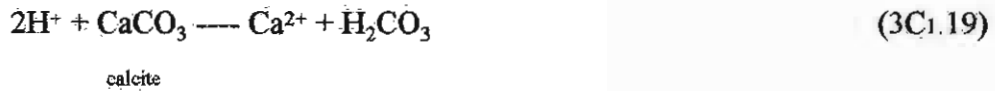
Weathering has occurred mainly on the surface of the rock, with only minor alteration to the interior of the specimen. Some jarosite and goethite were observed through thin section microscopy and SEM/EDX investigations as coatings on crystals and these minerals are the main products of weathering. They are both byproducts of oxidation of pyrite (eq 3C1.5) and pyrrhotite:



Jarosite precipitates from solution (eq 3C1.8) while hematite forms through dehydration reactions of ferrihydroxides (eqs 3C1.15 & 3C1.16).

Potential Environmental Impact

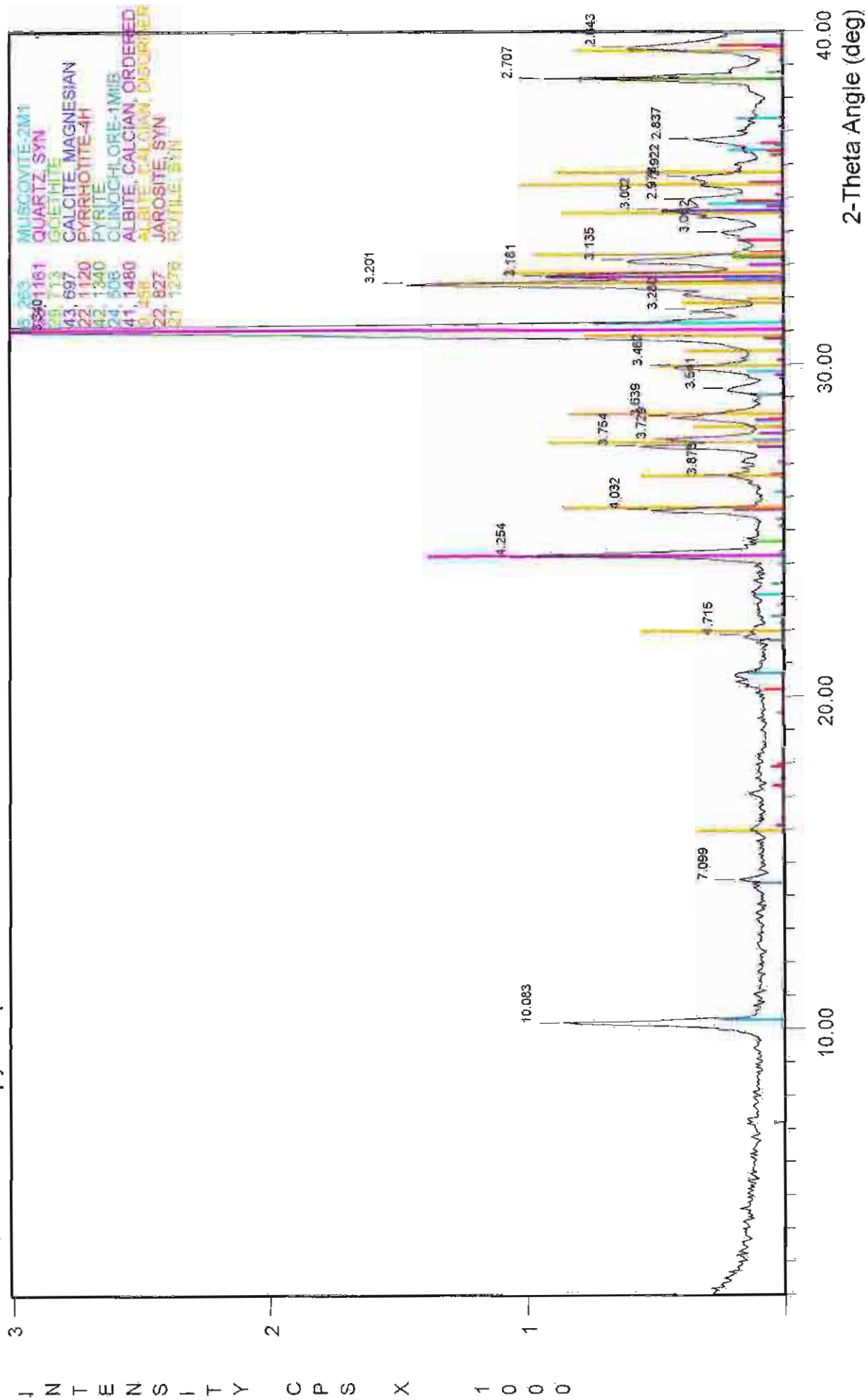
The dissolution of calcite is highly neutralising, but it would have no significant effect due to the small quantity present:



The specimen also contains 5-10% clinocllore, this aluminosilicate has a strong neutralising capacity because of its brucite-like layer $(\text{MgAl})_6(\text{OH})_{12}$ interlayers, and the dissolution of this mineral would have a significant effect on the AMD potential (Fordham, 1994). The products of weathering must have leached out of the system as only minor kaolinite was observed. Additional support for this theory is the absence of any Mg and Al weathering products.

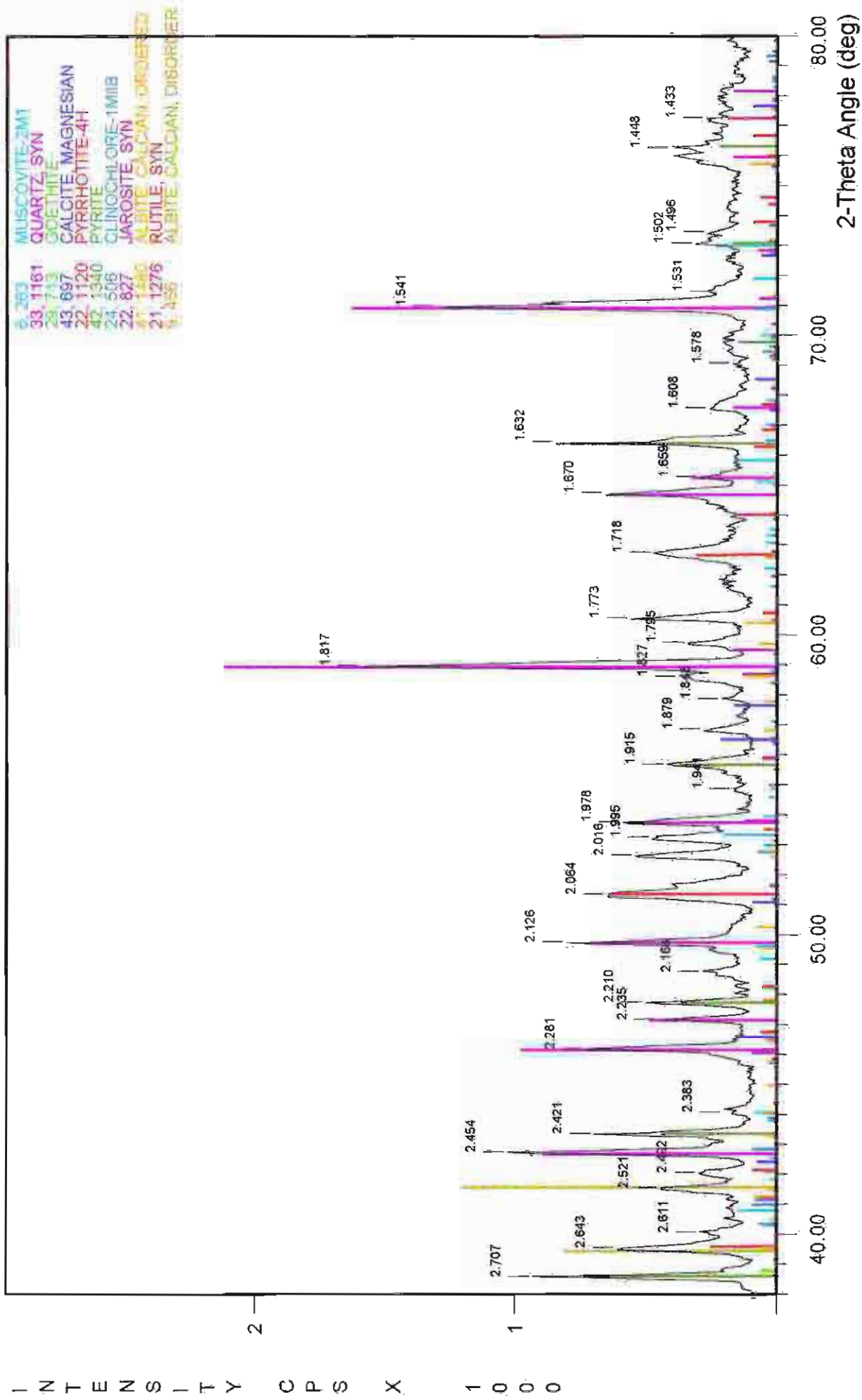
During SEM/EDX investigations, the clinocllore within this specimen did not appear to be weathering differently from the muscovite present. The muscovite present would also have some neutralising capacity (eq 3C1.9), and evidence of alteration was obtained through thin section microscopic analysis. Fig 3.26 (frame width 0.5mm) shows the degradation of a biotite crystal as its neutralising capacity is being utilized, producing a K leached end member aluminosilicate (Fig 3.26a & 3.26b). However the combination of all three minerals proves to be ineffective during the short term, as shown by the NNP of -233 kg H_2SO_4 per tonne.

ROCK 1 : Massive pyritic quartzite



File Name: A:\BRUKROCK.101

ROCK 1 : Massive pyritic quartzite



File Name: A:\BRUKROCK.101

ROCK 10 Fine grain pyrite-muscovite gneiss.

The main components determined via XRD and verified by optical microscopy are:

quartz	25-30%
muscovite	20-30%
pyrite	5-10%
jarosite	<5%
microcline & albite	<5%
marcasite	<5%

Optical microscopy revealed pyrite crystals were slightly to moderately weathered. Crystal form was well preserved although some pitting and degradation could be seen. The marcasite present is very much like pyrite in appearance, however it is more reactive. It sometimes shows tabular or pyramidal habit, but it is more likely found in radiating fibrous masses as an alteration product of sulfide degradation. It can be distinguished from pyrite by examination in polarized light since pyrite crystals appear to be isotropic or at most weakly birefringent while marcasite is strongly anisotropic.

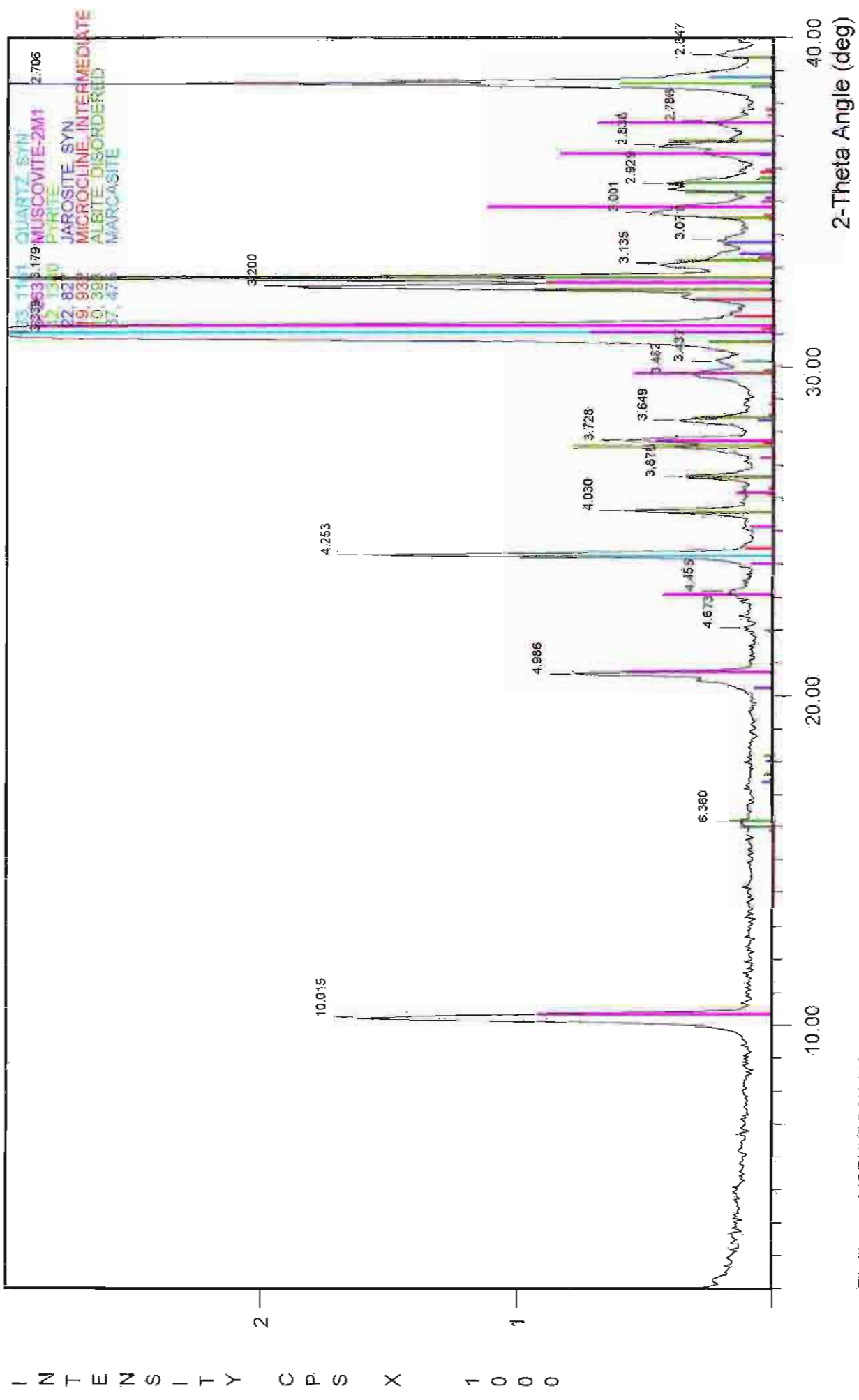
A black hard agglomeration of material was observed within the interior of the rock. This material was identified as a mixture of marcasite, sphalerite and pyrite. An agglomeration of such minerals suggests that it formed during the rocks development. Other such agglomerates may be present throughout this rock type, increasing its potential for acid generation, as large pure sulfide aggregates would be highly susceptible to weathering and acid formation.

A strong coating of jarosite and iron oxides has developed on the surface of the rock through the weathering of pyrite (eq 3C1.5), precipitation from solution (eq 3C1.8 & 3C1.15) and subsequent dehydration of any ferric oxyhydroxides (eq 3C1.16).

Potential Environmental Impact

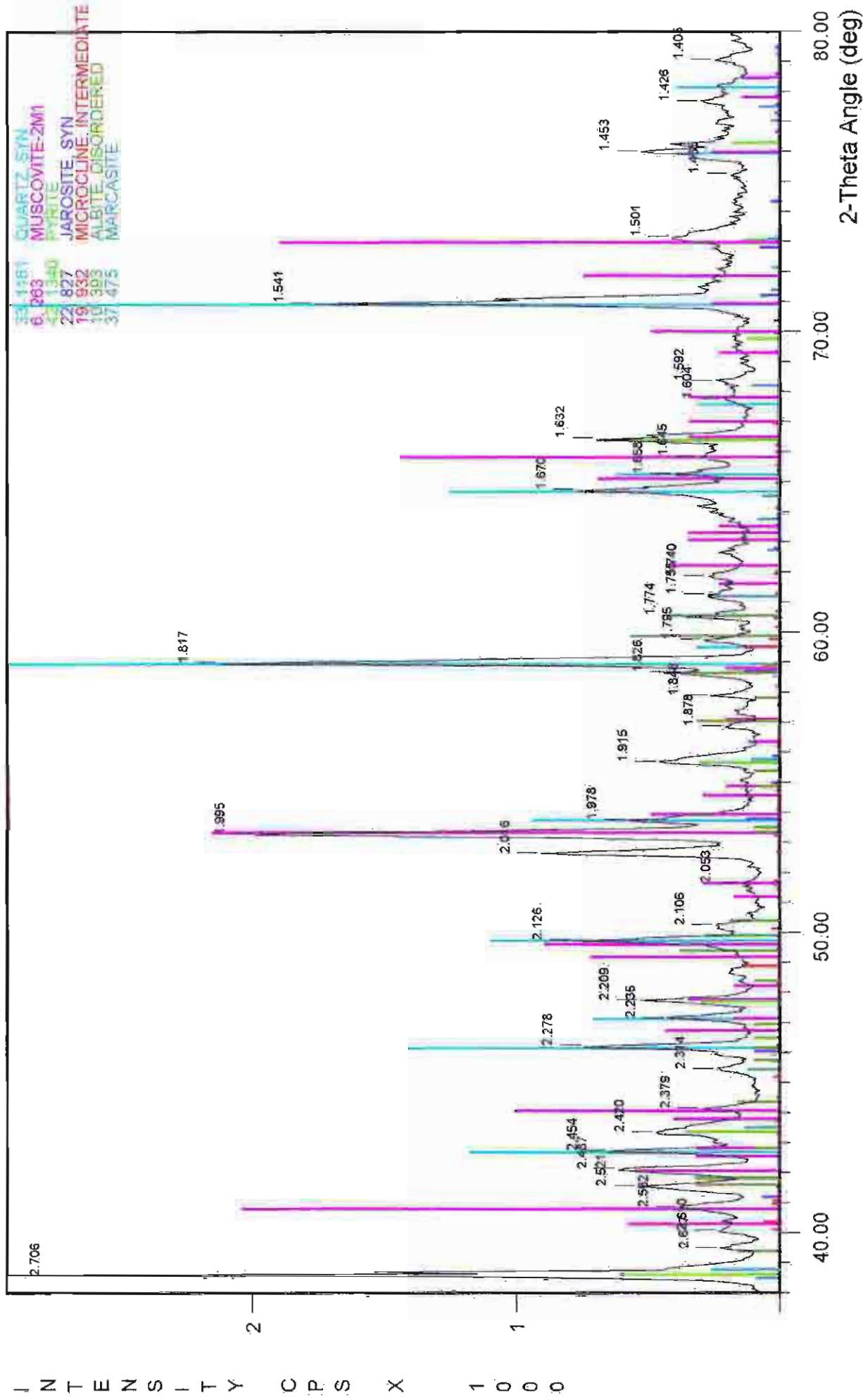
Muscovite within this pyrite-muscovite gneiss is the subdominant mineral, and one would expect to see evidence of its reaction with the AMD produced through pyrite oxidation. Thin section optical microscopy showed muscovite readily degrading as pyrite alters. Even though there is approximately twice as much muscovite as pyrite (determined through XRD and XRF), the neutralisation capacity of this mineral is obviously much less than the acid potential of the pyrite present, as shown by the NNP determined as -215.73 kg H₂SO₄ per tonne. The B.C Initial Research Test used to determine these results unfortunately does not measure the neutralisation potential of the slowly reacting aluminosilicates which are predominantly the neutralising minerals within this suite of rock. Thus over a long period of time the effect on the environment may be less than the original AMD flush through the waste rock dump would indicate.

ROCK 10 : Fine grained pyrite-muscovite gneiss



File Name: A:\BRUKROCK.110

ROCK 10 : Fine grained pyrite-muscovite gneiss



File Name: A:\BRUKROCK.110

ROCK 8 Moderately weathered pyrite-muscovite gneiss.

Main components determined via XRD and verified by optical microscopy are:

quartz	15-25%
muscovite	15-25%
pyrite	5-15%
jarosite	<5%
albite & microcline	<5%

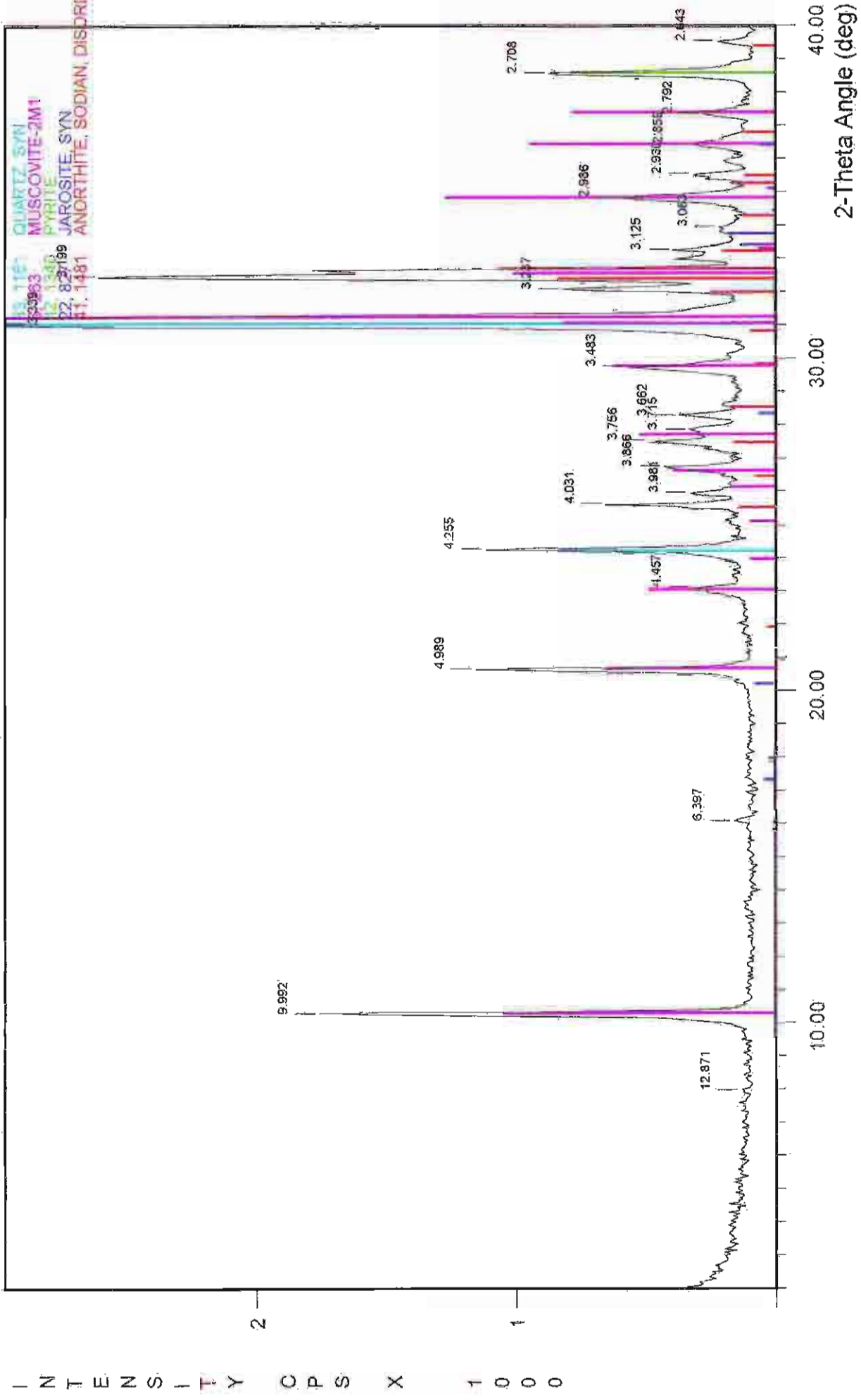
The majority of pyrite is fine grained. However a number of slightly larger crystals were observed which showed strong weathering features, leaving residual crystals within voids as the crystal degradation continued. Thin section analysis also showed strong alteration of the individual pyrite crystals while the surrounding muscovite crystals were totally degraded in some cases.

Jarosite and rozenite, identified by XRD of scrapings, formed on the rocks surface as a coating. Additionally minor amounts of sulfur was observed developing in depressions on the rock's surface. The jarosite exists as pale yellow rhombahedrals. Rozenite appears as a white powdery precipitate. The structure of individual crystals were not discernible without the aid of magnification. This mineral apparently forms by migration of solutions to a point of dessication when aqueous sulfate and ferrous ions contained in solution precipitate.

**Potential Environmental Impact**

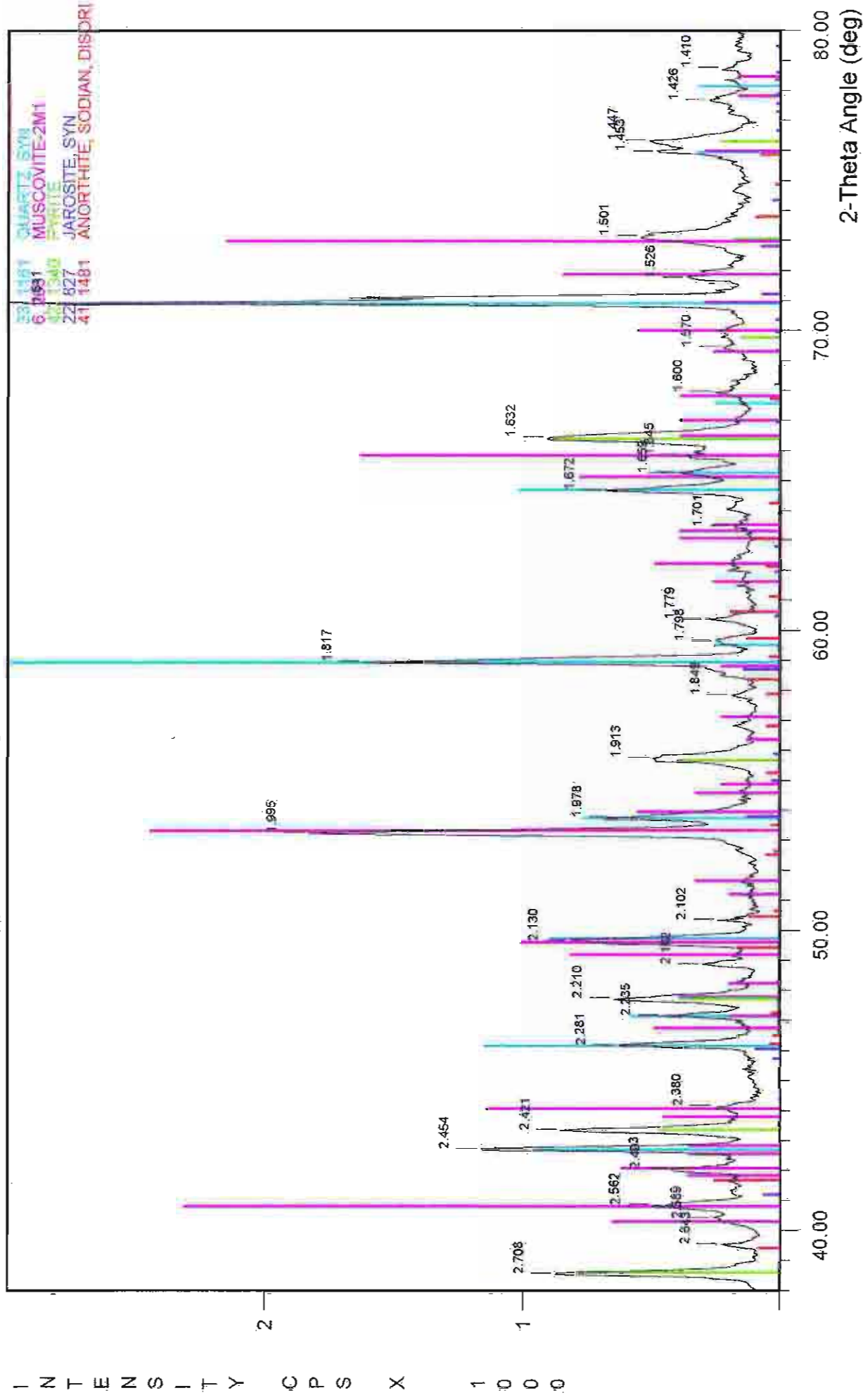
A NNP of -205 kg H₂SO₄ per tonne was determined for this rock. Thin section analysis allowed observation of muscovite degradation, thus this minerals neutralising capacity is being activated. However, because of its slow reactivity, (its effect is not taken into account using the B.C Initial Research Test) it is obviously ineffective in reducing the AMD potential significantly in the short term however over a long period of time would be more capable of neutralisation.

ROCK 8 : Moderately weathered pyritic-muscovite gneiss



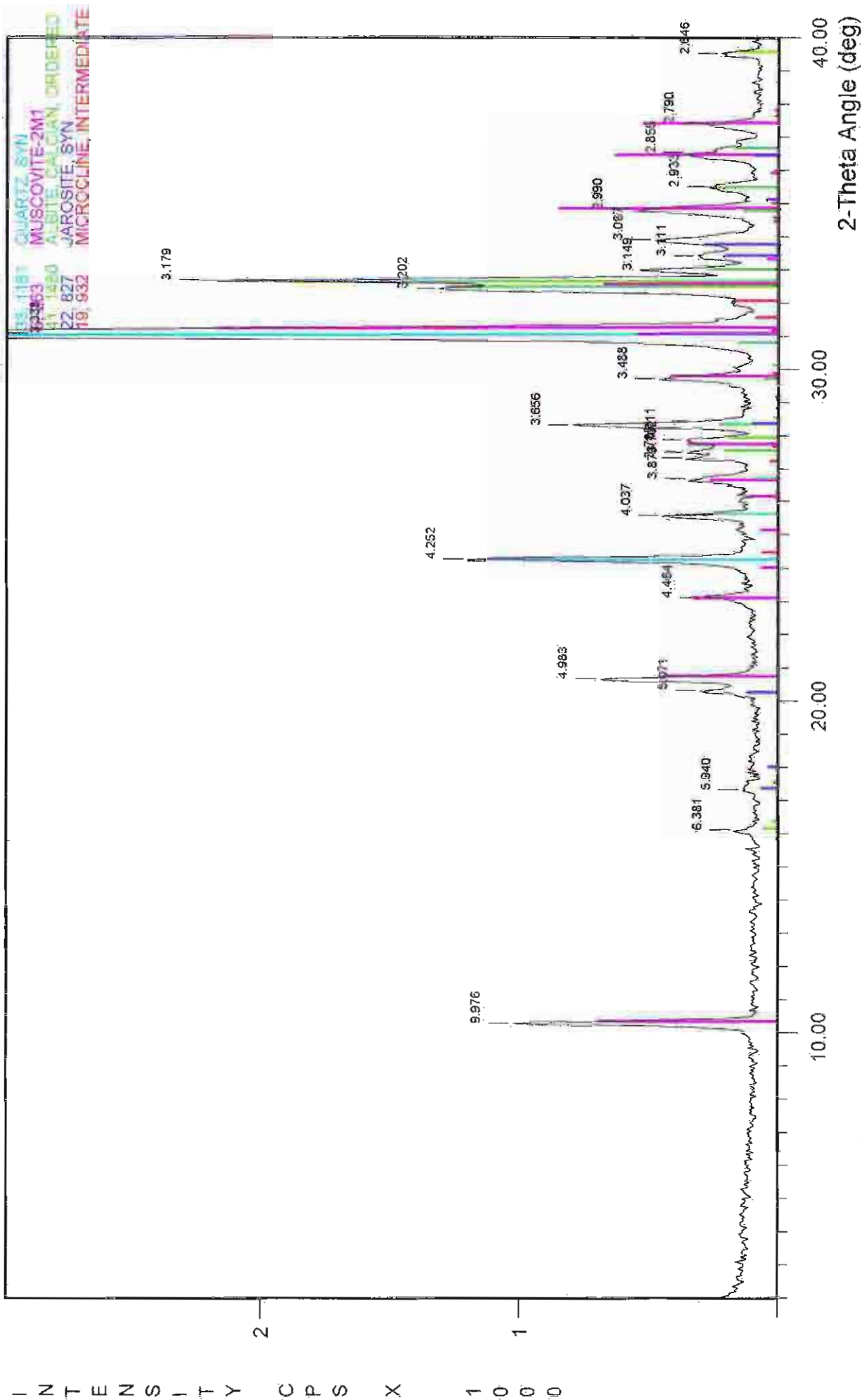
File Name: A:\BRUKROCK.108

ROCK 8 : Moderately weathered pyritic-muscovite gneiss



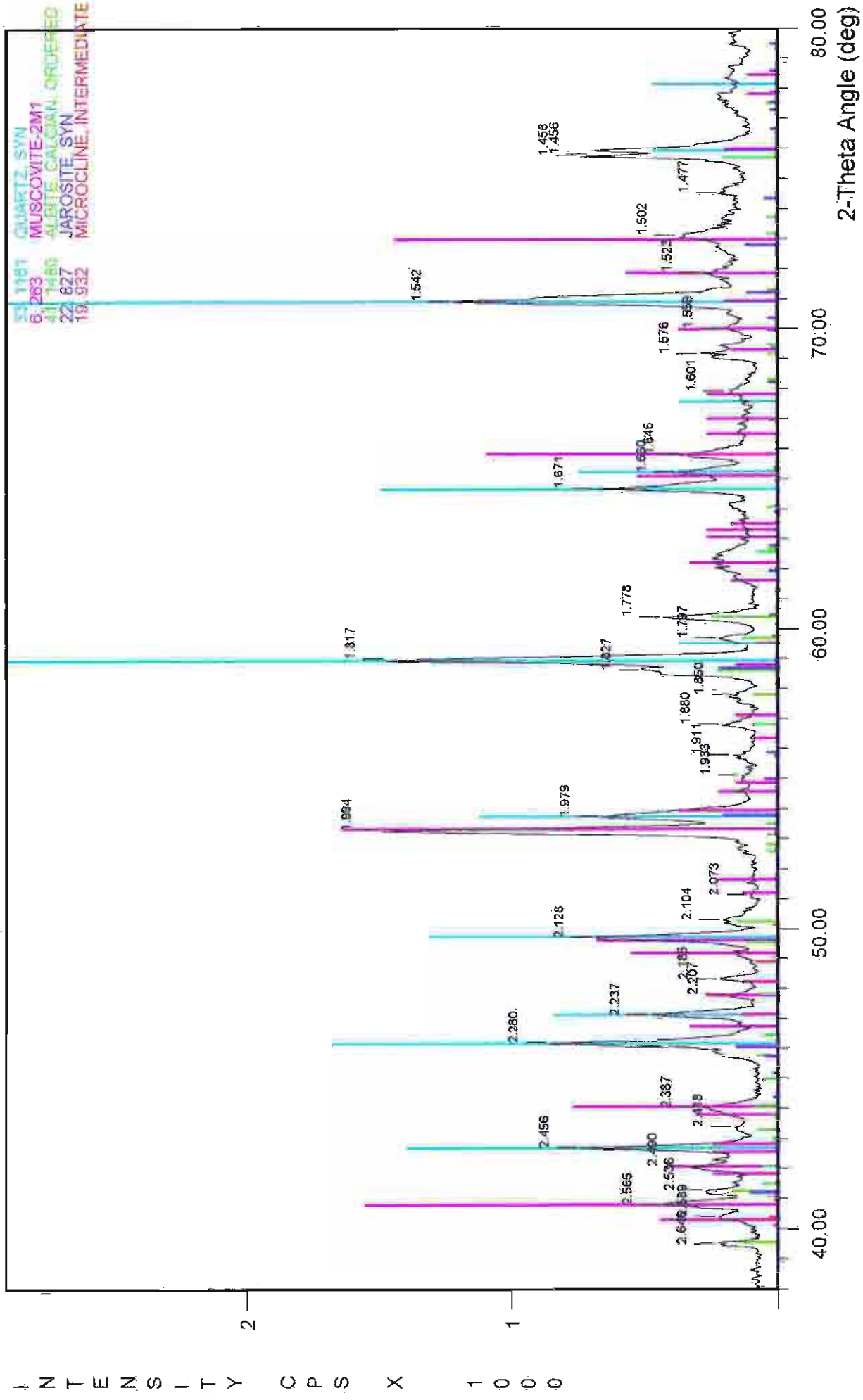
File Name: A:\BRUKROCK.108

ROCK 8 : Moderately weathered pyrite-muscovite gneiss (homogeneous light grey regions & jarosite)



File Name: A:\BRUKROCK.116

ROCK 8 : Moderately weathered pyrite-muscovite gneiss (homogeneous light grey regions & jarosite)



File Name: A:\BRUKROCK.116

ROCK 9 Highly weathered pyritic gneiss

Main components determined via XRD and verified by optical microscopy include:

quartz	25-35%
muscovite	20-30%
pyrite	5-10%
jarosite	<5%
albite & microcline	<5%

Handpicking of particular materials from the rock surface provided a means of identification of additional mineral phases via XRD and verified by SEM/EDX (Fig 3.13) and optical microscopy:

rozenite
spinel ferrian
rectorite
pyrophyllite
jarosite
marcasite
sulfur
hematite

SEM/EDX revealed many different secondary mineral phases formed in response to the highly acidic conditions (Fig 3.13 & 3.14). Several secondary phases were identified including fibrous halotrichite (Fig 3.15, 3.15a & 3.16), stringers of opal A (Fig 3.17 & 3.18), and barytes (BaSO₄). A platy-fibrous material was also observed and subsequently identified as a iron sulfate, most probably rozenite, as this mineral was identified through XRD (Fig 3.19 & 3.19a).

Fibrous rozenite, black amorphous sulfur, jarosite, fibrous halotrichite, hematite and opal A are all weathering byproducts of pyrite oxidation. The fibrous nature of rozenite and halotrichite suggest that they precipitated quickly from solution. Halotrichite forms in a similar manner to rozenite (eq 3C1.20):

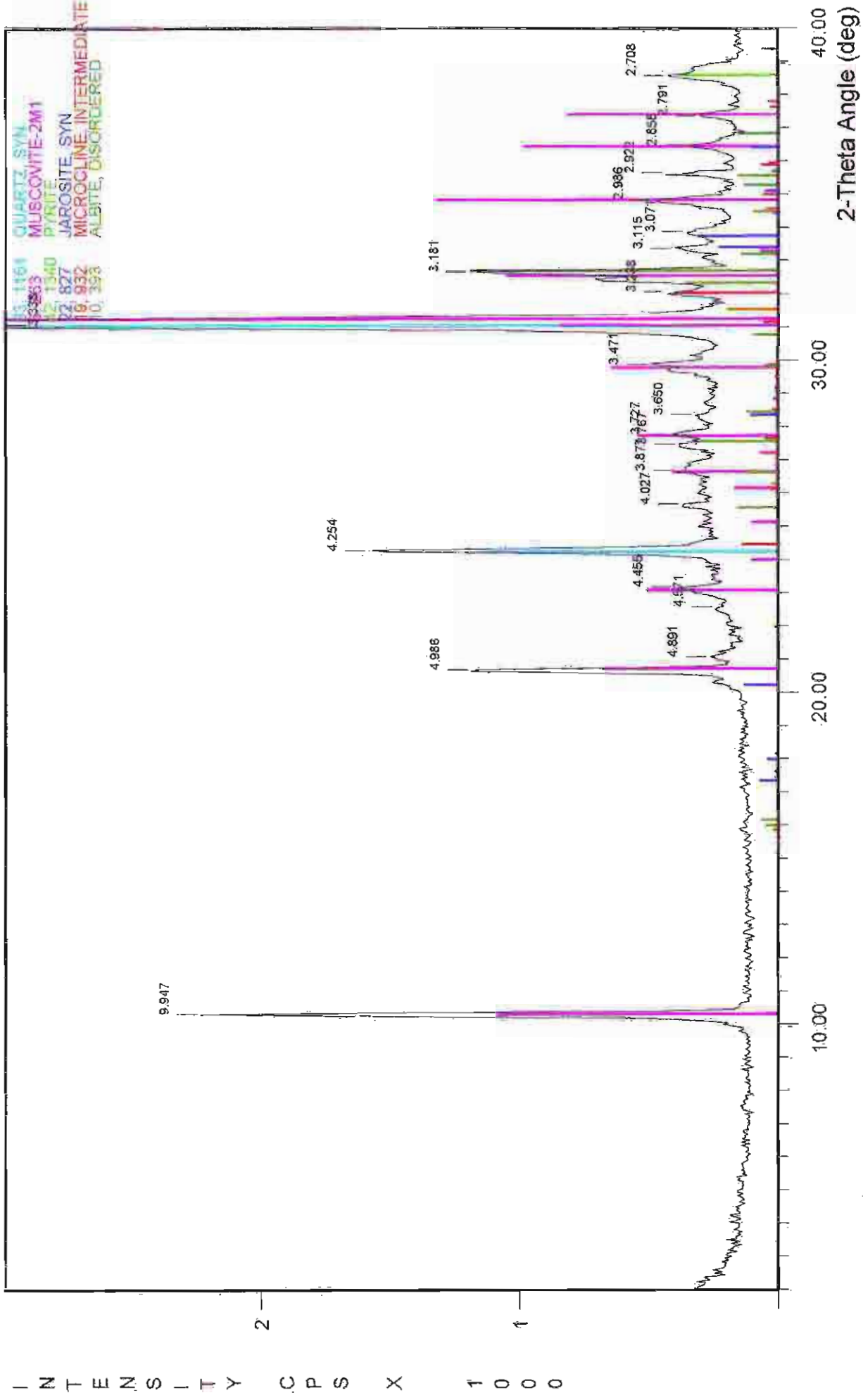


The opal A present occurs as stringers (Fig 3.17 & 3.18). This would suggest it developed as a residue after the dissolution of a pre-existing mineral phase. Evidence of this comes from opal observed in the shape of mica (Fig 3.20). It is thought that all other constituents of the mica have been leached out leaving only the framework structure made of silicon. Additional opal A was observed with little or no structure and this may have formed through direct precipitation from a silica-rich solution.

Potential Environmental Impact

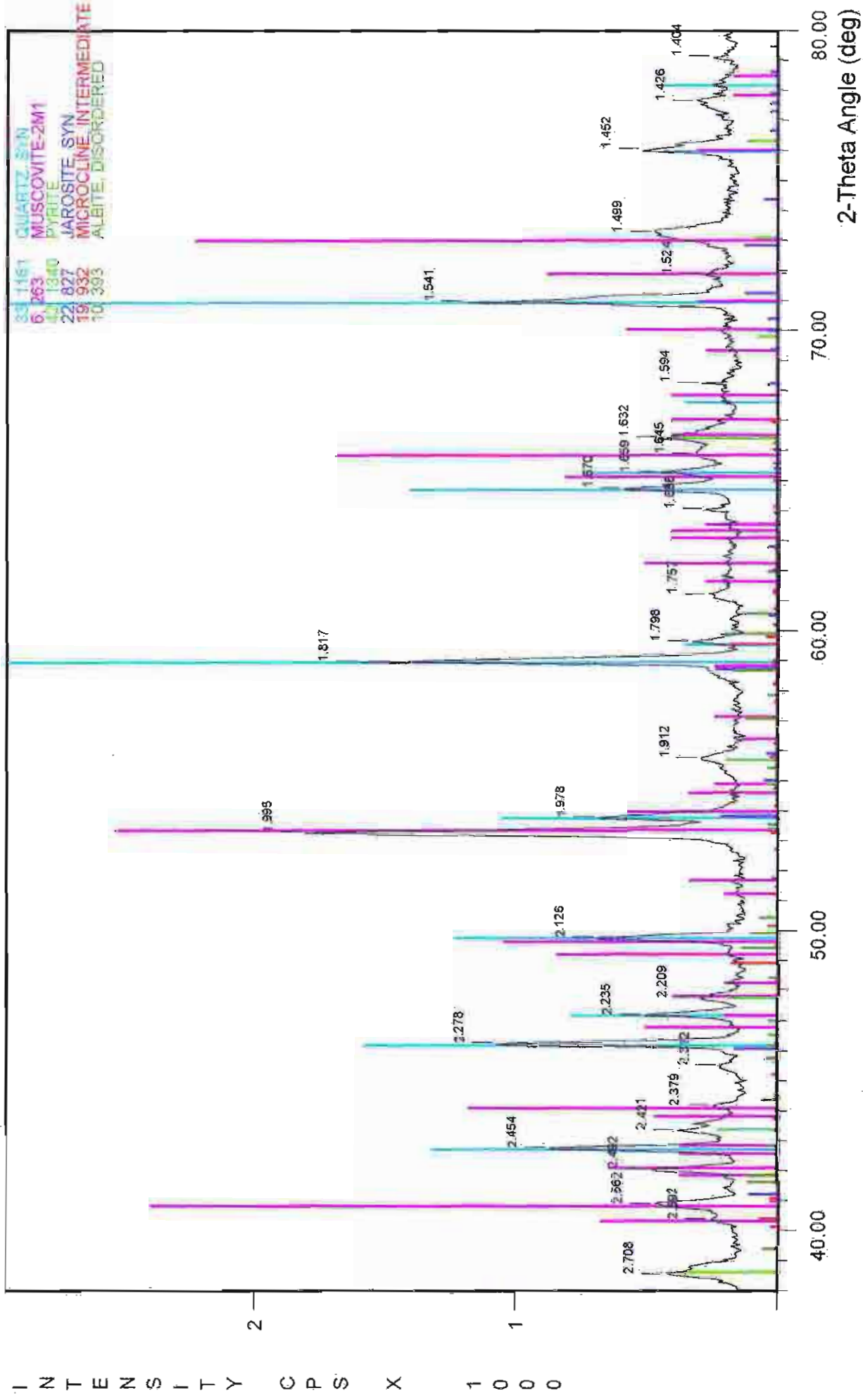
The impact to the surroundings that this rock represents is about the same as that of rock 8, which contains a similar amount of sulfides (% total S values of 5.6 and 6.7% respectively). Muscovite is the main mineral present with a potential neutralising capacity, and again the amounts are comparable in both rocks 9 and 8. Muscovite near the surface of the rock was strongly degraded but thin section analysis showed the muscovite present with the interior is mostly unaltered, reflecting the fine grained impervious nature of the rock. Thus this rock seems to be highly reactive at the surface, rather than throughout its matrix. When saturated for a period and allowed to dry, rozenite rapidly formed from high concentrations of iron and sulfate in solution. During subsequent analysis of the surface, sulfur was also identified as a weathering product of pyrite and thus when oxidised would also add more acid to the surrounds. The muscovite degradation on the surface does not seem to form any weathering products, and instead is highly leached, leaving only silica and opal residues in the system.

ROCK 9 : Highly weathered pyritic gneiss



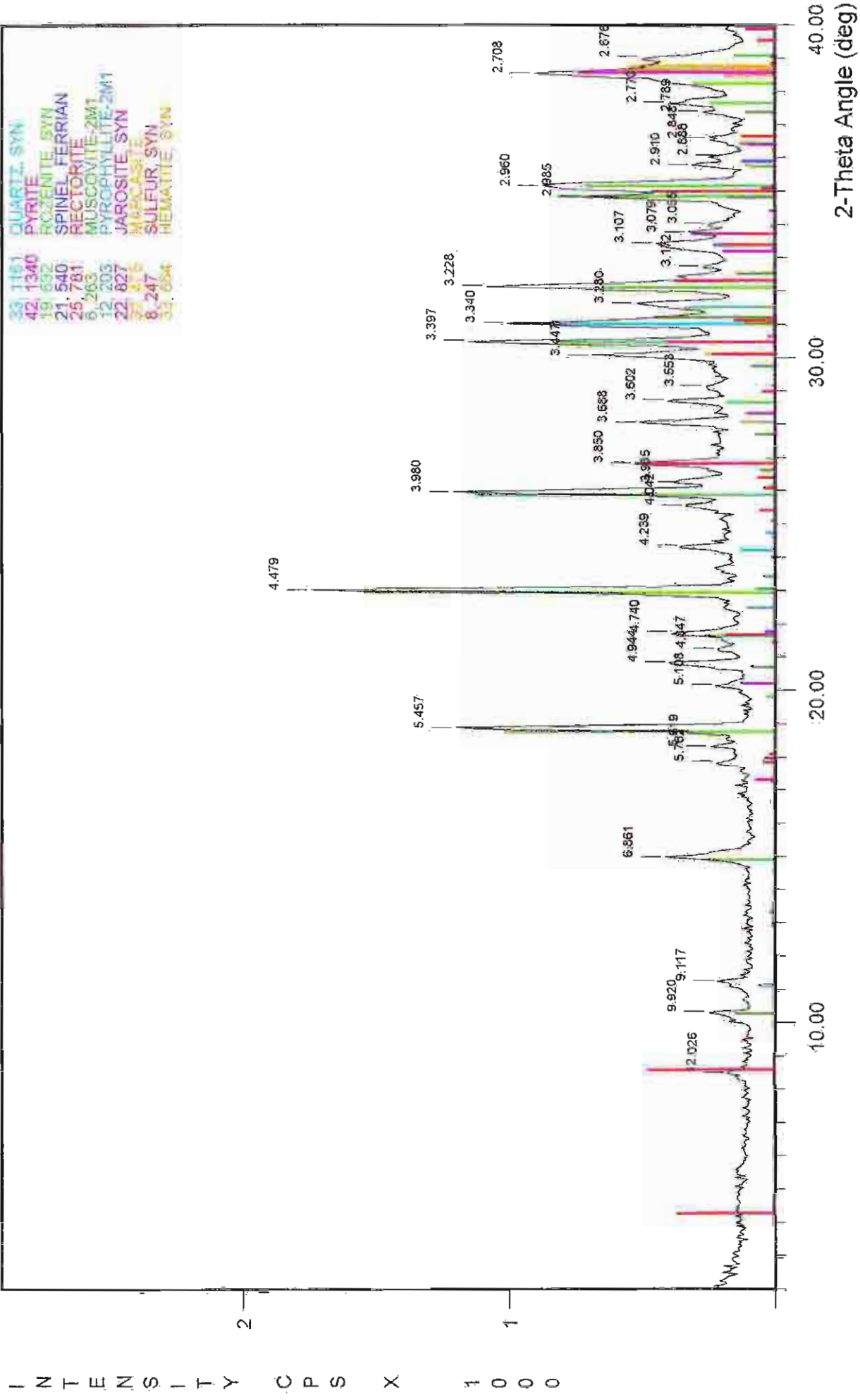
File Name: A:\BRUKROCK.109

ROCK 9 : Highly weathered pyritic gneiss



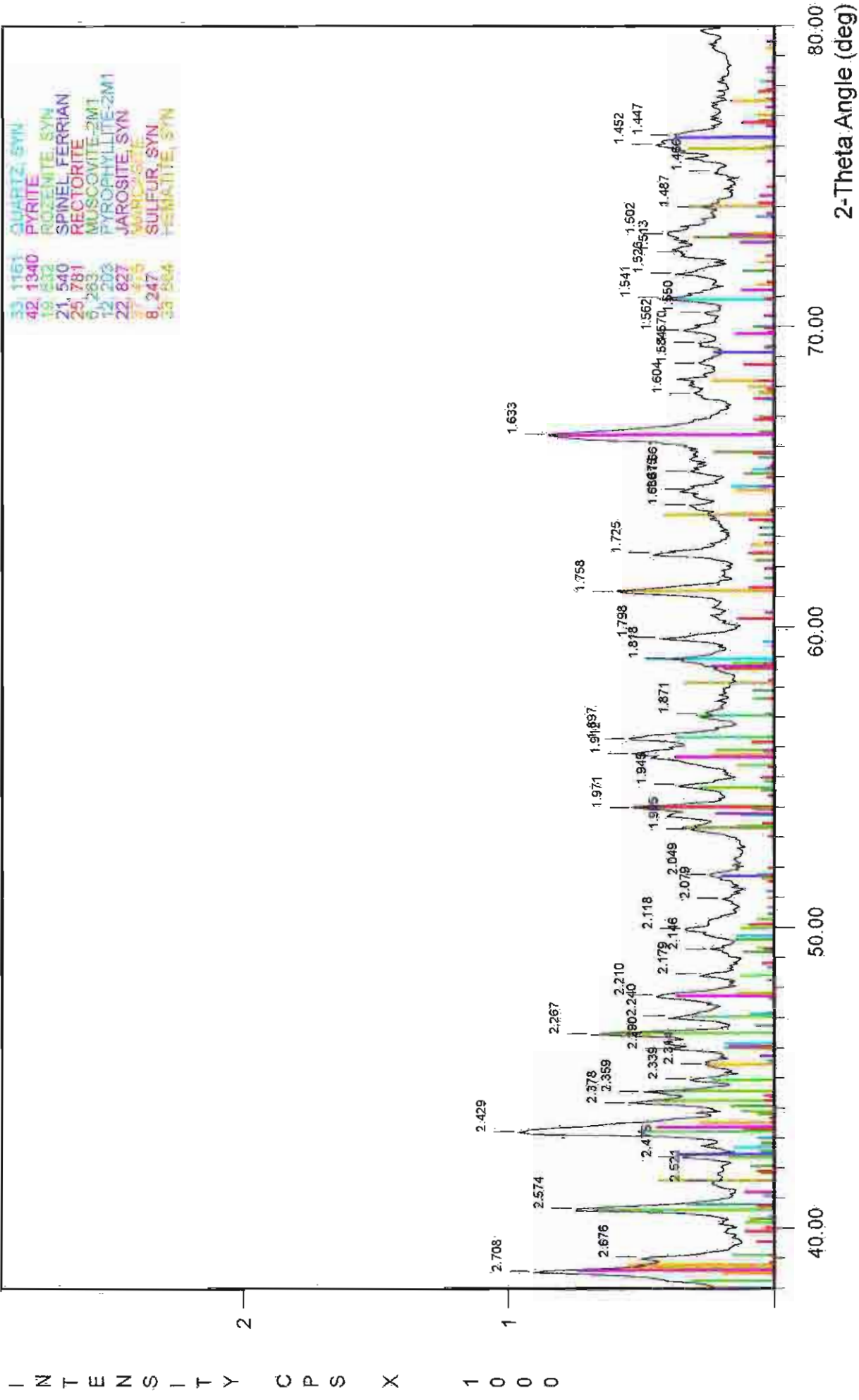
File Name: A:\BRUKROCK.109

ROCK 9: Highly weathered pyritic gneiss (surface material)



File Name: A:\BRUKROCK.117

ROCK 9: Highly weathered pyritic gneiss (surface material)



File Name: A:\BRUKROCK.117

ROCK 7 Highly weathered fine grained pyritic metasediment

This highly weathered metasediment has pyrite or evidence of pyrite homogeneously throughout, except for the .5mm surface coating that has developed as a result of weathering. The main components determined via XRD and verified by optical microscopy are:

quartz	20-30%
muscovite	15-25%
pyrite	5-15%
kaolinite	5-15%
hematite	<5%
jarosite	<5%
albite & microcline	<5%

Examined in thin section under the optical microscope, this metasediment has developed a skin as a result of the weathering process. At the surface jarosite and hematite are at peak proportions (determined from scrapings by XRD and XRF), while pyrite and albite are non-existent. Within 3mm of the surface, albite can be observed. Additionally boxwork structures are seen where pyrite has been degraded. Approximately 1cm below the surface pyrite crystals are apparent. They are very fine grained, and all crystals detected showed pitting to some extent. These changes can be explained via the penetration of water and oxygen; the resistant nature of different minerals quartz and muscovite vs albite and pyrite; and the weathering products jarosite (eq 3C1.18), and hematite (eq 3C1.16) they form.

Thin section microscopy indicated kaolinite is distributed throughout the rock matrix as a coating to quartz and muscovite alike, particularly as reaction rims along boundaries of muscovite and pyrite (Fig 3.21 (frame width 0.5mm)). Kaolinite is the main weathering product formed in response to the weathering of feldspars (eq 3C1.1, 3C1.2 and 3C1.3) and muscovite (eq 3C1.9), by reaction with the acid formed during pyrite oxidation (eq 3C1.5). Hematite is also a minor weathering products of this system and forms as red spheres and staining along regions where pyrite has been totally degraded, ie, surface regions (Fig 3.22 (frame width 0.5mm) & 3.22a).

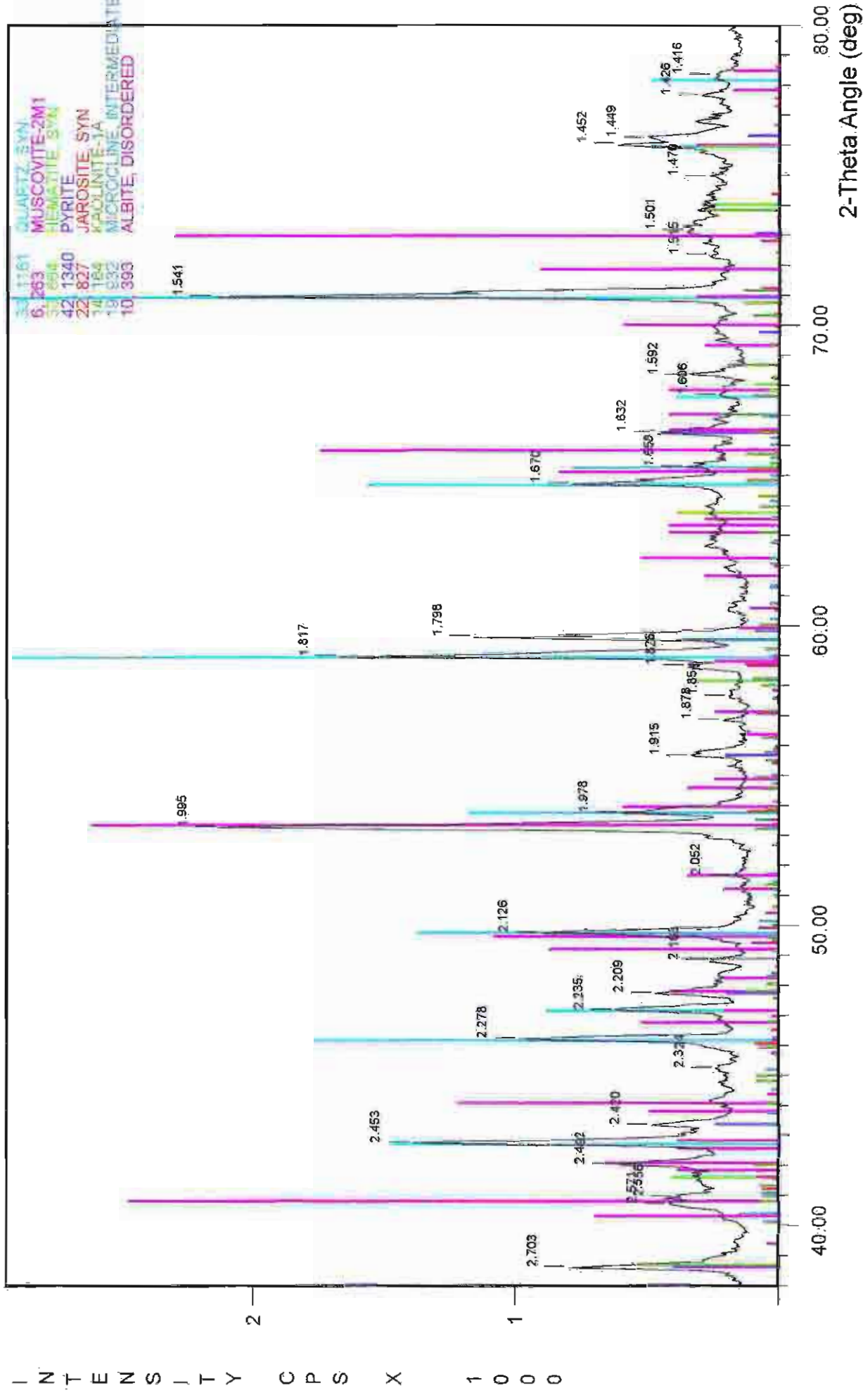
Potential Environmental Impact

The Net Neutralising Potential determined as -108 kg H₂SO₄ per tonne, is comparatively low, as a result of low total sulfur content of 3.6%. The neutralising capacity of the muscovite would have some effect. Even though this is a decrease in AMD potential compared to the other samples from Brukunga, compared to values observed at other mine sites around the world (for example, waste rock from Currough and Heath Steel, Canada, listed by Lawrence *et al*, (1989) is still comparatively high.

INTENSITY OF X 1000

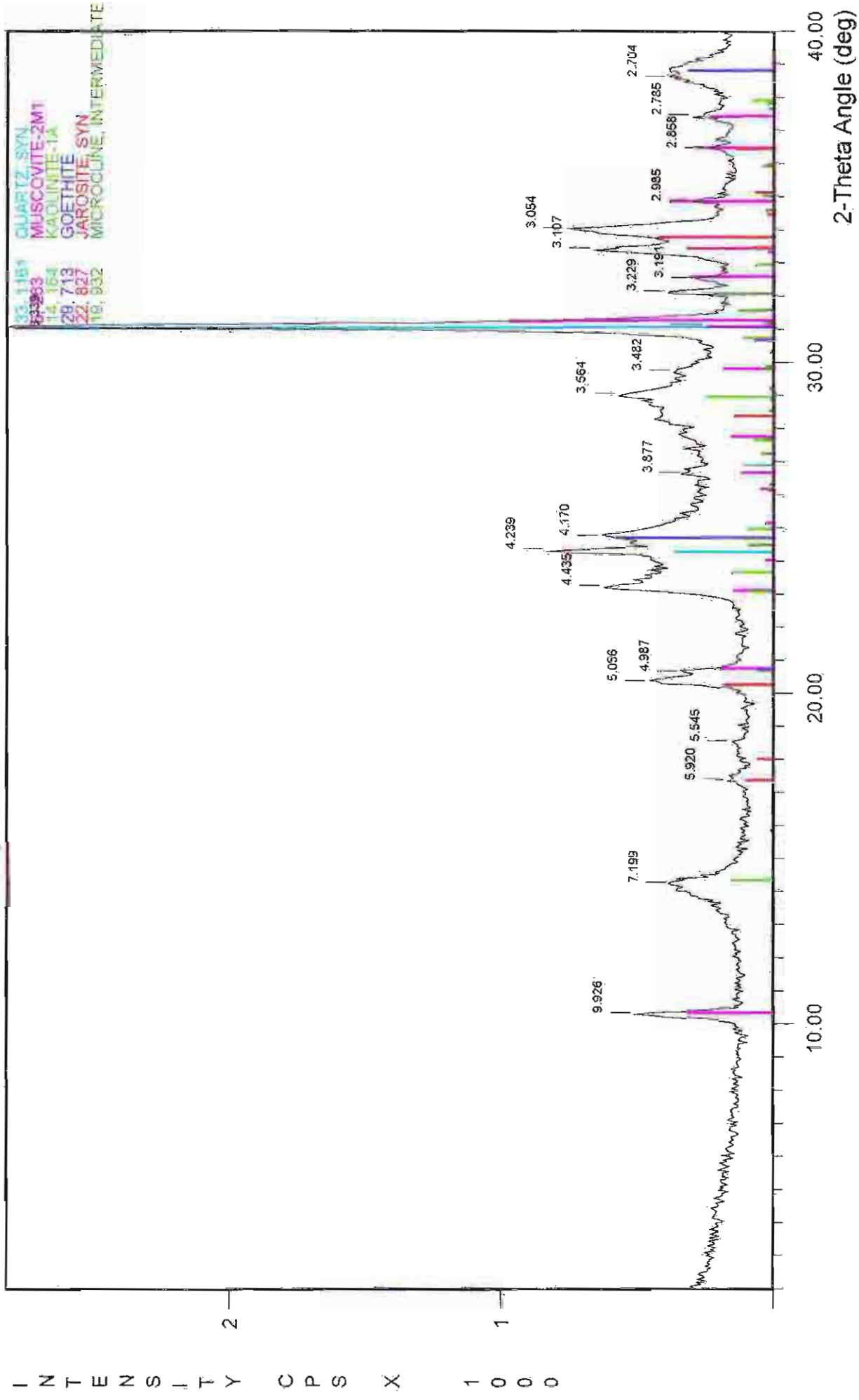


ROCK 7 : Highly weathered fine grained pyritic metasediment



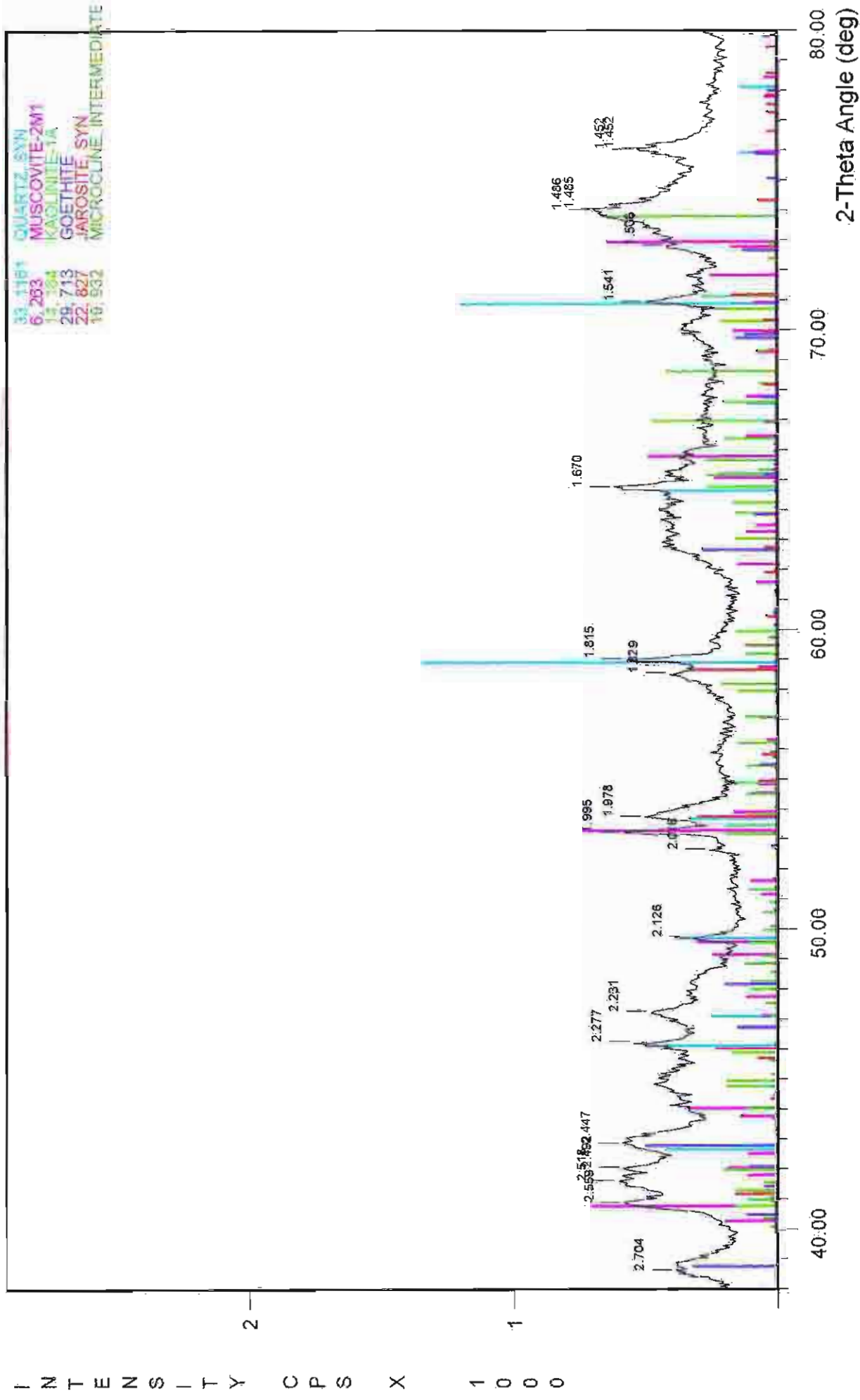
File Name: A:\BRUKROCK\107

ROCK 7 : Highly weathered fine grained pyritic metasediment (brown outer rim)



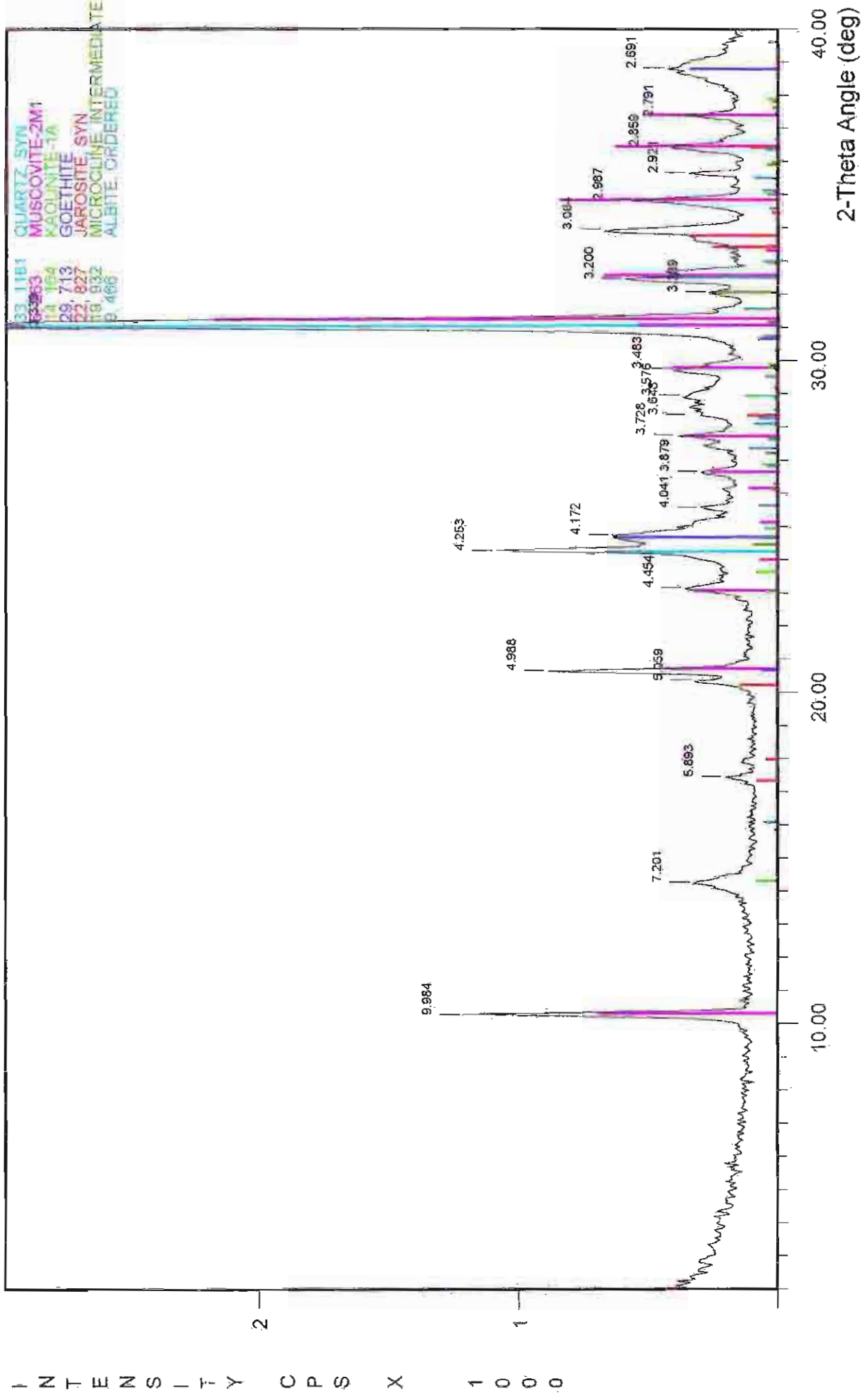
File Name: A:\BRUKROCK.118

ROCK 7 : Highly weathered fine grained pyritic metasediment (brown outer rim)



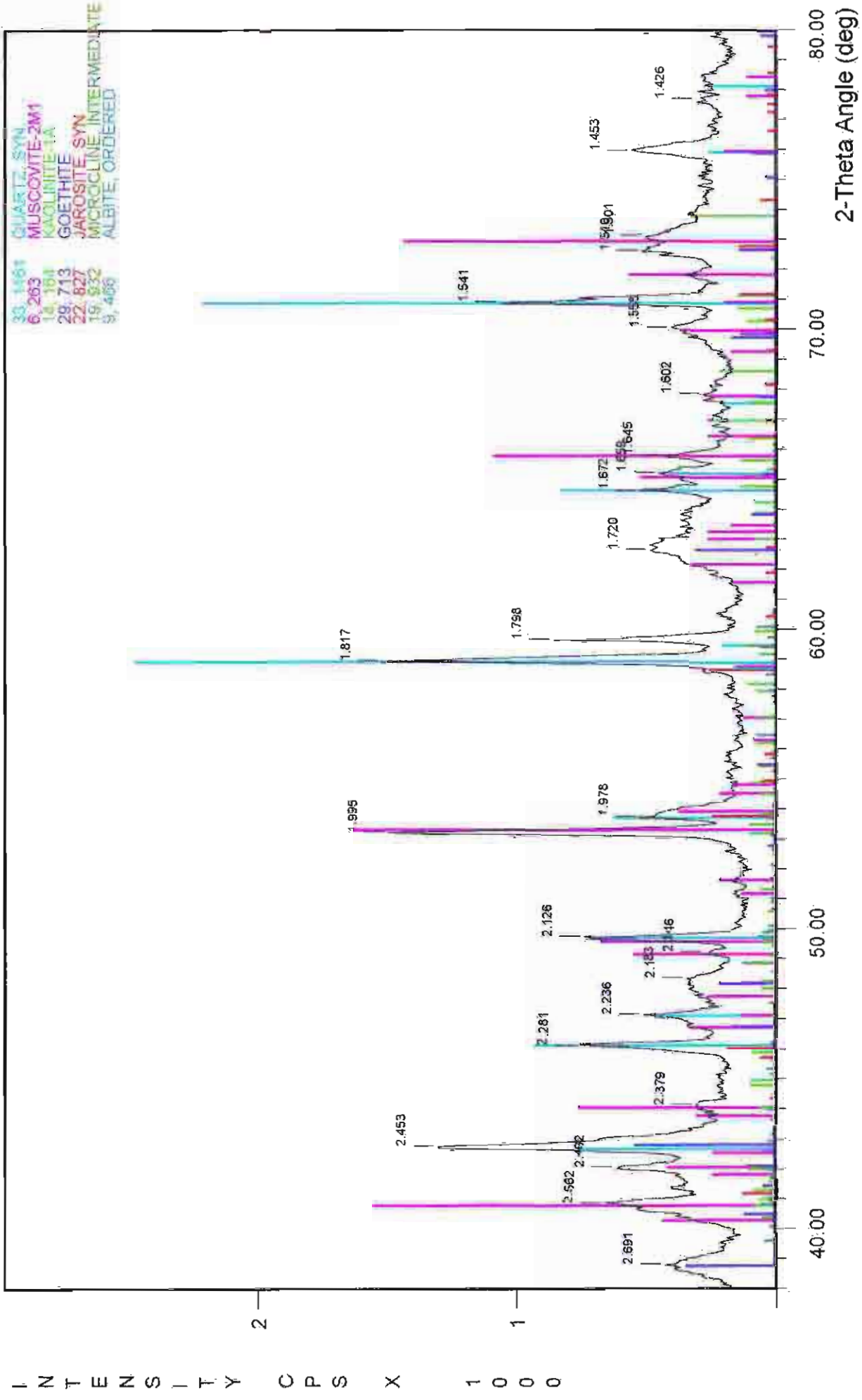
File Name: A:\BRUKROCK.118

ROCK 7 : Highly weathered fine grained pyritic metasediment (light grey interior)



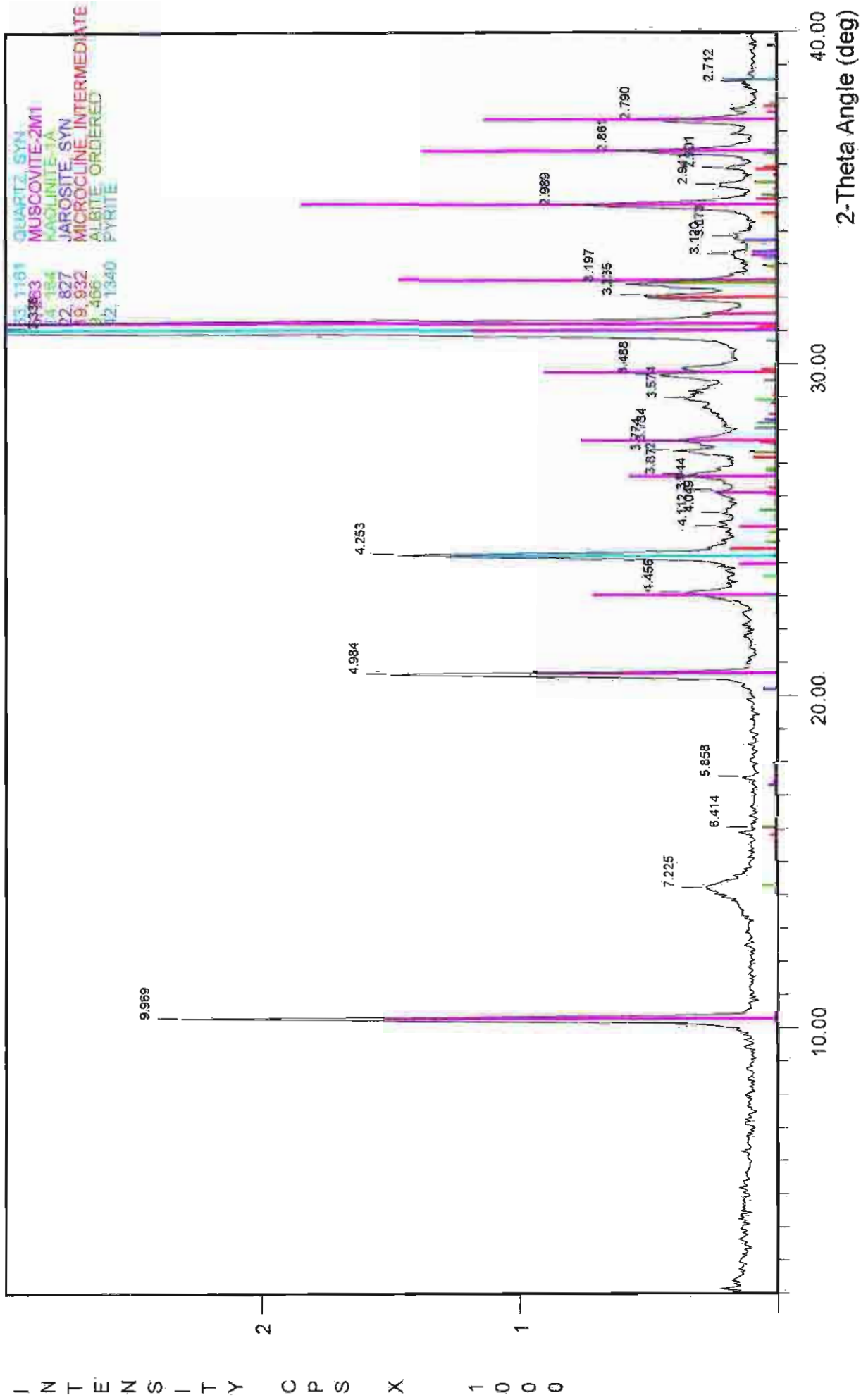
File Name: A:\BRUKROCK.119

ROCK 7 : Highly weathered fine grained pyritic metasediment (light grey interior)



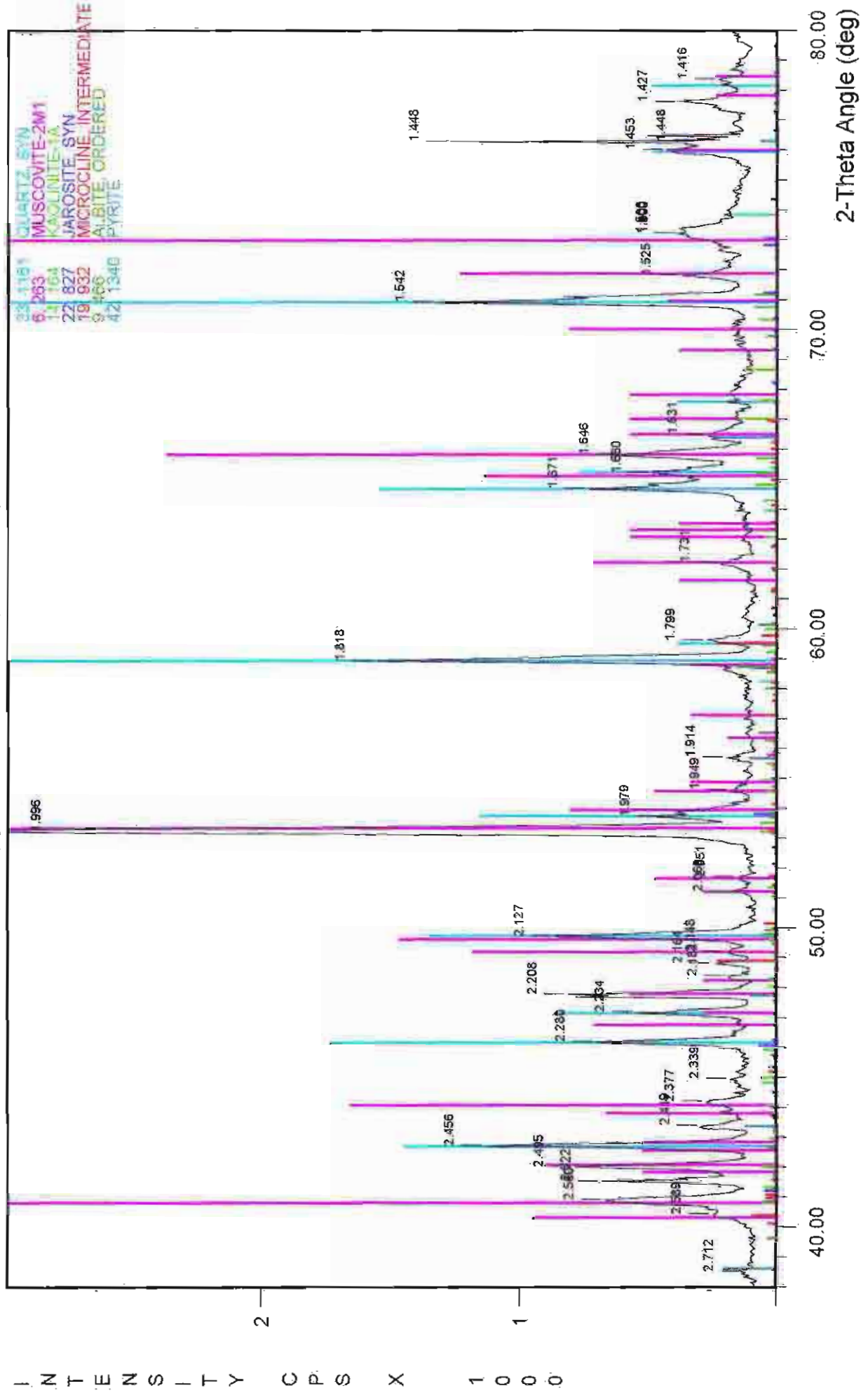
File Name: A:\BRUKROCK.119

ROCK 7 : Highly weathered fine grained pyritic metasediment (outer skin)



File Name: A:\BRUKROCK.120

ROCK 7 : Highly weathered fine grained pyritic metasediment (outer skin)



File Name: A:\BRUKROCK.120

ROCK 3 Micaceous Schist

Main components determined via XRD and verified by optical microscopy are:

muscovite	>30%
quartz	25-35%
albite	5-10%
pyrophyllite	<5%
clinochlore	<5%
calcite	<5%
hematite	<5%
tremolite	<1%
rutile	<1%

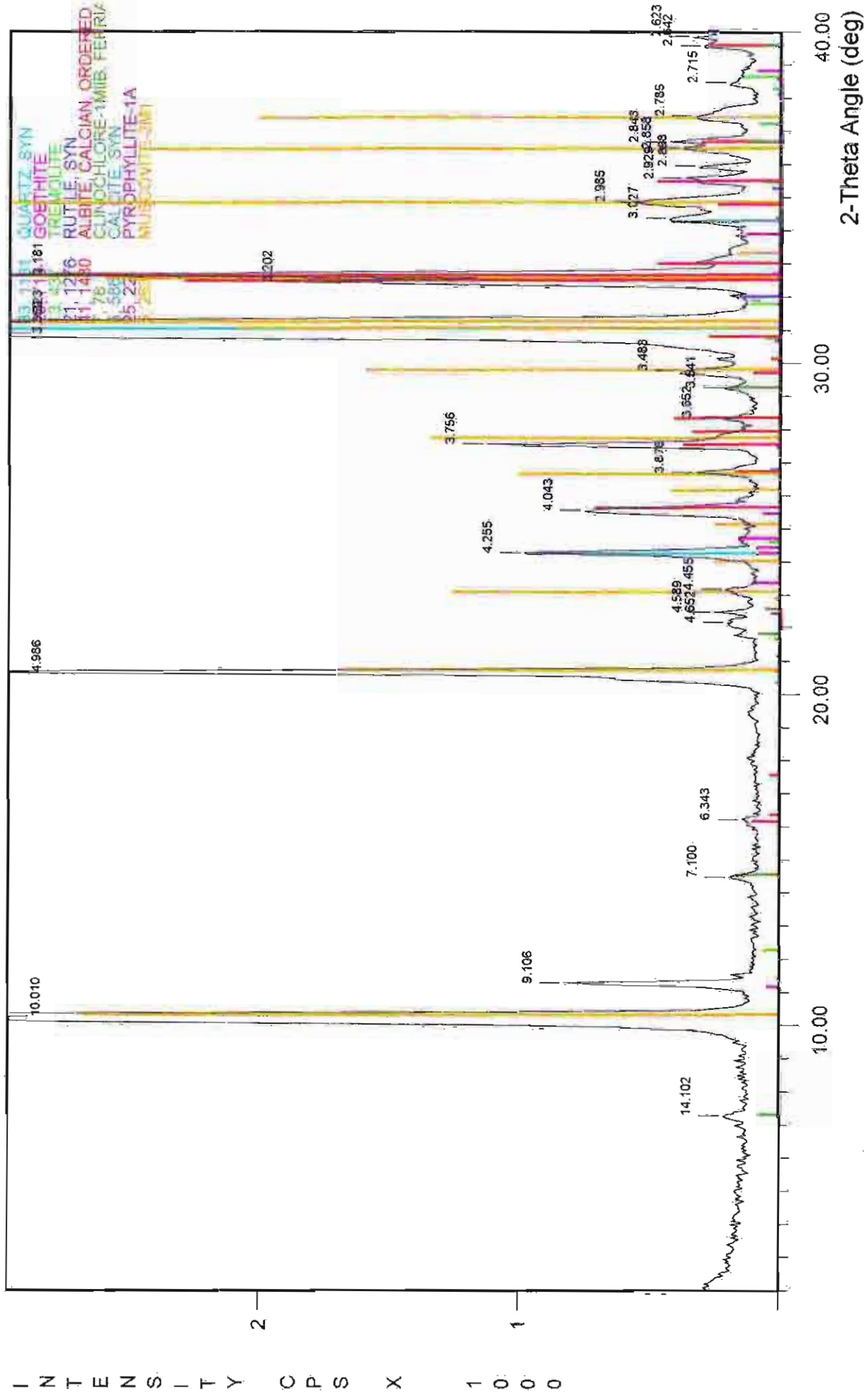
Optical microscopy identified small quantities of rozenite on the rock surface. SEM/EDX additionally identified pyrrhotite, pyrite, biotite, hornblende and monazite in small amounts (Fig 3C.4). XRF data (Table 3.4) indicate the presence of the sulfide minerals even though they were not detected by XRD. This very fine grained micaceous schist exhibited fine grained pyrite and pyrrhotite crystals forming a foliation within the specimen which was observed to be slightly crenulated.

The fine grained pyrite present was difficult to observe on the unbroken weathered surface under the optical microscope. Once cut and the rock split, small pyrite crystals could be observed in the interior of the sample. The crystals were strongly pitted and degraded. Thin section microscopy showed slightly altered mica - pyrite boundaries within the interior of the rock. Closer to the surface, increased pyrite weathering was observable (Fig 3.23 (frame width 0.5mm)). Muscovite was altered along cleavages and grain boundaries, leaving them stained red. This red staining can be attributed to the hematite previously identified through XRD.

Potential Environmental Impact

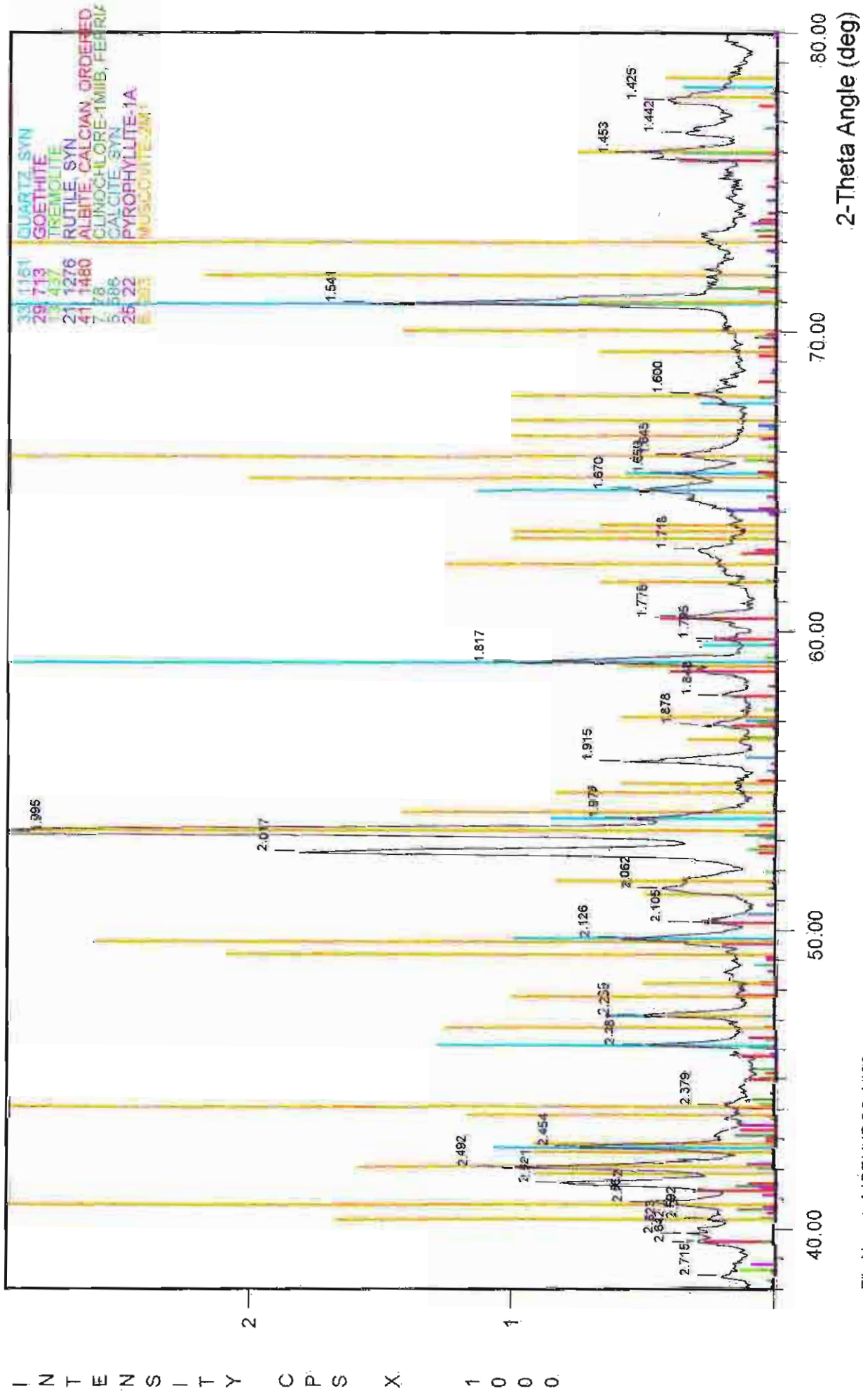
The moderate AMD potential (NPP = -79 kg H₂SO₄ per tonne) can be attributed to the low quantity of sulfide present in the specimen. Additionally the dissolution of neutralising minerals such as tremolite, calcite (eq 3C1.19), clinochlore, muscovite (eq 3C1.9) and biotite (eq 3C1.17) would have a major effect. SEM/EDX observations showed that there was little difference in the effects of weathering of any of the neutralising minerals. The only variations observed were related to the proximity of the minerals to pyrite crystals i.e. more degradation closer to the pyrite decomposing crystal.

ROCK 3 : Micaceous Schist



File Name: A:\BRUKROCK.103

ROCK 3 : Micaceous Schist



File Name: A:\BRUKROCK.103

ROCK 12 Highly crystalline, highly weathered metasediment

Two separate XRD samples were used to identify the main components of this specimen. These data combine to give a whole rock analysis of;

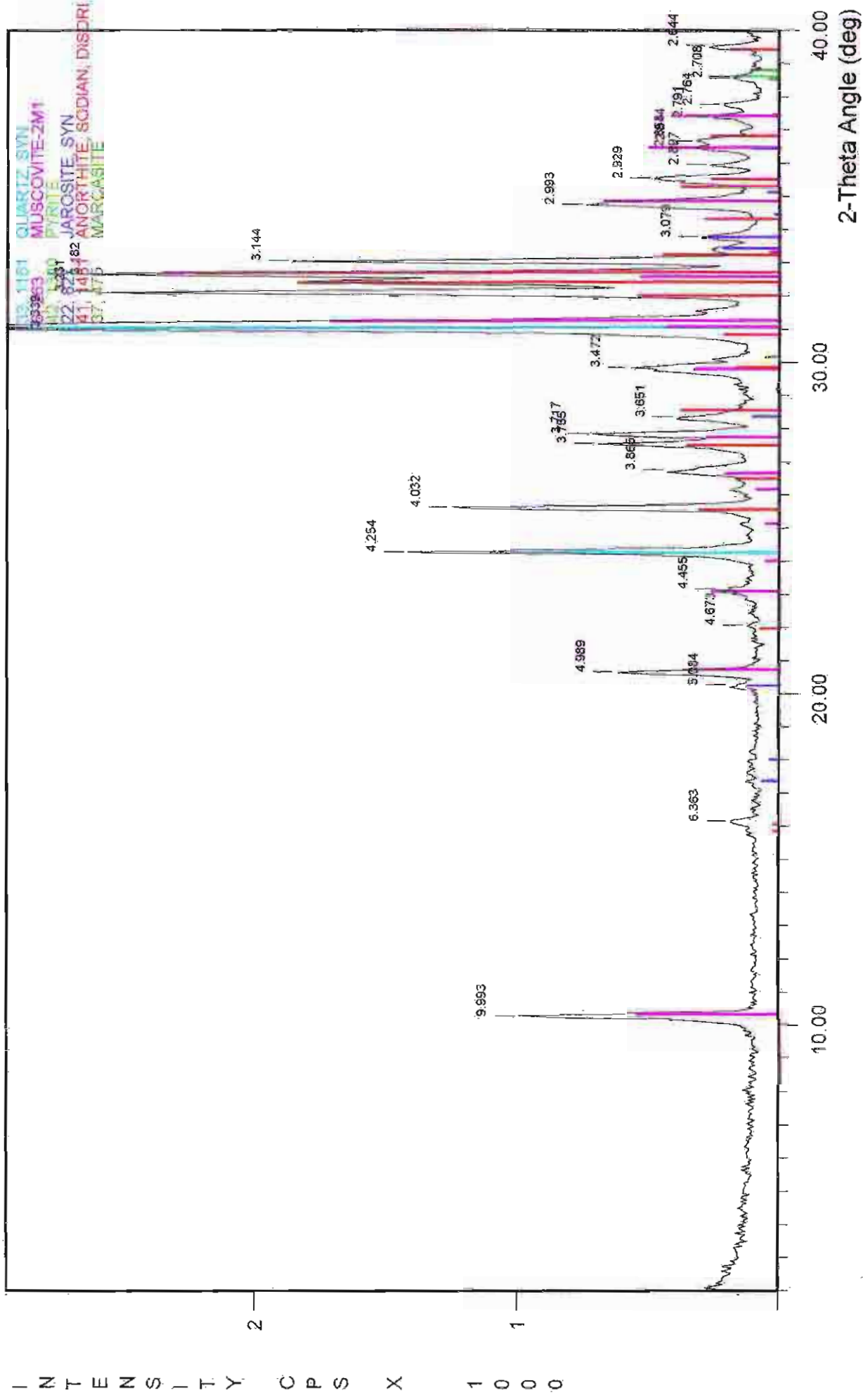
quartz	20-30%
muscovite	10-20%
albite	
anorthite	} 5-10%
microcline	
marcasite	<5%
pyrite	<5%
jarosite	<5%

Optical microscopy indicated the occurrence of minor rozenite on the surface. Only minor pyrite could be identified, and these were highly degraded and showed strong pitting. Thin section observations indicated the presence of jarosite-filled structures formed in response to the weathering and removal of pyrite and possibly pyrrhotite crystals. Muscovite along boundaries of pyrite showed strong weathering and alteration. However, muscovite at further distances away, remain unaltered. A pale yellow coating of jarosite formed on the surface and at fractures. Its thickness was thought to be a function of the orientation of the rock to prevailing weathering conditions ie. the access of oxygen and water to the rock.

Potential Environmental Impact

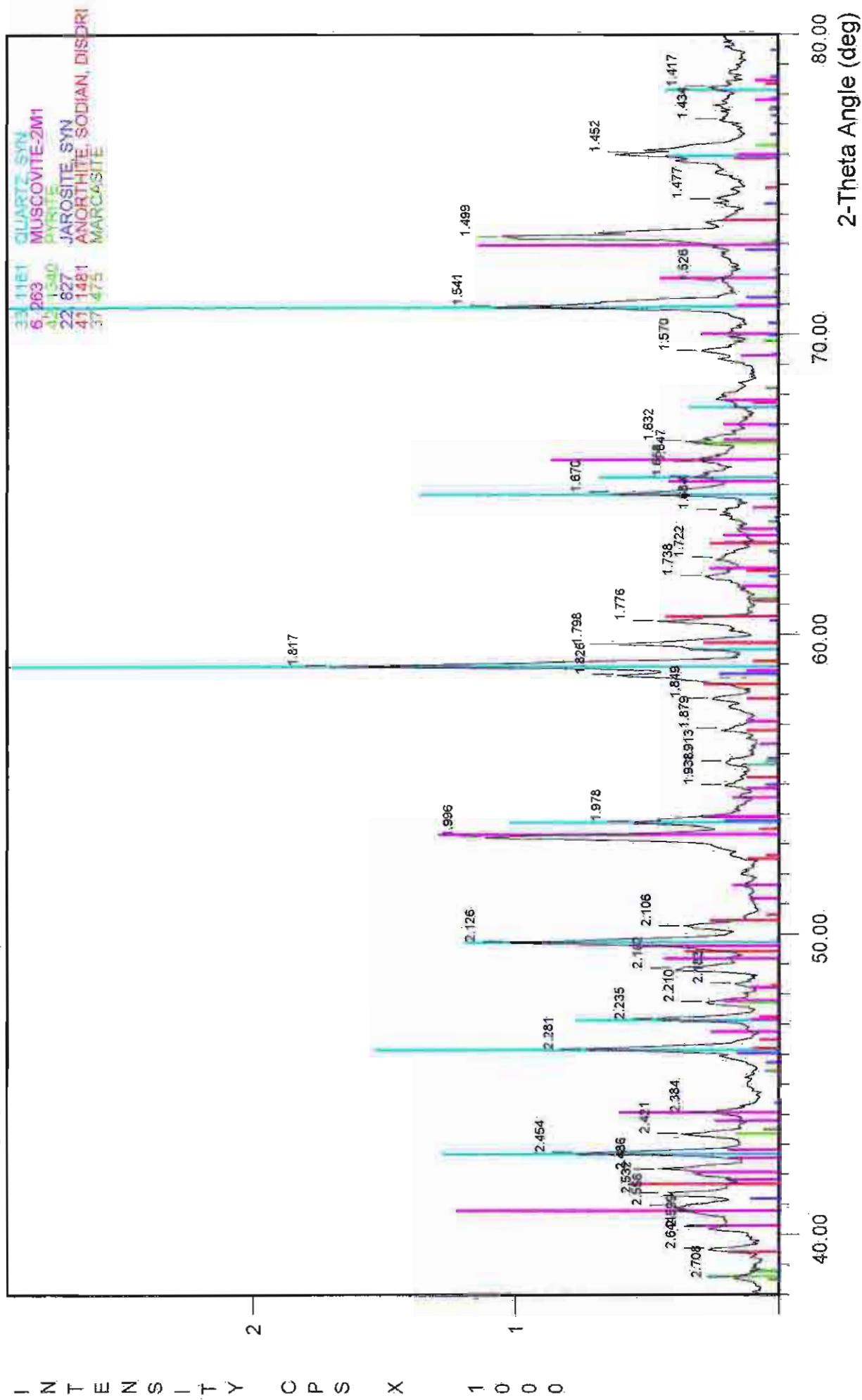
The lower AMD potential (NNP of -77 kg H₂SO₄ per tonne) compared to other Brukunga rock samples can be attributed to the low amount of sulfides present. Additionally some AMD produced would be neutralised through the dissolution of the muscovite present. Evidence of this was observed via high magnification microscopy where muscovite in contact with pyrite is highly degraded and covered with iron staining and jarosite. As with Rock 3, this rock type would have much lower environmental impact than most of the rocks at Brukunga.

ROCK 12 : Highly crystalline, highly weathered metasediment



File Name: A:\BRUKROCK.112

ROCK 12 : Highly crystalline, highly weathered metasediment



File Name: A:\BRUKROCK.112

ROCK 2 Tremolite rich metasediment

Main components determined via XRD and verified by SEM/EDX and optical microscopy are:

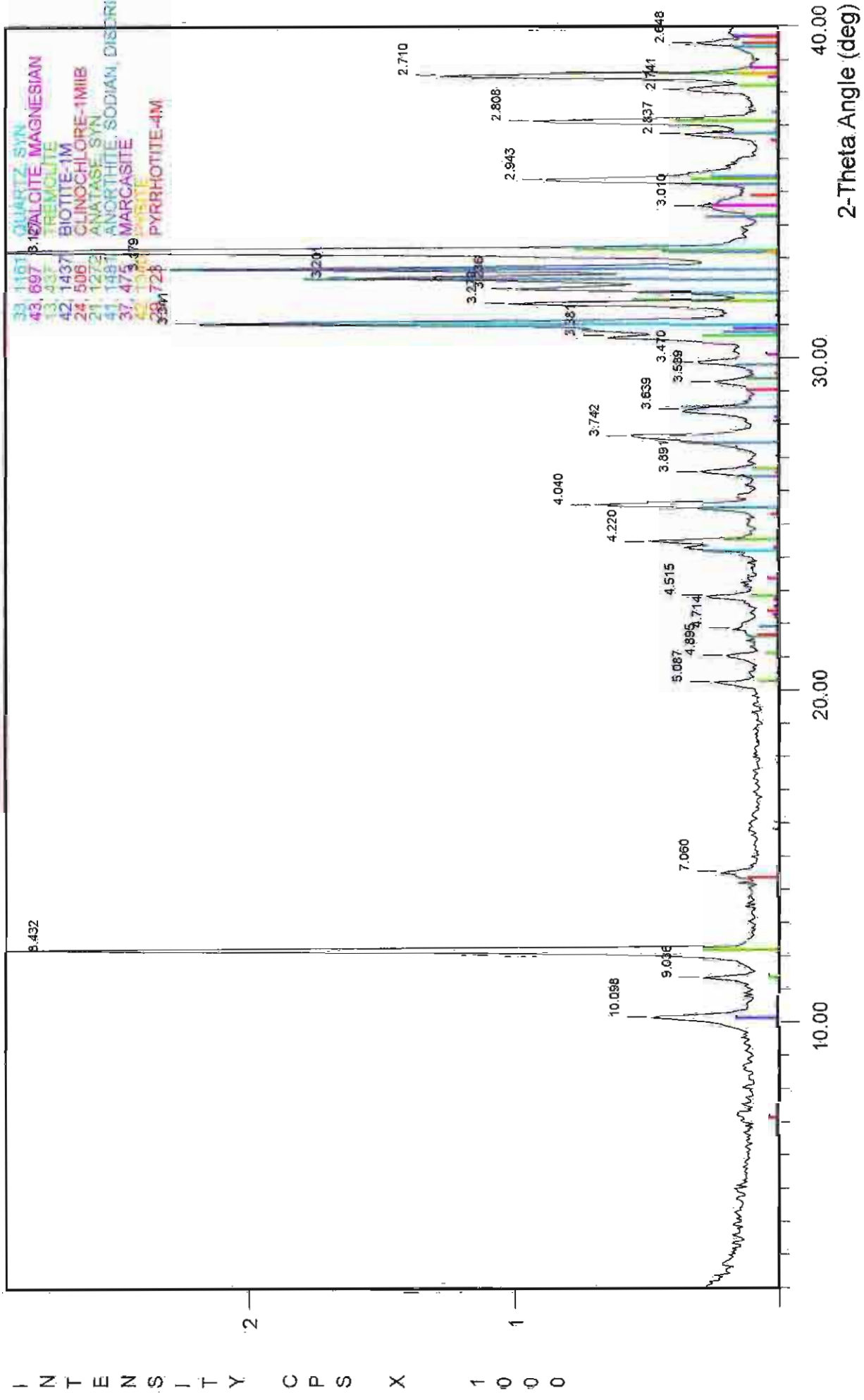
Tremolite	20-60%
biotite	15-25%
quartz	5-10%
anorthite	5-10%
calcite	<5%
clinochlore	<5%
marcasite	<5%
pyrite & pyrrhotite	<5%
anatase	<1%

SEM/EDX observations indicated this sample is a homogeneous tremolite-rich metasediment (Fig 3C.5, 3C.5a & 3C.5b). The high quantity of tremolite was also verified through XRF data (Table 3.5), as notably high amounts of magnesium and calcium. Optical microscopy indicated pyrite is in small quantities with weathering restricted to the surface or along fractures of the rock. This is indicative of the fine grained impervious nature of the rock, allowing only small amounts of the water and oxygen to enter along these sites. The main products of weathering include jarosite and other iron oxyhydroxides forming a conspicuous coating along fracture sites and surface.

Potential Environmental Impact

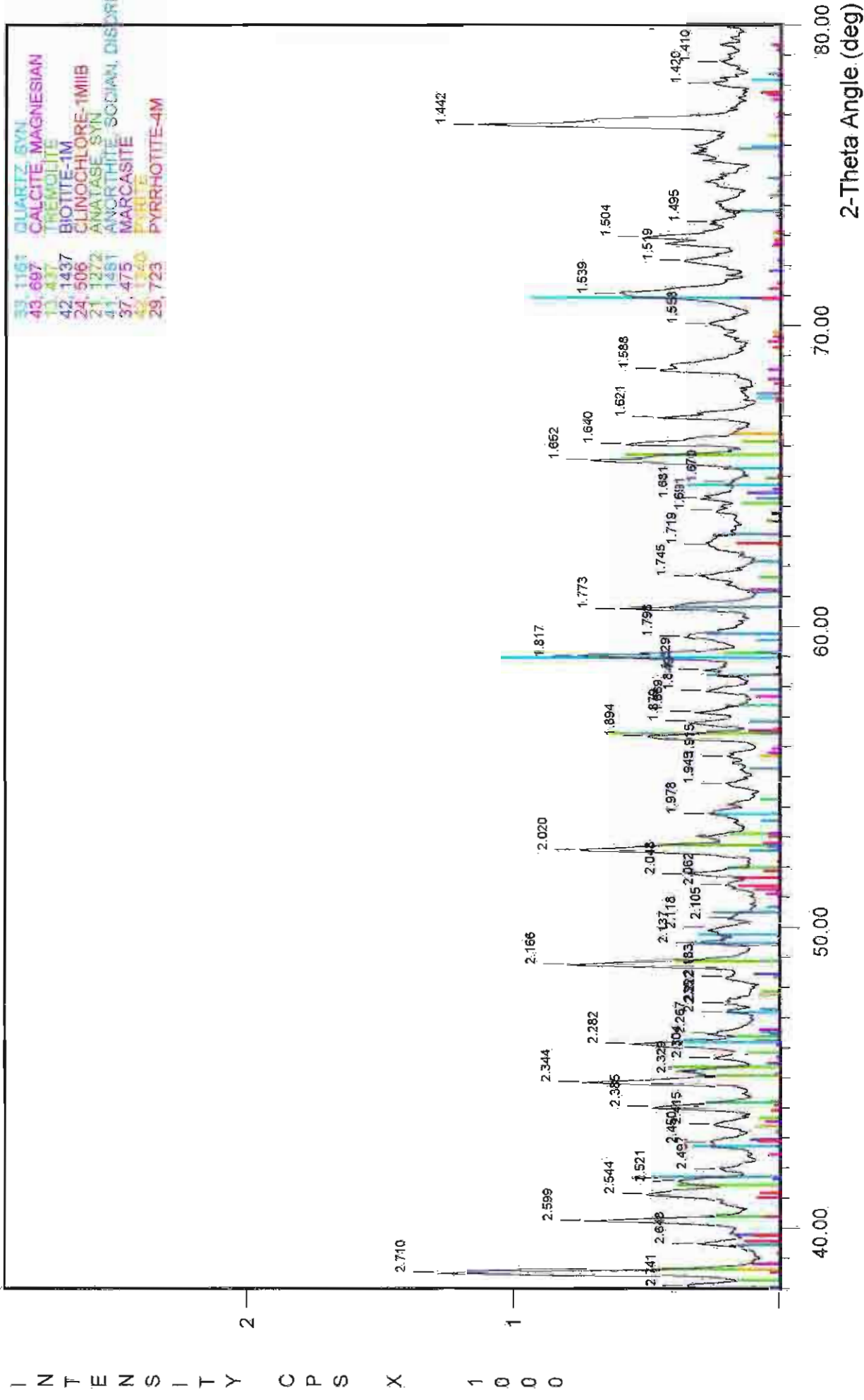
The NNP of -17 kg H₂SO₄ is due to the low quantity of sulfides present. Some of the AMD produced would be neutralised through the dissolution of the biotite (eq 3C1.17), calcite (eq 3C1.19) and clinochlore. However, using high magnification thin section microscopy, only minor weathering could be observed throughout the interior of the sample. Few weathering products have formed, and the majority of the boundaries between pyrite and host rock crystals are sharp. From this, it is suggested that the fine grained impervious nature of this rock is responsible for little or no reactions taking place. Thus the effect on the environment is low, as a consequence of the physical and chemical properties of this tremolite-rich rock.

ROCK 2 : Tremolite rich metasediment



File Name: A:\BRUKROCK.102

ROCK 2 : Tremolite rich metasediment



File Name: A:\BRUKROCK 102

ROCK 4 Highly weathered schist, originally pyritic

Two separate XRD samples were analysed to determine the main components of this weathered schist, these were then verified through optical microscopy:

quartz	20-30%
rectorite & muscovite	15-25%
halloysite & kaolinite	<10%
albite	<5%
rutile and anatase	<1%

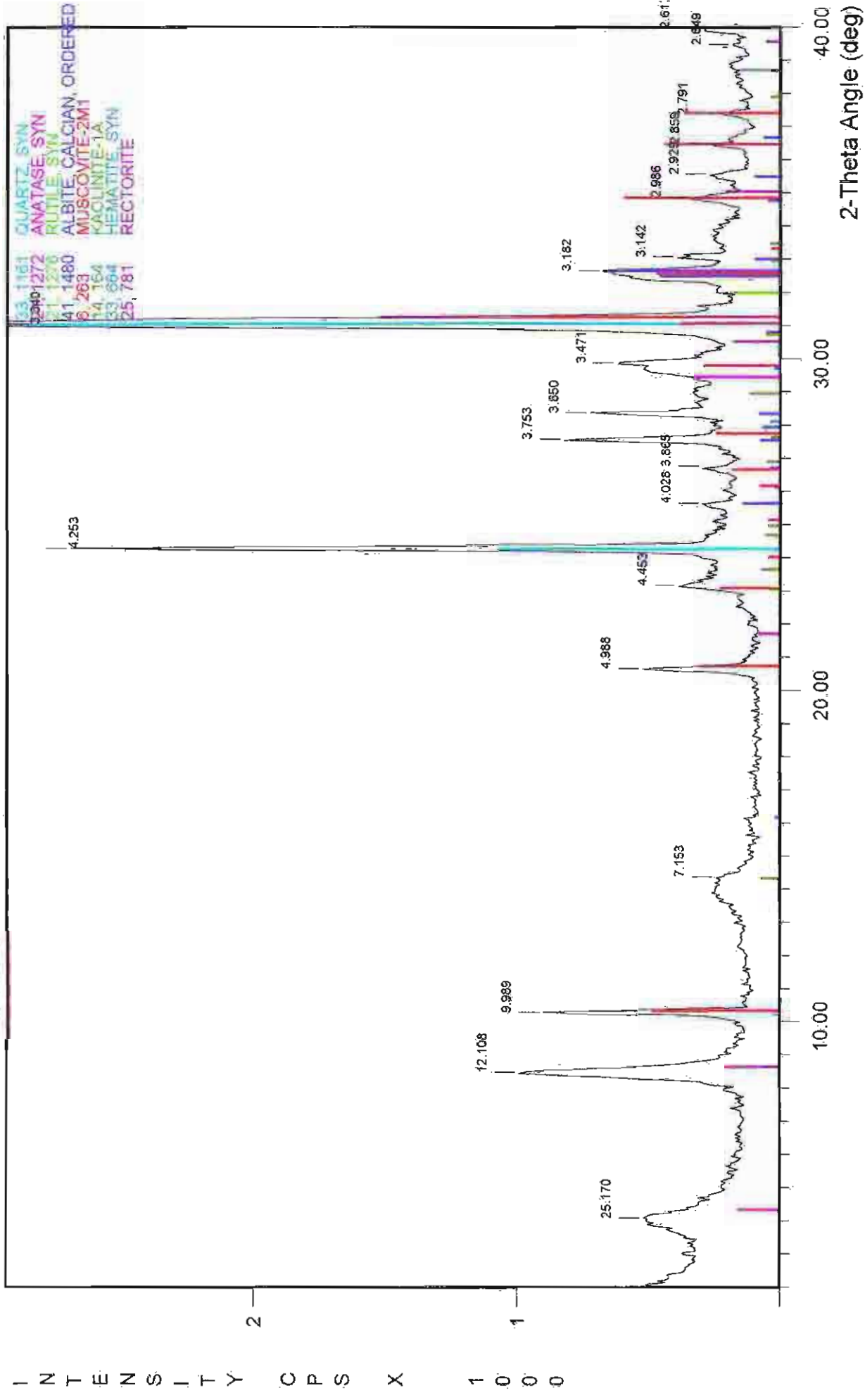
A separate XRD sample was taken from a white rim existing on this specimen. This rim may represent a highly weathered surface region, and contains only halloysite, muscovite and quartz because all other phases have been weathered out. Alternatively, it may represent a region created during the formation of this rock, in which no pyrite formed. This seems the more appropriate option as no iron stained voids exist (from which pyrite has been removed) in this section whereas they are a main feature of the rock's interior.

The total S% of this rock is 0.7% which may indicate some sulfide is still present. However, no sulfides were observed microscopically, and it is more probable the S represents minor amounts of sulfate formed during the oxidation of the original sulphides. Additionally thin section microscopy allowed identification of extensive red-orange staining associated with pyrite weathering voids. SEM/EDX investigations of thin sections identified them as iron oxyhydroxides, localised hematite spheres and minor jarosite (which could account for the sulfur content). This iron staining was usually confined between fractured pieces of mica which may indicate a highly leached environment where dissolved iron was moving through the rock. Such an environment would also account for the absence of any major amounts of sulfates and other weathering products.

Potential Environmental Impact

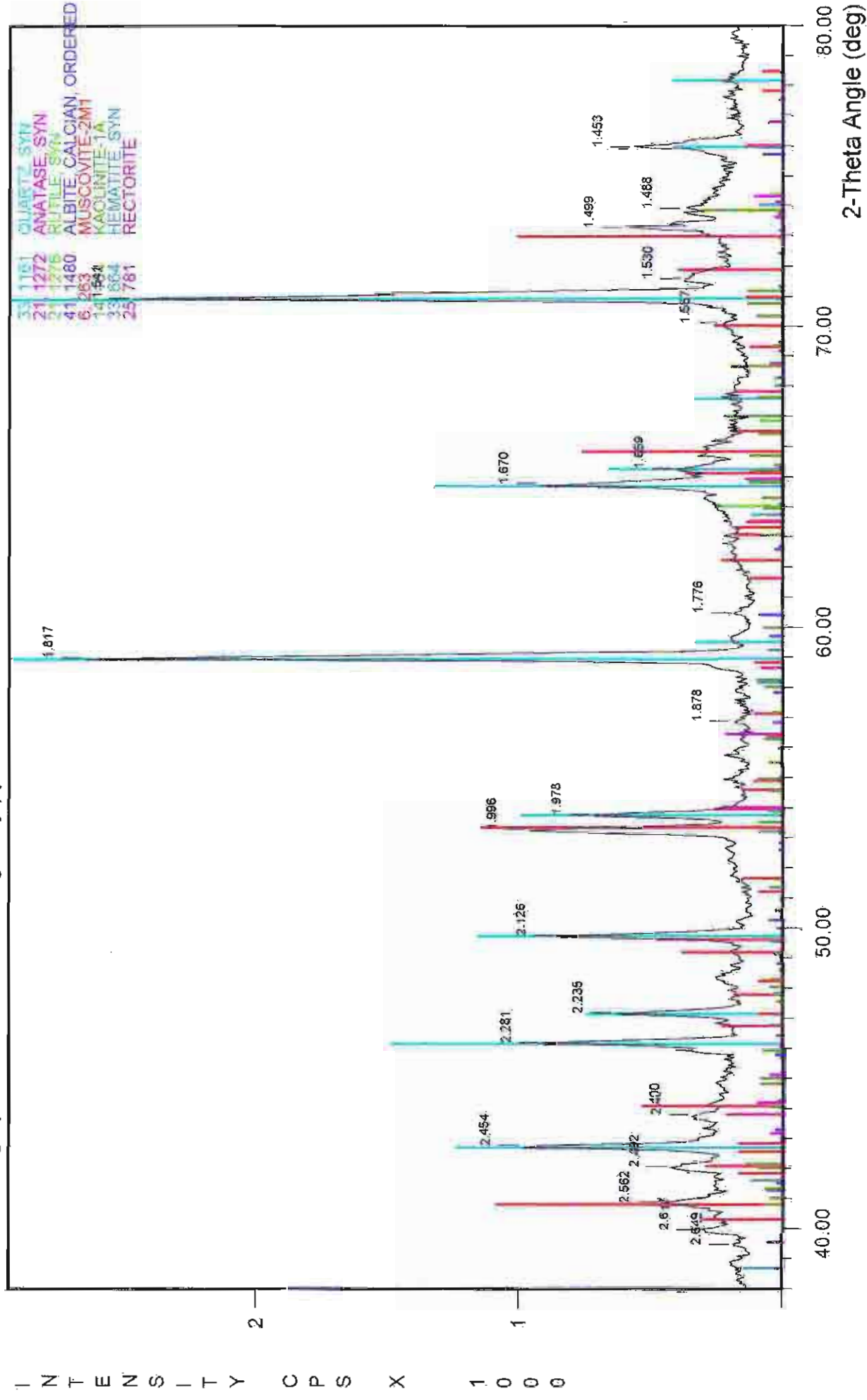
It is because of the very low total S% that the AMD potential of this sample is very low (NNP = -1 kg H₂SO₄ per tonne). Additionally the presence of micas would neutralise most of the relatively small amounts of AMD produced. Thus this rock type is not expected to have any major effect on the surrounding environment. However, the observation of iron staining associated with pyritic voids, indicates that the unweathered counterpart of this rock type would probably represent a significant hazard to the surroundings.

ROCK 4 : Highly weathered schist, originally pyritic



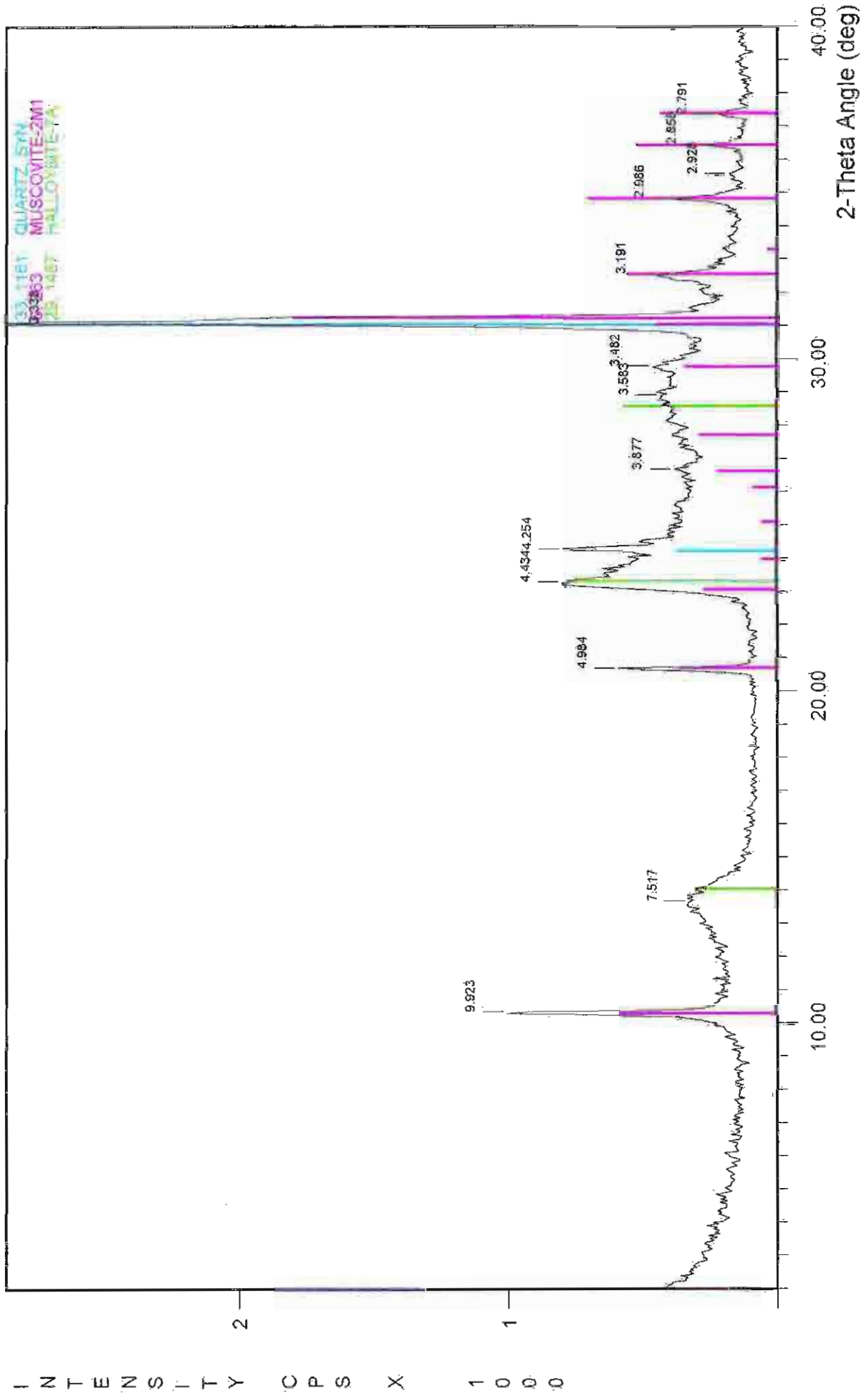
File Name: A:\BRUKROCK.104

ROCK 4 : Highly weathered schist, originally pyritic



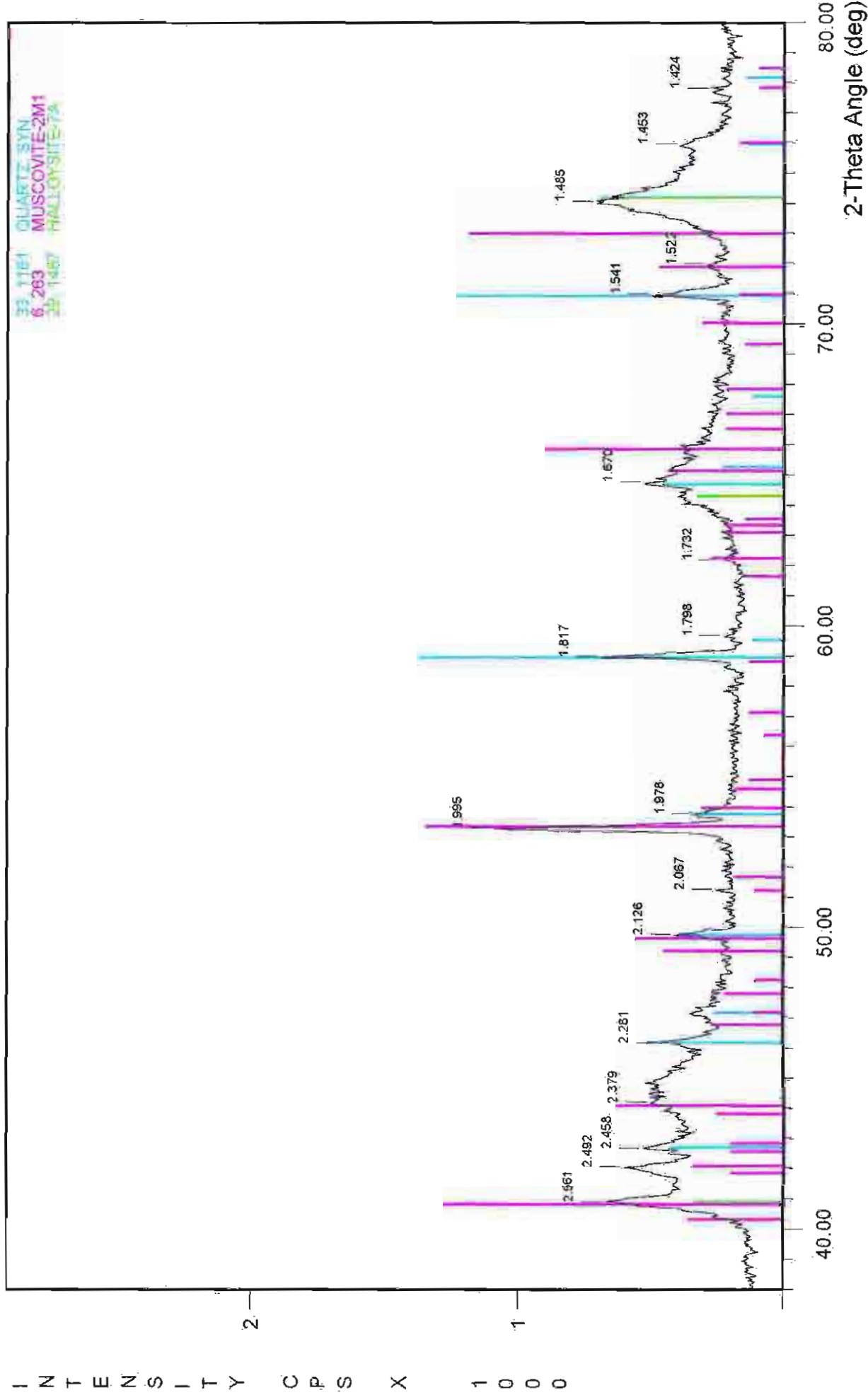
File Name: A:\BRUKROCK\104

ROCK 4 : Highly weathered schist, originally pyritic (white rim)



File Name: A:\BRUKROCK.115

ROCK 4 : Highly weathered schist, originally pyritic (white rim)



File Name: A:\BRUKROCK\115

APPENDIX C2

Mineral Investigation of tailings and development of cemented layers

&

Presentation of data referred to in Chapter 3, Section B.

Figures referred to in Chapter 3 - Section B follow.

Page 174: Figures representing EDX spectra obtained during SEM investigations, and are presented for verification of the presence of the specific minerals observed.

Page 175: Tables and figures concerning the physical attributes of the tailings, including void ratio vs depth, porosity vs depth & wet, dry and particle density vs depth.

Page 179: Flow chart using the physical characteristics of the tailings to determine NNP.

Page 180: Presentation of the detailed classification of hole 8.

Page 181: Mineral Investigations of tailings and development of cemented layers.

Page 195: Detailed description of the tailings.

Page 205: XRD Traces.

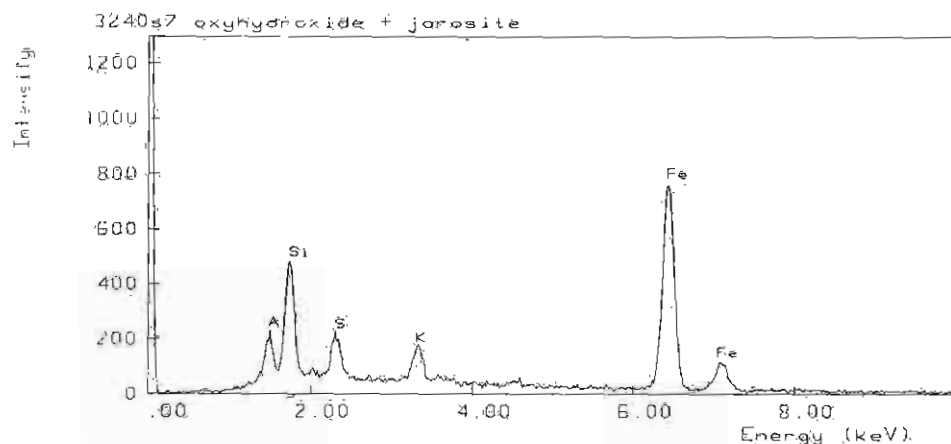


Fig 3.31a

Ferrihydrite with minor jarosite, developed in cemented layer at 1.04m depth.

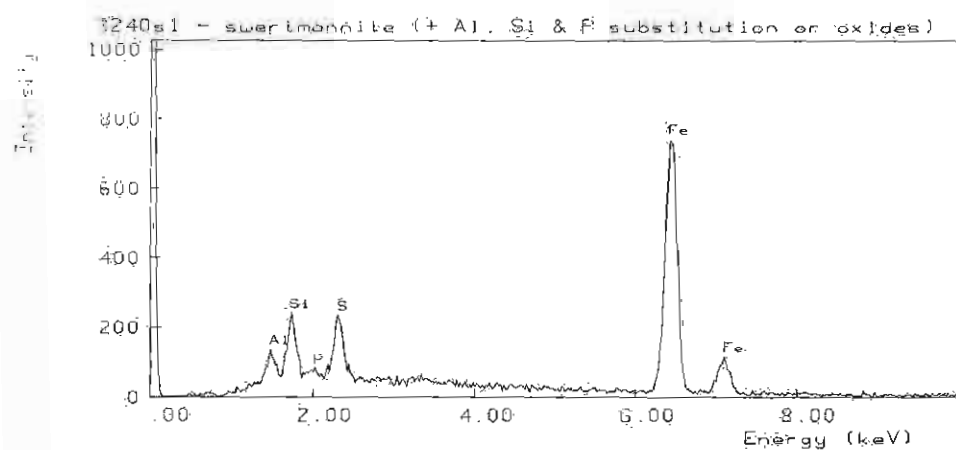


Fig 3.31b

Swertmannite with minor contaminants of Si and P as oxides or substitutions developed in cemented layer at 1.04m depth.

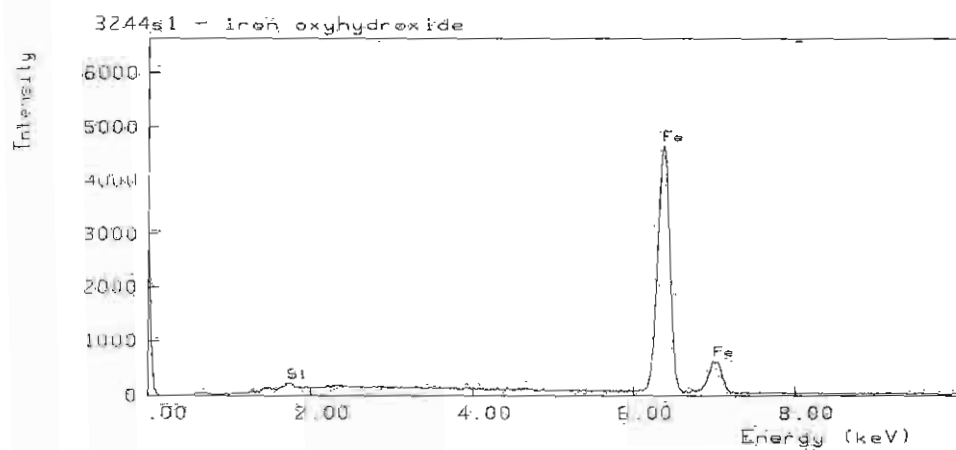


Fig 3.34a

Iron oxyhydroxide as small platy deposits in main cement developed at 1.37m depth.

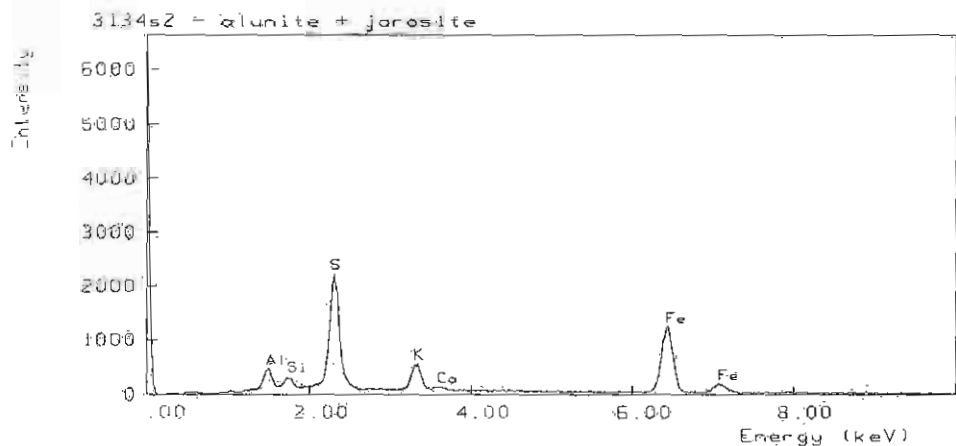


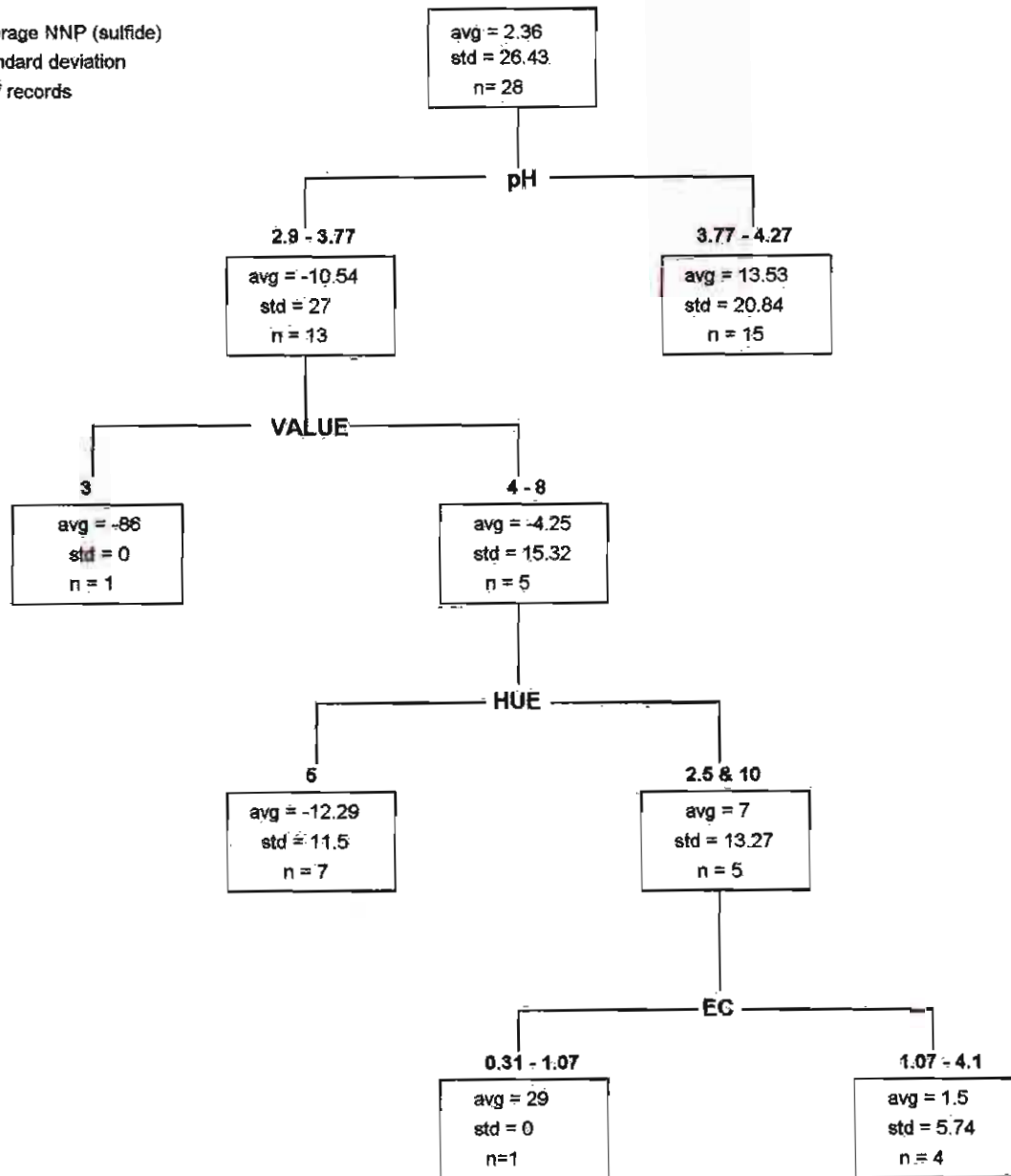
Fig 3.35a

Jarosite and alunite developed above main cemented layer at 1.37m depth.

Fig 3C.9 Flow chart using the physical characteristic of the tailings to determine NNP.

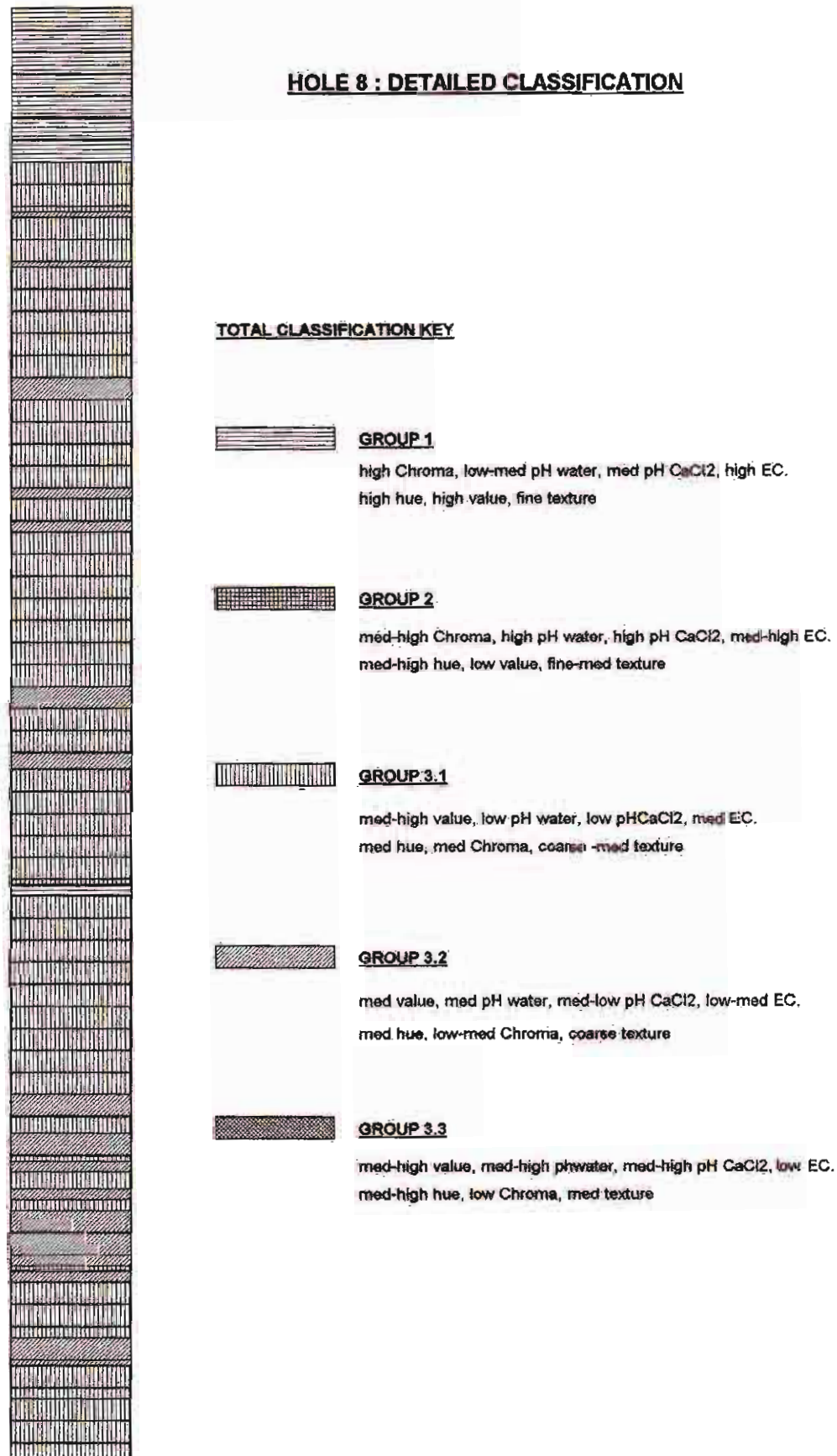
LEGEND

Average NNP (sulfide)
standard deviation
of records



pH of the sample gives an indication of NNP, as pH decreases, NNP becomes more negative (ie less neutralising potential). Colour gives an indication of whether or not the tailings have already been slightly oxidised and therefore has less acid potential (AP), ie more positive NNP. Whereas the sample identified with 'value' of 3, ie very dark indicates that it has not been oxidised at all and has a very high acid potential due to the high sulfide content (NNP -86 kg CaCO₃ equi/tonne). A similar situation exists when discussing 'hue', where the redder (ie. hue 2.5 and 10) samples are more oxidised, and thus some of the acid potential has been exhausted producing a positive NNP.

Fig 3C.10 Detailed Classification of hole 8.



Description of the tailings and the development of cemented layers

The top 1m consists of porous medium-sized sand, the majority of which is gangue mineral grains with strong coatings of jarosite and ferrihydrite (Fig 3C.11). XRD analysis did not indicate the presence of pyrite and SEM/EDX investigations verified its absence. The lack of evidence maybe due to the strong coating (>2um) of jarosite reducing its EDX signature. However it is fair to say that at this depth oxidation of pyrite is essentially complete, so that little or no pyrite is present and only secondary minerals formed during this process, along with degraded gangue minerals, remain.

SEM/EDX and XRD investigations determined the type of gangue minerals present (Fig 3C.11a, 3C.11b, 3C.11c, & 3C.11d). SEM/EDX showed the variable nature of grain coatings ranging from jarosite to iron oxyhydroxides identified through XRD as ferrihydrite. Lower magnification investigation of the coatings showed it to have a hygroscopic appearance typical of ferrihydrite (Jambor and Blowes, 1994), along with smaller rhombahedral crystals of jarosite (Fig 3C.12 & Fig 3C.12a). At higher levels of investigation discrete particles of the iron oxyhydroxide could be seen (Fig 3C.13 & Fig 3C.13a). This iron compound did not portrays a regular structure indicative of any particular iron mineral, and its shape is probably dictated by the surrounding host grain morphology as it formed.

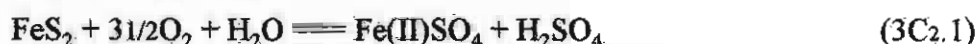
Within this shallow region XRD also identified amounts of strengite ($\text{Fe}(\text{PO}_4) \cdot 2\text{H}_2\text{O}$). This is a surface or near surface product formed by the alteration of iron-containing phosphates, and particularly forms in gossans. Strengite is often associated with microcrystalline apatite. Chlorapatite ($\text{Ca}_5(\text{PO}_4)_3\text{Cl}$) was identified through XRD also. This mineral is chiefly found in veins in gabbroic rocks and is often associated with rutile, magnetite, pyrrhotite and tremolite. Chlorapatite is observed at different depths down the profile, its presence or absence is presumably due to variations in the ore being processed. Strengite is also observed at different depths throughout the profile. This maybe a function of leaching although strengite is only slightly soluble. Its presence may be due to development of the gossan prior to mining and thus can be regarded as a relict mineral and not a secondary mineral formed at depth.

Between 0.98-1.37m different specimens were selected for SEM/EDX to observe cemented layers and the material separating them. Iron is the predominant element in the cemented areas, although isolated patches of S associated with Fe were detected by SEM/EDX between aggregates and identified as jarosite. H, C and O are not detected

by EDX, but their presence is assumed in association with Fe, in the absence of signature of other expected combinations such as S.

The cement has a reddish brown, cloudy appearance and forms coatings around vesicular aggregates and other discrete mineral grains. Marked irregularities exist within micro environments, as shown by graded bedding and obvious changes in depositional regimes. Coarse material is deposited on fine, forming a sharp textural contrast indicative of a hiatus in deposition. Infilling of the inter-aggregate pores is favoured under saturated conditions, where leachate reaches saturation with respect to ferrihydrite, jarosite or schwertmannite.

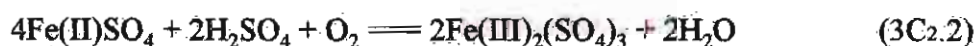
Nordstrom (1982) and Fanning and Fanning (1989) suggest a series of intermediate steps that may occur prior to the development of the iron oxyhydroxides and sulfates. Nordstrom (1982) explained that the precursor secondary soluble sulfate minerals are most commonly formed during dry periods as evaporation promotes the rise of subsurface waters to the upper-most soil surface by capillary action. As these waters reach the upper portion of the tailings, they become progressively more concentrated and finally precipitate various salts. This is an important intermediate step preceding the precipitation of the more common insoluble iron minerals eg jarosite. Fanning and Fanning (1989) showed that the oxidation of FeS_2 to give ferrous sulfate and acid can be written as



Additionally they explain that both ferrous sulfate and sulfuric acid are very soluble and are normally dissociated in water. Then under desiccation conditions (eg at the surface by drying) different FeSO_4 minerals (eg. szomolnokite $\text{FeSO}_4 \cdot \text{H}_2\text{O}$; rozenite $\text{FeSO}_4 \cdot \text{H}_2\text{O}$; ferroxahydrite, $\text{FeSO}_4 \cdot 6\text{H}_2\text{O}$; or melanterite, $\text{FeSO}_4 \cdot 7\text{H}_2\text{O}$) may form depending on humidity conditions.

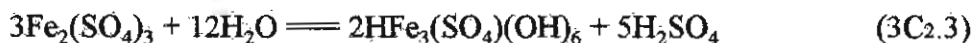
Under conditions of continuous dryness, melanterite dehydrates to rozenite $\text{FeSO}_4 \cdot 4\text{H}_2\text{O}$. If these minerals are still in contact with soil water or humid air, they oxidise.

Fanning and Fanning (1989) express the oxidation of ferrous sulfate to ferric sulfate as



As mentioned previously this reaction and/or others involving the oxidation of Fe(II) to Fe(III) are greatly accelerated by the bacteria *Thiobacillus ferrooxidans* (Ivarson *et al*; Nordstrom, 1982, see Appendix D).

Fanning and Fanning (1989) explain ferric sulfate is also quite soluble, under desiccation conditions, but, it may precipitate as minerals such as copiapite, a hydrated ferric sulfate. Hydrolysis of ferric sulfate to basic ferric sulfate can be expressed as



Fanning and Fanning suggest however that it is more commonly jarosite, $\text{KFe}_3(\text{SO}_4)_2(\text{OH})_6$ that is produced, with the K arising mainly from acidic weathering of silicates.

It should be noted that the presence of melanterite and rozenite etc. is not a precursor to jarosite. However the reactions that must take place before jarosite will precipitate are consistent with the formation of these minerals. The reactions include the oxidation of sulfide, the oxidation of Fe^{2+} to Fe^{3+} and then the hydrolysis of ferric sulfate to basic ferric sulfate.

It is obvious from this discussion that the formation of secondary minerals in this system is a complicated one. Nordstrom (1982) and Fanning and Fanning (1989) have shown the development of jarosite through a series of steps. Ferrihydrite and schwertmannite are not unlike jarosite in that for both minerals Fe^{2+} must be oxidised to Fe^{3+} , and additionally they must be hydrolysed to a certain extent.

The formation of this secondary mineral suite is dictated by the surrounding conditions of the environment. Bigham *et al* (1992) have attempted to integrate available information to produce a tentative biogeochemical model for mineral formation from mine drainage. They explain under conditions of low pH, high dissolved SO_4 (3000-4000 ug/mL) and sustained bacterial activity, jarosite or related basic ferric sulfates will form, provided suitable metal cations (eg K, Na) are also available. In the case of Brukunga tailings suitable K would be present from the break down of feldspars and micas during acid neutralisation reactions.

Schwertmannite forms most readily within a narrow pH range of 3-4. *Acidophilic bacteria* may therefore be active, assisting in the formation of the required oxidation of Fe under field conditions. While the mineral can form in the presence of excess SO_4 ,

concentrations in the range of 1000-3000 ug/mL appear to be optimal (Bigham *et al* 1992).

In mine drainage with $\text{pH} > 5$ the abiotic oxidation of Fe^{2+} can proceed rapidly, and the dominant mineral product of Fe^{2+} being ferrihydrite. Precipitation of this mineral seems fairly insensitive to SO_4 . Carlson and Schwertmann (1981) explain that although thermally unstable with respect to and less well ordered than lepidocrocite and goethite, ferrihydrite seems to be kinetically favoured under conditions where Fe(III) is supplied at a high rate, such as during rapid oxidation of dissolved Fe(II) .

Once formed, natural ferrihydrite seems to resist transformation to more stable forms longer than it does when produced in pure, but otherwise comparable, synthetic systems, which convert to goethite and/or hematite within months or years. Stability is due to dissolved compounds which have a high affinity for the ferrihydrite surface. They are chemically absorbed and not only suppress ordering of the ferrihydrite, but also inhibit the formation of hematite or goethite. Chemically absorbed silicate is one of the main stabilization factors.

Observations of the cemented layers indicate the main products are in fact jarosite and ferrihydrite, and yet the two seem to develop in different pH conditions. McSweeney and Madison (1988) suggest that the pH of the solution in the intra-aggregate pores could be slightly more acidic than that in the bulk solution, because the smaller pores are in immediate contact with or in very close proximity to a source of oxidisable S. This condition would favour formation of jarosite rather than ferrihydrite. In locations further away from sulfides, pH may be higher and precipitation of ferrihydrite would be favoured. As the progressive cementation of the inter-aggregate pores occurs, this reduces permeability of the horizon to downward flow and enhances capillary flow through the intra-aggregate pores, improving the conditions likely for the formation of potentially soluble Fe-sulfates. It should be noted that there is little direct evidence for the presence of specific soluble Fe-sulfates through XRD analysis. This is due to the great difficulty of isolating and making positive identification of solids present in small quantities in the tailings.

Because of the importance of cemented layers as a morphological feature of the developing profile and because of its potential effect on drainage and oxygen diffusion, the material lying between the depths of 0.99-1.48m was examined in fine detail. This includes the cemented layers and oxidised material between them; the cemented layer

at the boundary between visibly oxidised and unoxidised material; along with material beneath the boundary with little or no evidence of alteration.

0.99m depth - Pinkish grey layer

SEM/EDX investigations showed microscale graded bedding with regions of loose conglomerates of coarse anorthite, quartz and muscovite of average size 10-12µm, with intermittent denser regions of particles sized between 20 and 40µm. The denser region contained infilling of siliceous quartz, ferrihydrite and gypsum along with minor jarosite around orientated finer particles of biotite, muscovite and K feldspar (Fig 3C.14). XRD indicated the presence of all gangue minerals previously mentioned along with tremolite and confirmed the presence of gypsum.

1.03m depth - Brown silt layer

SEM/EDX investigations showed microscale graded bedding similar to 0.99m depth, but here the majority of the cementing is due to well-developed small rhombahedral crystals of jarosite (Fig 3C.15). The cement occurs throughout the profile although it concentrates along interlayers of fine orientated particles. XRD analysis suggested the presence of pyrite but SEM/EDX investigations did not verify this.

1.04m depth - Strongly cemented minor hard pan

SEM/EDX investigations indicate the cements present are a combination of ferrihydrite (Fig 3.31a), jarosite and schwertmannite (Fig 3.31b). Schwertmannite is present only as small groups of crystals, unlike the jarosite and ferrihydrite which make up the bulk of the material. XRD analysis confirm the presence of ferrihydrite and jarosite. K-alpha X-ray imaging was undertaken on this cemented layer (Fig 3.32). Large concentrations of Fe and minor S occur in the centre of the layer, corresponding to decreased amounts of Al and Si. The K-alpha image for the cemented layer at 1.04m indicates it is not a major region for absorption of cations leached from shallower regions. Also at this depth XRD indicated the presence of pyrite but it was not detected by SEM/EDX.

1.09m depth - Strongly cemented minor hard pan

Microscale graded bedding has dictated the development of this layer. Cracks have developed subsequent to sampling due to the occurrence of coarse loosely compacted

layers adjacent to the cemented areas. Cements have been concentrated in regions corresponding to a texture change ie. developed in the coarser material directly above a fine orientated sedimentary layer (Fig 3C.16). Cements are a combination of gypsum (Fig 3C.17 & Fig 3C.17a), jarosite and ferrihydrite (Fig 3C.18). SEM/EDX showed the typical hygroscopic nature of ferrihydrite, suggesting jarosite may only be a minor constituent to the cement in this case. This is supported by the spectrum collected using the SEM/EDX (Fig 3.34a) showing major Fe with only minor S and K in the system. Schwertmannite does not seem to be a main constituent in this cement as Fe/S ratio of 8:1 was not observed. XRD indicated that both chlorapatite and minor pyrite is also present at this depth.

1.13m depth - Strongly cemented layer

This sample showed a strong depositional hiatus with large 200um-400um particles being deposited on particles of less the 20um. In general the cement present in the finer textured layer is jarosite and gypsum with minor ferrihydrite as small pockets. XRD traces support their presence. XRD did not indicate any pyrite at this depth but chlorapatite was identified. The larger grains above the layer are strongly coated with jarosite and gypsum, but this coating is almost non existent below this layer. This is thought to be a function of deposition of suspended material as flow is restricted.

1.25m depth - Strongly cemented layer

Again cementing is dictated by textual changes down the profile. XRD indicates the cement is a mixture of ferrihydrite, gypsum and jarosite. SEM/EDX investigations also indicated the presence of opal (Fig 3C.19, 3C.19a & 3C.20) as a major cementing agent. Fig 3C.19a indicates a large quantity of Si with a minor jarosite signature. This spectrum along with the morphology of the cements suggest that opal is in fact a major constituent of the cement in this layer. XRD indicated the presence of pyrite and covellite. Covellite is a well documented CuS produced in AMD systems through the replacement of iron sulfide in shallow depths during oxidation. The formation can be represented as



1.27m depth - Uncemented region

Coatings of both jarosite and ferrihydrite were observed through SEM/EDX. XRD analysis confirms the presents of these and suggest the presence of bassanite. Bassanite ($\text{CaSO}_4 \cdot \text{H}_2\text{O}$) probably formed as a tertiary mineral during the sample preparation when heated in the oven. XRD also indicates the occurrence of tremolite at this depth, which is confirmed through SEM/EDX analysis (Fig 3C.21). XRD suggests the present of pyrite but SEM/EDX investigations were unable to confirm this. Covellite was identified just below this region through XRD at 1.34m depth. This again is indicative of fine particles of ferrihydrite and jarosite flowing suspended down the profile. Here they have coated the particles due to adsorption on negatively charged surfaces, but there is no textual changes so they haven't completely dropped out of suspension and formed a cemented layer.

1.37m depth - Boundary cemented layer between oxidised and reduced material forming a discrete well-developed cemented layer

The cement that makes up this layer varies in composition horizontally (Fig 3.33). Variations are thought to occur in response to infiltrating water flushing material downward and depositing it in channels and spaces between skeleton grains. This would effectively plug much of the lower horizon. Intermittent and repetitive infiltration appears to have alternated with times of evaporation which initiated the precipitation of secondary minerals. Variations in precipitation would be simply due to the prevailing conditions of the time, how saturated the solution was with respect to each mineral, and the flow path available for its movement.

SEM/EDX investigations indicate the cements present are a mixture of iron oxyhydroxide, minor jarosite and alunite. The hygroscopic morphology of the majority of the material suggests the iron oxyhydroxide is ferrihydrite, and XRD confirms this. Small areas of the layer show well-developed denser (increased atomic density) crystals of thin platy minerals (Fig 3.34). SEM/EDX investigations of this material indicate it is a iron oxyhydroxide, but presumably not ferrihydrite due to its distinctly different morphology (Fig 3.34a). Higher in the profile above the cemented layer, discrete crystals of jarosite and alunite occur as strong coatings of grains (Fig 3.35 & 3.35a). K-alpha X-ray imaging was undertaken on the boundary layer (Fig 3.36). This layer corresponds to the high concentrations of Fe and S. Fe and S are also present in large quantities above the layer as the material has leached down, become saturated and precipitated before reaching the discrete ferrihydrite band. A decrease is observed

directly below the cemented boundary layer. Unlike the cemented layer at 1.04m depth, this layer also shows high quantities of Al, Si, Ca & K. This indicates that the cement is acting as an entrapping material with Al, Si, Ca and K becoming incorporated into the layer.

Vermiculite was also observed at this depth and additionally at 1.38m depth through XRD. Vermiculite does not occur elsewhere in the profile and it is thought to have moved through the profile and its travel has been terminated because of the impervious nature of this cemented region. Its origin could be from wind blown soil prior to the dam covering or from relict weathering material formed in the mine prior to mining. It could also be a residue after prolonged acid neutralisation reactions of an aluminosilicate such as clinocllore. It is the deposition of this fine colloidal clay carried down by percolating waters that acts as a obstruction in many of the pore spaces and help to restrict the flow of mobile ions.

1.39-1.40m depth - Reduced material directly below the boundary.

Only very minor jarosite is present as coating to some pyrite grains (Fig 3C.22a). Trace amounts of copper-sulfur minerals are also present (Fig 3C.22 & 3C.22b). This is probably covellite as it was identified through XRD higher in the profile. XRD was unable to detect this material at this depth probably due to the minor amounts present. SEM/EDX also indicated the presence of apatite (Fig 3C.22c) in the tailings. Earlier observations would suggest this is actually chlorapatite.

1.47-1.48m depth -Reduced material representative of remaining reduced material.

This material is suggested to be representative of the remaining material down the profile (Fig 3C.23). This does not include the paleosurfaces present, nor the secondary minerals occurring at depth as ions are leached from the oxidised zone. Sulfides have increased in quantity and type. Pyrrhotite (Fig 3C.24 & 3C.24a) is present along with minor galena (Fig 3C.24b) and sphalerite (Fig 3C.24c).

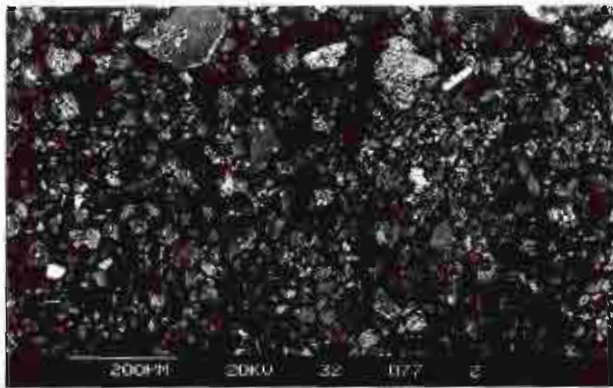


Fig 3C.11 Gangue minerals with coatings of jarosite and ferrihydrite - top 1m tailings.

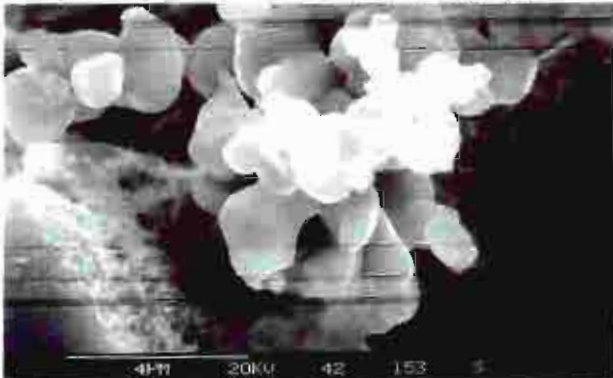


Fig 3C.13 Close up of iron oxyhydroxide cement, ferrihydrite within top 1m of tailings.

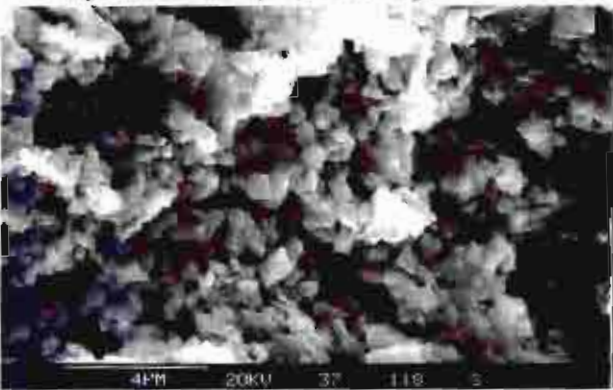


Fig 3C.15 Jarosite cement within brown silt layer at 1.03m depth.

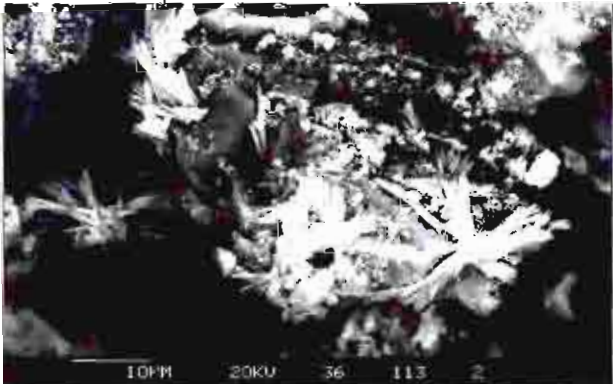


Fig 3C.17 Close up of gypsum crystals, within cemented layer at 1.09m depth.

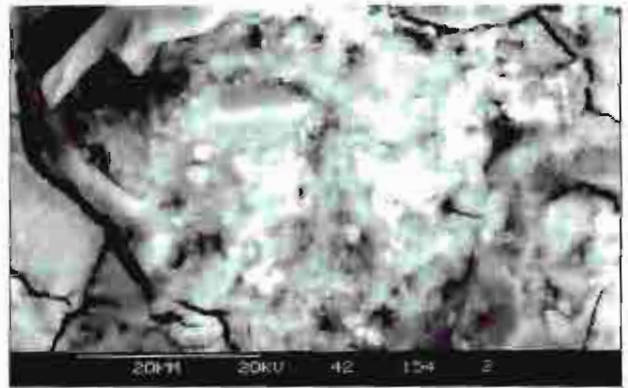


Fig 3C.12 Cement within top 1m of tailings, shows hygroscopic nature of ferrihydrite.

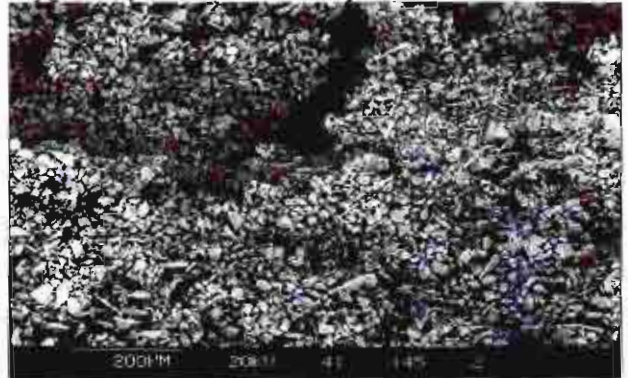


Fig 3C.14 Microscale graded bedding developed throughout tailings, but illustrated here at 0.99m.

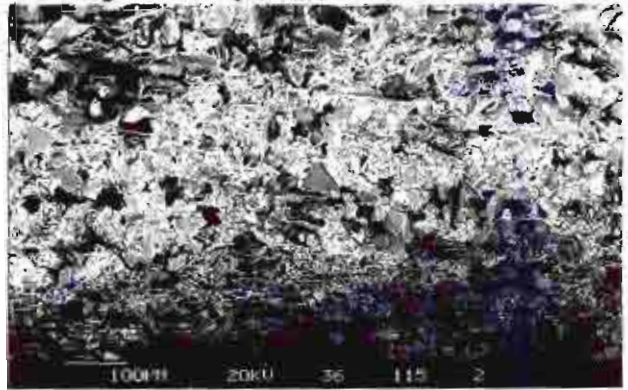


Fig 3C.16 Cement developed above textural variations.

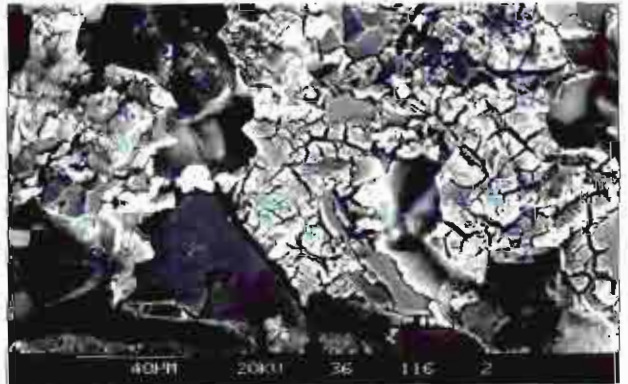


Fig 3C.18 Close up of hygroscopic ferrihydrite crystals within cemented layer at 1.09m depth.

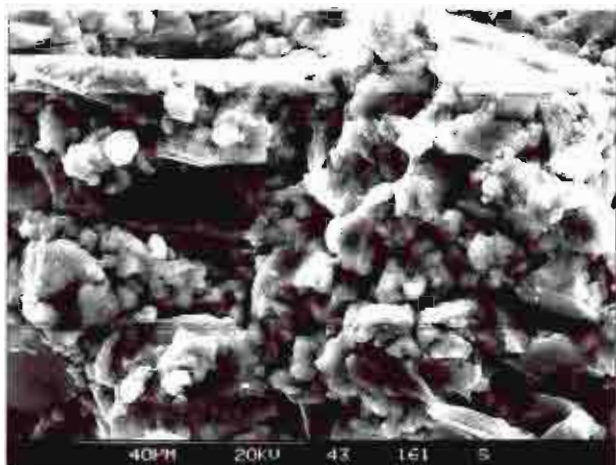


Fig 3C.19 Opal developed in cemented layer at 1.25m depth.

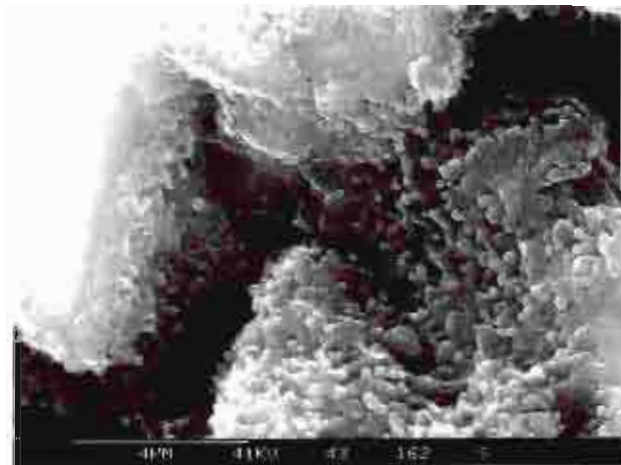


Fig 3C.20 Close up of opal cement at 1.25m depth.

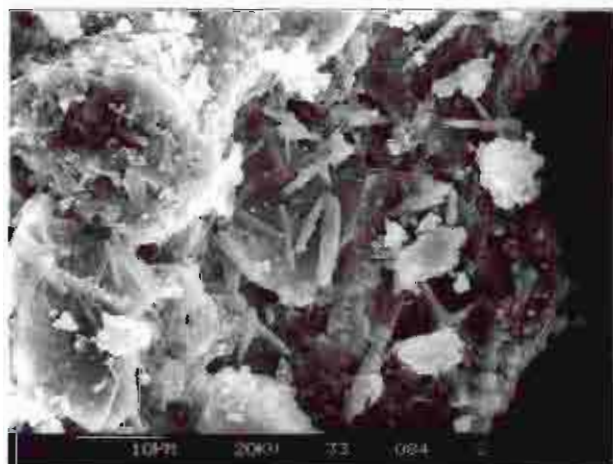


Fig 3C.21 Tremolite remnants of main ore, observed within an uncemented layer at 1.27m depth.

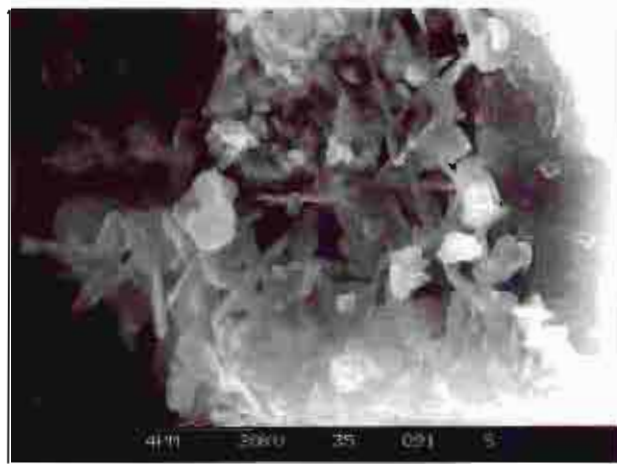


Fig 3C.22 Copper-sulfur mineral, probably covellite, developed as replacement product of iron sulfide, observed at 1.39-1.41m depth.

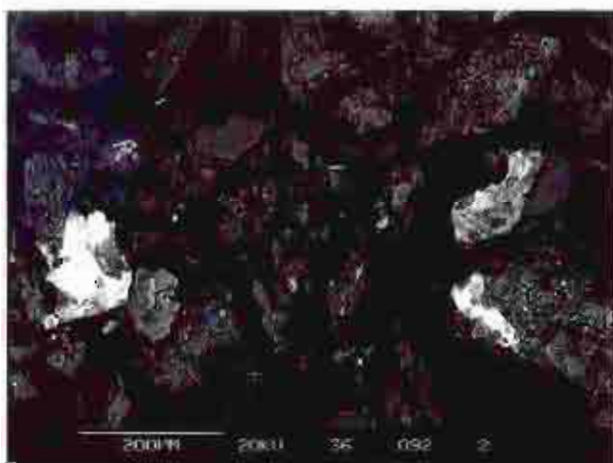


Fig 3C.23 Tailings within zone B, ie below main oxidised zone, 1.47-1.48m depth, larger quantities of sulfides, with little or no oxides present.

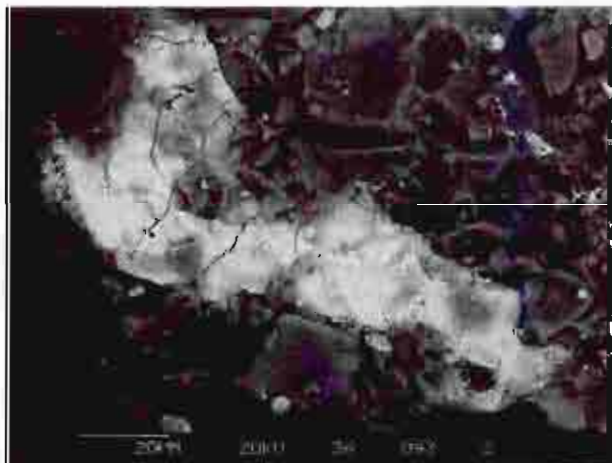


Fig 3C.24 Pyrrhotite, with minor galena and sphalerite present in unoxidised zone B, 1.47-1.48m depth.

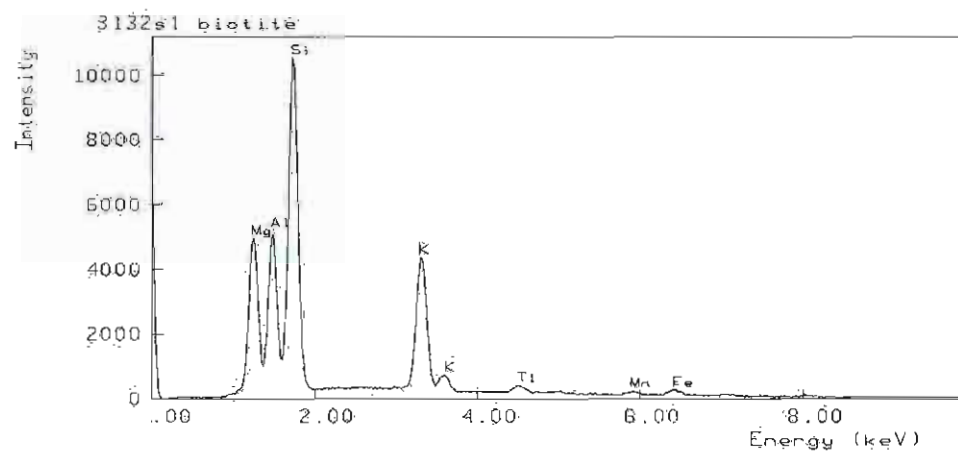


Fig 3C.11a

Biotite present
as gangue
mineral in top
1m of tailings.

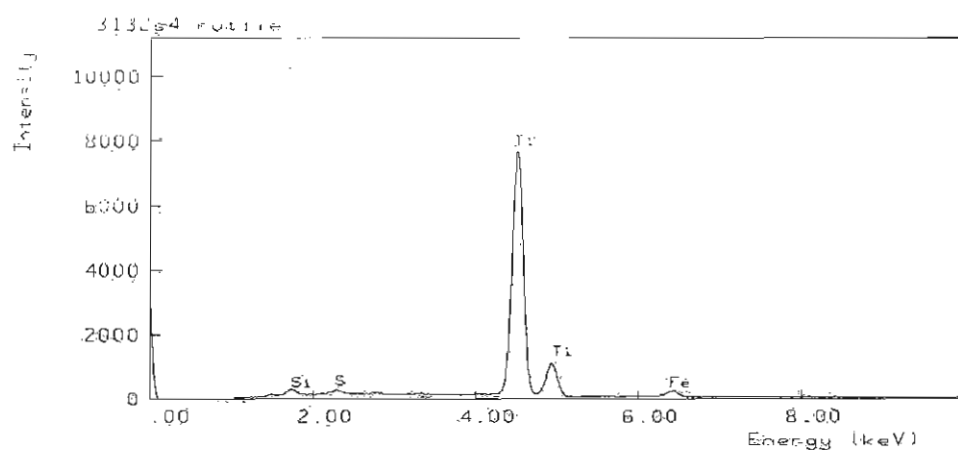


Fig 3C.11b

Rutile present
as gangue
mineral in top
1m of tailings.

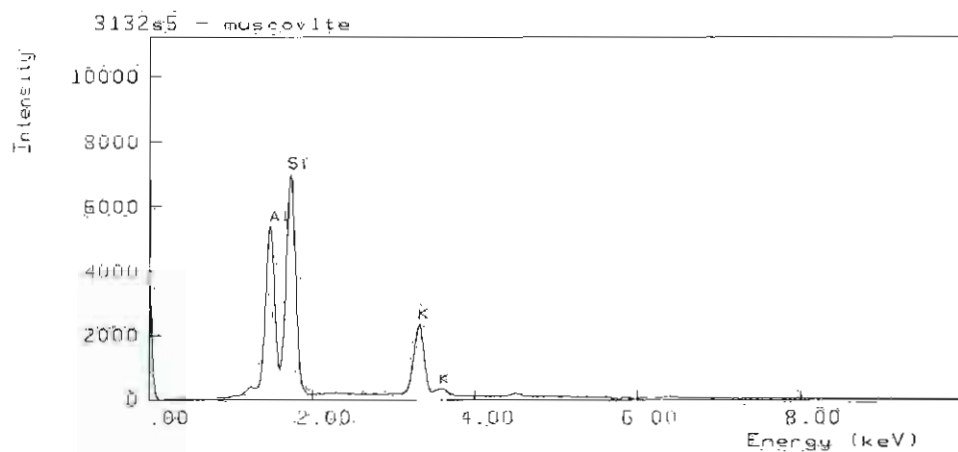


Fig 3C.11c

Muscovite
present as
gangue mineral
in top 1m of
tailings.

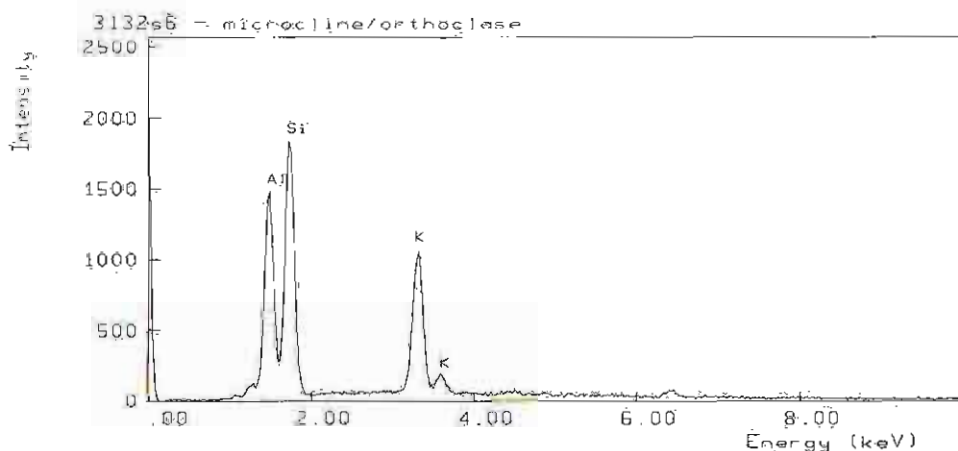


Fig 3C.11d

Feldspar
present as
gangue mineral
in top 1m of
tailings.

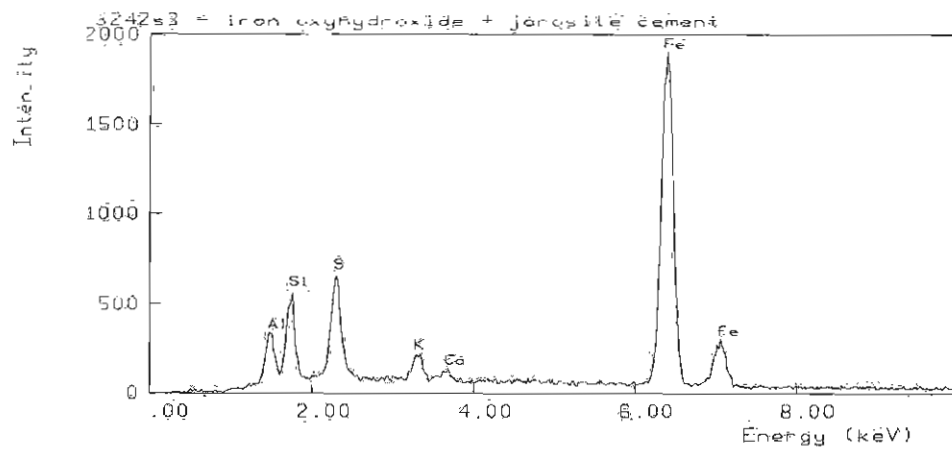


Fig 3C.12a

Iron oxyhydroxide : ferrihydrite and minor jarosite coatings on gangue minerals in top 1m of tailings

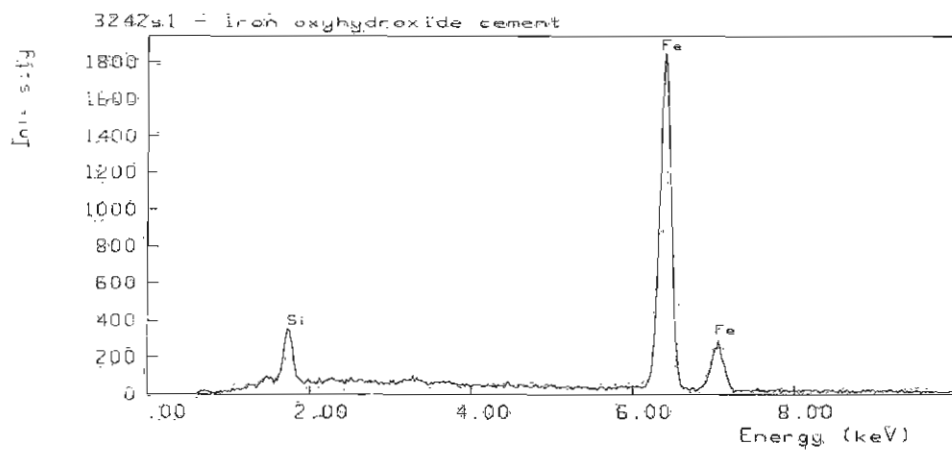


Fig 3C.13a

Dominant gangue mineral coating - Iron oxyhydroxide: ferrihydrite developed within top 1m of tailings

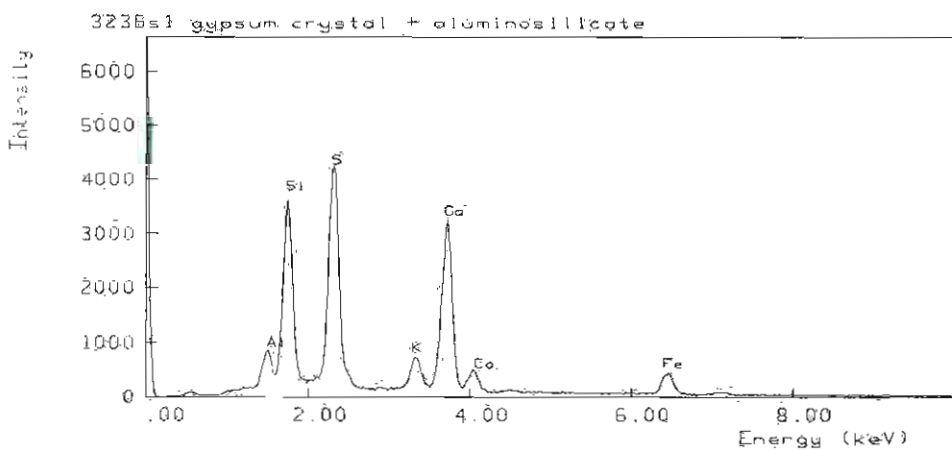


Fig 3C.17a

Gypsum developed in cemented layer at 1.09m depth

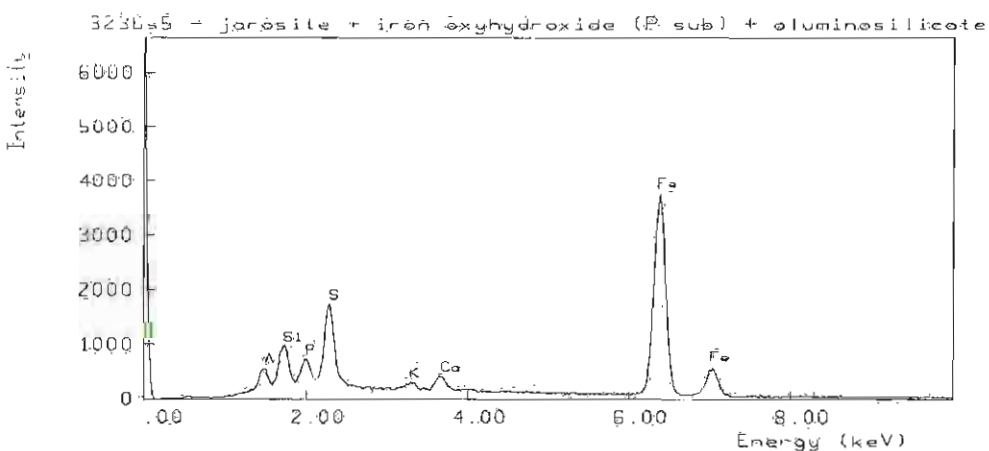


Fig 3C.18a

Iron oxyhydroxide: ferrihydrite and minor jarosite developed in cemented layer at 1.09m.

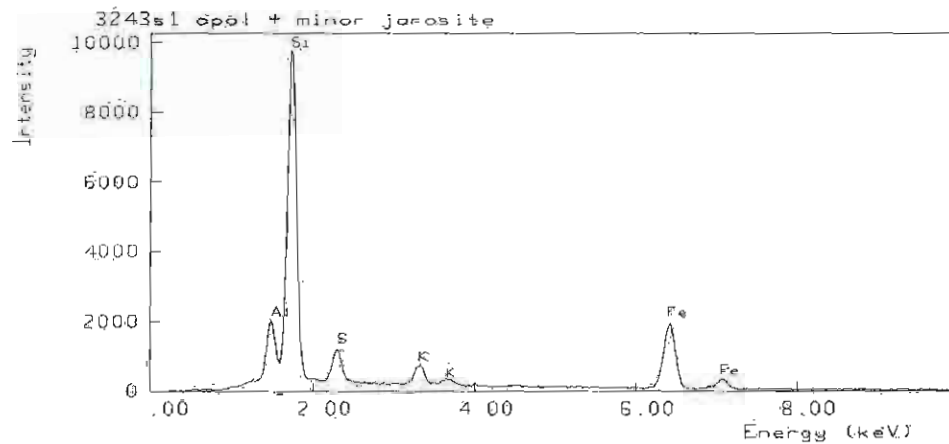


Fig 3C.19a

Opal and minor jarosite developed within cemented layer at 1.25m depth

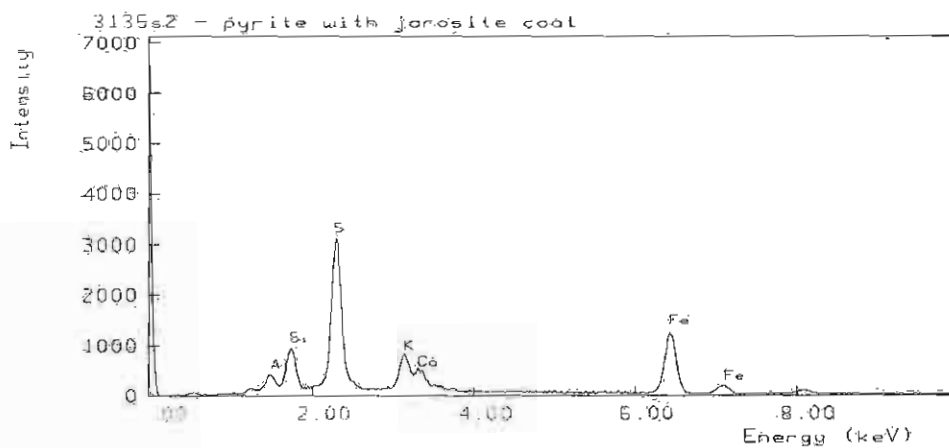


Fig 3C.22a

Pyrite crystals present within cemented boundary layer at 1.37m depth with jarosite coating.

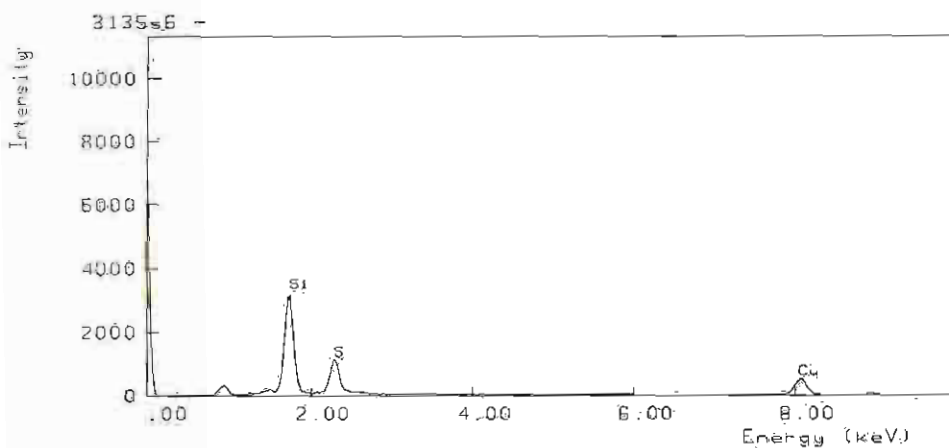


Fig 3C.22b

Copper sulfur mineral developed within cemented layer at 1.37m depth.

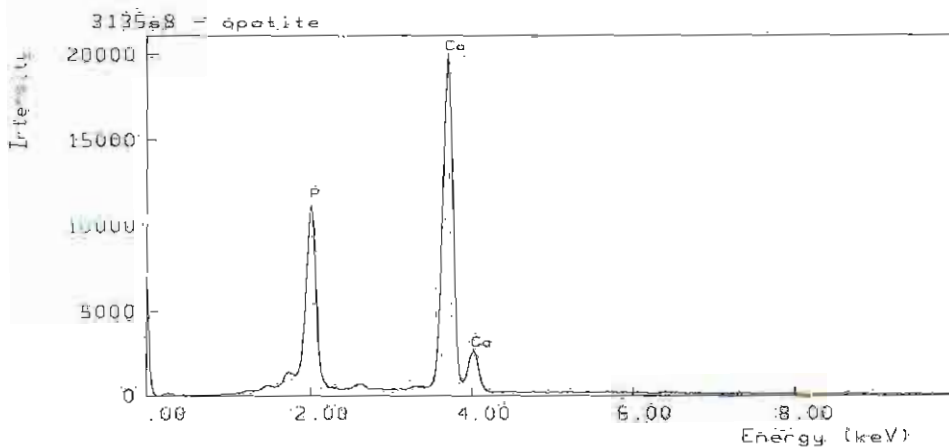


Fig 3C.22c

Apatite present within cemented layer at 1.37m depth.

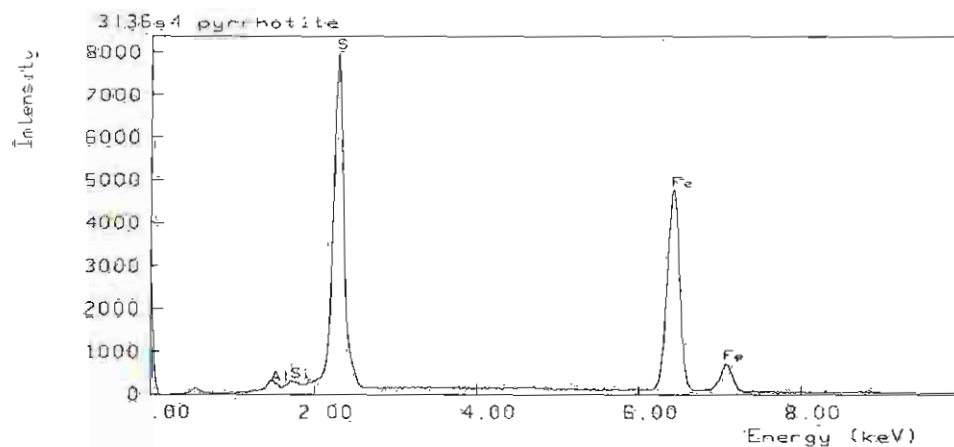


Fig 3C.24a

Pyrrhotite present in unoxidised material at 1.47m depth (below cemented boundary layer).

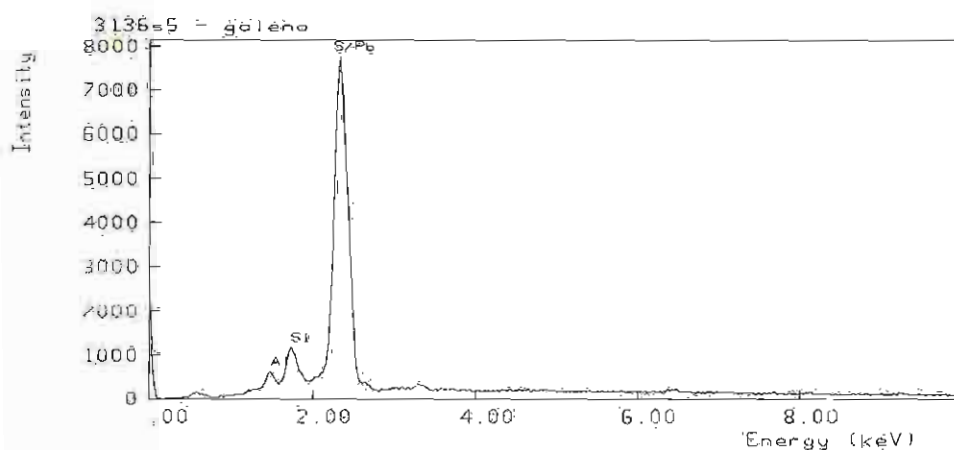


Fig 3C.24b

Galena present in unoxidised material at 1.47m depth (below cemented boundary layer).

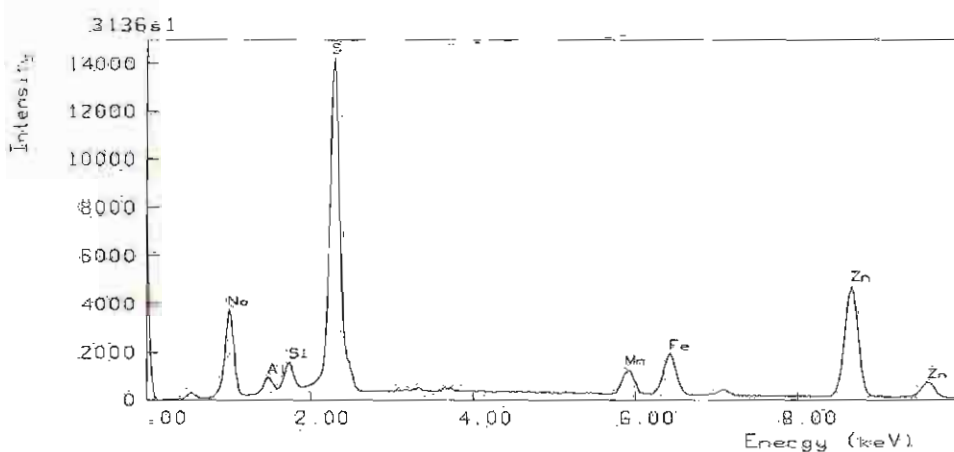


Fig 3C.24c

Sphalerite and contaminants present in unoxidised material at 1.47m depth (below cemented boundary layer).

Detailed Description of Tailings

An extensive description of colours, textures, pH, EC and moisture content observed down the profile follows, demonstrating the variability of the tailings material.

0-2cm	dark brown (10YR 3/3) organic top cover
2-18cm	brownish yellow (10YR 5/8) soil and waste rock
18-25cm	brownish yellow (10YR 5/8) loamy fine sand, pH 4, E.C.0.23/mS, moisture content 2%
25-85cm	dark yellowish brown (10YR 4/6) medium sand, pH 3.71, E.C 1.83/mS, moisture content 4.06%
85-92cm	predominantly brownish yellow (10YR 6/6) loamy medium sand with layers of light grey (5Y 7/1) silts, pH 3.75, E.C 2.46/mS, moisture content 11.15%

CORE 1 0.92--1.23m

Mixture of fine grained sand and silt size interlayers of material, highly oxidised material not restricted to either texture. Only pink grey (5YR 6/2) and a brown (7.5YR 5/4) restricted to silt, all other colours developed in all texture types. Because of the range of colours observed and the intricate nature of the sample, it was decided to obtain identification of the colour range present in each section see Fig 3.27 for positioning.

0.92-1.02m	7.5YR 8/2 pinkish white 7.5YR 7/2 pinkish grey 10YR 5/8 yellowish brown 10YR 6/8 brownish yellow 10YR 7/8 yellow 10YR 8/8 yellow
1.02-1.04m	7.5YR 5/4 brown
1.04-1.05m	2.5YR 6/0 light grey
1.05-1.06m	5Y 7/3 pale yellow
1.06-1.08m	7.5YR 7/1 light grey
1.12-1.22m	10YR 5/8 yellowish brown 10YR 6/8 brownish yellow 10YR 7/8 yellow 10YR 8/8 yellow
1.22-1.25m	5YR 6/2 pinkish grey
1.25-1.27m	10YR 6/1 light grey
ave. pH 3.9, ave. E.C 1.07/mS	

Core 2 1.24-1.61m

Predominantly medium sand with minor layers of fine sand and silts.

1.24-1.38m In this upper oxidised zone layers are formed via different oxidation state which is not restricted to any texture type. This oxidised zone has a mixture of colours including

2.5Y 8/8 yellow

10YR 8/8 yellow brown

10YR 7/6 yellow

10YR 6/1 light grey

10YR 8/3-7/3 pale to very pale grey

1.38-1.40m The boundary between oxidised and reduced is predominantly medium sand and minor fine sand, colours include

7.5 YR 6/8 reddish brown

7.5YR 5/6 strong brown

1.40-1.61 In this reduced region, layers are observed in silts only, the majority of material being medium sand with minimal variation.

1.40-1.45m 2.5Y 3/1 very dark grey

1.45-1.61m 2.5 Y 3/1 very dark grey

2.5Y 4/1 dark grey

2.5Y 5/1 grey

2.5Y 6/1 light grey

ave pH 3.62, ave E.C 1.84/mS

1.6-1.69m predominantly olive (5Y 4/3) with minor amounts of yellow (2.5Y 7/6) medium sand, pH 4.04, E.C. 2.03/mS, moisture content 6.25%

1.69-1.85m predominantly very dark grey (5Y 3/1) with minor amounts of yellow (2.5Y 7/6) loamy medium sand, pH 3.87, E.C. 3.7/mS, moisture content 6.6%

1.85-1.9m	silt layers of varying colours, (mm scale)	dark grey grey light grey grey	(2.5Y 4/0) (2.5Y 5/0) (10YR 7/1) (10YR 6/1)
	pH 3.78, E.C.1.67/mS, moisture content 14.81%		

1.9-1.97m dark grey (2.5Y 4/0) loamy fine sand, pH 3.78, E.C. 1.67/mS, moisture content 7.92%

1.97-2.1m dark grey (2.5Y 4/0) loamy medium sand, pH 3.95, E.C. 1.3/mS, moisture content 6.63%

2.1-2.14m	silt layers of varying colour, (mm scale)	grey dark grey yellow	(2.5Y 5/0) (2.5Y 4/0) (2.5Y 7/6)
	pH 4.04, E.C. 1.34/mS, moisture content 5.13%		

2.14-2.17m grey (5Y 5/1) loamy fine sand, pH 4.04, E.C. 1.34/mS, moisture content 5.13%

Appendix C2 Detailed Tailings Mineralogy

2.17-2.22m	grey (5Y 5/1) and dark grey (2.5Y 4/0) loamy medium-fine sand, pH 3.8, E.C.1.52/mS, moisture content 11.96%
2.22-2.28m	olive grey (5Y 5/2) loamy fine sand, pH 3.67, E.C. 2.39/mS, moisture content 6.29%
2.28-2.39m	dark grey (5Y 4/1) loamy fine sand, pH 3.94, E.C. 1.65/mS, moisture content 5.41%
2.39-2.48m	a mixture of dark olive grey (5Y 3/2) and yellow (2.5Y 7/6) loamy fine-medium sand, pH 4.06, E.C. 1.45/mS, moisture content 7.02%
2.48-2.55m	mixture of yellow (2.5Y 7/6) loamy fine- medium sand and light grey (5Y 7/1) to grey (5Y 6/1) silts, pH 4.05, E.C. 1.71/mS, moisture content 10.34%
2.55-2.67m	mixture of olive (5Y 4/3) fine-medium sand and light grey (5Y 7/1) to grey (5Y 6/1) silts, pH 4.18, E.C. 1.47/mS, moisture content 11.31%
2.67-2.7m	olive grey (5Y 4/2) loamy fine sand, pH 4.04, E.C. 1.52/mS, moisture content 11.03%
2.7-2.95m	grey (5Y 5/1) to olive grey (5Y 5/2) loamy fine - medium sand, pH 4.25, E.C. 1.42/mS, moisture content 13.95%
2.95-3.15m	yellowish brown (10YR 5/5) loamy fine-medium sand, pH 3.73, E.C. 2.58/mS, moisture content 7.67%
3.15-3.35m	a mixture of olive (5Y 4/3) and yellow (2.5Y 7/6) loamy fine sand, pH 3.75, E.C. 6.72/mS, moisture content 6.1%
3.35-3.55m	a mixture of dark greyish brown (2.5Y 4/2)loamy fine sand and light grey (5Y 7/2), pale yellow (5Y 7/4) and yellow (2.5Y 7/6) silt, pH 3.45, E.C. 1.98/mS, moisture content 9.57%
3.55-3.67m	dark grey (5Y 4/1) to very dark grey (5Y 3/1) loamy medium sand, pH 3.56, E.C. 1.51/mS, moisture content 6.98%
3.67-4.10m	very dark grey (5Y 3/1) loamy medium sand, pH 3.78, E.C. 0.88/mS, moisture content 6.81%
4.10-4.27m	olive grey (5Y 4/2) and dark olive grey (5y 3/2) medium sand, pH 4.12, E.C. 1.51/mS, moisture content 4.81%
4.27-4.32m	olive grey (5Y 4/2) medium sand, pH 4.08, E.C. 0.92/mS, moisture content 6.05%

Appendix C2 Detailed Tailings Mineralogy

4.32-4.37m	silt layers of varying colour, (mm scale)	olive yellow pale yellow light grey dark grey	(2.5Y 6/8) (5Y 7/4) (5Y 7/2) (5Y 4/1)
	pH 3.47, E.C. 1.32/mS, moisture content 10.14%		
4.37-4.39m	olive (5Y 5/3) loamy fine-medium sand, pH 3.47, E.C. 1.32/mS, moisture content 10.14%		
4.39-4.41m	silts layers of varying colour, (mm scale)	olive grey olive olive light grey grey olive yellow	(5Y 5/2) (5Y 5/3) (5Y 4/3) (5Y 6/1) (5Y 5/1) (5Y 6/6)
	pH 3.48, E.C. 1.48/mS, moisture content 11.45%		
4.41-4.51m	olive grey (5Y 4/2) medium sand, pH 3.79, E.C. 1.29/mS, moisture content 6.11%		
4.51-4.66m	dark olive grey (5Y 3/2) medium sand, pH 3.99, E.C. 1.02/mS, moisture content 8.13%		
4.66-4.76m	layers of sand (2-5mm thick) and silts (.5-1mm thick) of varying colour,	dark grey grey light grey light olive grey	(5Y 4/1) (5Y 5/1) (5Y 6/1) (5Y 6/2)
	pH 3.96, E.C. 1.03/mS, moisture content 8.23%		
4.76-4.82m	dark olive grey (5Y 3/2) loamy medium sand, pH 3.93, E.C. 1.02/mS, moisture content 5.05%		
4.82-5.18m	dark olive grey (5Y 3/2) medium sand, pH 3.89, E.C. 1.07/mS, moisture content 4.43%		
5.18-5.25m	loamy fine sand layers of varying colour,	pale yellow brownish yellow light grey olive grey olive	(5Y 7/3) (10YR 6/8) (5Y 6/1) (5Y 5/2) (5Y 5/3)
	pH 3.4, E.C. 2.66/mS, moisture content 11.02%		
5.25-5.41m	olive (5Y 3/2) fine-medium sand, pH 3.31, E.C. 1.72/mS, moisture content 14.2%		

Appendix C2 Detailed Tailings Mineralogy

5.41-5.55m	a mixture of light olive brown (2.5 Y 5/6 & 5/4) loamy fine -medium sand with grey (5Y 3/1) and pale yellow (5Y 7/4) silts, pH 3.47, E.C. 2.28/mS, moisture content 7.66%		
5.55-5.89m	olive (5Y 4/3) loamy medium sand, pH 4.07, E.C. 1.12/mS, moisture content 4.62%		
5.89-5.98m	a mixture of olive (5Y 5/4) silts and olive (5Y 5/3) loamy fine-medium sand, pH 3.54, E.C. 1.72/mS, moisture content 5.9%		
5.98-6.15m	olive (5Y 4/4) loamy medium sand, pH 3.88, E.C. 1.24/mS, moisture content 5.25%		
6.15-6.22m	a mixture of olive (5Y 4/4) loamy medium sand and loamy fine sand layers of varying colour, (mm scale)	grey olive yellow light olive brown greyish brown	(2.5Y 5/0) (2.5Y 6/6) (2.5Y 5/3) (2.5Y 5/2)
	pH 3.74, E.C. 1.61/mS, moisture content 6.16%		
6.22-6.4m	silt layers of varying colour, (mm scale)	grey olive yellow light olive brown greyish brown	(2.5Y 5/0) (2.5Y 6/6) (2.5Y 5/3) (2.5Y 5/2)
	pH 3.92, E.C. 1.2/mS, moisture content 5.24%		
6.4-6.49m	loamy fine sand layers of varying colour, (.5-2mm scale)	light olive brown grey pale yellow light yellowish brown light olive brown	(5Y 5/3) (5Y 5/1) (5Y 7/4) (5Y 6/3) (5Y 5/3)
	pH 3.51, E.C. 1.8/mS, moisture content 20.77%		
6.49-6.59m	a mixture of grey (5Y 5/1) and light olive brown (5Y 5/4) loamy fine sand, pH 3.01, E.C. 2/mS, moisture content 22.08%		
6.59-6.75m	layer of fine sand and silts of varying colour,	light olive brown olive grey brownish yellow pale olive	(2.5Y 5/6) (5Y 5/2) (10YR 6/6) (5Y 6/3)
	pH 3.39, E.C. 1.59/mS, moisture content 13.51%		

Appendix C2 Detailed Tailings Mineralogy

6.75-6.87m saturated loamy fine sand layers of varying colours,
grey (5Y 5/1)
olive grey (5Y 5/2)
grey (2.5Y 5/0)
dark grey (2.5Y 6/3)
pH 3.46, E.C. 1.77/mS, moisture content 28.23%

CORE 6.87-7.12m

6.87-6.93m loamy fine sand and intermittent (3mm) layers of medium sand
6.93-6.96m medium sand
6.96-7.12m loamy fine sand and intermittent (3mm) layers of medium sand

Minor sand layers occur above major yellow brown oxidised bands

Slight cementing at 7.01-7.02m oxidised layer, other oxidised layers show no cementing. Colours of oxidised layers include

7.5 YR 5/6 strong brown
10YR 6/6 brownish yellow
10YR 6/4 light brownish yellow
10YR 6/3 pale brown
10YR 5/3 brown
2.5Y 7/4 pale yellow

The majority of the profile is reduced, colours include

5Y 3/1 very dark grey
5Y 4/1 dark grey
5Y 5/1 grey
5Y 6/1 light grey

ave pH 3.45, ave E.C 1.85, moisture content 23.9%

7.20-7.27m olive (5Y 4/3) loamy fine sand,
pH 3.46, E.C. 1.77/mS, moisture content 28.08%

7.27-7.34m dark grey (2.5Y 4/1) and grey (2.5Y 5/1) loamy fine sand,
pH 3.44, E.C. 1.99/mS, moisture content 31.45%

7.34-7.44m olive grey (5Y 4/2) medium sand,
pH 3.88, E.C. 1.39/mS, moisture content 4.6%

7.44-7.69m olive grey (5Y 4/2) loamy fine sand,

7.69-7.79m a mixture of dark greyish brown (2.5Y 4/2) loamy fine-medium sand
and silt of varying colour
olive yellow (2.5Y 6/6)
pale yellow (2.5Y 7/3)
light yellowish brown (2.5Y 6/4)
light grey (2.5Y 7/2)
pH 3.4, E.C. 1.85/mS, moisture content 17.21%

7.79-7.88m light olive brown (2.5Y 5/6) loamy fine sand,
pH 2.52, E.C. 2.89/mS, moisture content 15.32%

Appendix C2 Detailed Tailings Mineralogy

7.88-7.97m	a mixture of dark greyish brown (2.5Y 4/2) and light olive brown (2.5Y 5/6) medium sand with layered silts of varying colour	olive yellow (2.5Y 6/6) light grey (2.5Y 7/2) light grey (2.5Y 7/1)
7.97-8.05m	layered loamy fine sand	olive yellow (2.5Y 6/6) dark greyish brown (2.5Y 4/2) light olive brown (2.5Y 5/6) light grey (2.5Y 7/1)
	pH 3.44, E.C. 1.67/mS, moisture content 8.43%	
8.05-8.15m	dark olive grey (5Y 3/2) loamy fine-medium sand	
8.15-8.24m	olive grey (5Y 4/2) loamy fine sand	
8.24-8.35m	a mixture of olive (5Y 5/3) and olive grey (5Y 4/2) loamy fine sand, pH 3.34, E.C. 2.42/mS, moisture content 22.18%	
8.35-8.45m	olive grey (5Y 5/3) loamy fine sand	
8.45-8.57m	dark olive grey (5Y 4/2) loamy medium sand	
8.57-8.68m	dark olive grey (5Y 3/2) medium sand, pH 4.06, E.C. 1.14/mS, moisture content 24.38%	
8.68-8.96m	dark olive grey (5Y 3/2) loamy fine sand	
8.96-9.05m	a mixture of olive (5Y 5/3) and olive grey (5Y 4/2) loamy fine sand, pH 3.52, E.C. 1.96/mS, moisture content 21.16%	
9.05-9.13m	a mixture of olive (5Y 5/3 & 4/2) loamy fine sand, moisture content 2.42%	
9.13-9.27m	a mixture of olive (5Y 5/4) and grey (5Y 5/1) loamy fine sand, pH 3.71, E.C. 2.71/mS, moisture content 11.9%	
9.27-9.37m	grey (5Y 5/1) loamy fine sand, pH 3.71, E.C. 2.71/mS, moisture content 11.9%	
9.37-9.45m	increased water content, dark grey (5Y 4/1) loamy fine sand, pH 3.41, E.C. 1.51/mS, moisture content 12.91%	
9.45-9.53m	decreased water content, dark grey (5Y 4/1) loamy fine sand, pH 4.06, E.C. 3.93/mS, moisture content 31.38%	
9.53-9.6m	water content decreased further, grey (5Y 4/1) loamy fine sand, pH 3.07, E.C. 2.48/mS, moisture content 14.65%	

Appendix C2 Detailed Tailings Mineralogy

9.6-9.68m	saturated dark grey (5Y 4/1) loamy fine sand, pH 3.25, E.C. 3.03/mS, moisture content 30.37%
9.68-9.77	dark grey (5Y 4/1) silt, pH 2.9, E.C. 3.13/mS, moisture content 26.03%
9.77-9.86m	free water observed in a mixture of olive grey (5Y 4/2) fine sand and layered silts of grey (5Y 5/1) and dark grey (5Y 5/2), pH 3.56, E.C. 3.47/mS, moisture content 20.93%
9.86-9.95m	saturated olive grey (5Y 4/2 & 5/2) loamy fine sand, pH 2.8, E.C. 3.45/mS, moisture content 28.47%
9.95-10.02m	a mixture of olive grey (5Y 4/2) and dark grey (2.5Y 4/0) loamy fine sand, pH 2.75, E.C. 3.97/mS, moisture content 25.89%
10.02-10.08	a mixture of very dark grey (2.5Y 3/0) and grey (5Y 5/1) silt, pH 3.04, E.C. 2.87/mS, moisture content 13.97%
10.08-10.18m	saturated dark grey (5Y 4/1 & 2.5Y 4/0) silt, pH 3.11, E.C. 3.04/mS, moisture content 23.82%
10.18-10.25m	predominantly dark olive grey (5Y 3/2) fine sand with a layered silt sequence of varying colour <div style="display: flex; justify-content: flex-end; align-items: center; margin-left: 20px;"> <div style="text-align: right; margin-right: 10px;">dark grey very dark grey olive</div> <div style="text-align: left;">(5Y 4/1) (2.5Y 3/0) (5Y 5/3)</div> </div> pH 3.45, E.C. 2.15/mS, moisture content 13.88%
10.25-10.33m	mixture of olive grey (5Y 4/2) and olive (5Y 5/3) loamy fine sand, pH 3.55, E.C. 1.42/mS, moisture content 9.53%
10.33-10.45m	mixture of grey (2.5Y 5/0) silt and olive (5Y 4/3) fine sand, pH 3.4, E.C. 1.58/mS, moisture content 12.31%
10.45-10.52m	dark olive grey (5Y 3/2) fine sand, pH 3.5, E.C. 1.53/mS, moisture content 9.56%
10.52-10.59m	predominantly dark olive grey (5Y 3/2) to olive grey (5Y 4/2) fine-medium sand, with lenses of light olive brown (2.5Y 5/6) silt, oxidised in situ, pH 3.47, E.C. 1.75/mS, moisture content 11.38%
10.59-10.68m	layered silt sequence of varying colour <div style="display: flex; justify-content: flex-end; align-items: center; margin-left: 20px;"> <div style="text-align: right; margin-right: 10px;">grey light olive brown dark brown dark greyish brown</div> <div style="text-align: left;">(5Y 5/1) (2.5Y 5/6) (10YR 3/3) (2.5Y 4/2)</div> </div> pH 3.48, E.C. 2.93/mS, moisture content 30.7%

Appendix C2 Detailed Tailings Mineralogy

10.68-10.77m predominantly olive grey (5Y 4/2) fine-medium sand with layered silt
sequence of varying colour light olive brown (2.5Y 5/3)
dark grey (2.5Y 4/0)
olive grey (5Y 5/2)
pH 3.34, E.C. 1.73/mS, moisture content 26.02%

10.77-10.83m dark greyish brown (2.5Y 4/2) silt,
pH 3.64, E.C. 2.56/mS, moisture content 29.5%

CORE 10.83-11.3m

10.89-10.93m brown (7.5YR 5/2) and grey (7.5YR 5/1) silt

10.93-11.07m a mixture of dark reddish grey (5Y 4/2), brown (7.5 YR 5/2), grey (7.5YR 5/1) and light olive brown (2.5Y 5/3) loamy fine sand

11.07-11.16m dark grey (2.5YR 4/1) medium sand

11.16-11.30m dark reddish grey (5Y 4/2) loamy fine sand
ave pH 3.75, E.C 0.72/mS, moisture content 32.2%

11.3-11.37m increased water content in dark greyish brown (2.5Y 4/2) loamy fine sand, pH 3.49, E.C. 2.46/mS, moisture content 29.5%

11.37-11.45m further increased water content in layered silt sequence of varying colour dark greyish brown (2.5Y 4/2) grey (5Y 5/1)
pH 3.29, E.C. 2.46/mS, moisture content 28.56%

11.45-11.53m mixture of grey (5Y 5/1) silt and olive grey (5Y 4/2) loamy fine-medium sand, pH 3.18, E.C. 2.92/mS, moisture content 22.92%

11.53-11.65m mixture of dark grey (5Y 4/1) loamy medium-fine sand and grey (5Y 5/1) silt, pH3.51, E.C. 2.82/mS, moisture content 24.27%

11.65-11.75m saturated grey (5Y 5/1) loamy fine sand,
pH 3.42, E.C. 4.1/mS, moisture content 50.49%.

11.75-11.87m saturated dark grey (5Y 4/1) loamy medium sand,
pH 3.79, E.C. 3.38/mS, moisture content 41.13%

11.87-11.95m saturated dark grey (5Y 4/1) loamy fine sand,
pH 3.64, E.C. 2.49/mS, moisture content 28.32%

12-12.5m CORE

12.01-12.05m dark grey (5Y 4/1) loamy fine sand
12.05-12.06m very dark greyish brown (2.5Y 3/2) silt
12.06-12.11m dark grey (5Y 4/1) loamy fine sand
12.11-12.15m dark olive grey (5Y 3/2) loamy fine sand-silt
12.15-12.20m dark to very dark grey (5Y 4/1 & 3/1) loamy fine sand
12.20-12.21m olive grey (5Y 5/2) silt
12.21-12.25m dark to very dark grey (5Y 4/1 & 3/1) loamy fine sand
12.25-12.27m olive grey (5Y 5/2) silt
ave pH 3.22, ave E.C 2.16/mS, moisture content 23.9%, ave. Eh 127 mv

12.5-13m CORE

12.50-12.57m dark grey (5Y 4/1) medium sand
12.57-12.82m interbanded fine to medium sands with silts of varying colour
sand 5Y 4/1 dark grey
5Y 5/1 grey
silt 5Y 6/2 light olive grey
5Y 6/1 grey
5Y 7/2 light grey
ave pH 2.56, ave E.C 0.89/mS, moisture content 23.9%, ave. Eh 11.5 mv

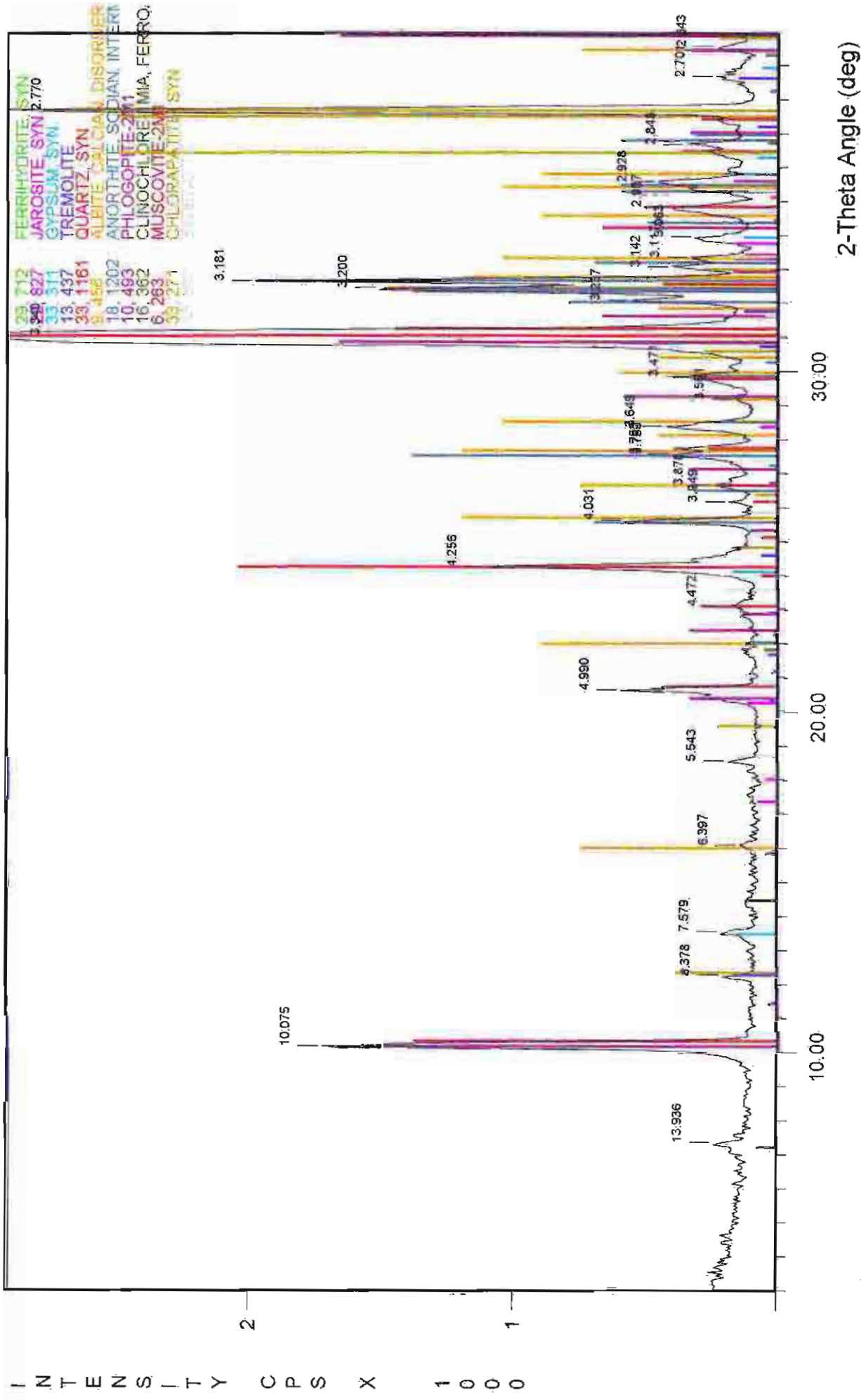
14-14.5m CORE

14.0-14.05m mainly grey (5Y 5/1) loamy fine sand, with single bands of olive grey (5Y 5/2) and dark olive grey (5Y 3/2)
14.05-14.15m dark grey (5Y 4/1) to very dark grey (5Y 3/1) fine - medium sand
14.15-14.17m dark grey (5Y 4/1) silt
ave pH 3.98, ave E.C 0.73/mS, moisture content 22.5%, ave. Eh 24 mv

17.5-18m CORE

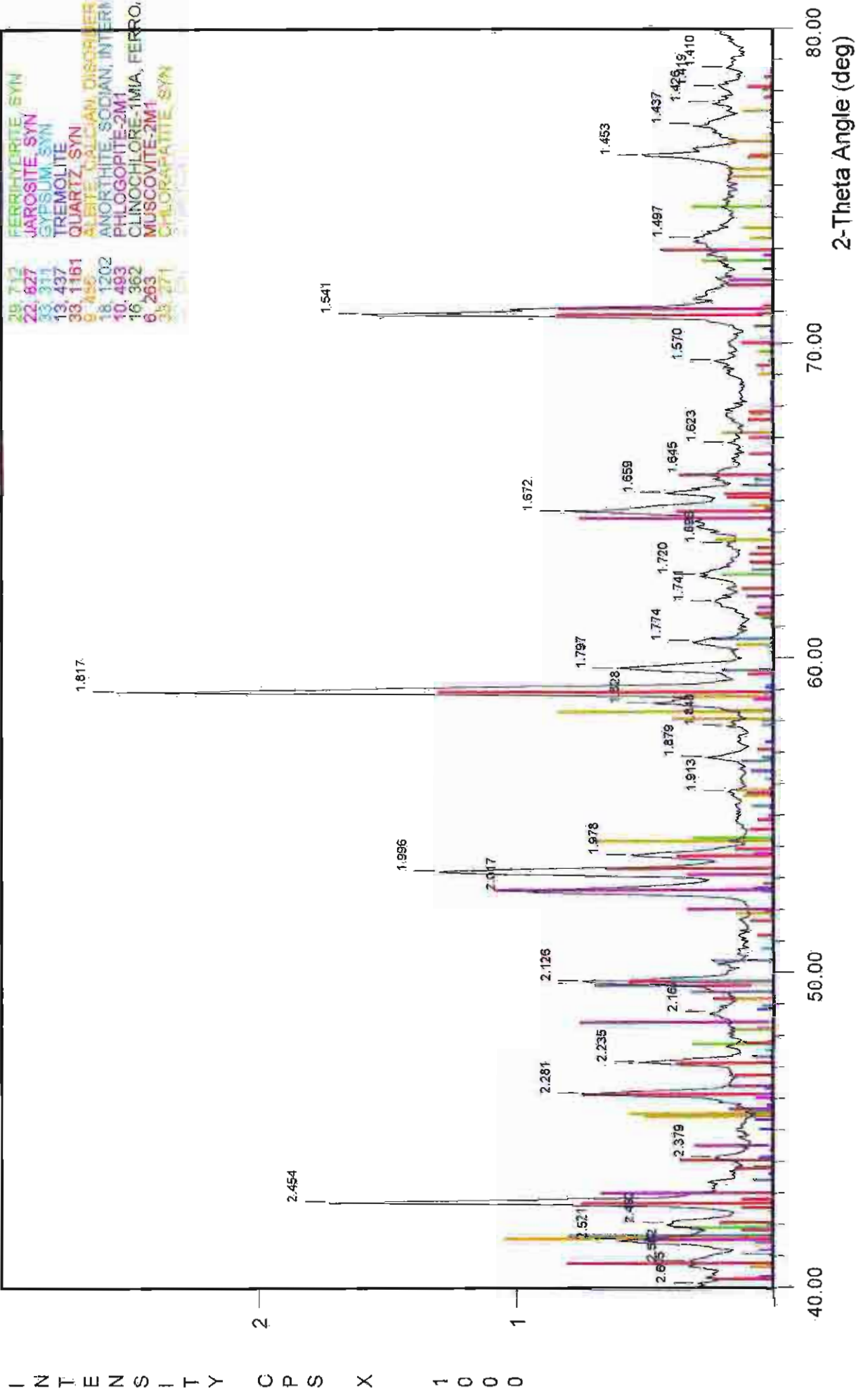
17.5-17.6m tailings base: brown (7.5YR 5/2) medium sand plus gravel
pH 4.09, E.C 2.2/mS, moisture content 21.7%, Eh
17.6-17.65m tailings base brown (7.5YR 5/2) loamy fine-medium sand
17.65-17.76m redoximorphic depletion zone, dark grey (5Y 3/1) to dark olive grey (5Y 3/2) loamy fine-medium sand matrix with mottles of yellowish brown (10YR 5/4) and strong brown (7.5YR 4/4) colour.
pH 4.02, E.C 1.94/mS, moisture content 21.7%, ave. Eh 135.3 mv
17.76-17.85m redoximorphic accumulation zone, dark grey (5Y 3/1) to dark olive grey (5Y 3/2) loamy fine-medium sand matrix with mottles of varying colours including
2.5 YR 4/6 red
2.5YR 4/4 reddish brown
7.5 YR 5/6 strong brown
7.5YR 5/6 strong brown
7.5YR 6/6 reddish yellow
10YR 6/6 brownish yellow
pH 4.02, E.C 1.93/mS, moisture content 21.9%, ave. Eh 124 mv.

0.65-0.70m brownish yellow fine-medium sand



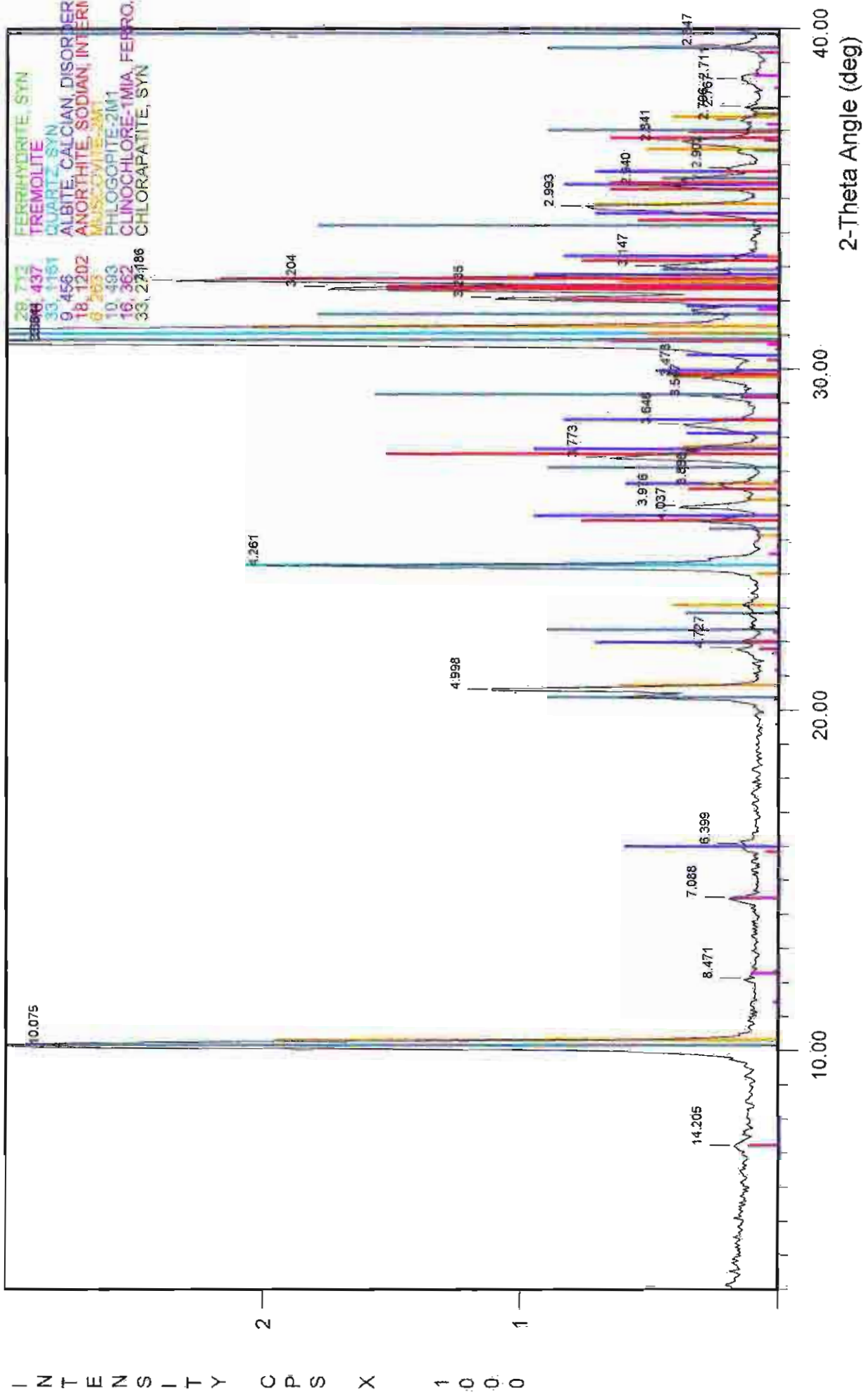
File Name: A:\0.68M

0.65-0.70m brownish yellow fine-medium sand



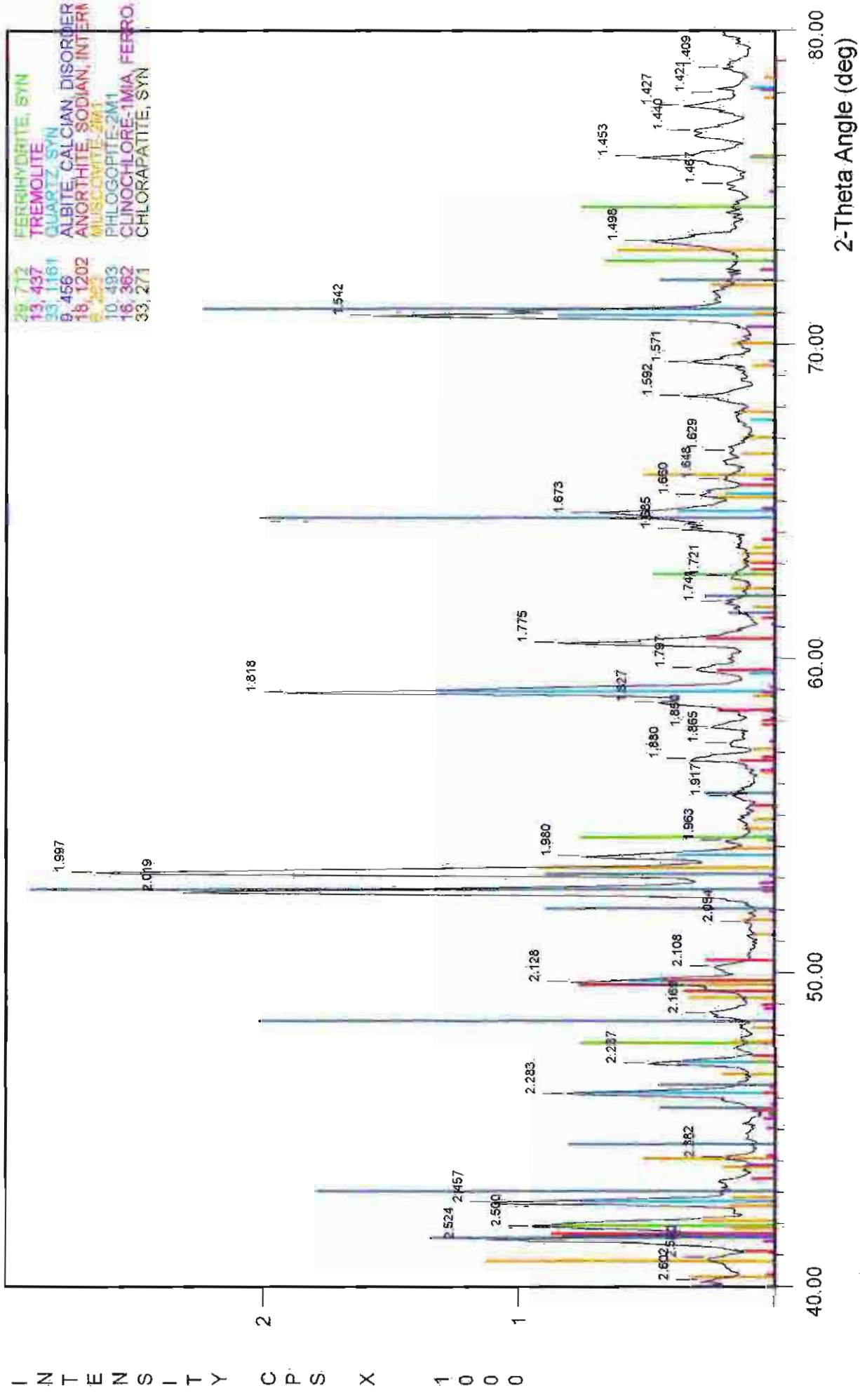
File Name: A:10.68M

98cm orange medium sand layer



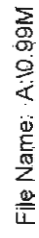
File Name: A:\0.98M

98cm orange medium sand layer

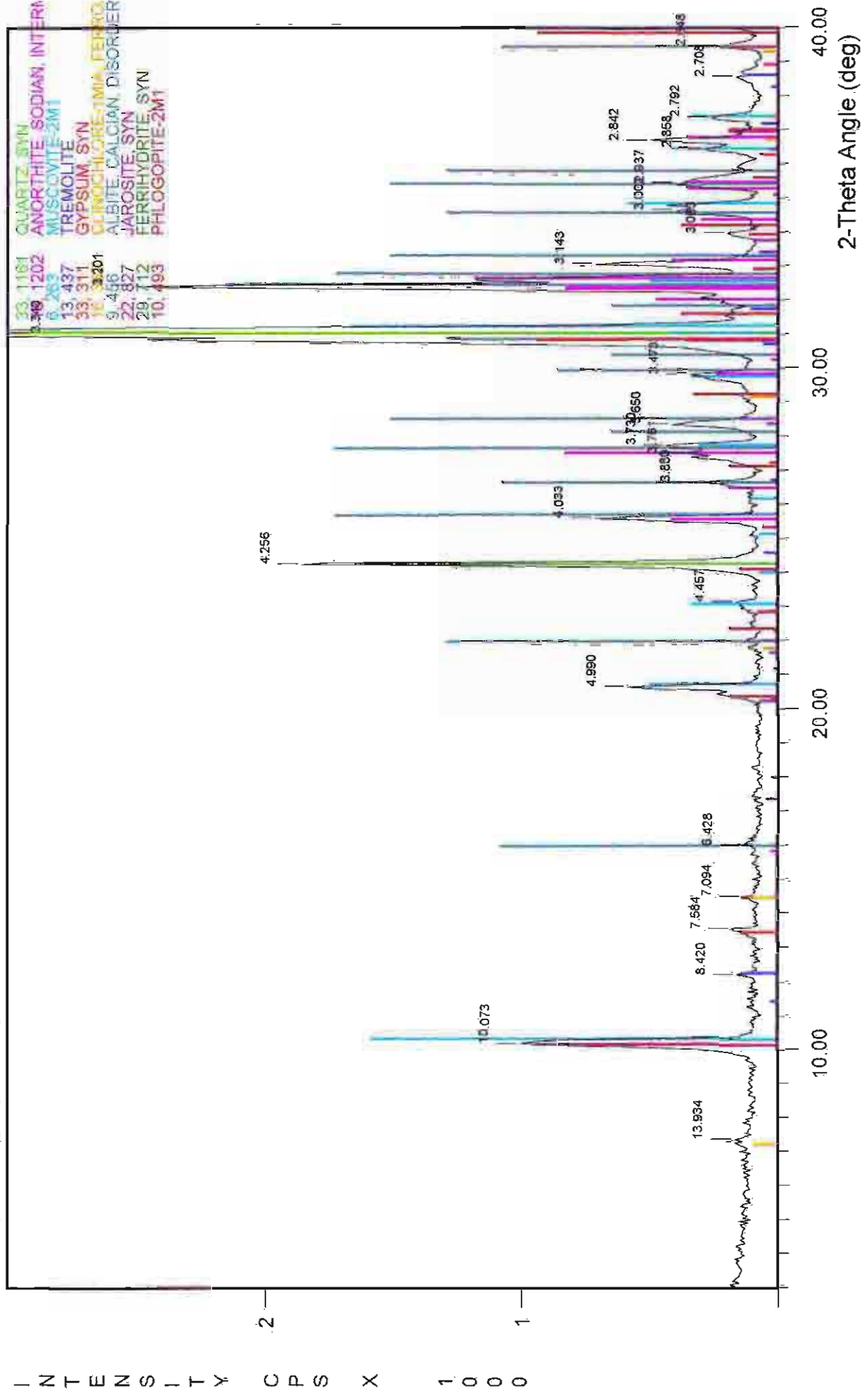


File Name: A:\0.98M

INTENSITY CPS X 1000

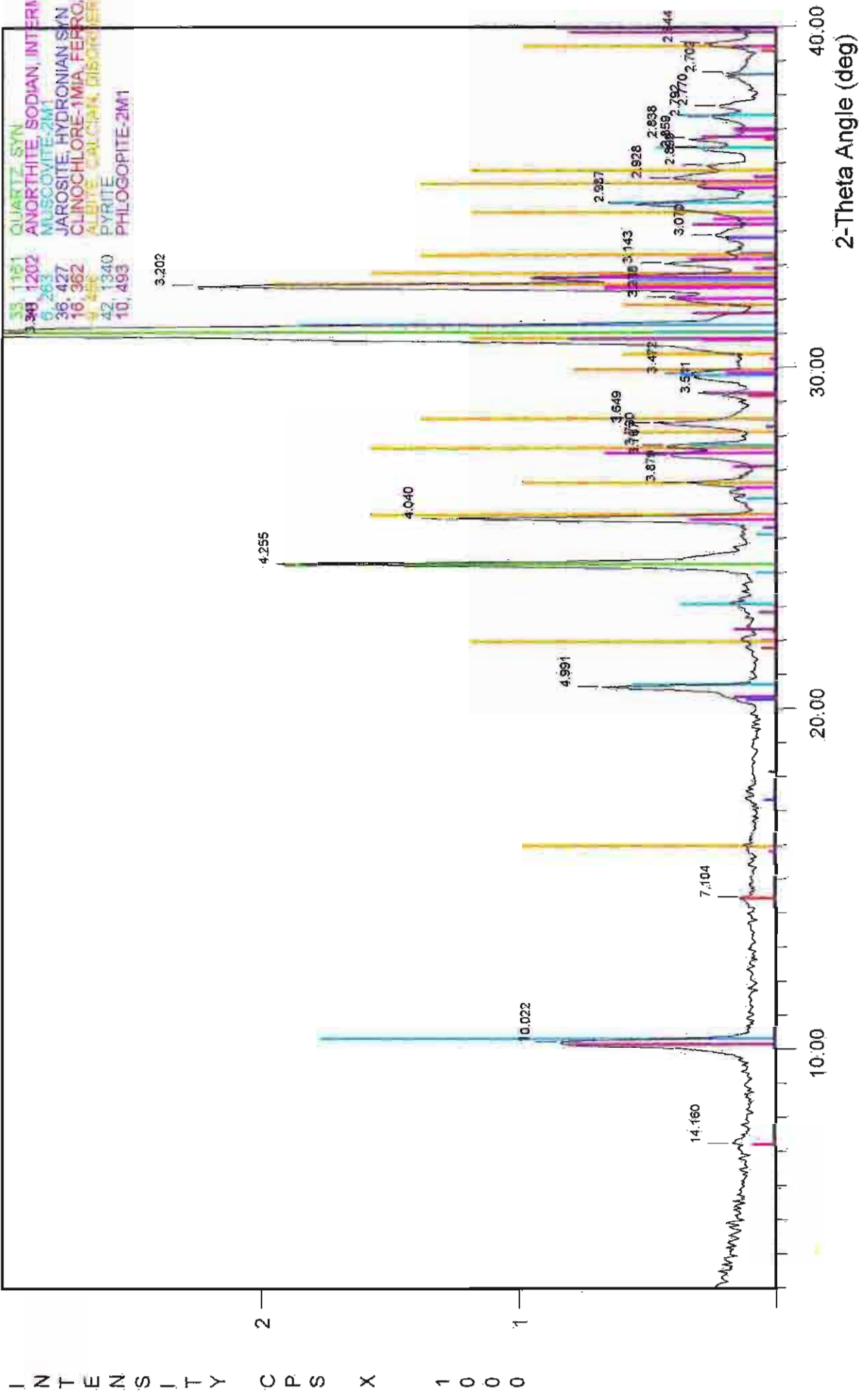


99cm pinkish grey silt region



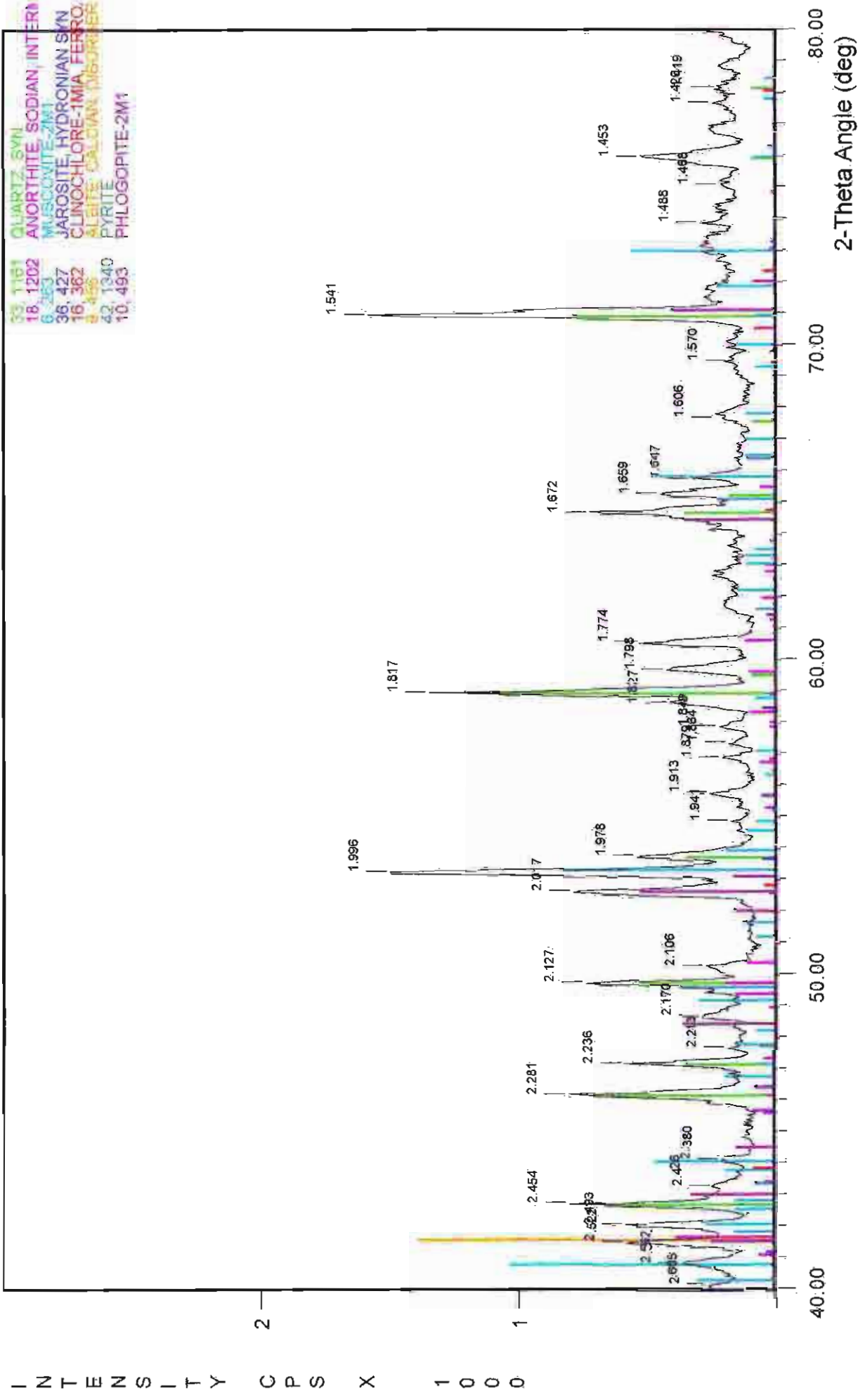
File Name: A:\0.99M

103cm brown silt layer

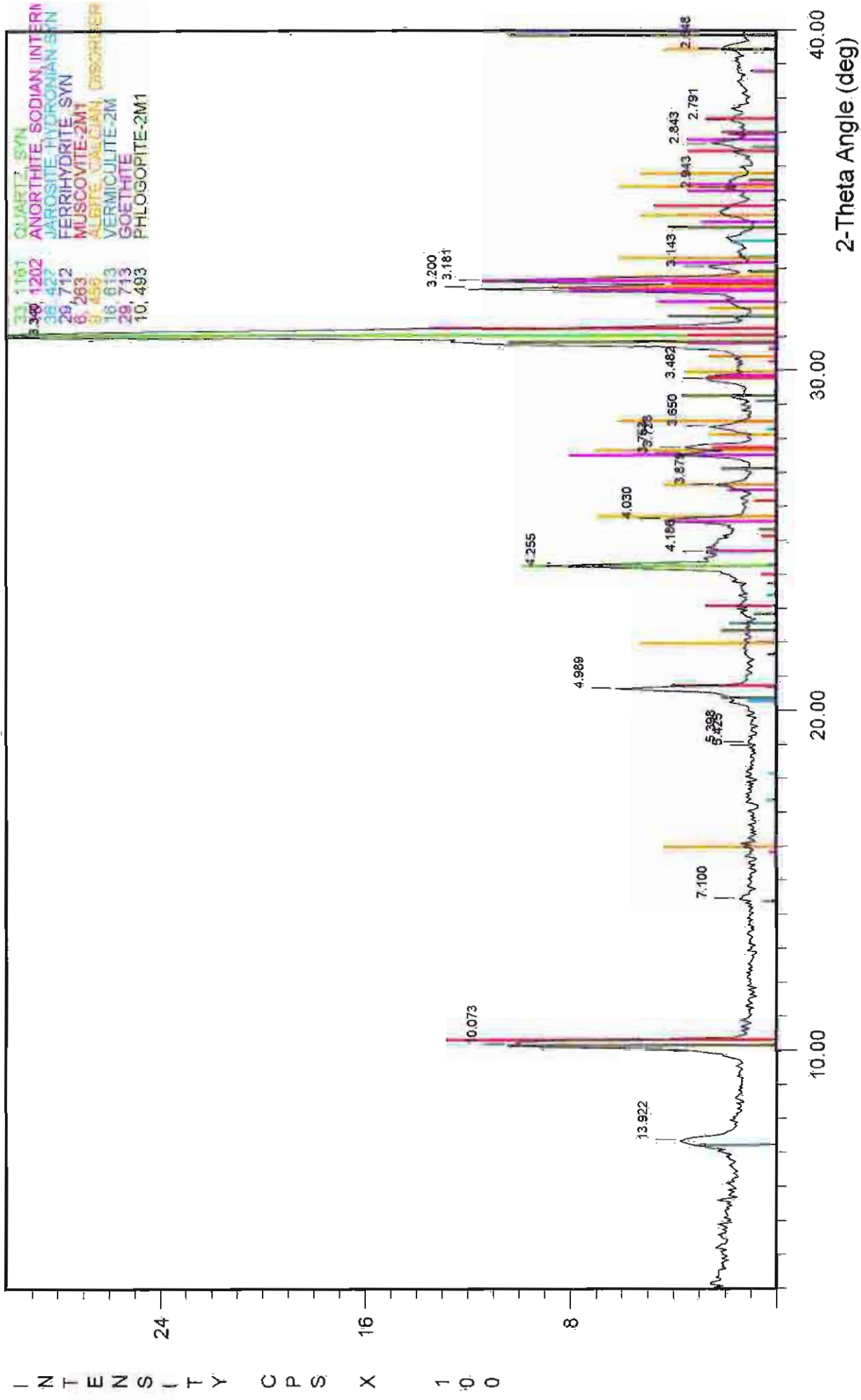


File Name: A:\11-03M

103cm brown silt layer

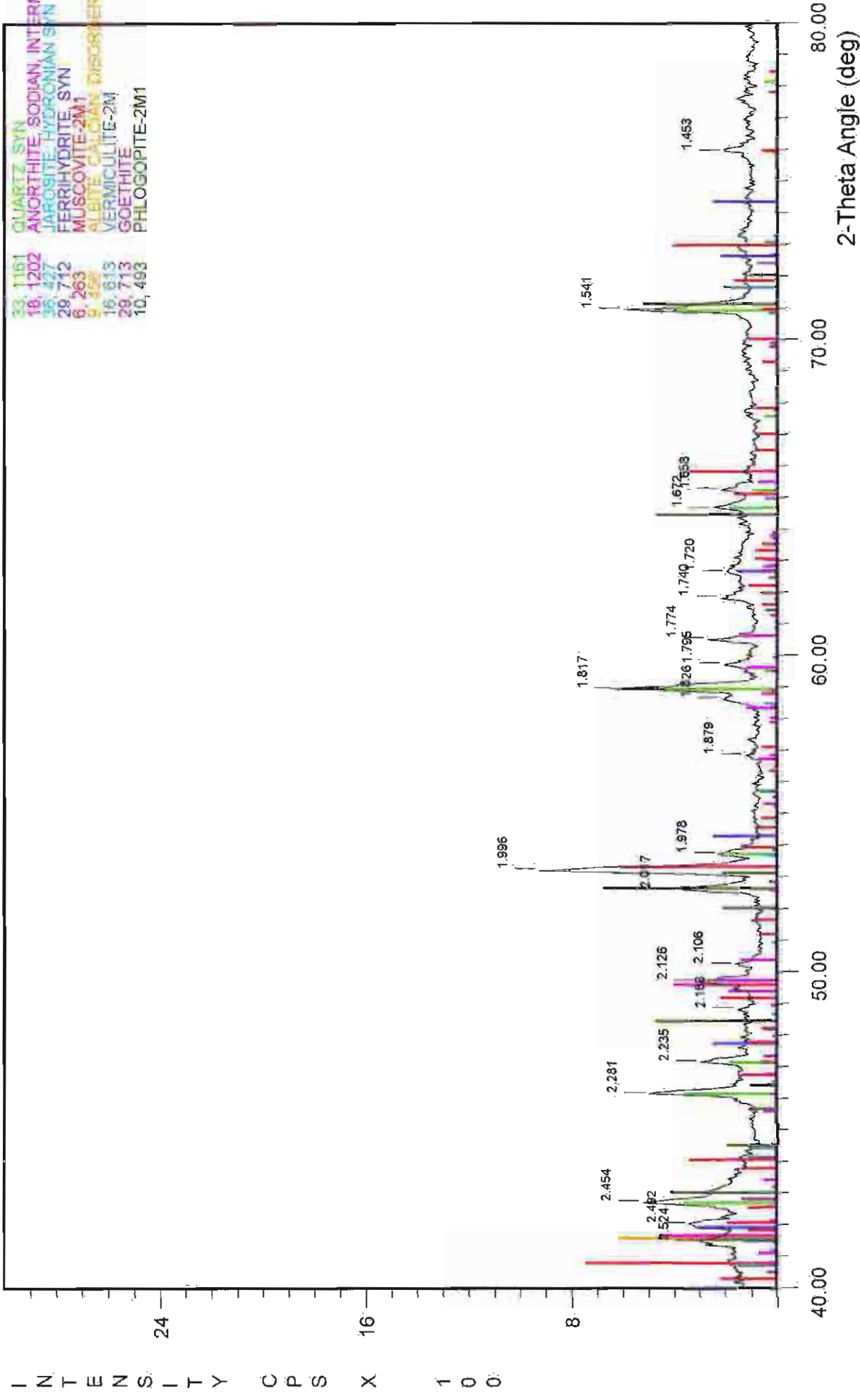


104cm cemented layer - single grain



File Name: A:\11-04MCLS

104cm cemented layer - single grain

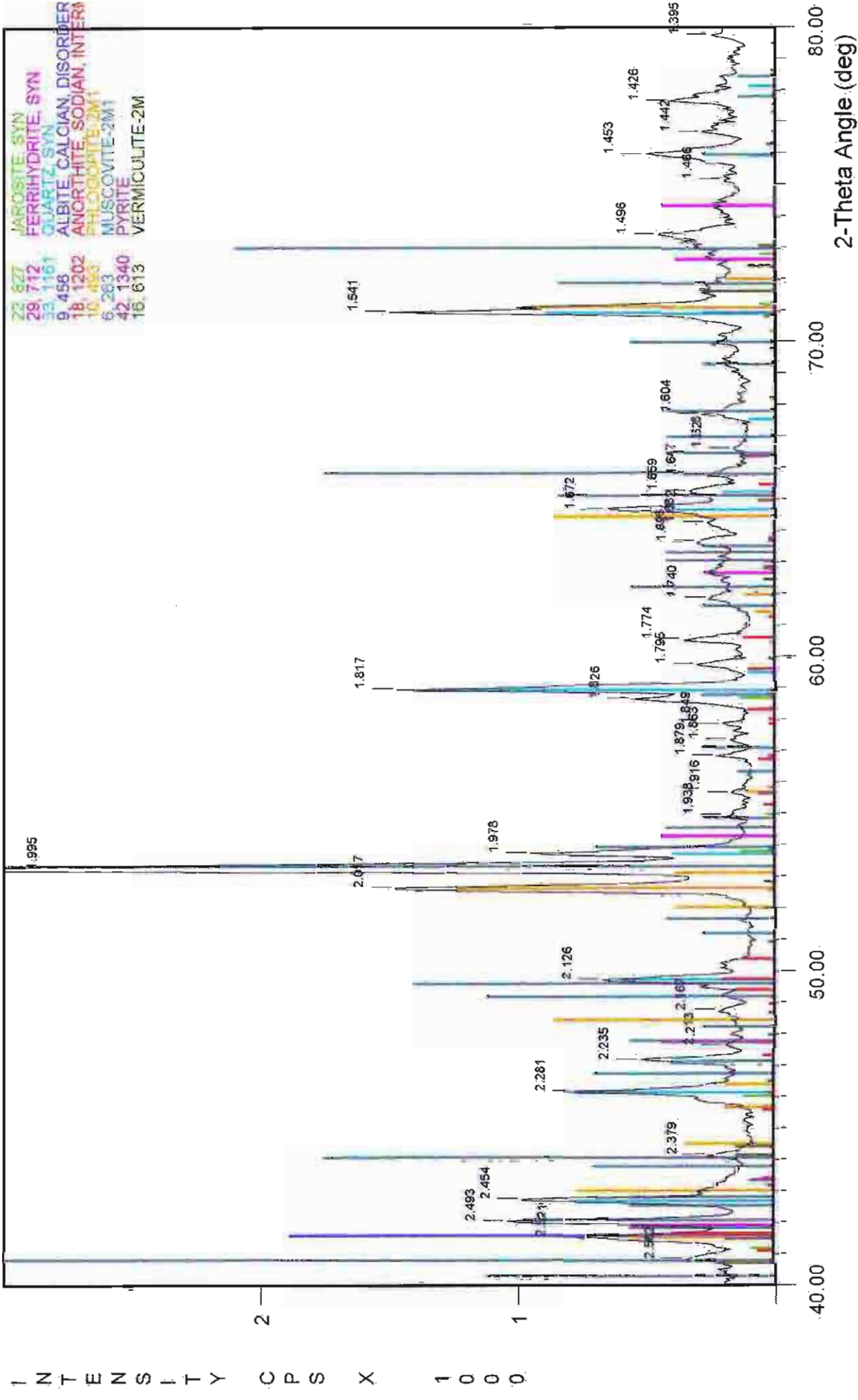


File Name: A:\11-04MCLS

- T E N S - T Y C P S X 1 0 0 0

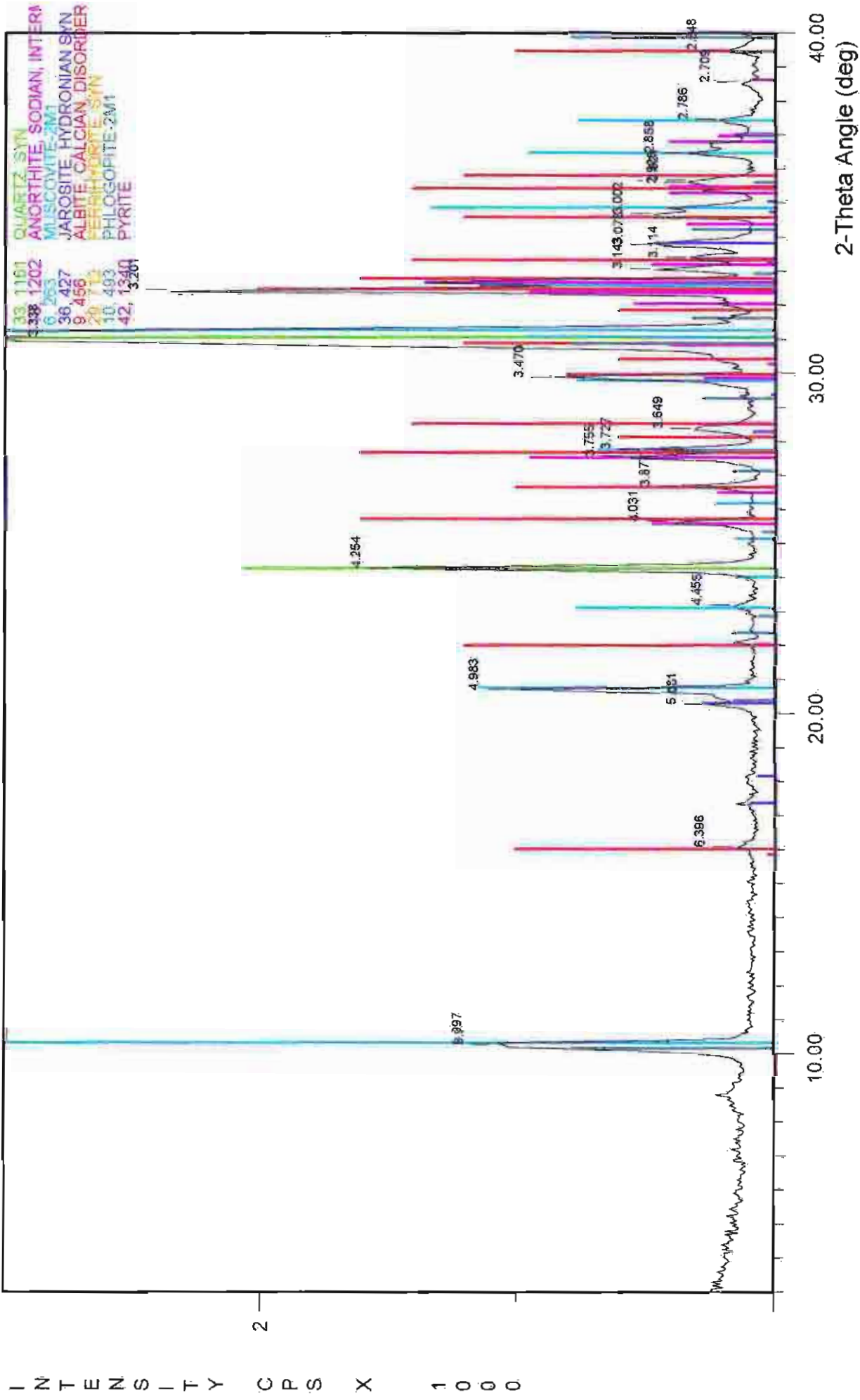


104cm cemented layer



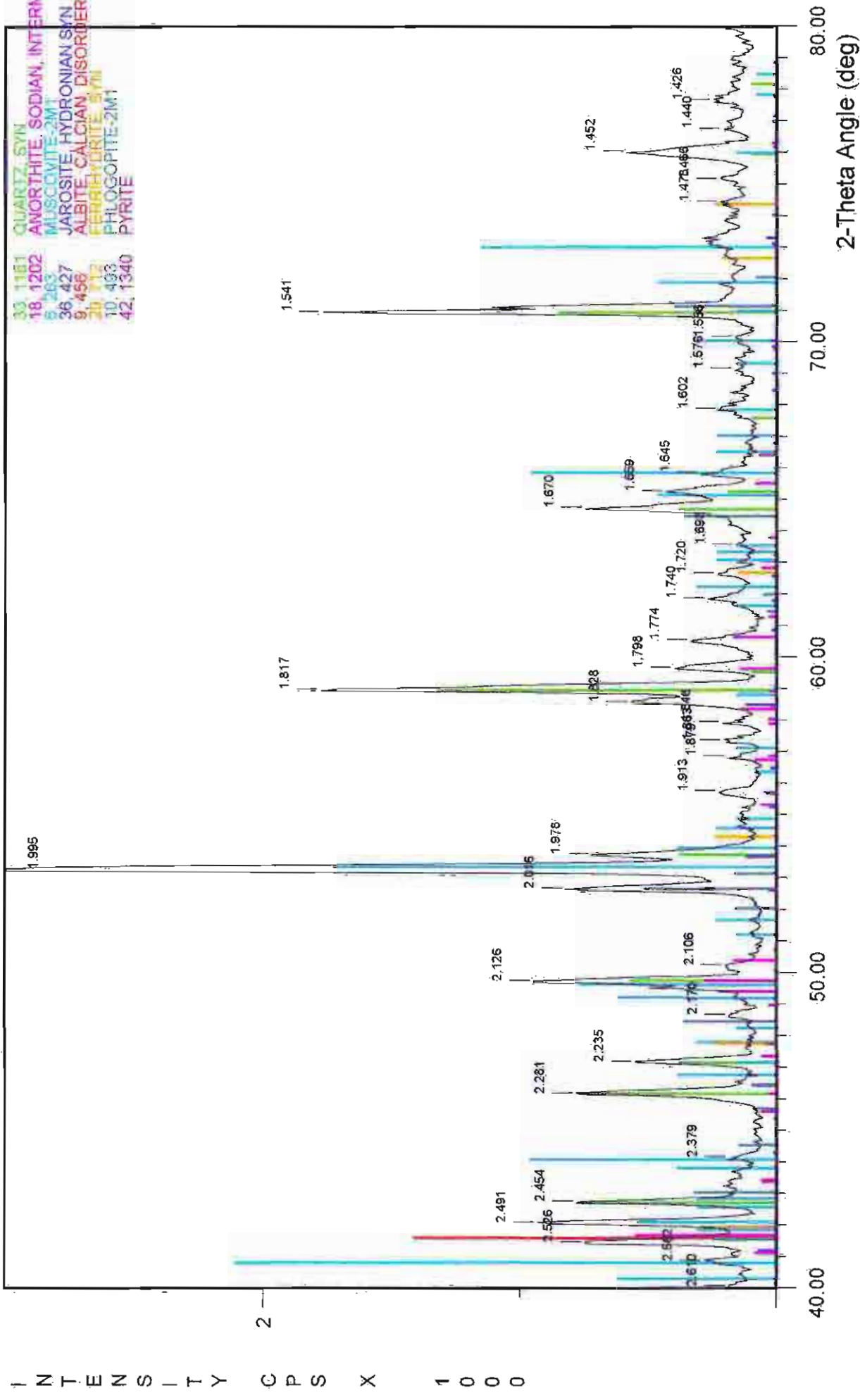
File Name: A:\1-04MCLB

106cm pale yellow silt layer



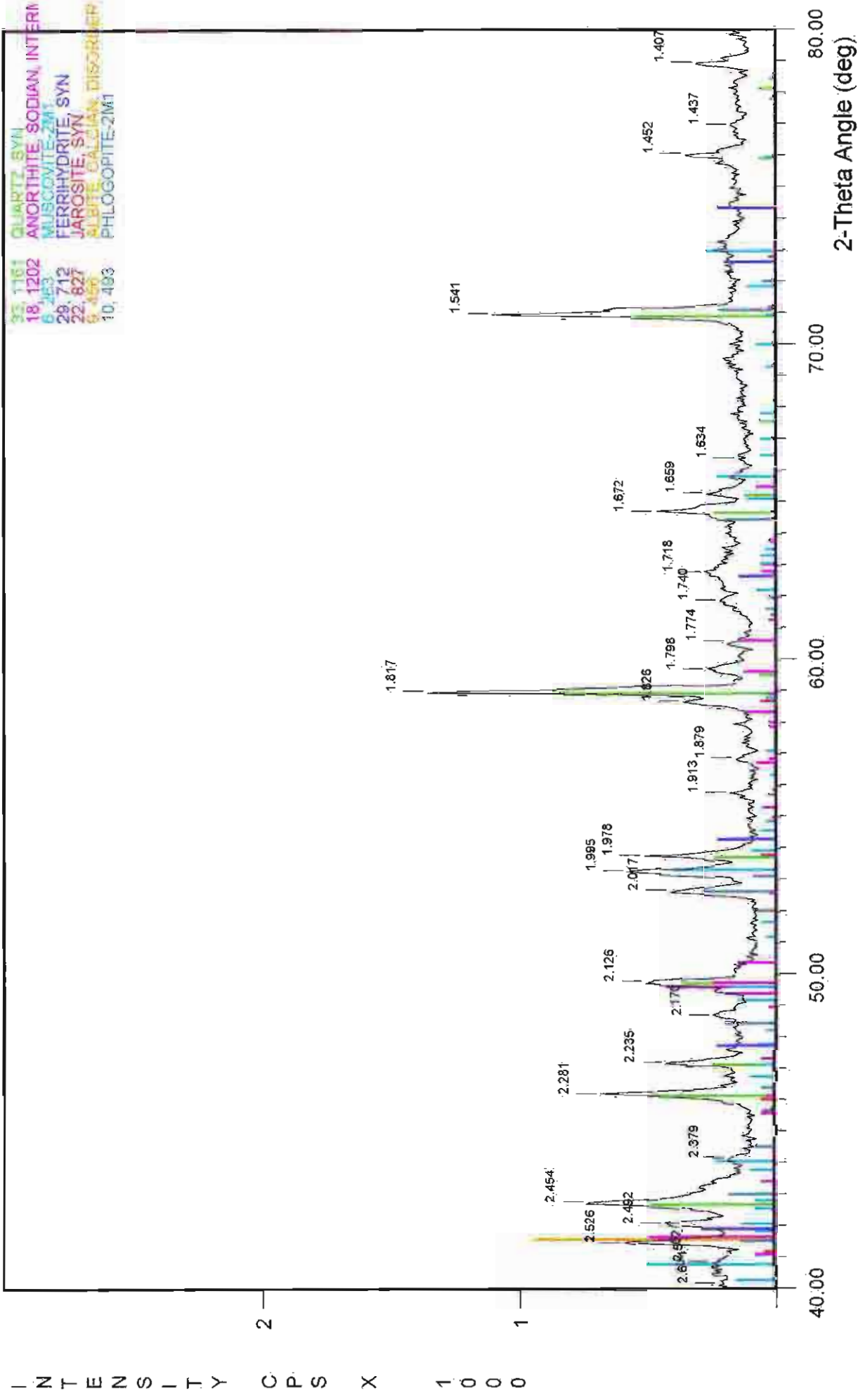
File Name: A:\11-06M

106cm pale yellow silt layer.



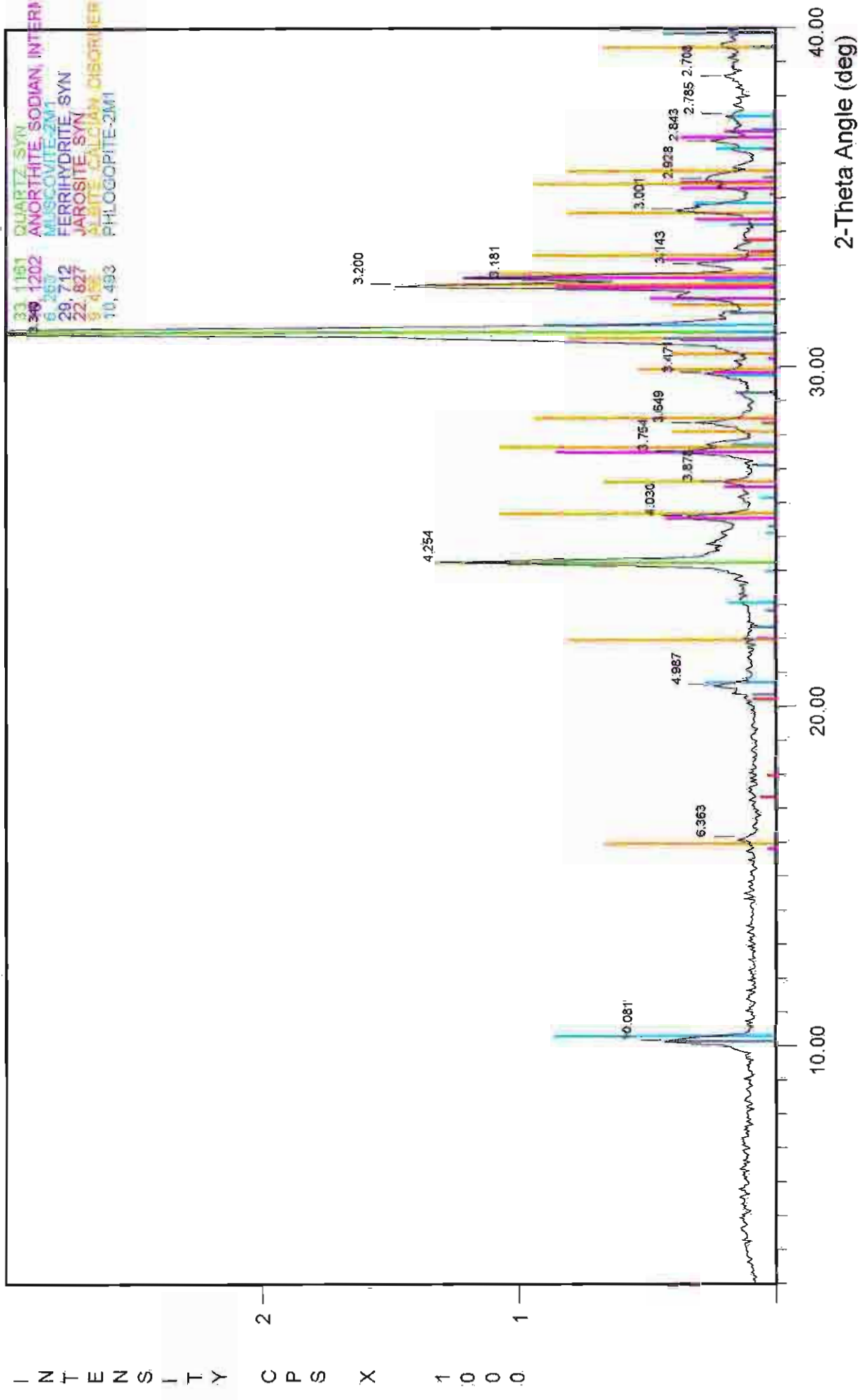
File Name: A:\V-06M

109cm cemented layer - single grain



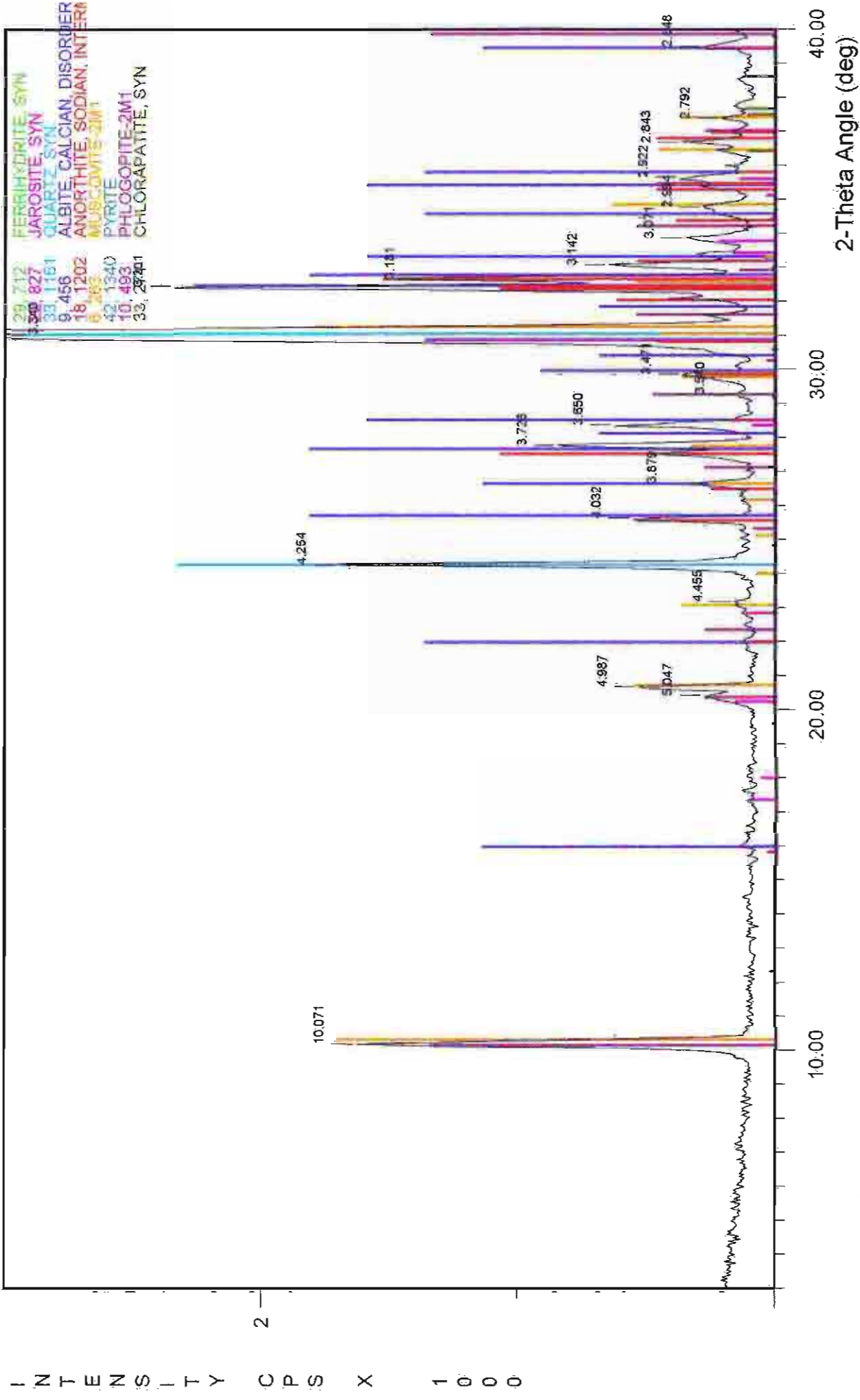
File Name: A:11-09MCLS

109cm cemented layer - single grain



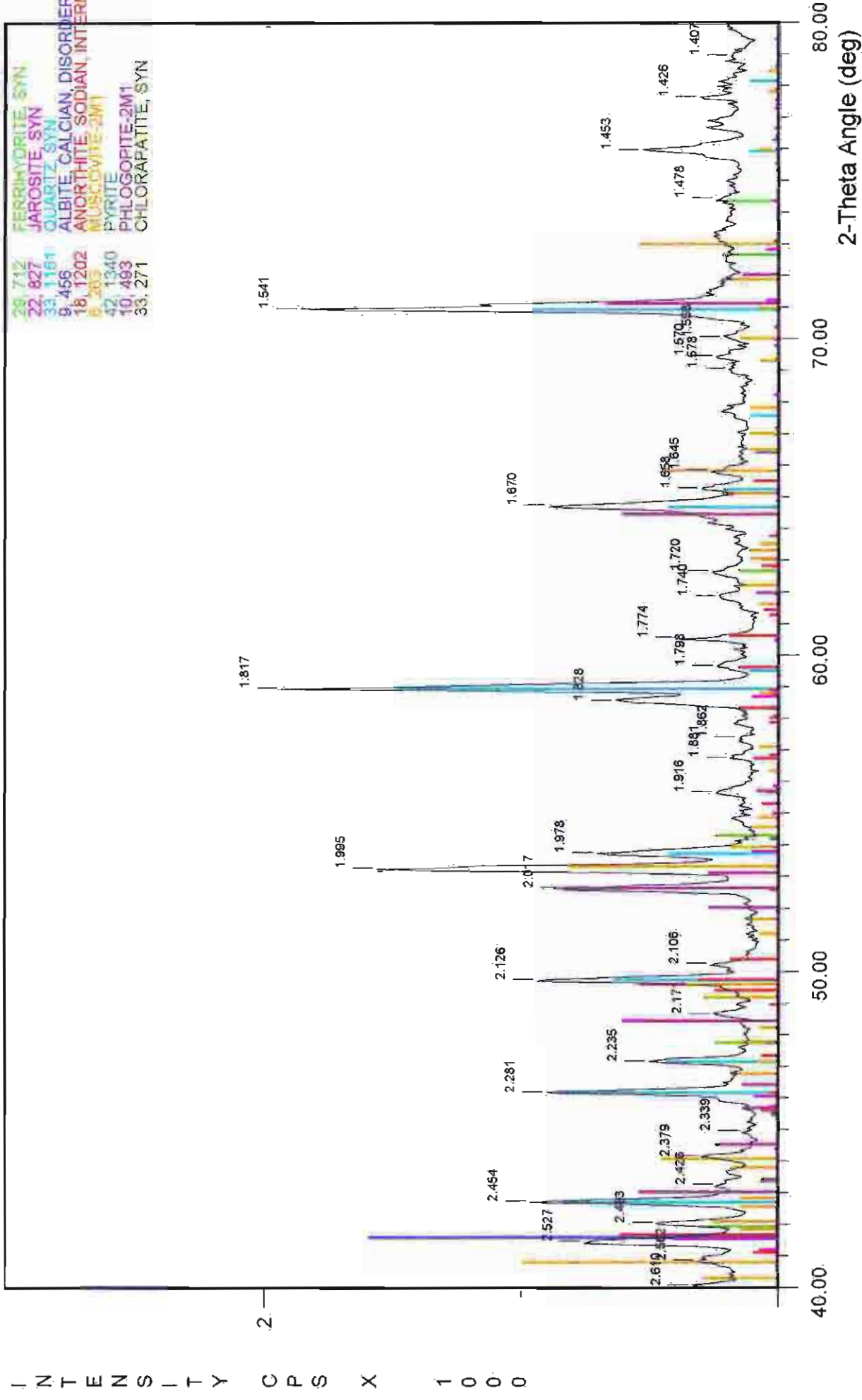
File Name: A11-09MCLS

109cm cemented layer

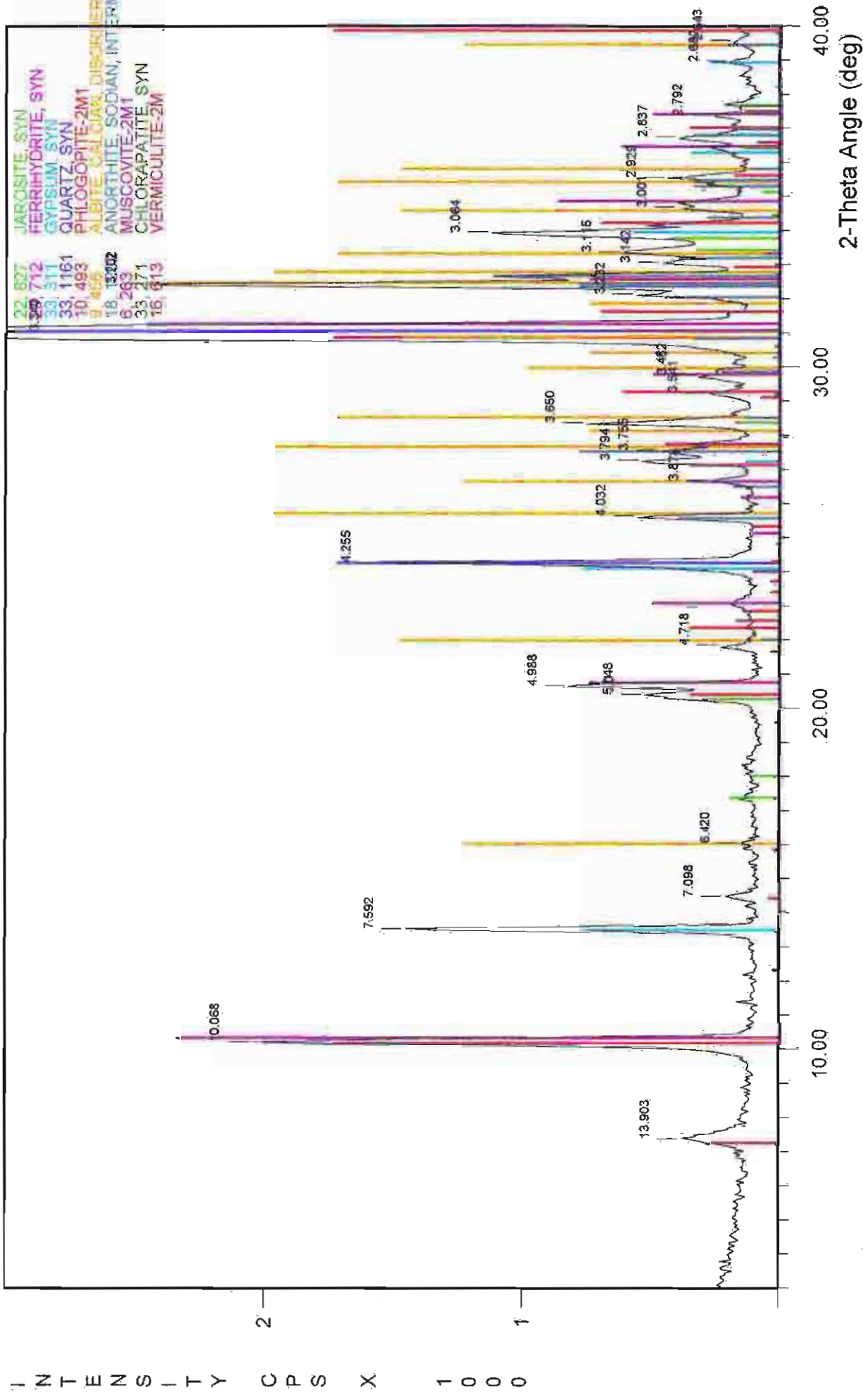


File Name: A\11-09MCLB

109cm cemented layer

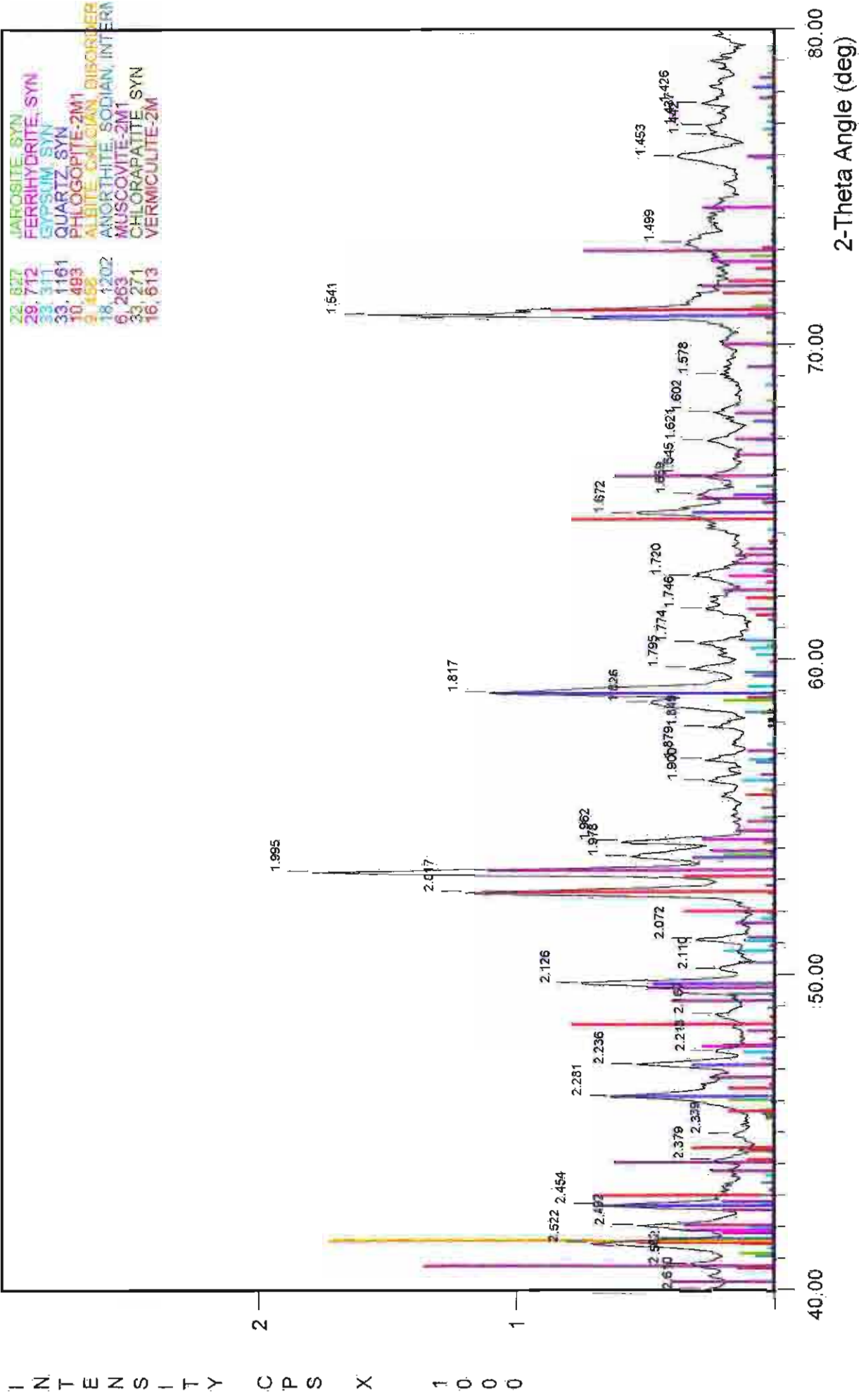


113cm cemented layer

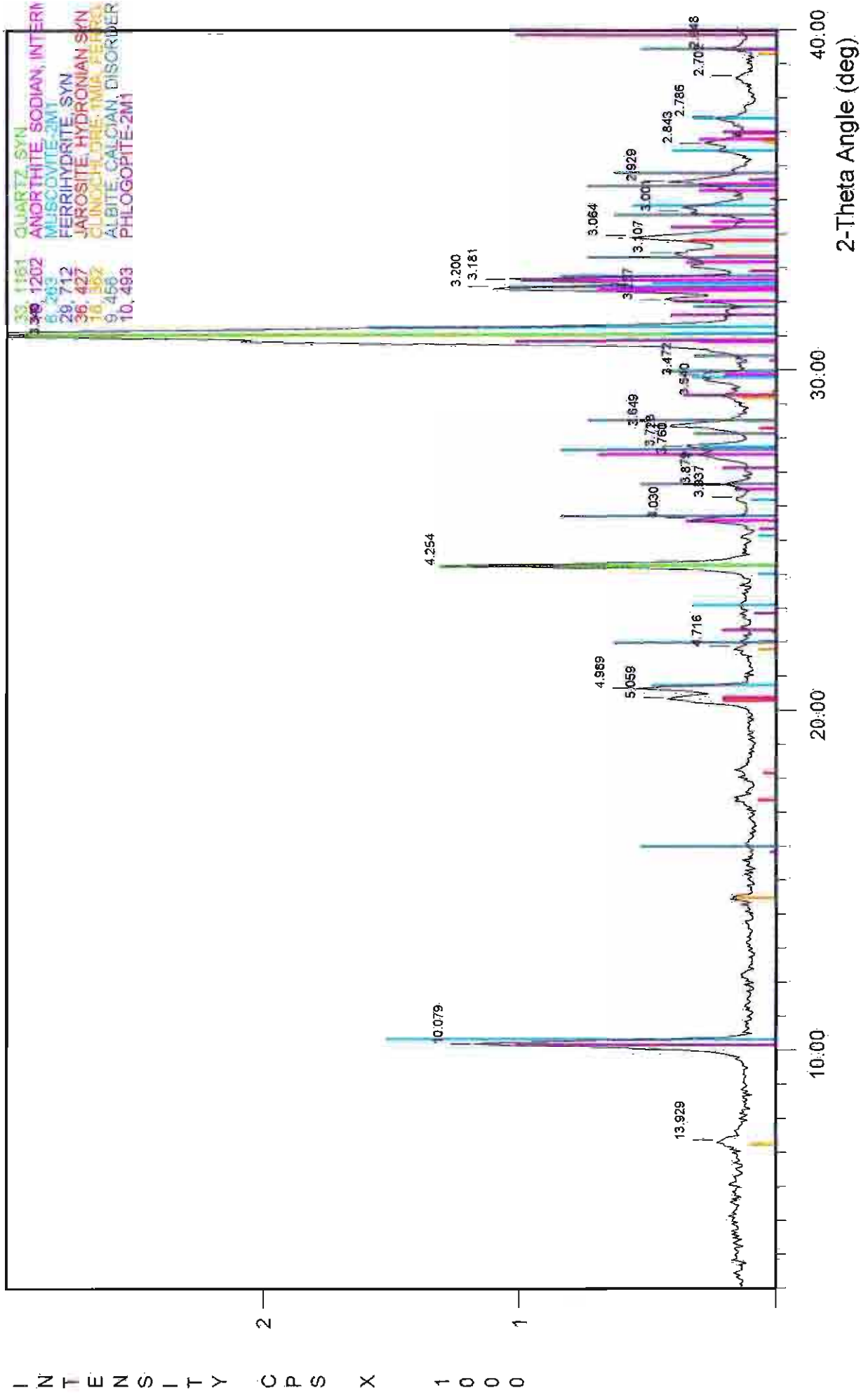


File Name: A:\1-13MCLB

113cm cemented layer

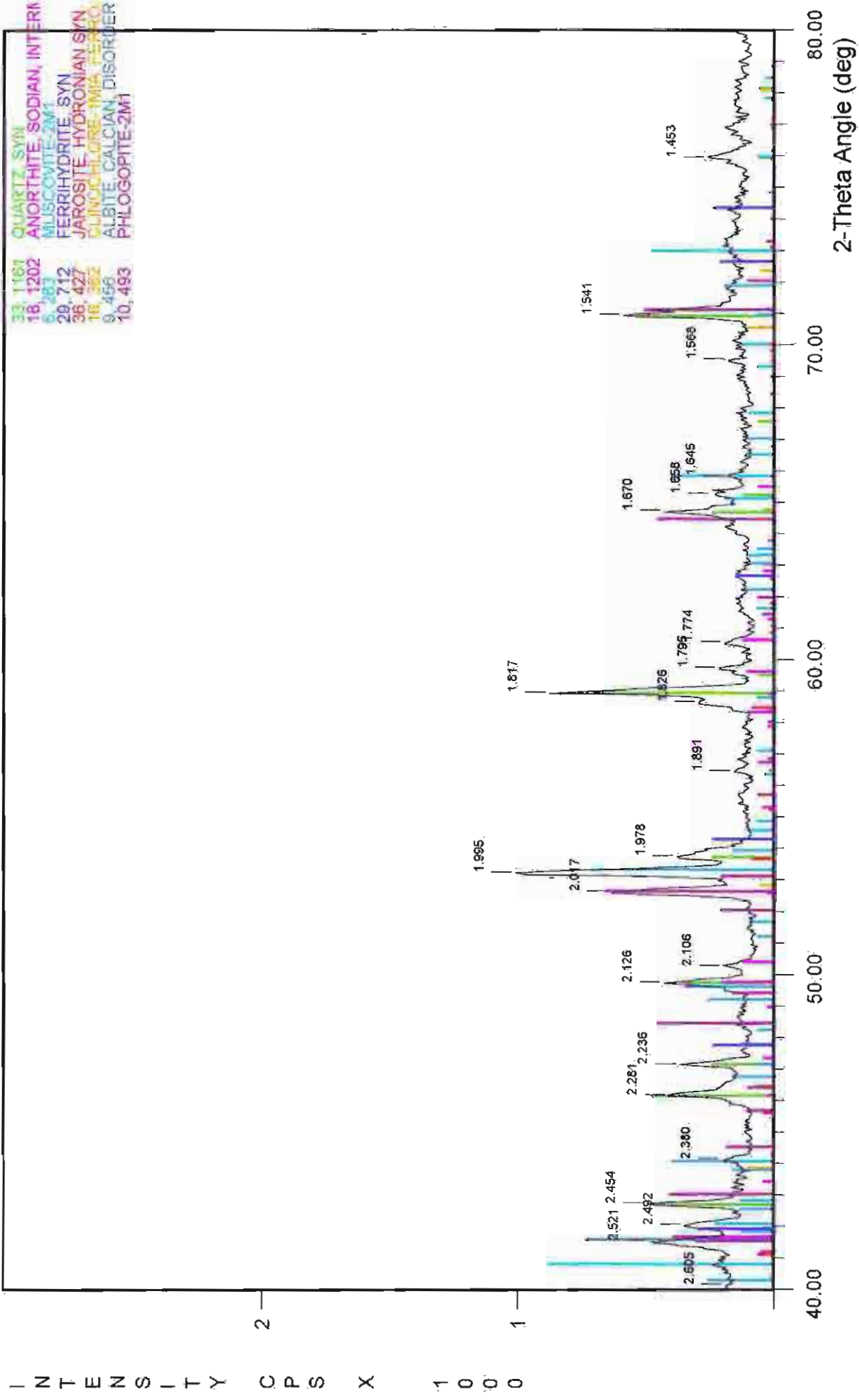


113cm cemented layer - single grain



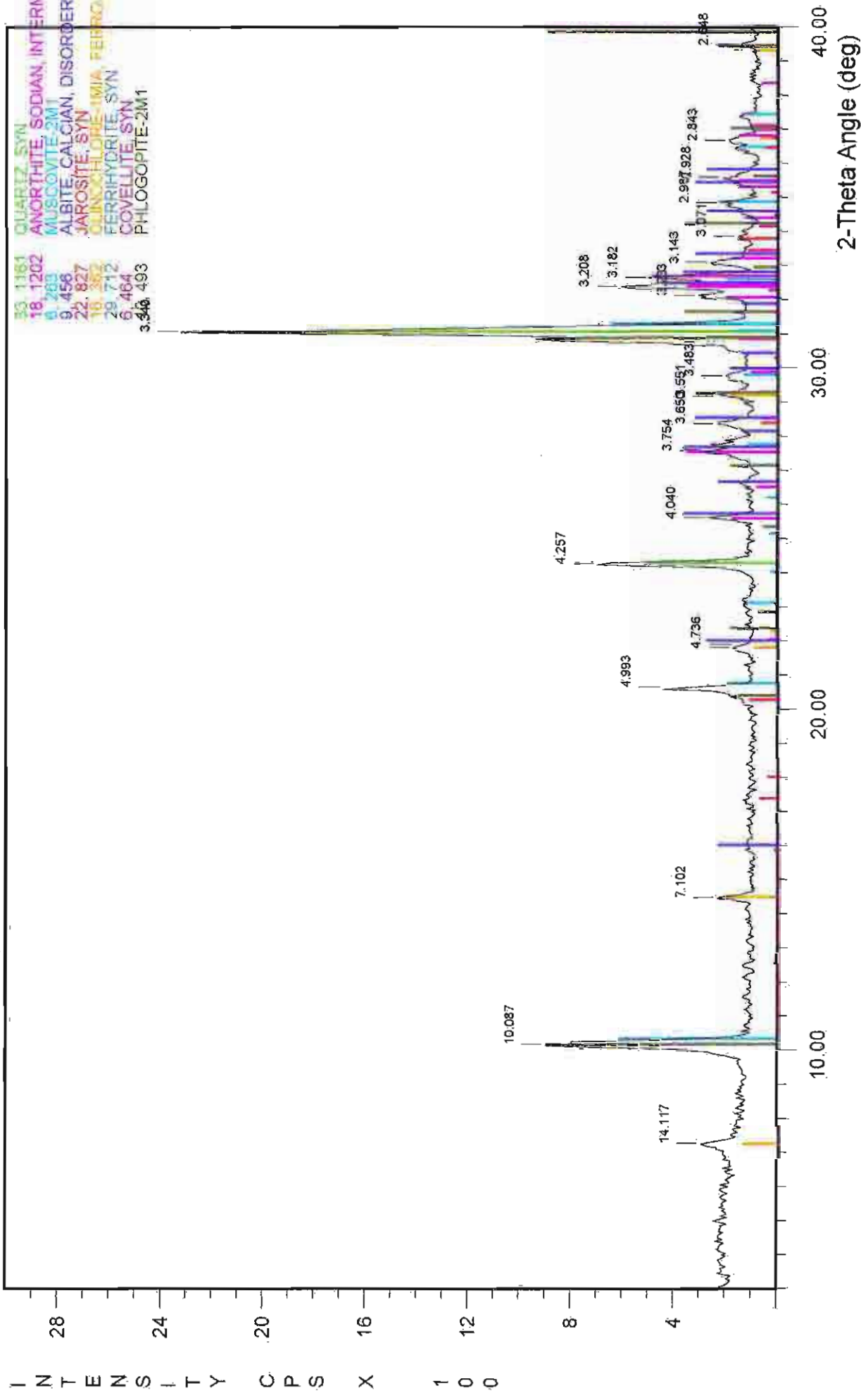
File Name: A\11-13MCLS

113cm cemented layer - single grain



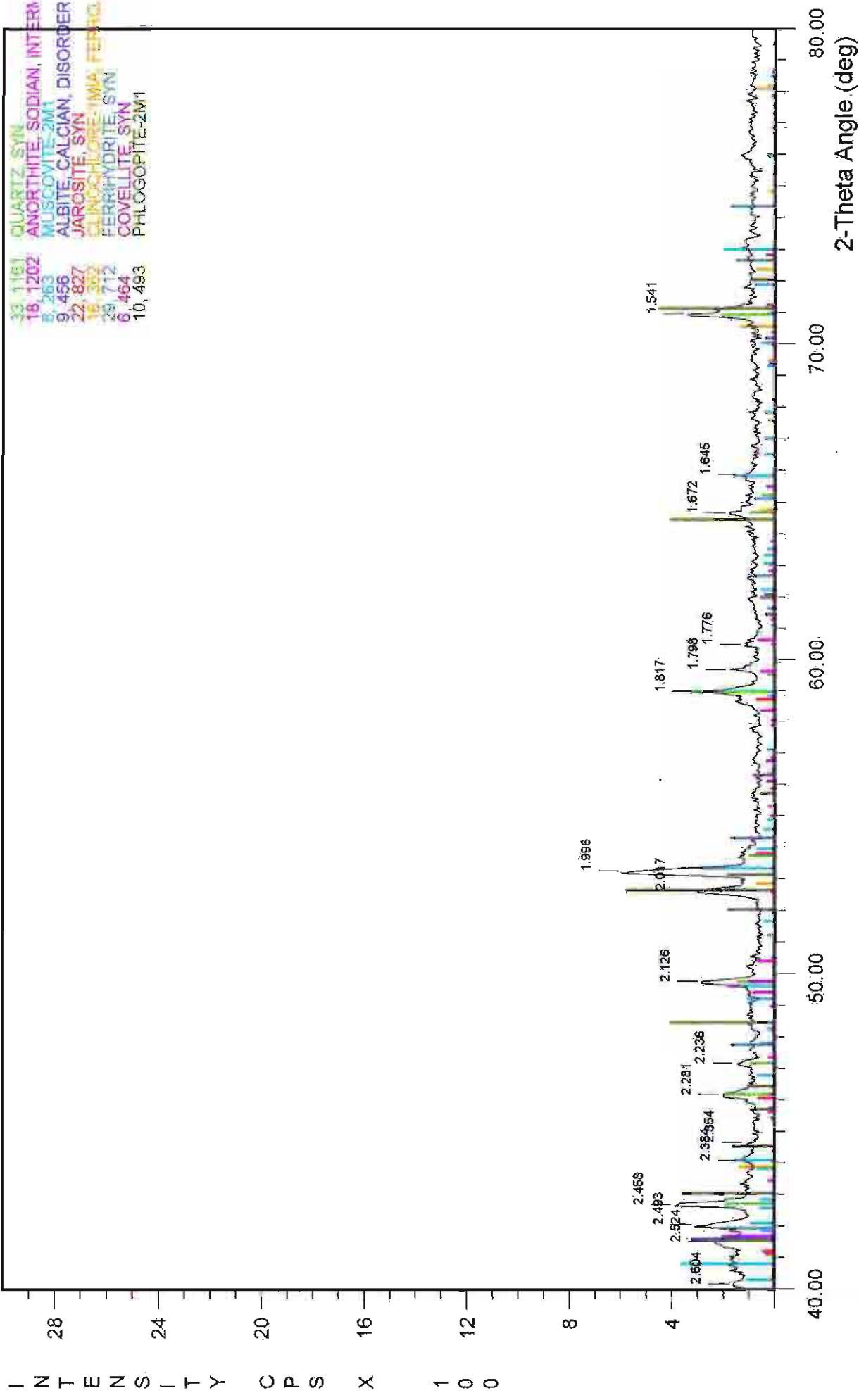
File Name: A:\11-13MCLS

124cm.cemented layer - single grain



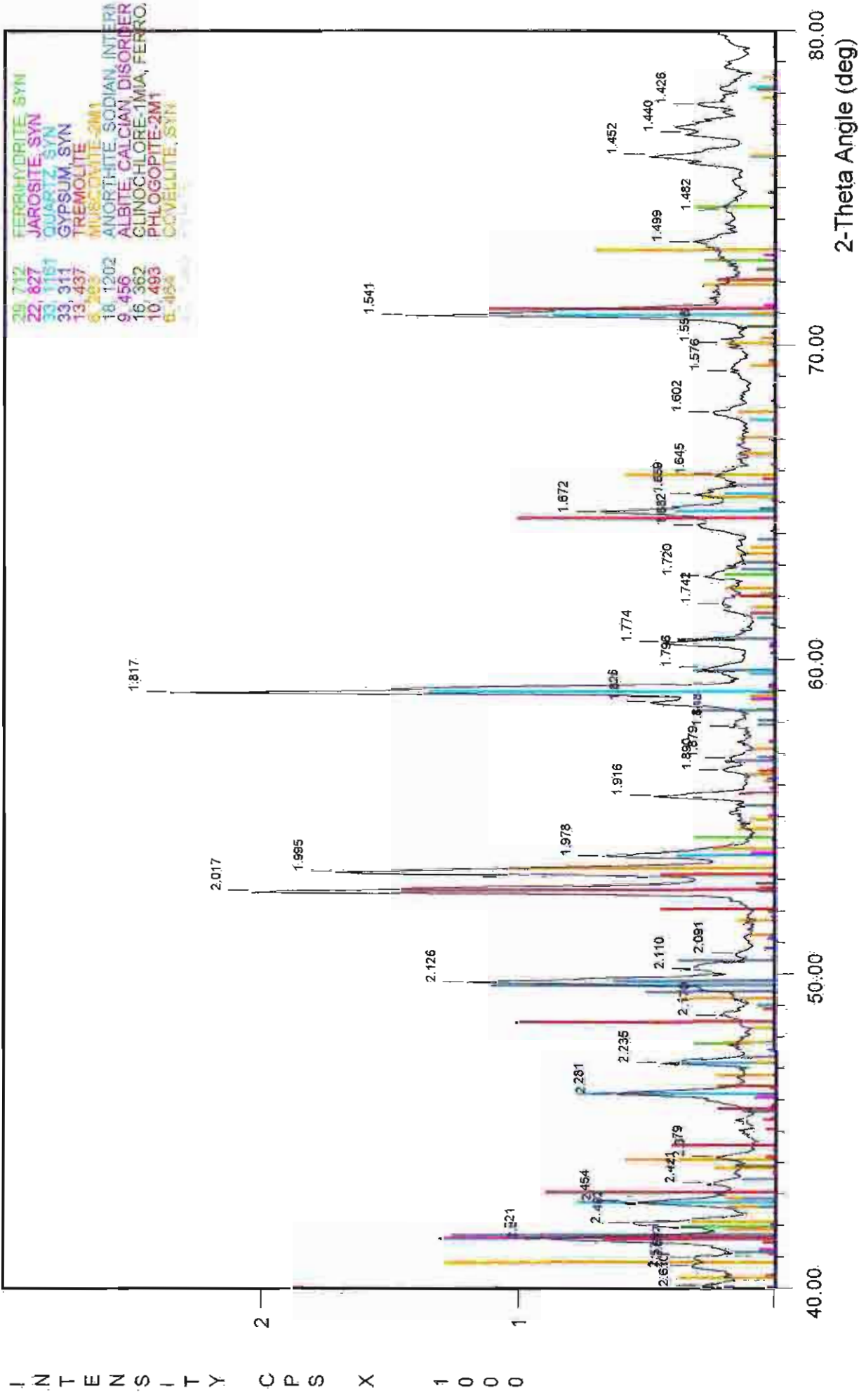
File Name: A:\1-24\MCLS

124cm cemented layer - single grain



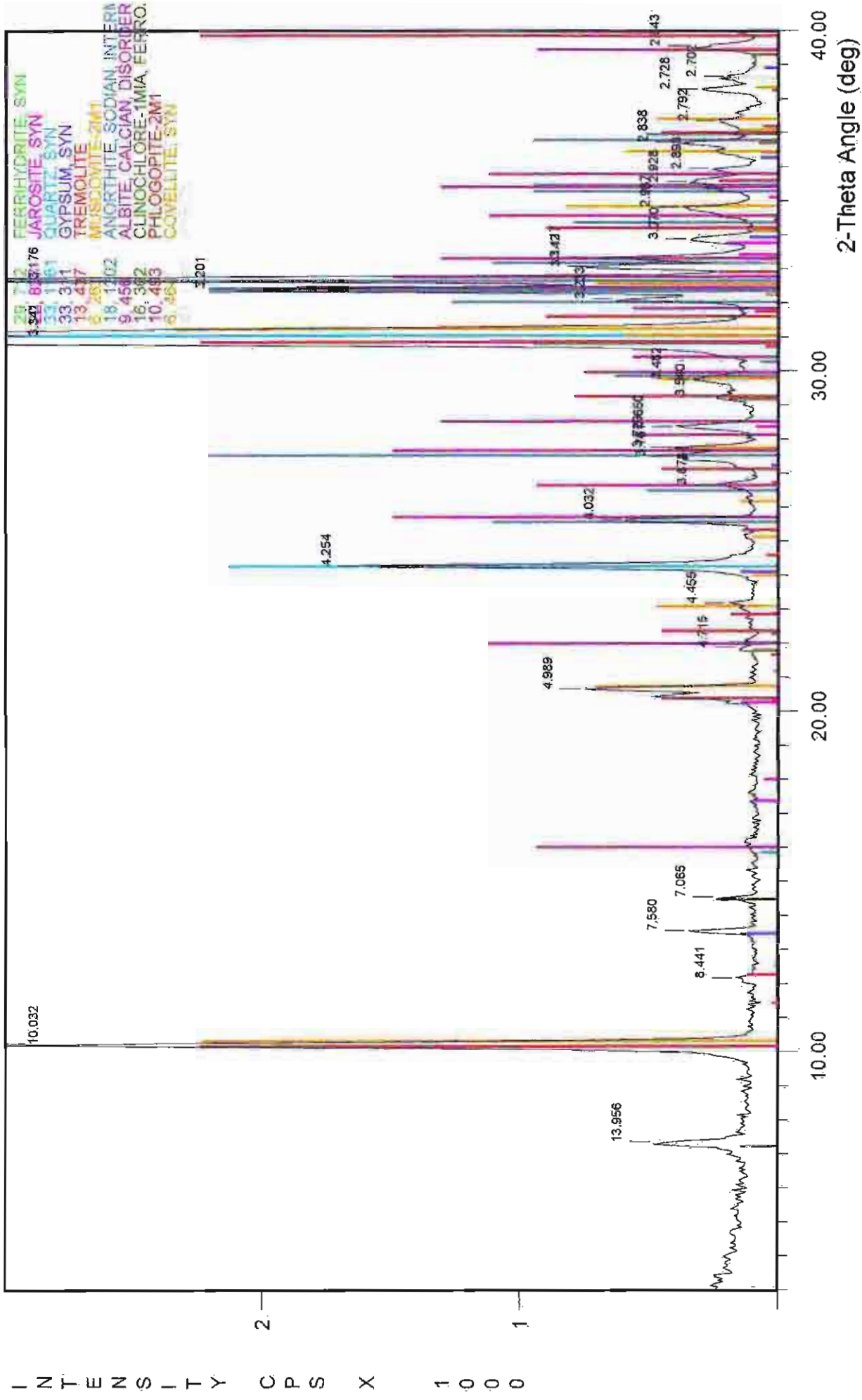
File Name: A:\1-24M\CLS

MA 124cm cemented layer



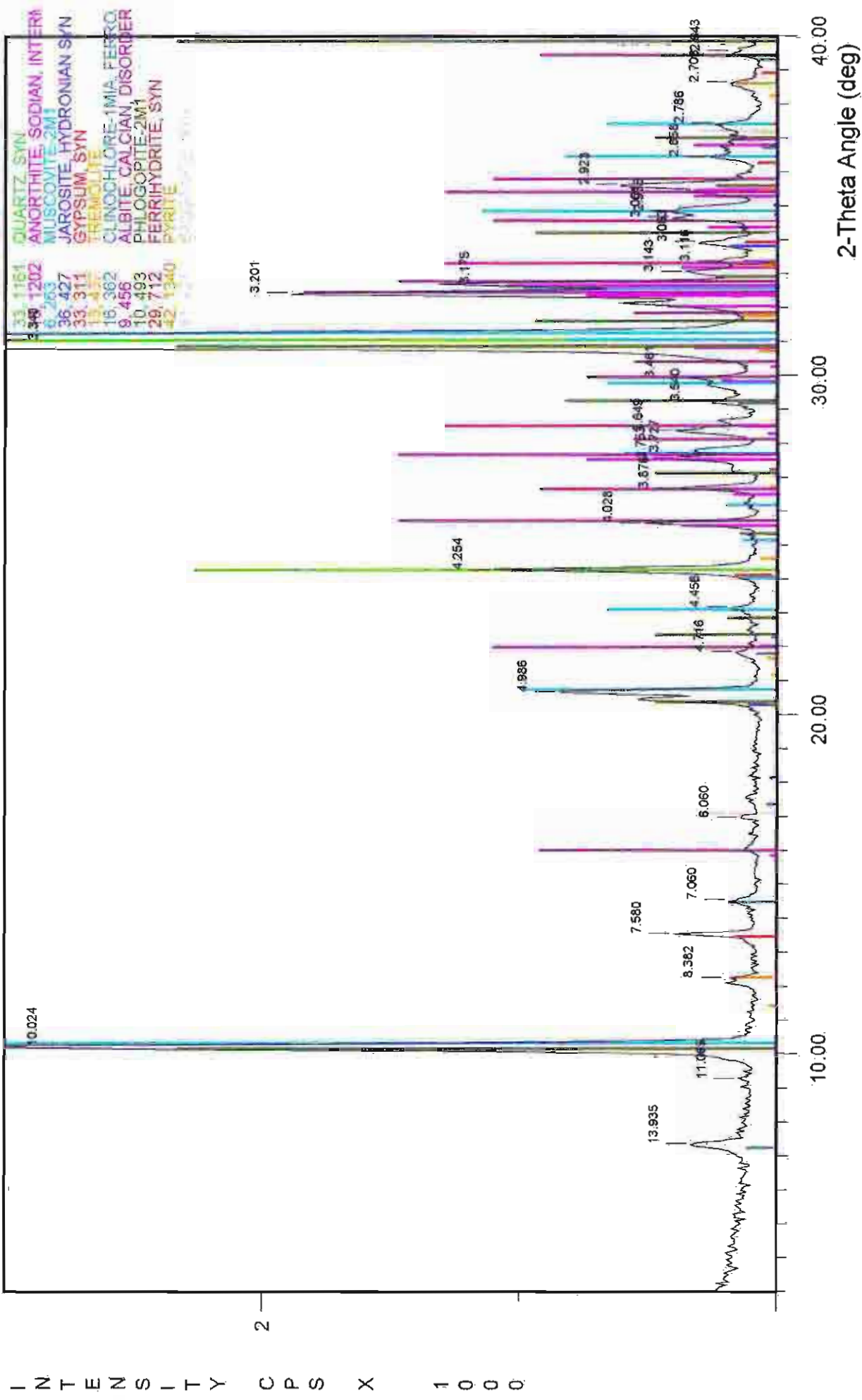
File Name: A:\1-24MCLB

MA 124cm cemented layer



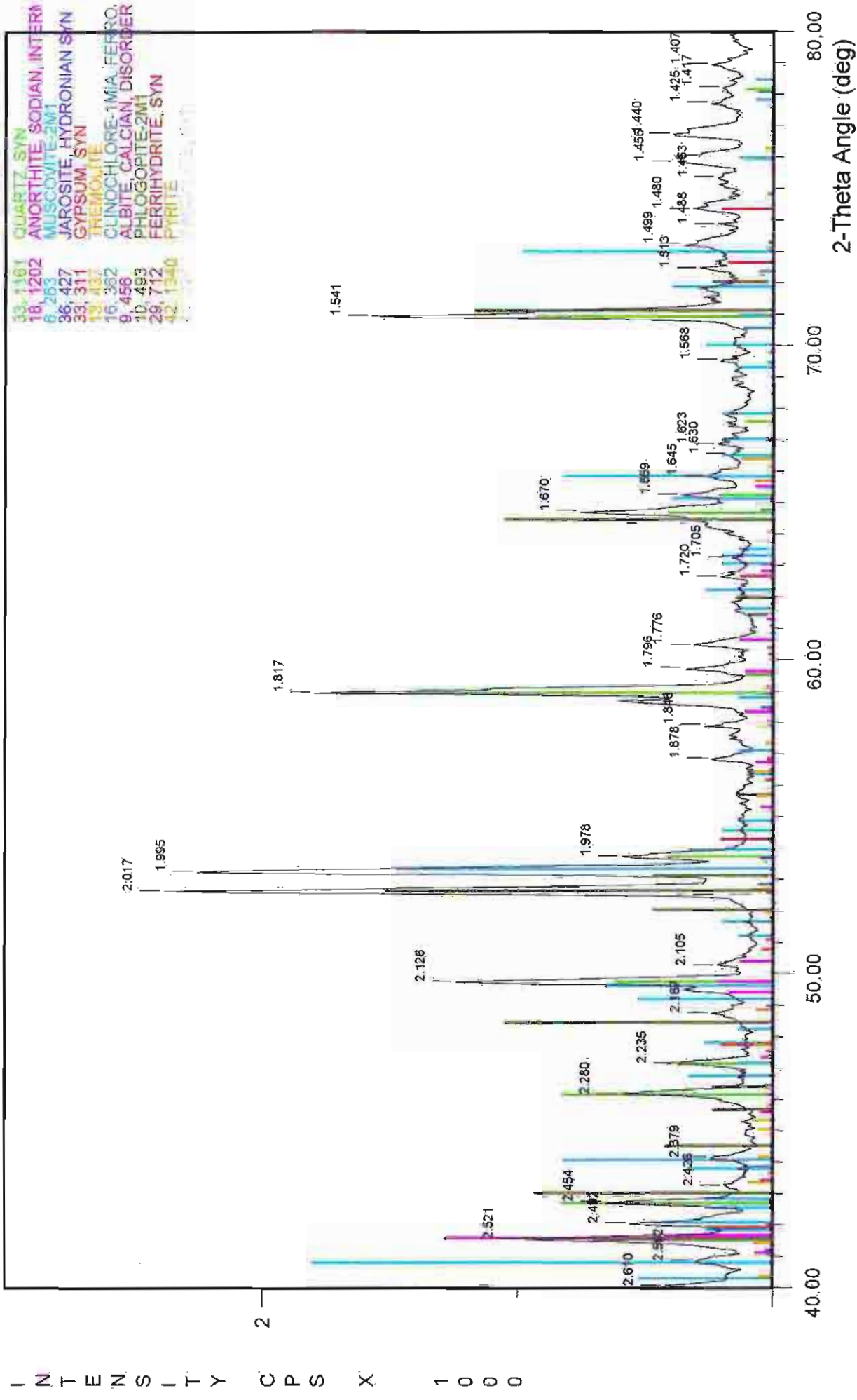
File Name: A:\11-24\MCLB

128cm light grey-yellow medium sand layer



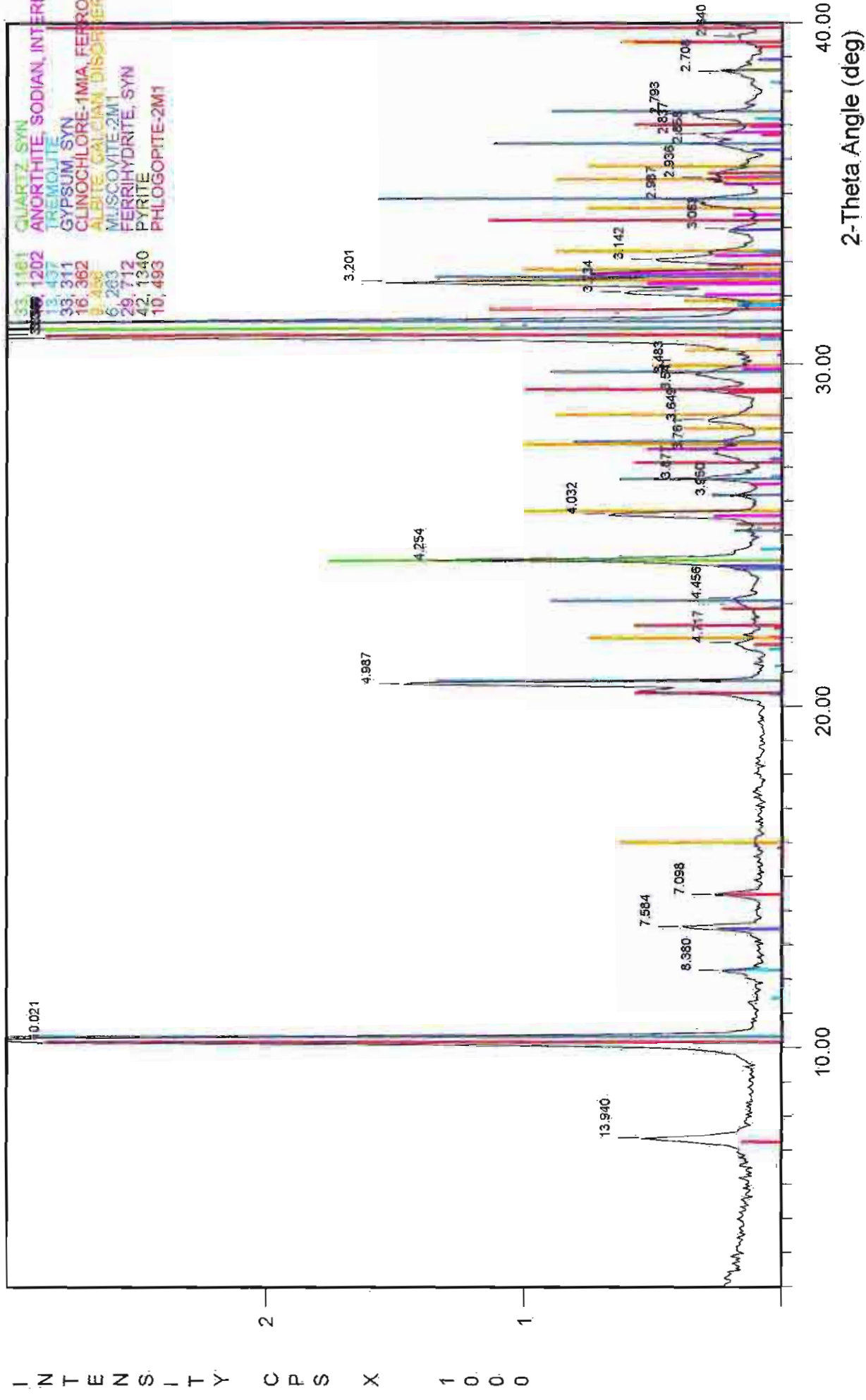
File Name: A:\1-28M

128cm light grey-yellow medium sand layer



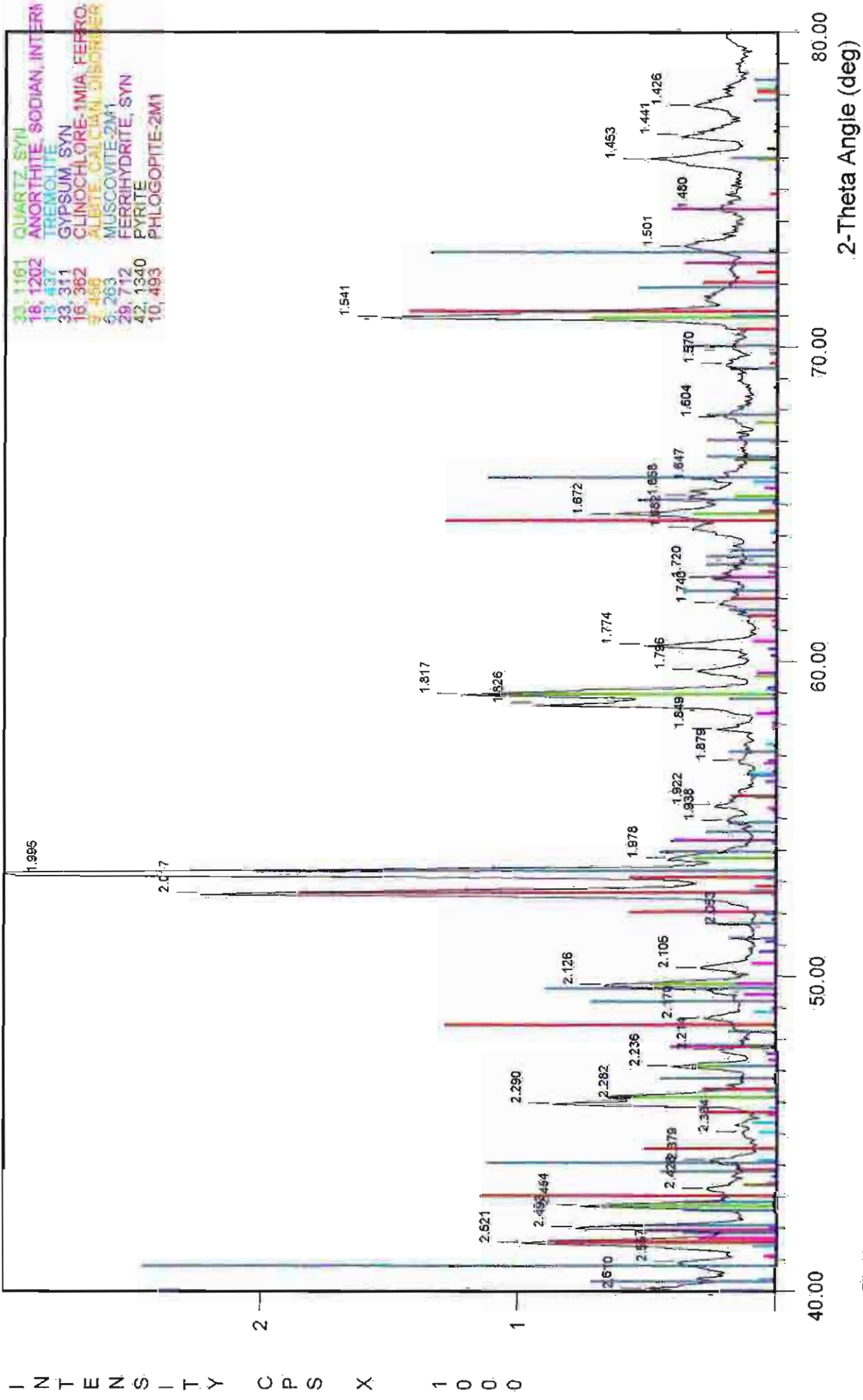
File Name: A:\V-28M

MA 129.5cm orange medium sand layer



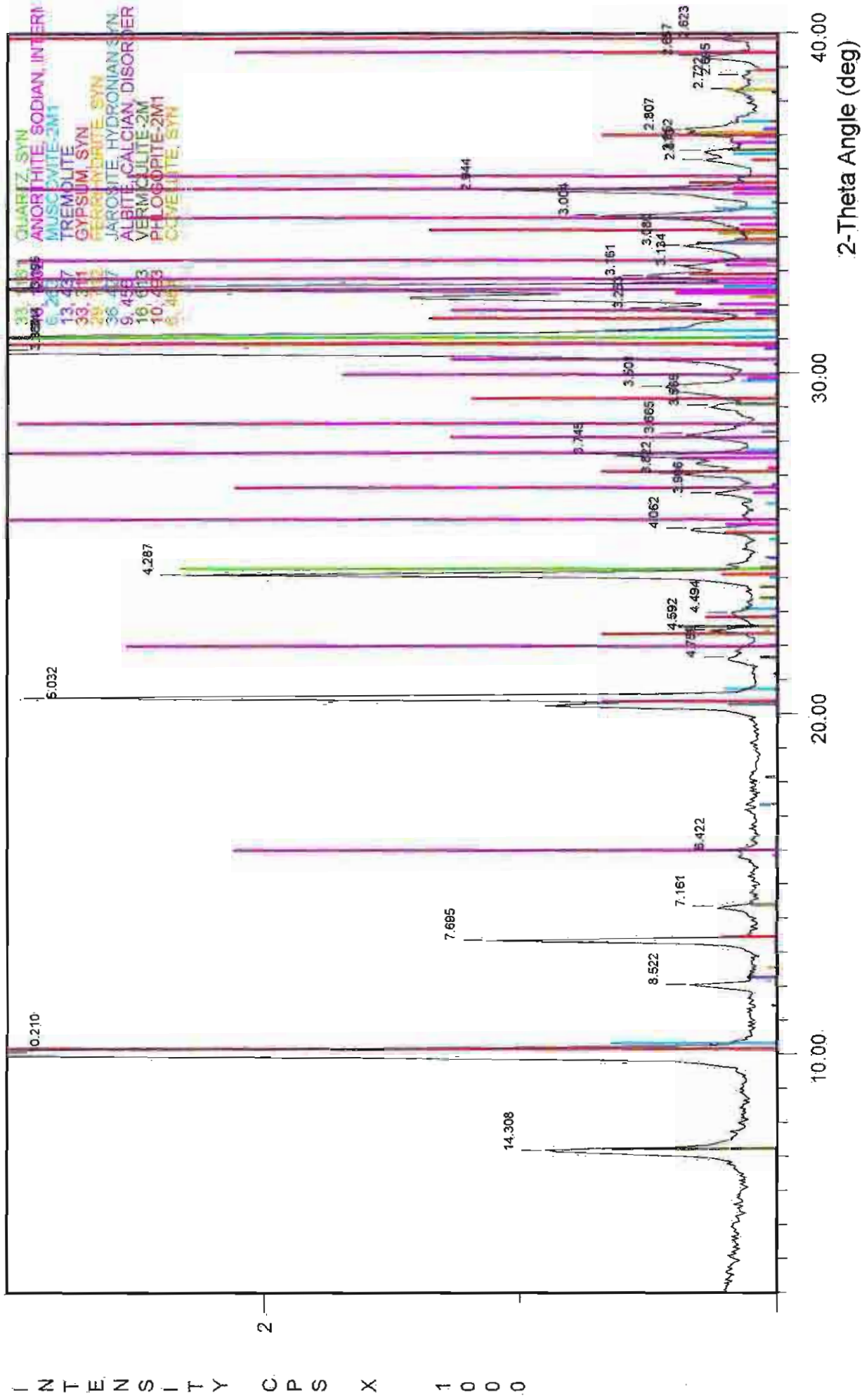
File Name: A:\1-295M

MA 129.5cm orange medium sand layer

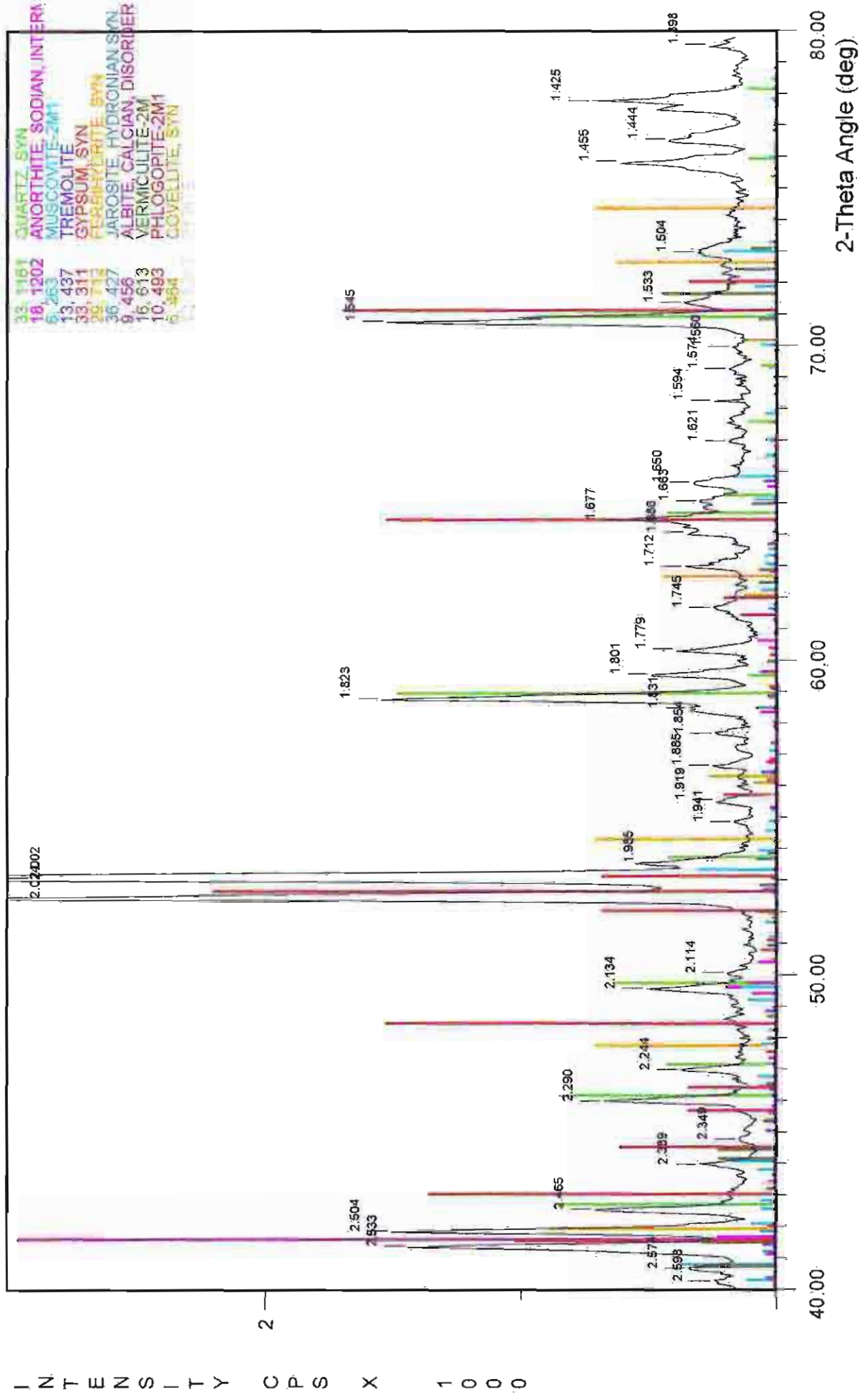


File Name: A:\1-295M

134cm cemented orange medium sand layer

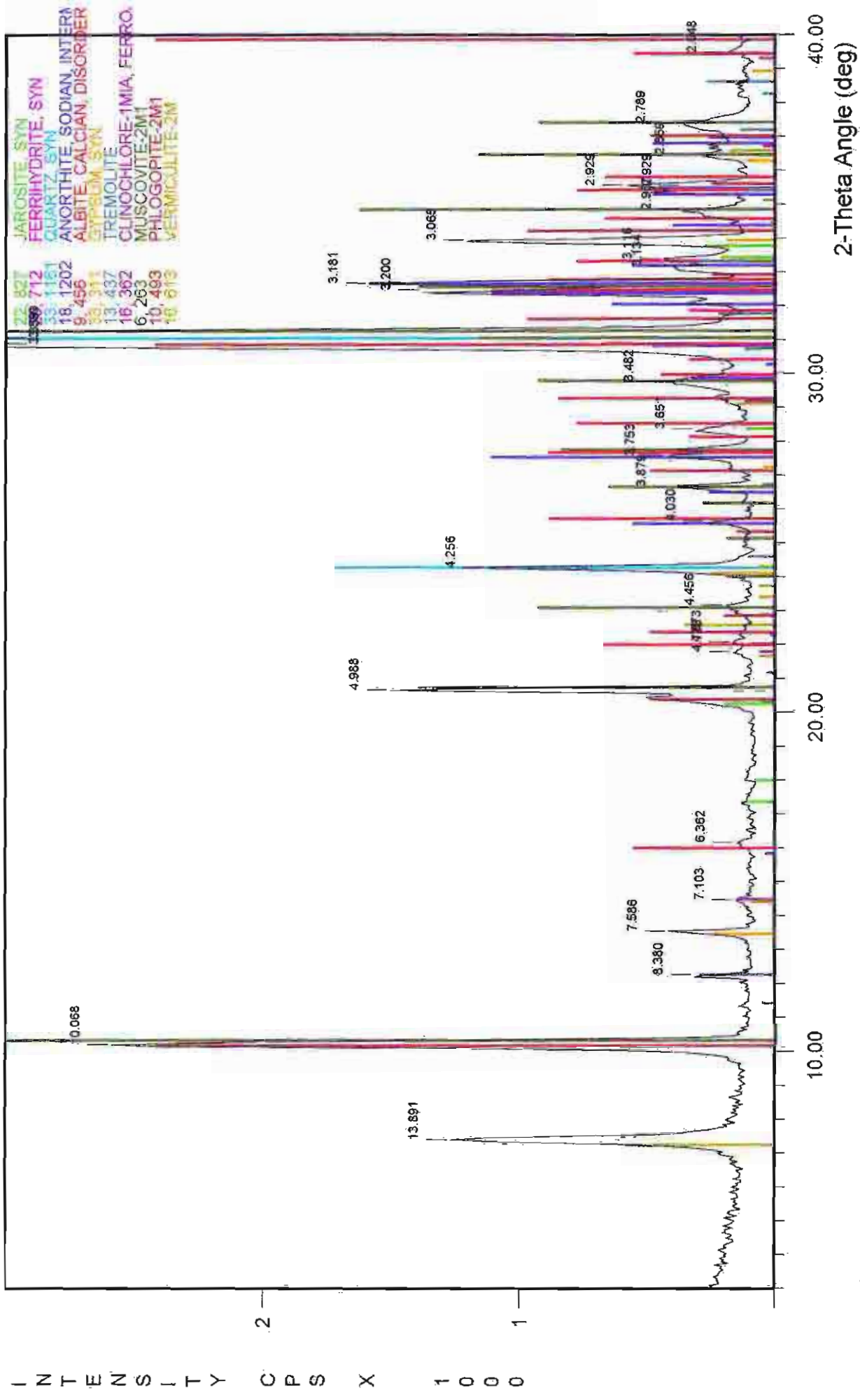


134cm cemented orange medium sand layer



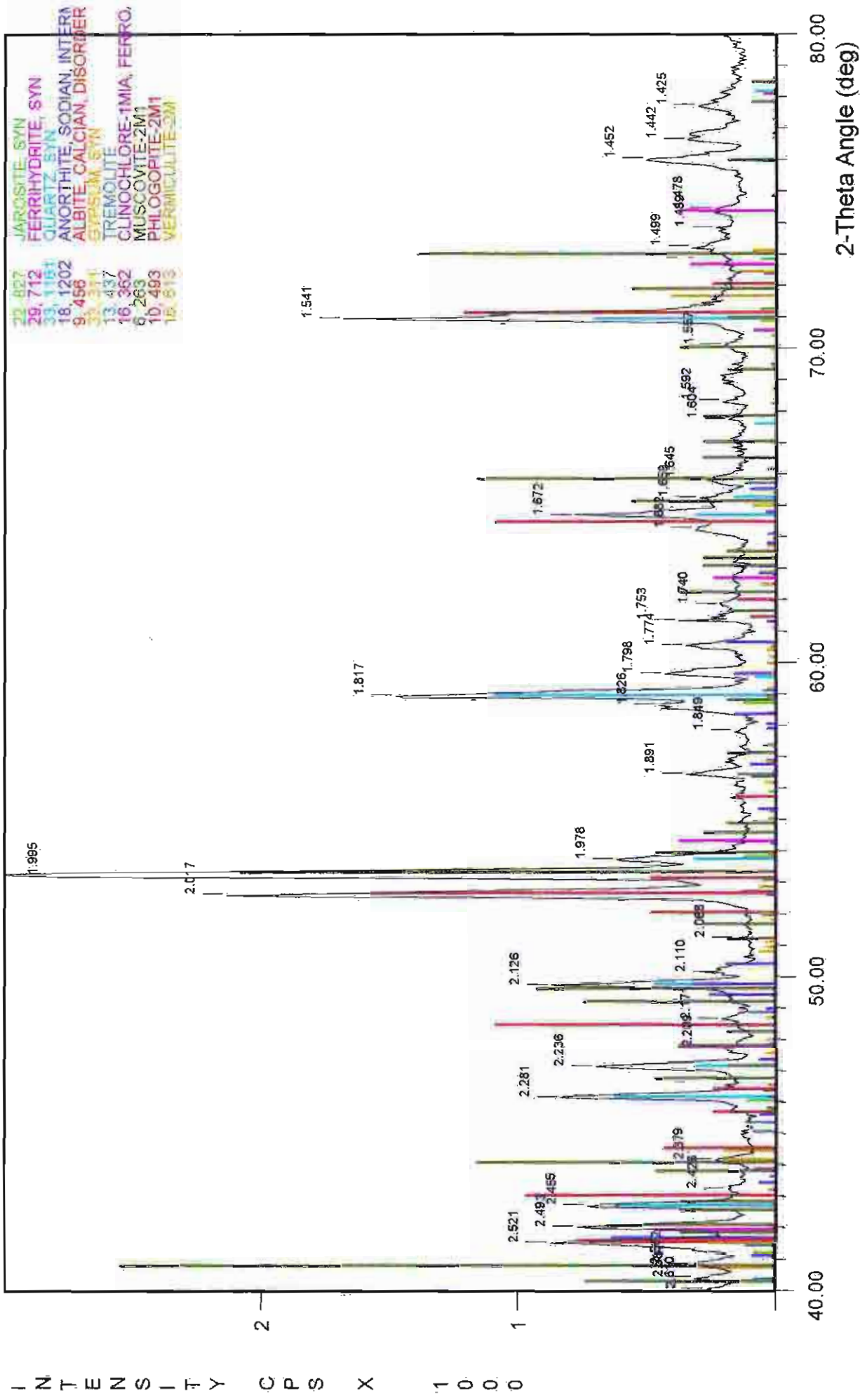
File Name: A:\11-34M

137cm cemented boundary layer



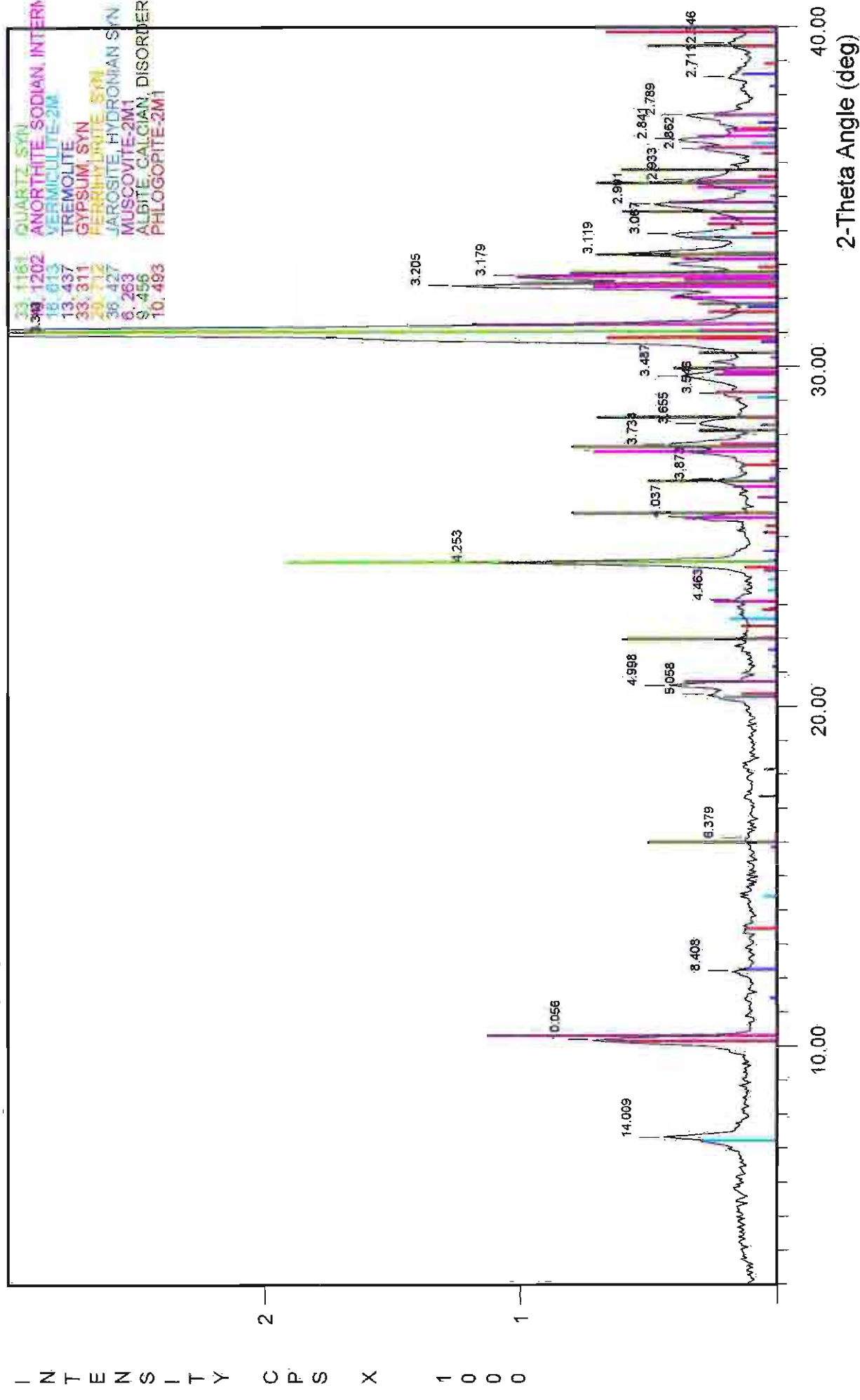
File Name: A:\1-37MCLB

137cm cemented boundary layer



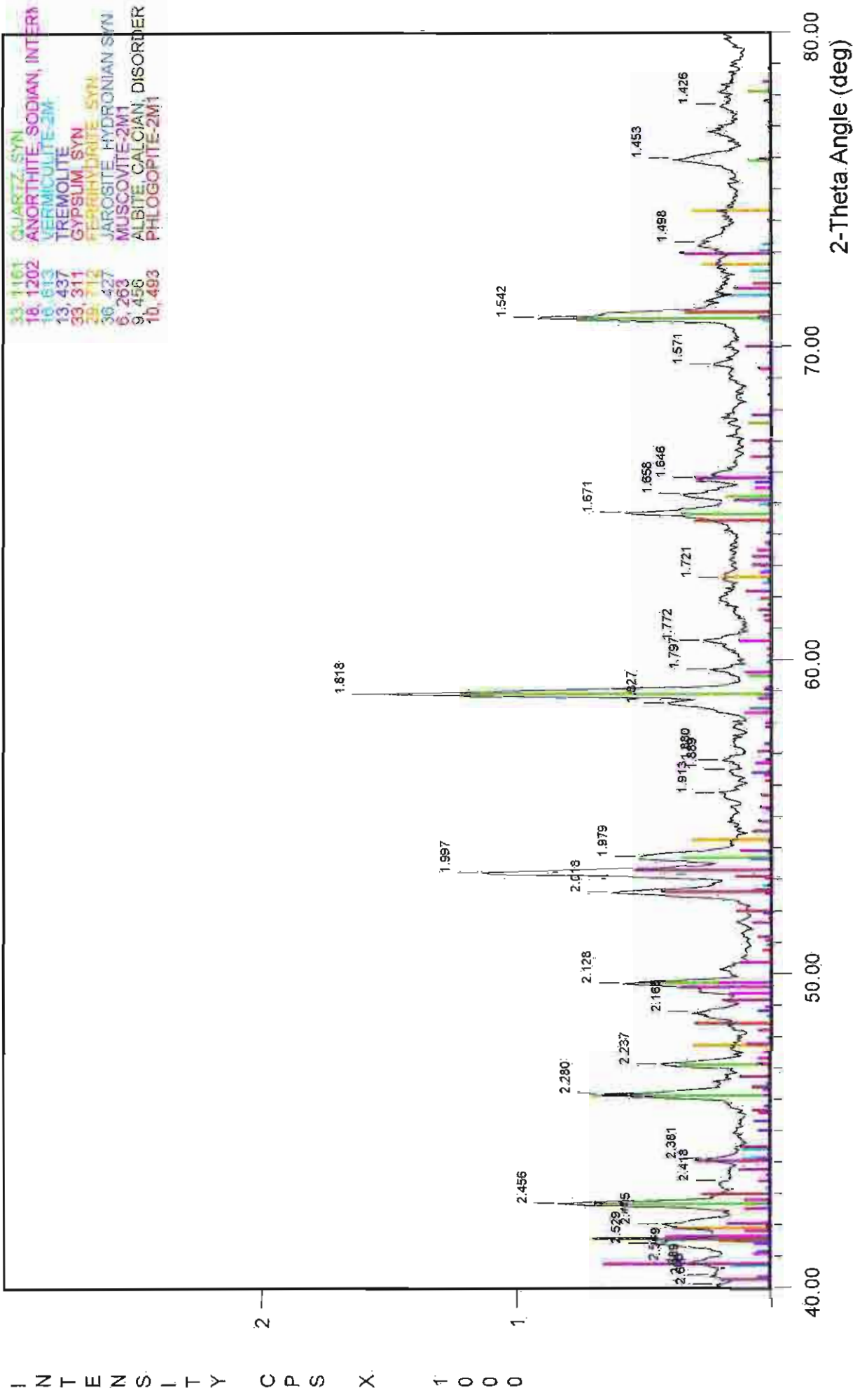
File Name: A\11-37MCLB

137cm cemented boundary layer



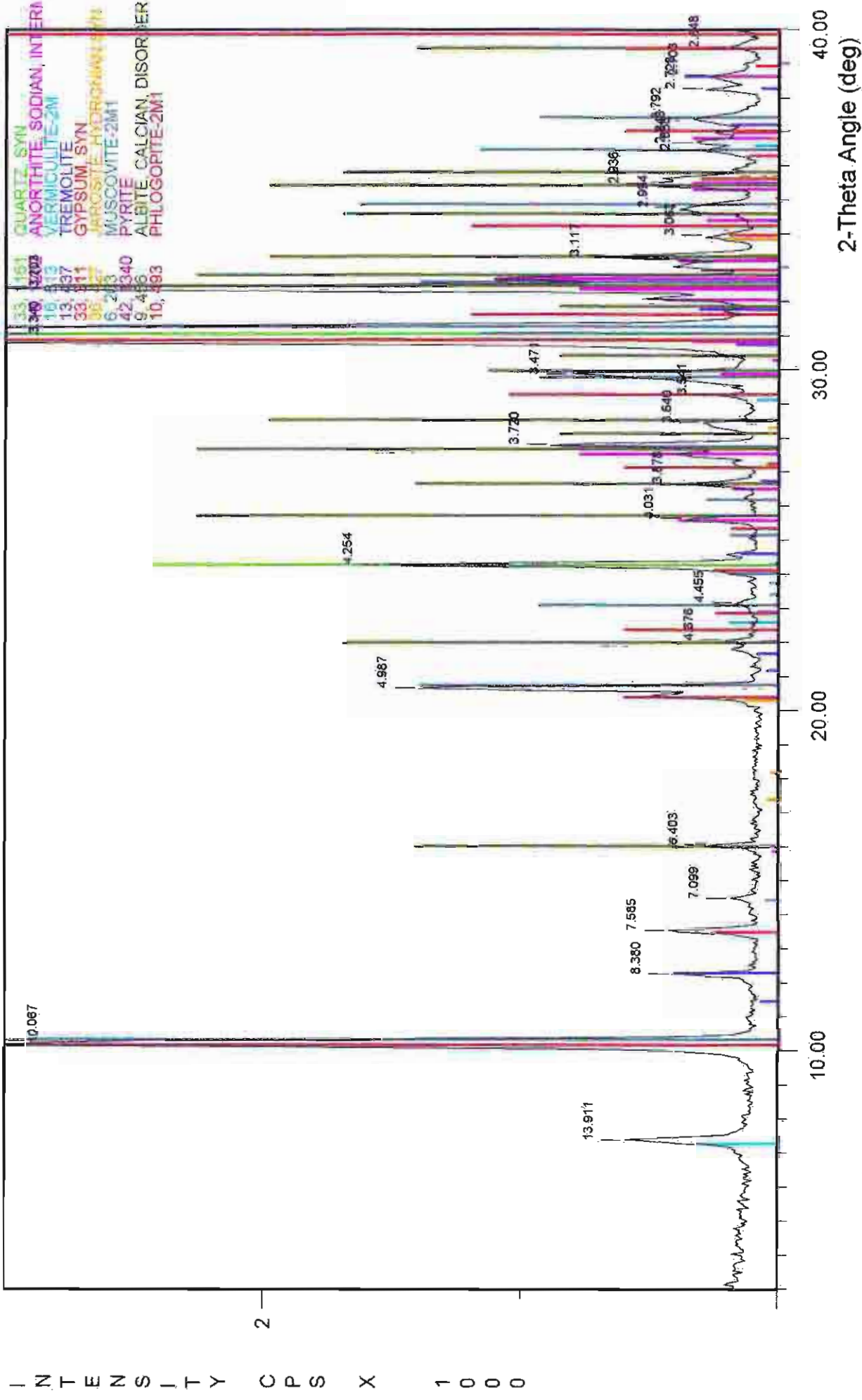
File Name: A:\1-37MCLS

137cm cemented boundary layer

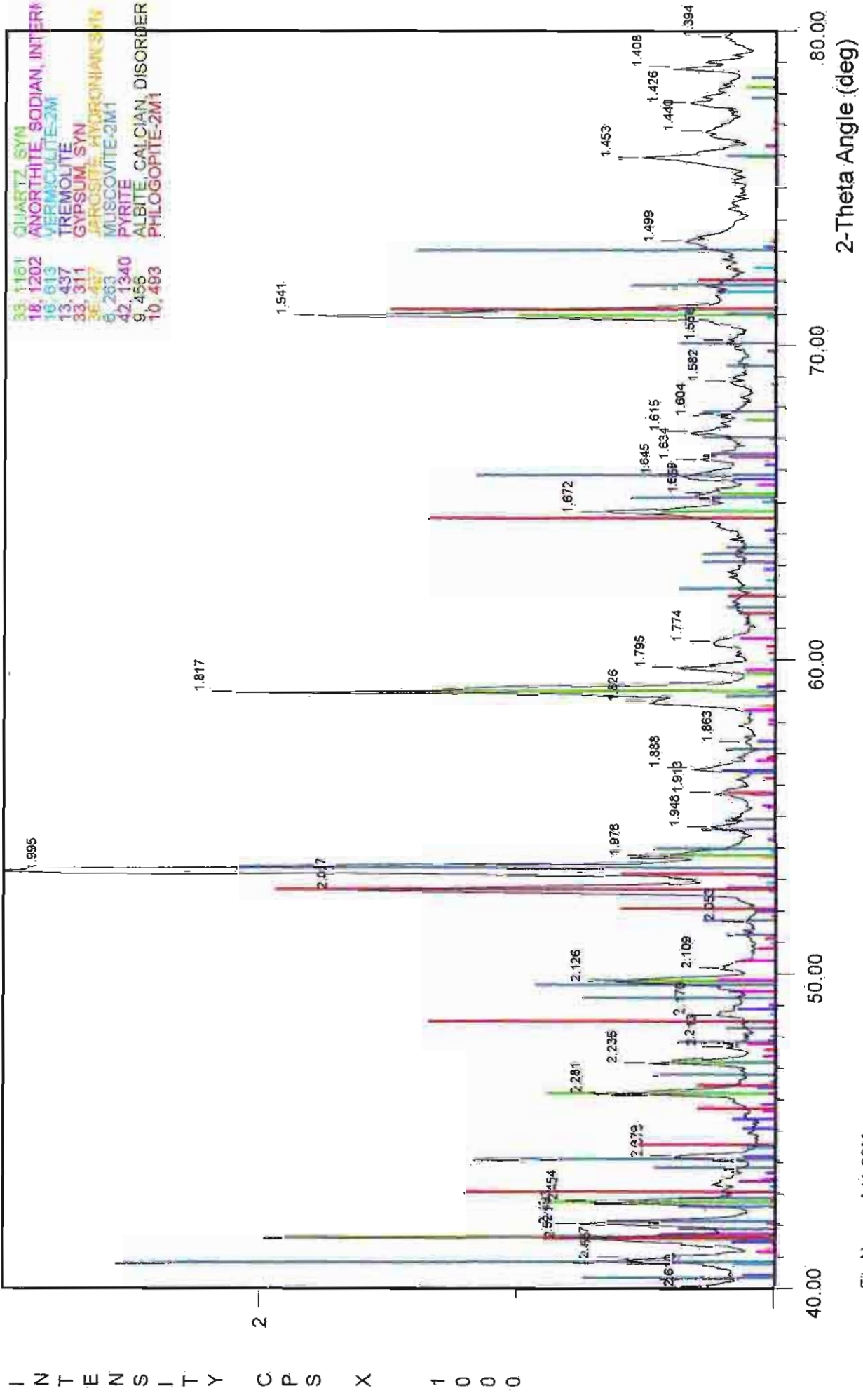


File Name: A:\1-37MCLS

MA 138cm light grey yellow layer

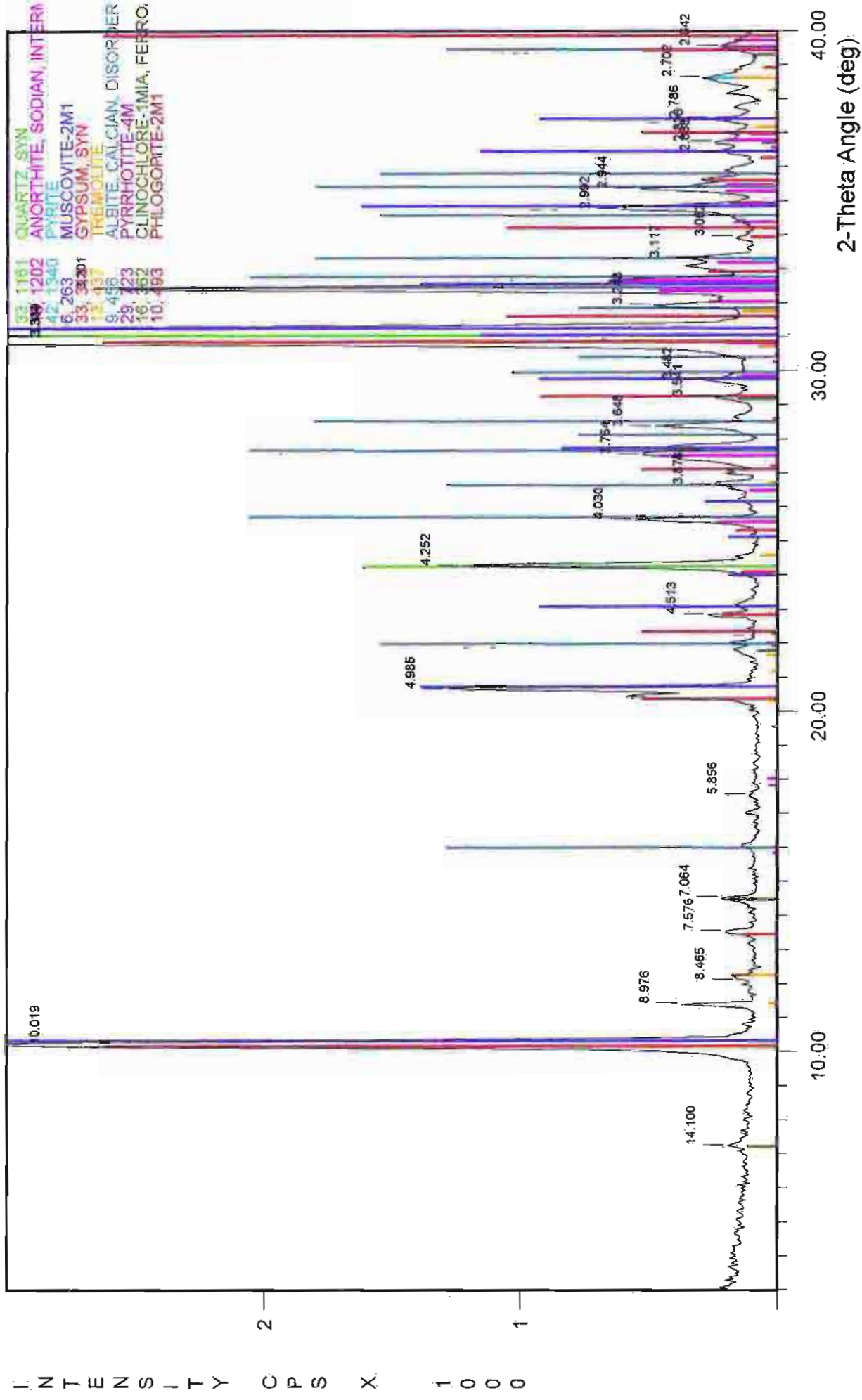


MA 138cm light grey yellow layer



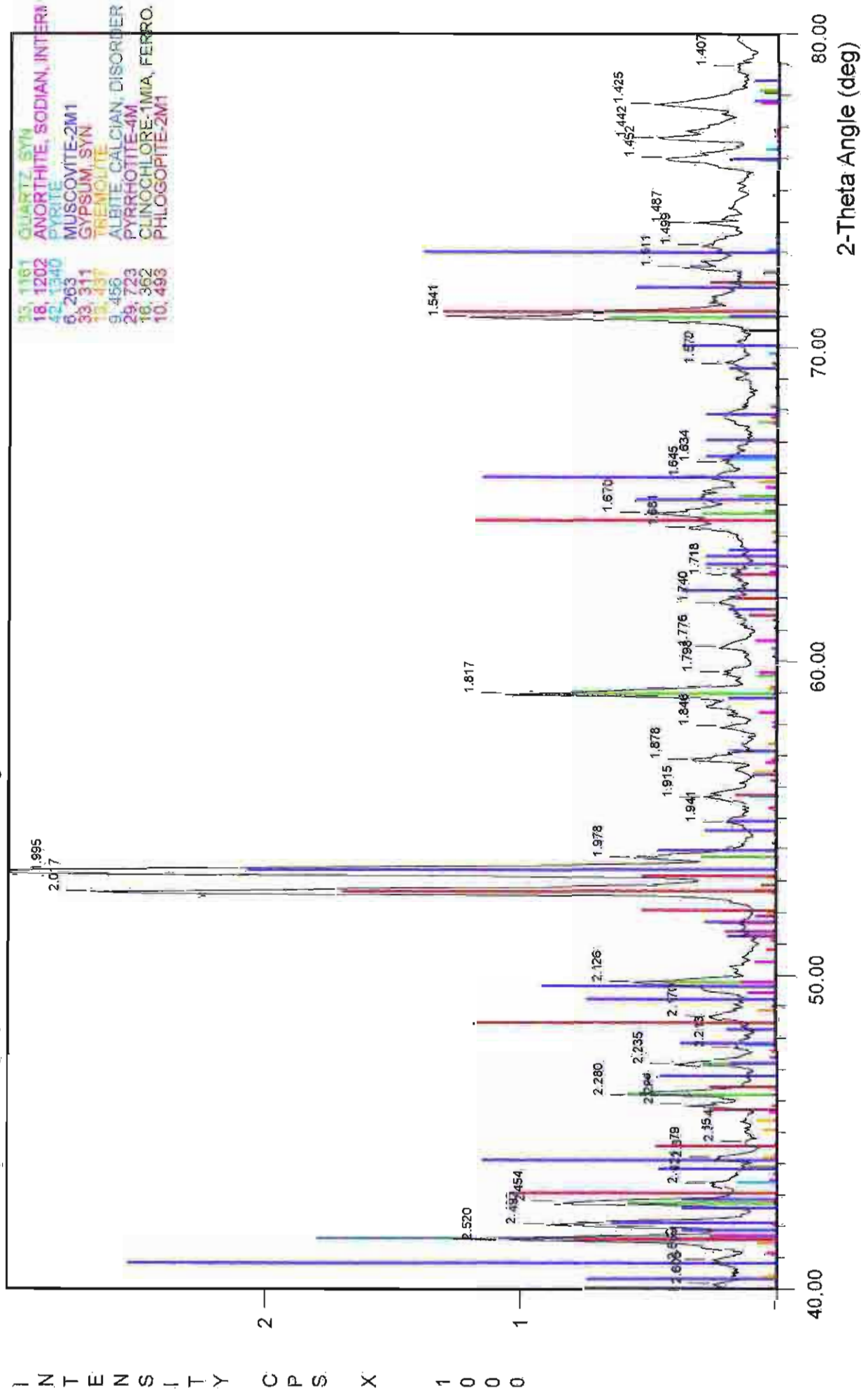
File Name: A:\1-38M

139.5cm top of dark grey fine - medium sand region



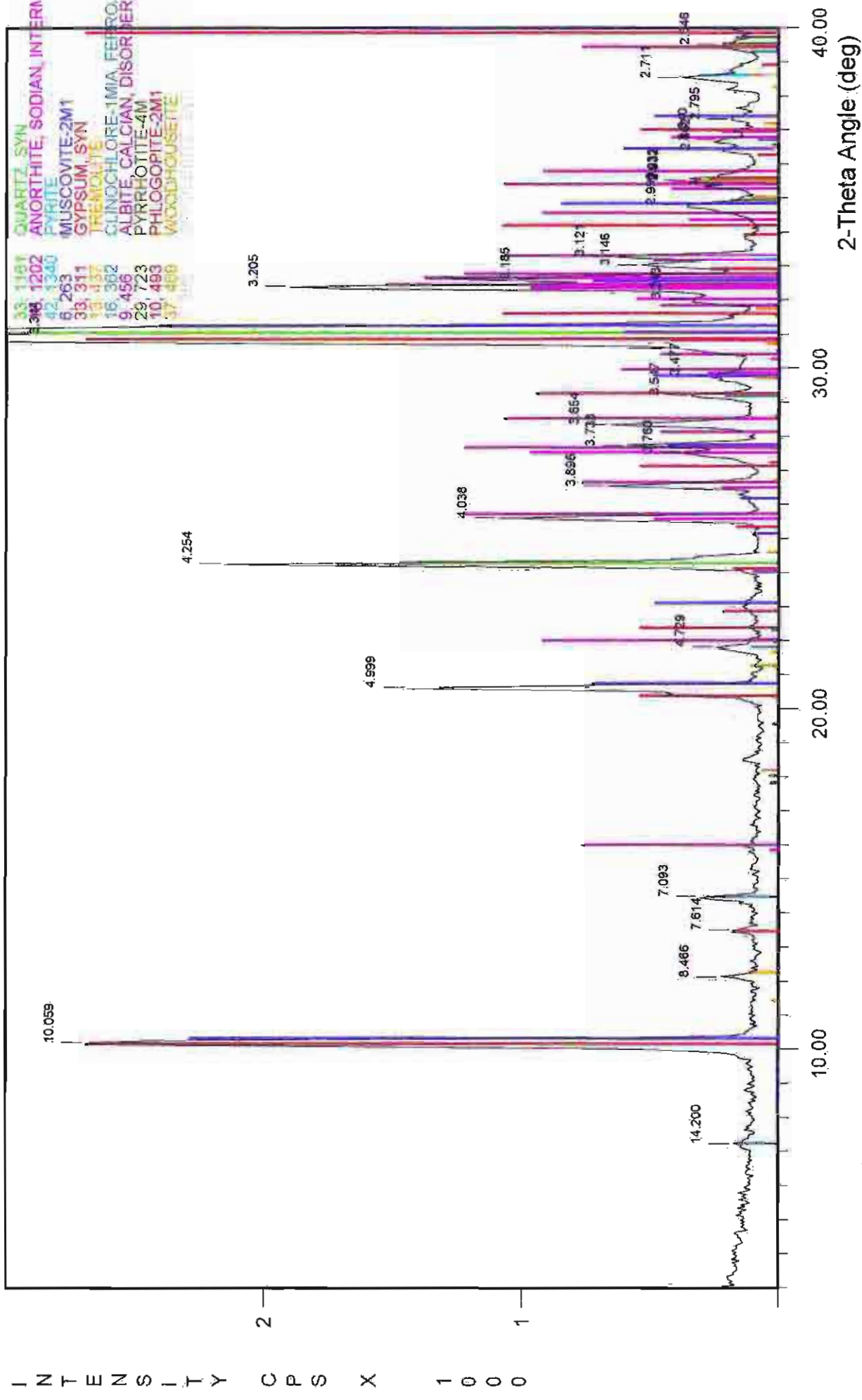
File Name: A:\1-395M

139.5cm top of dark grey fine - medium sand region



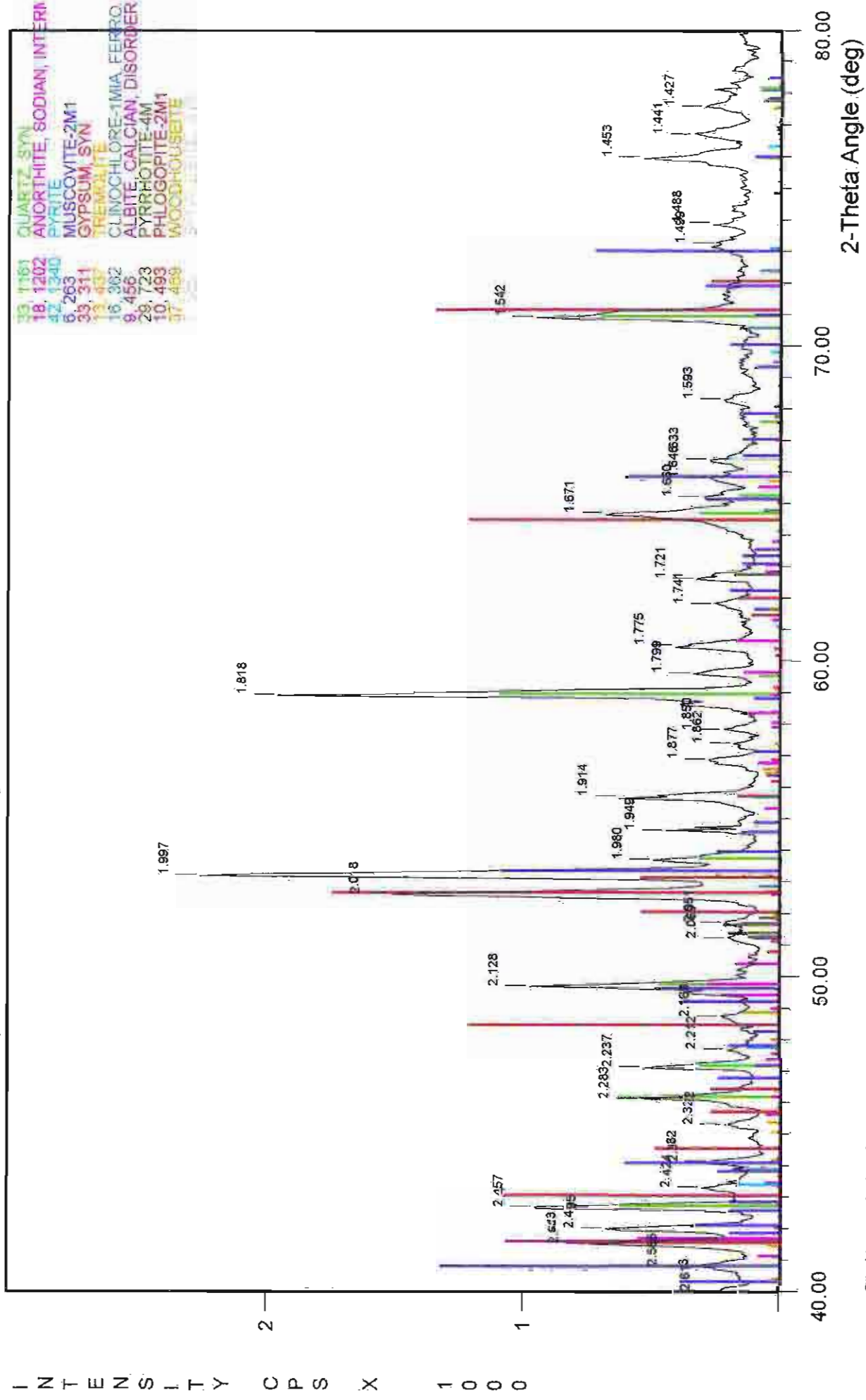
File Name: A:\1-395M

141cm base of dark grey fine medium sand region



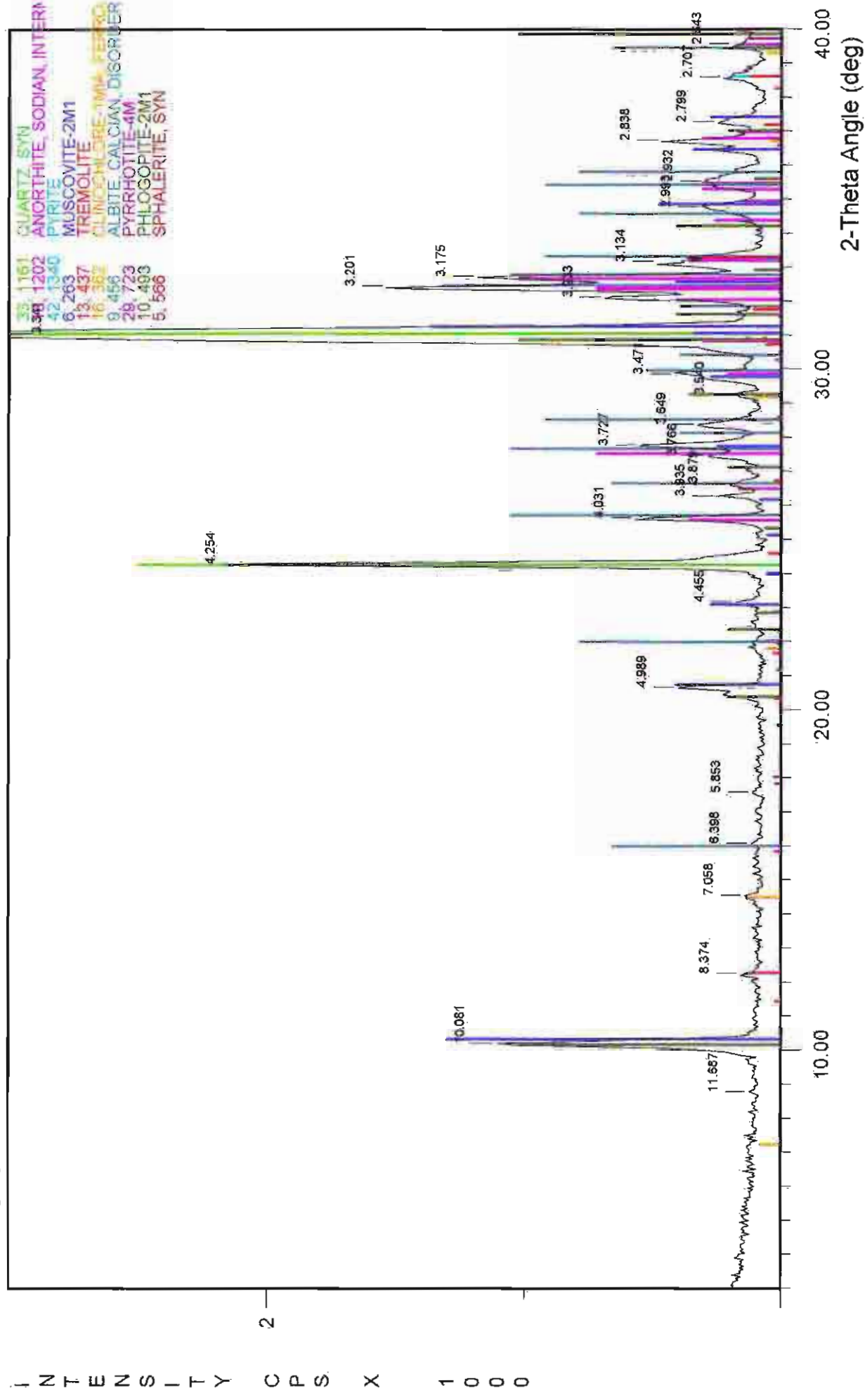
File Name: A:\11-41M

141cm base of dark grey fine medium sand region



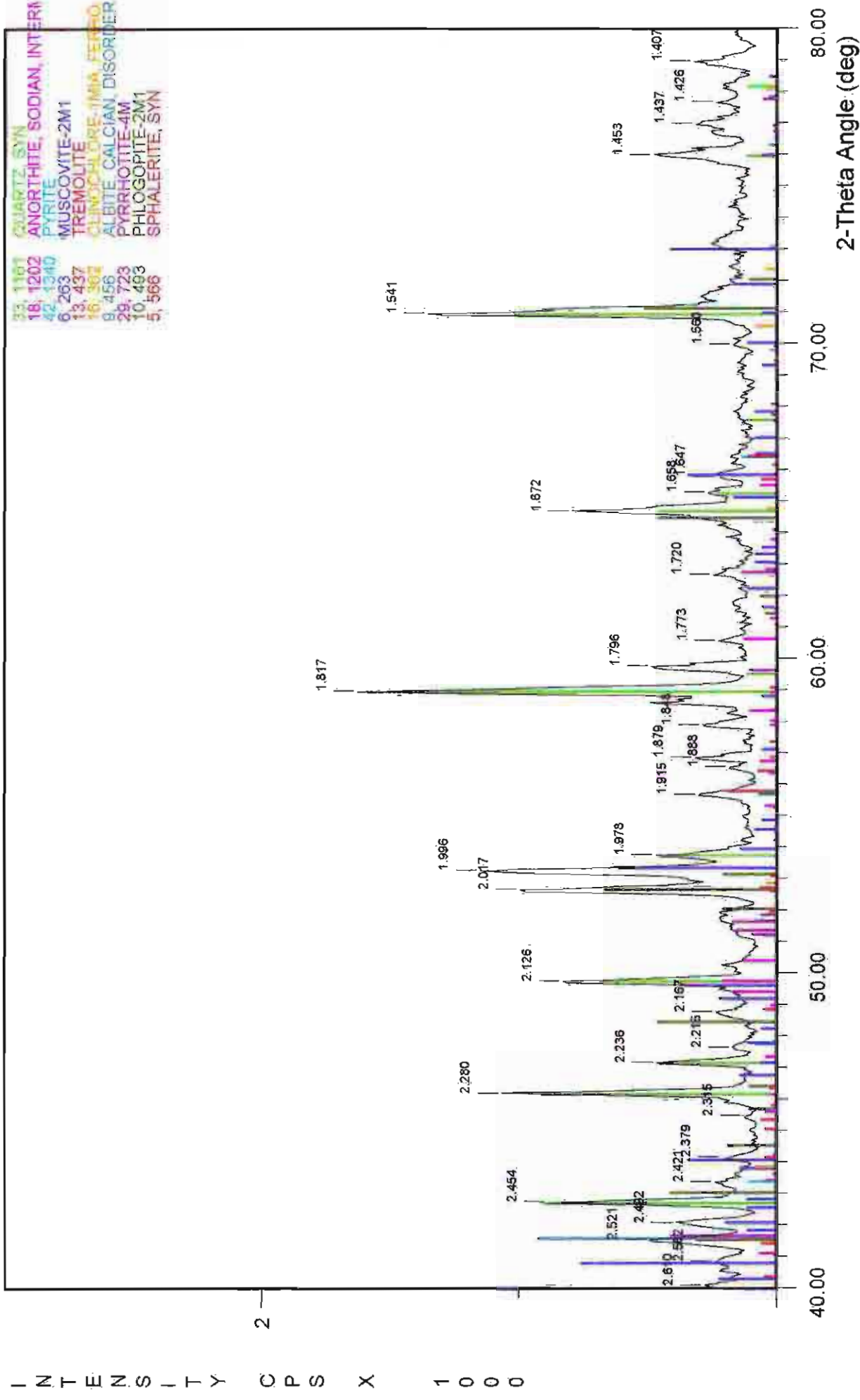
File Name: A:\1-41M

144cm grey medium sand



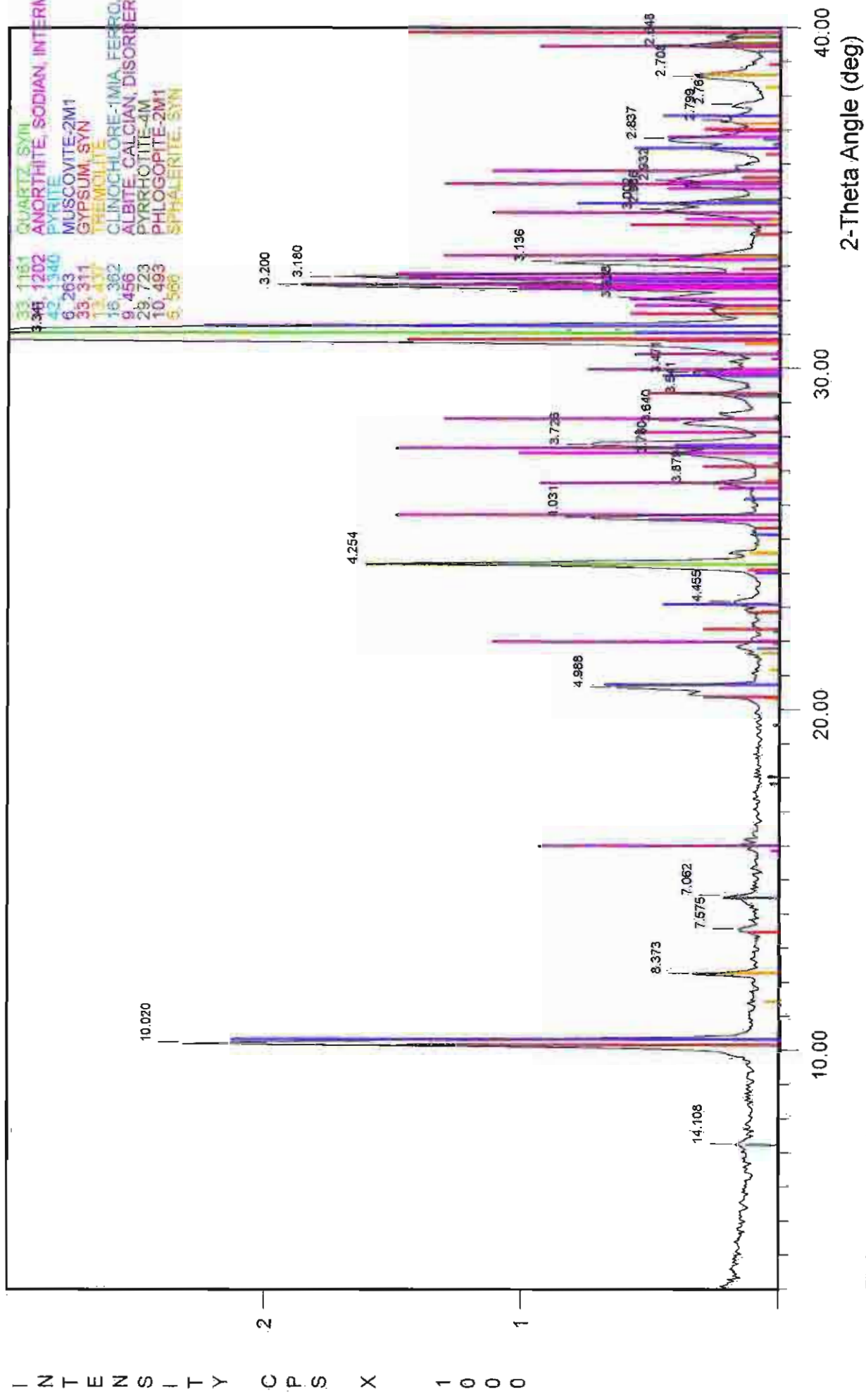
File Name: A\11-44M

144cm grey medium sand



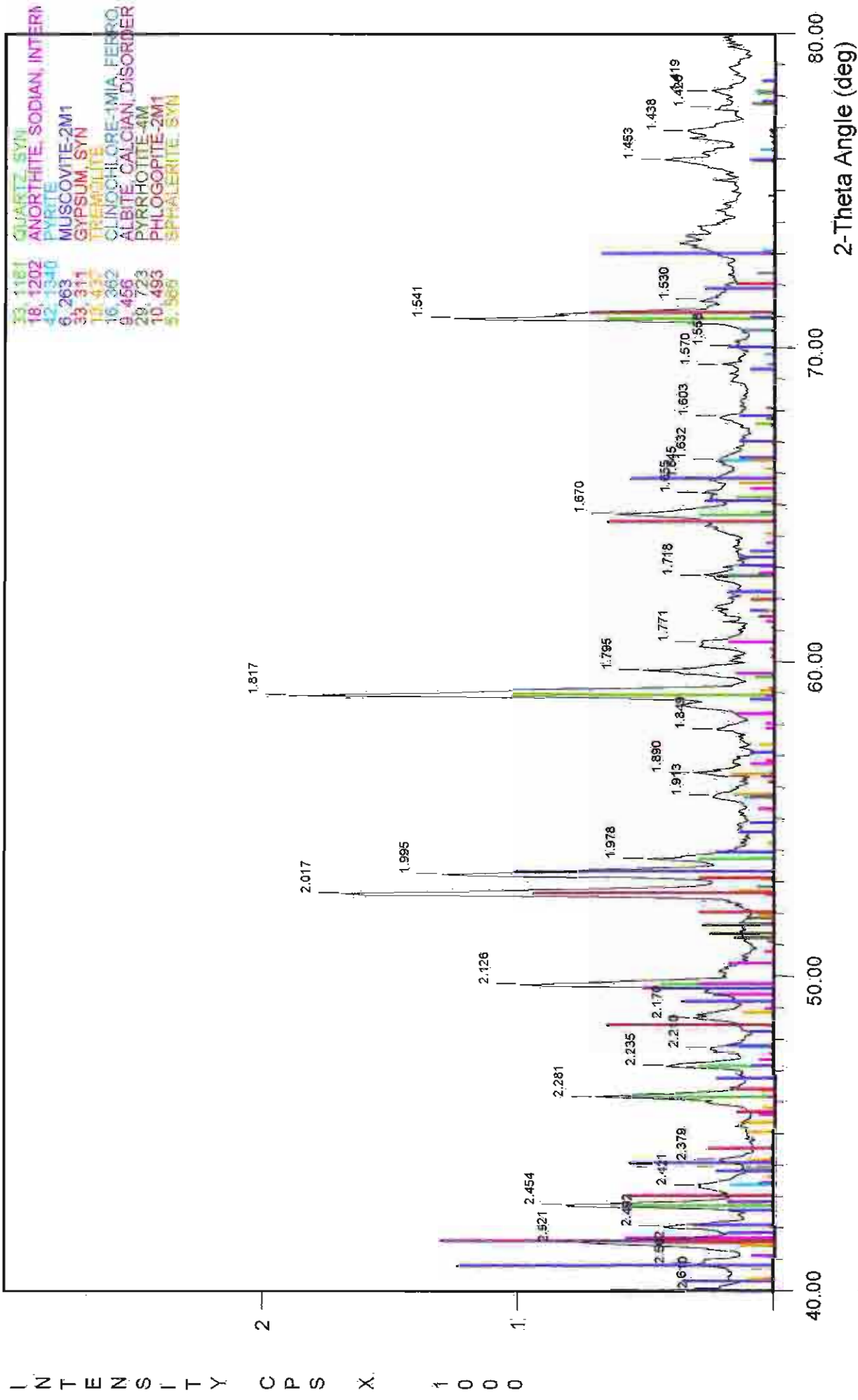
File Name: A:\1-44M

144.5cm grey fine sand - silt layer



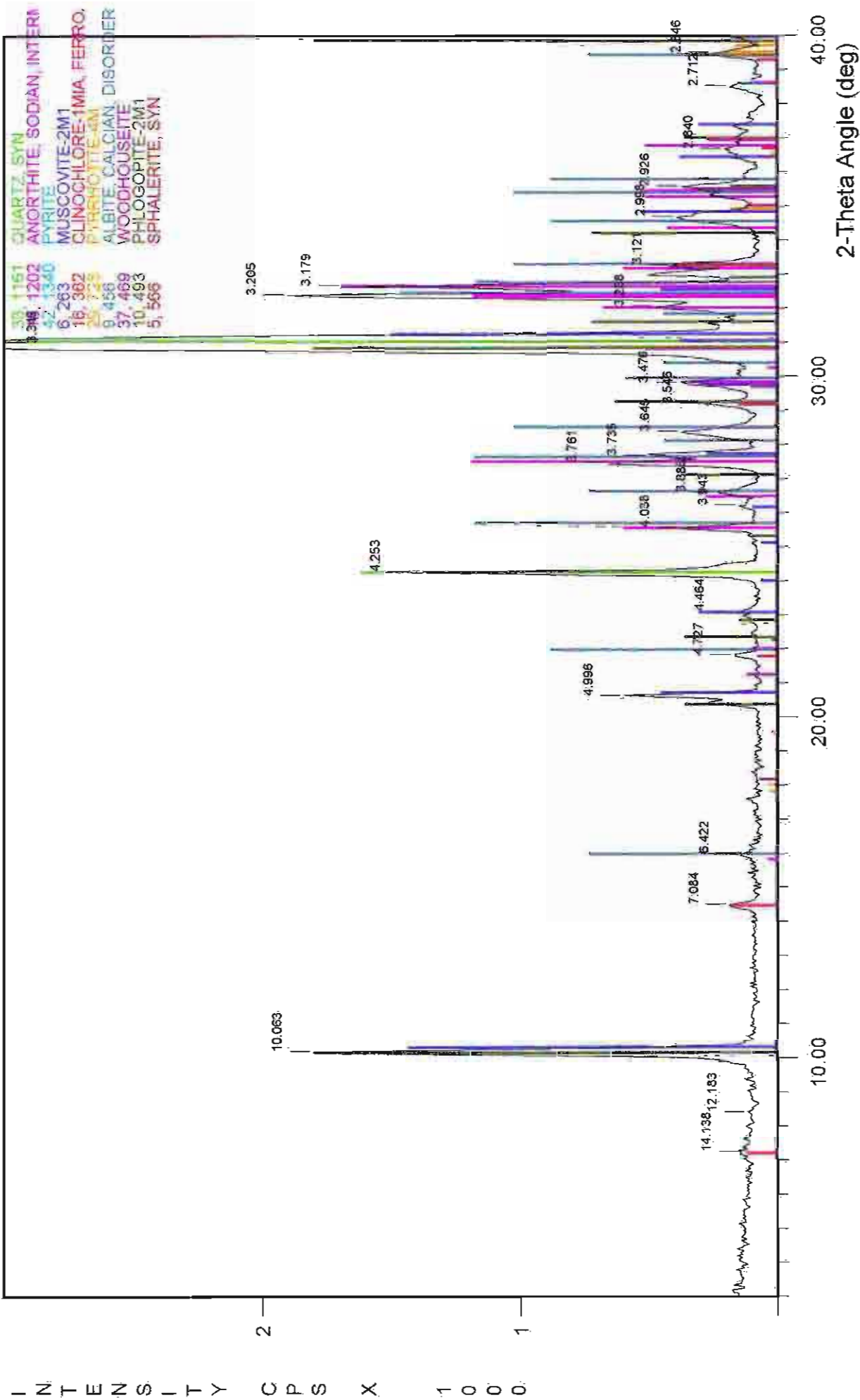
File Name: A:\1-445M

144.5cm grey fine sand - silt layer



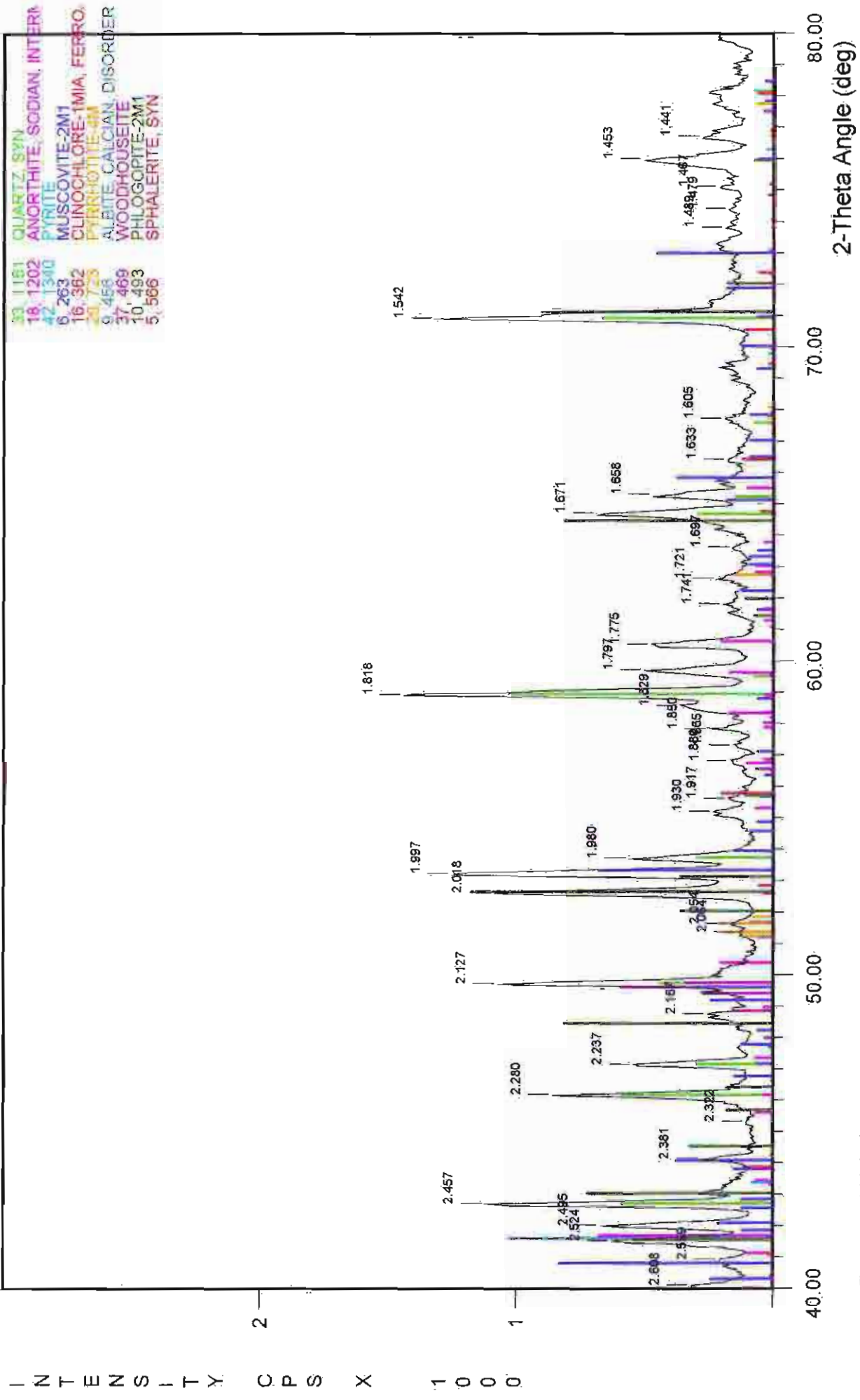
File Name: A:\1-445M

145.5cm banded light grey & grey silt layer



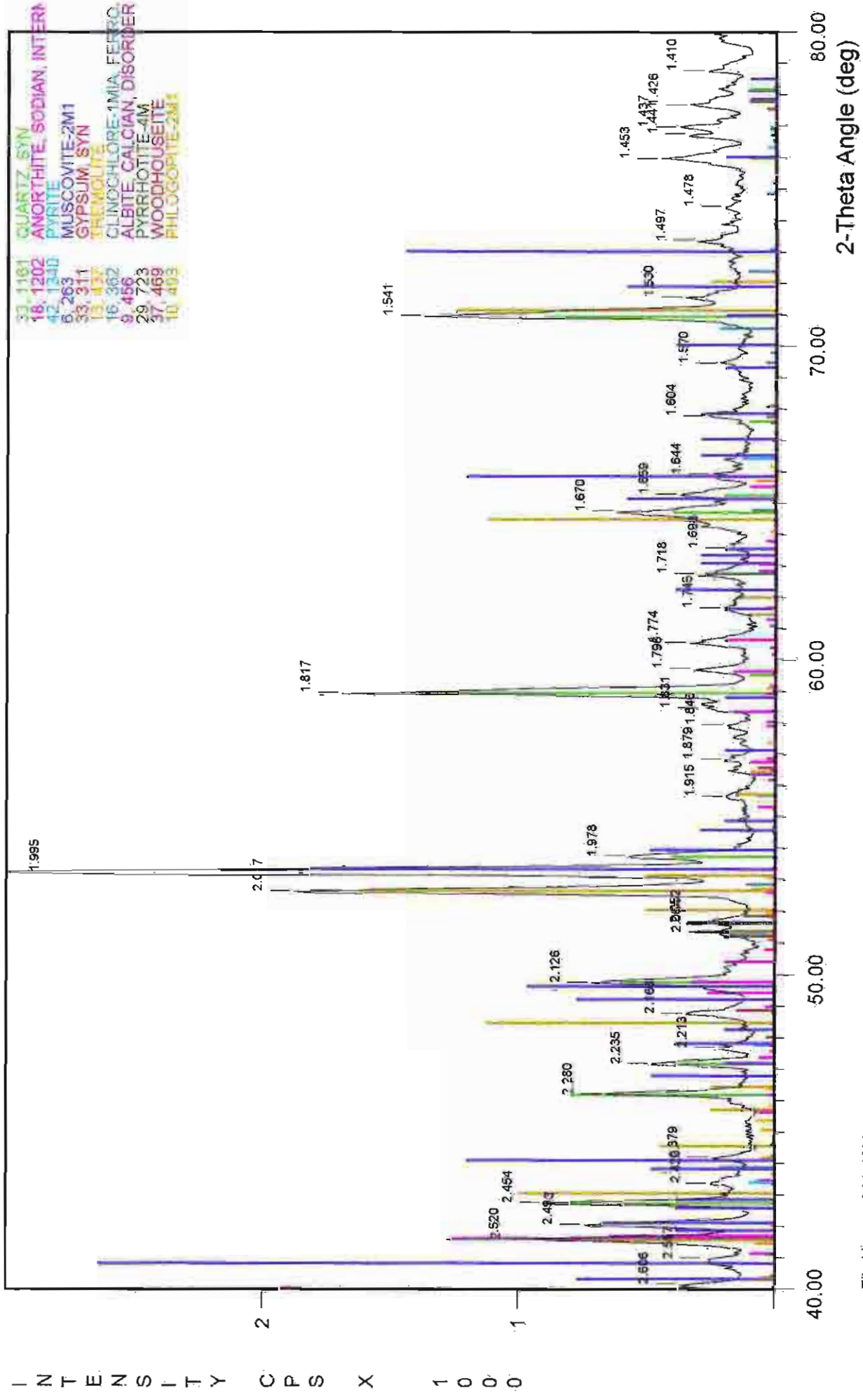
File Name: A\1-455M

145.5cm banded light grey & grey silt layer



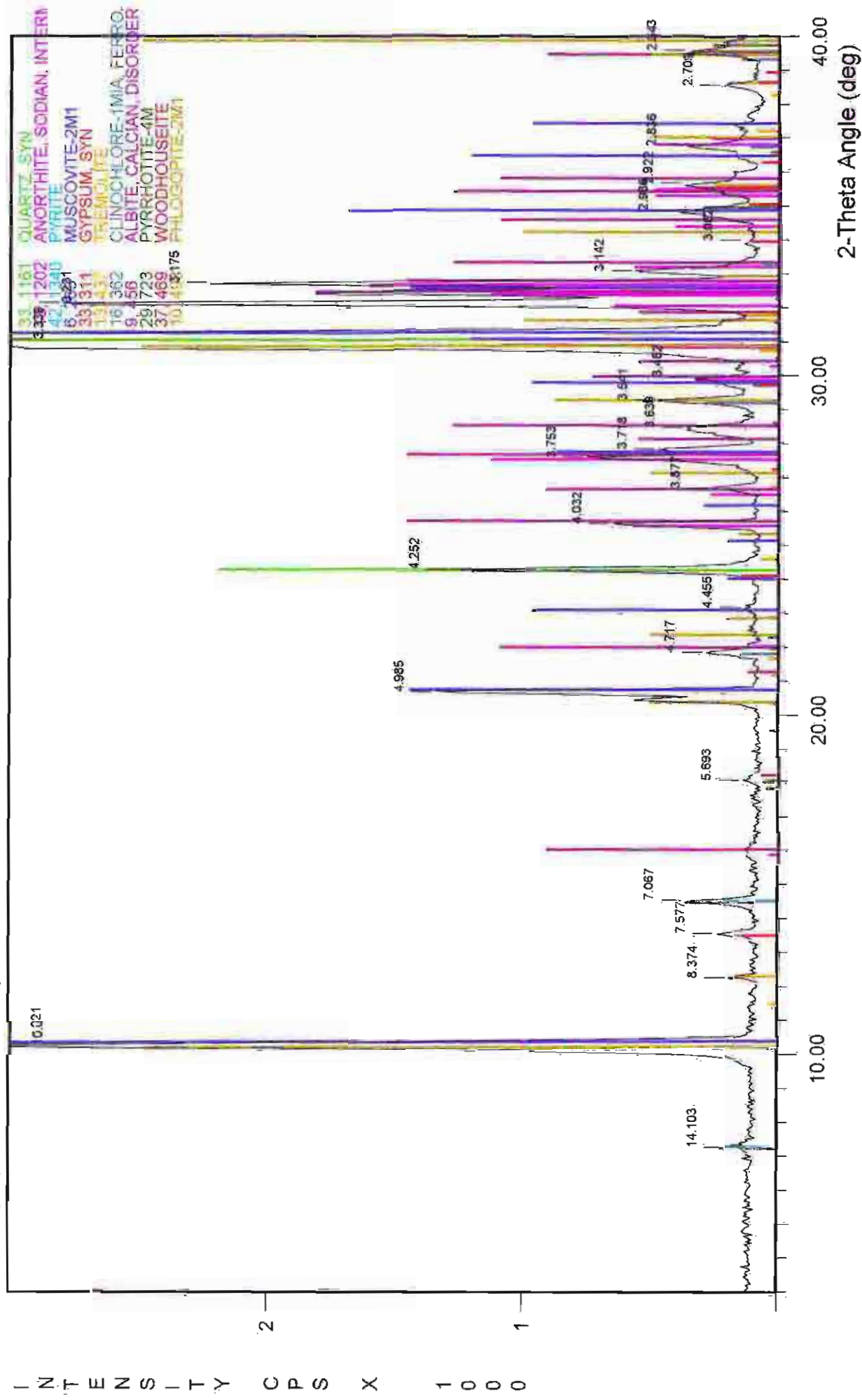
File Name: A:\1-455M

148cm grey medium sand layer.



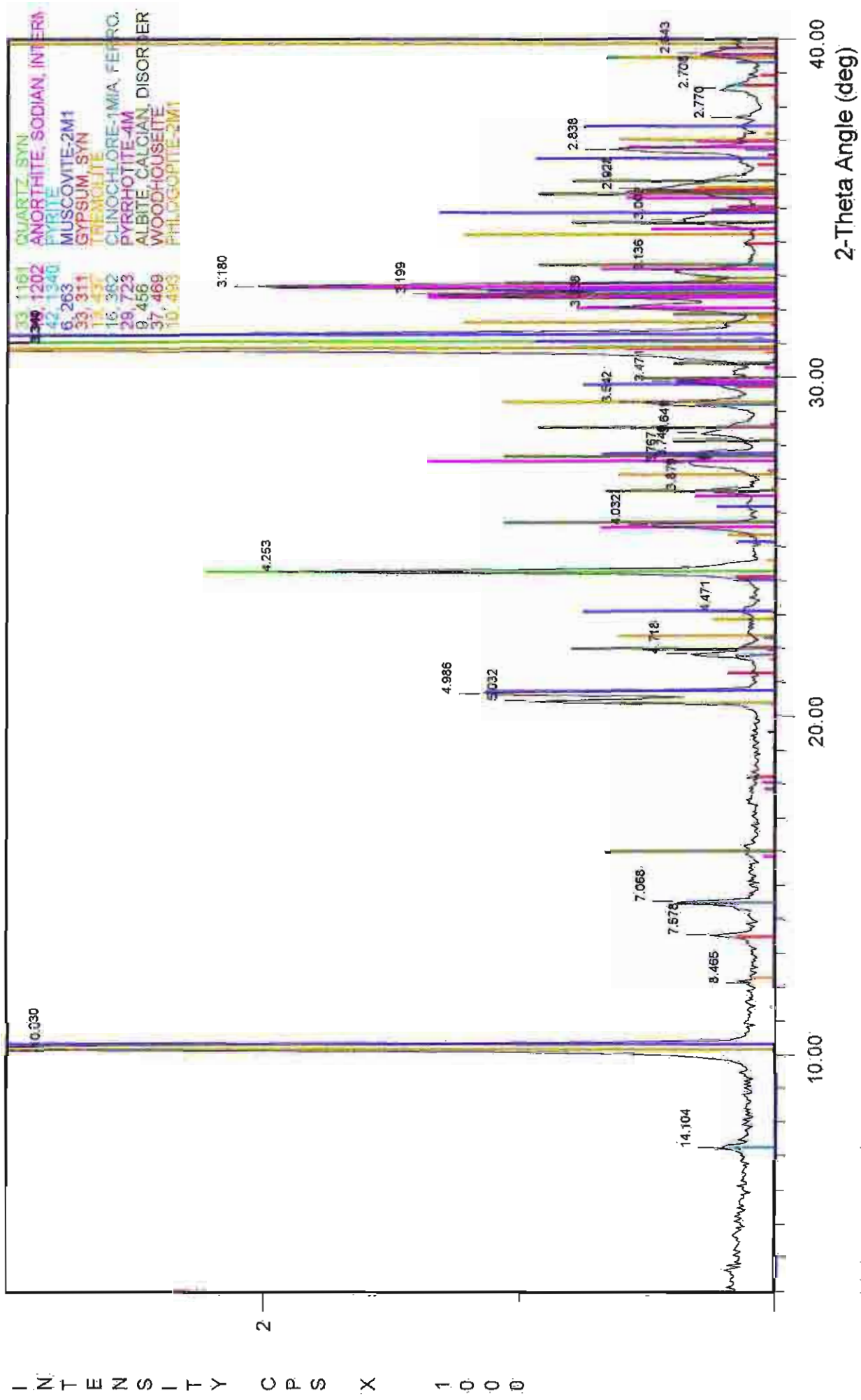
File Name: A:\1-48M

148cm grey medium sand layer



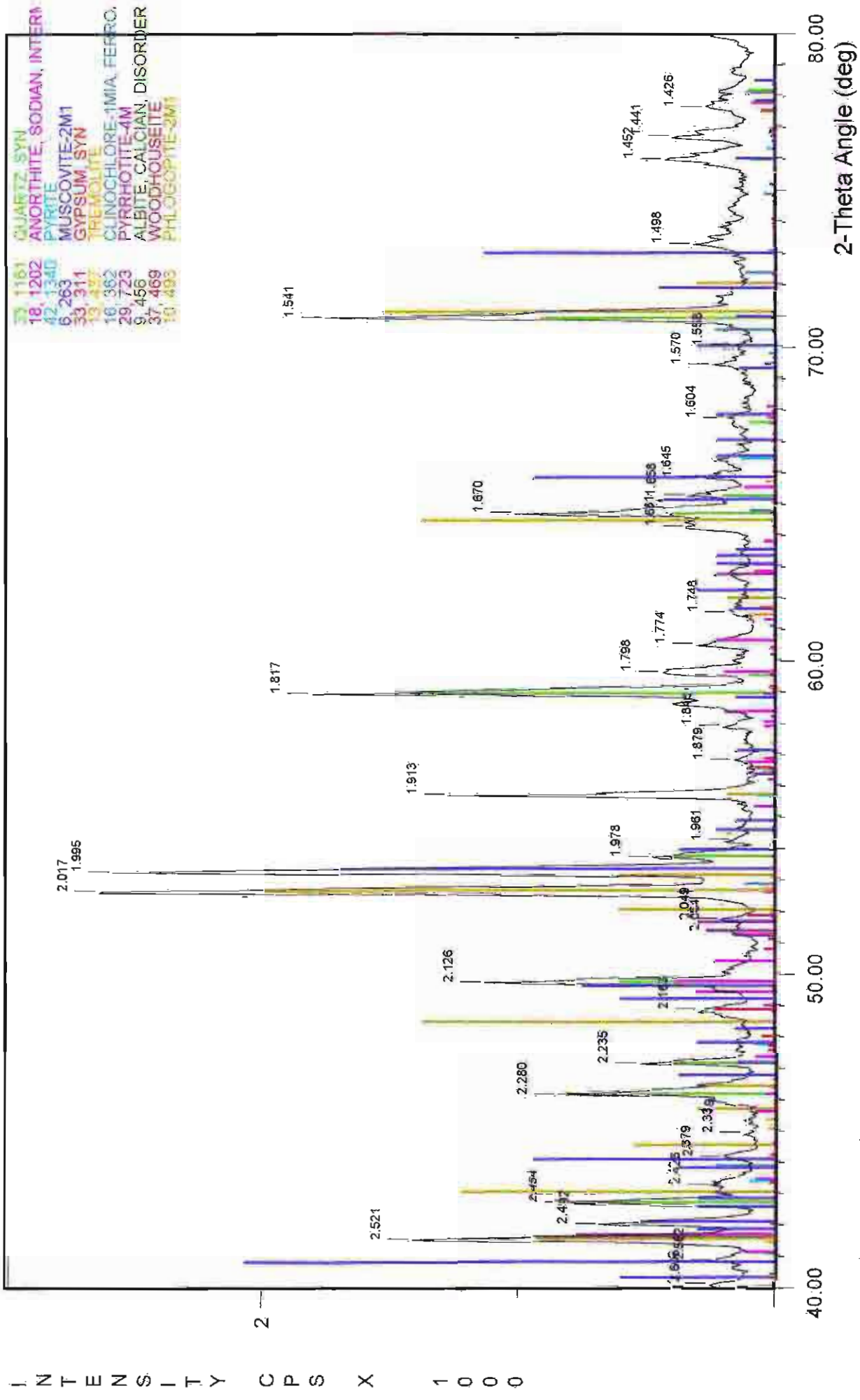
File Name: A:\1-48M

149.5cm banded light grey & grey silt layer



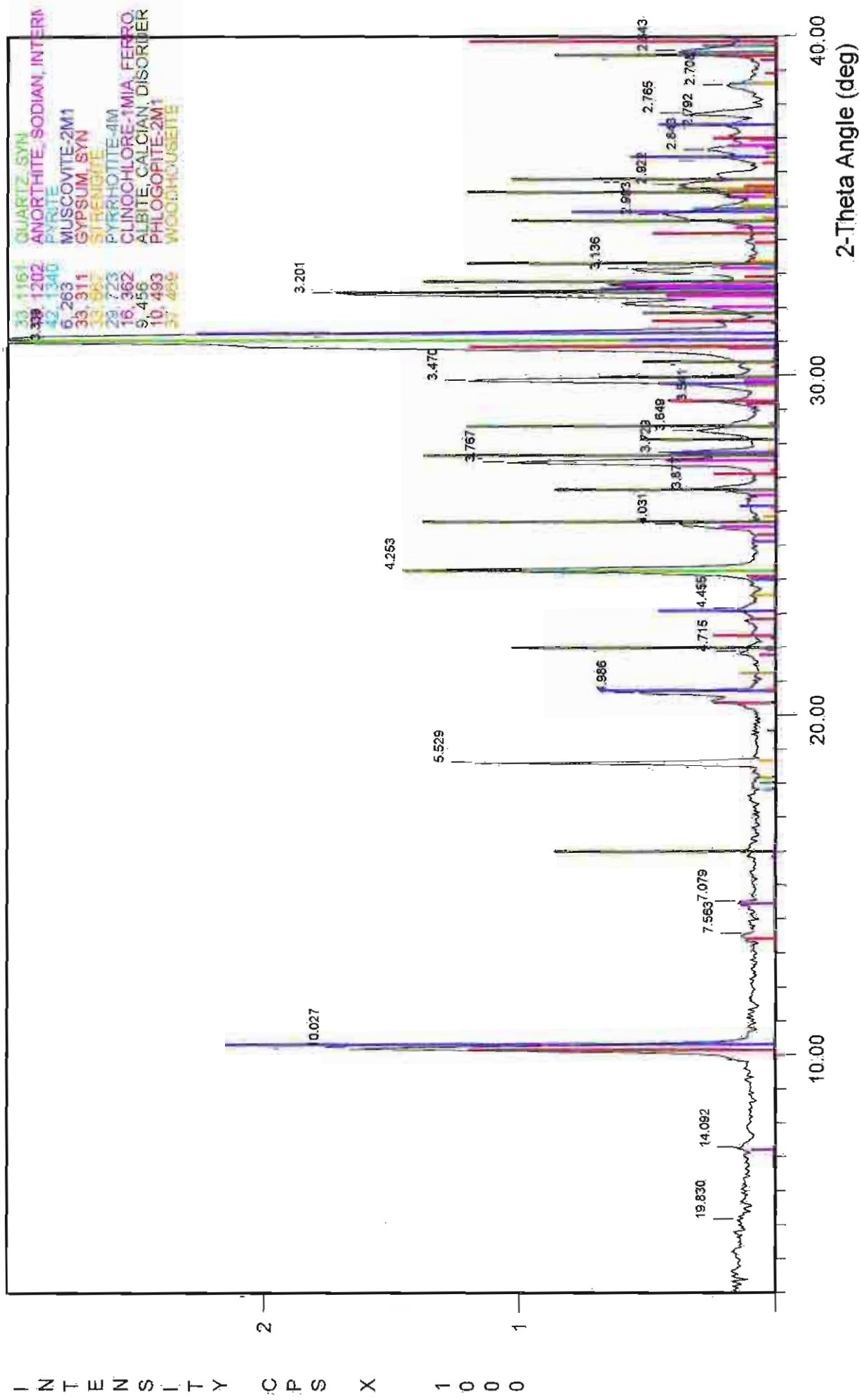
File Name: A:\1-495M

149.5cm banded light grey & grey silt layer



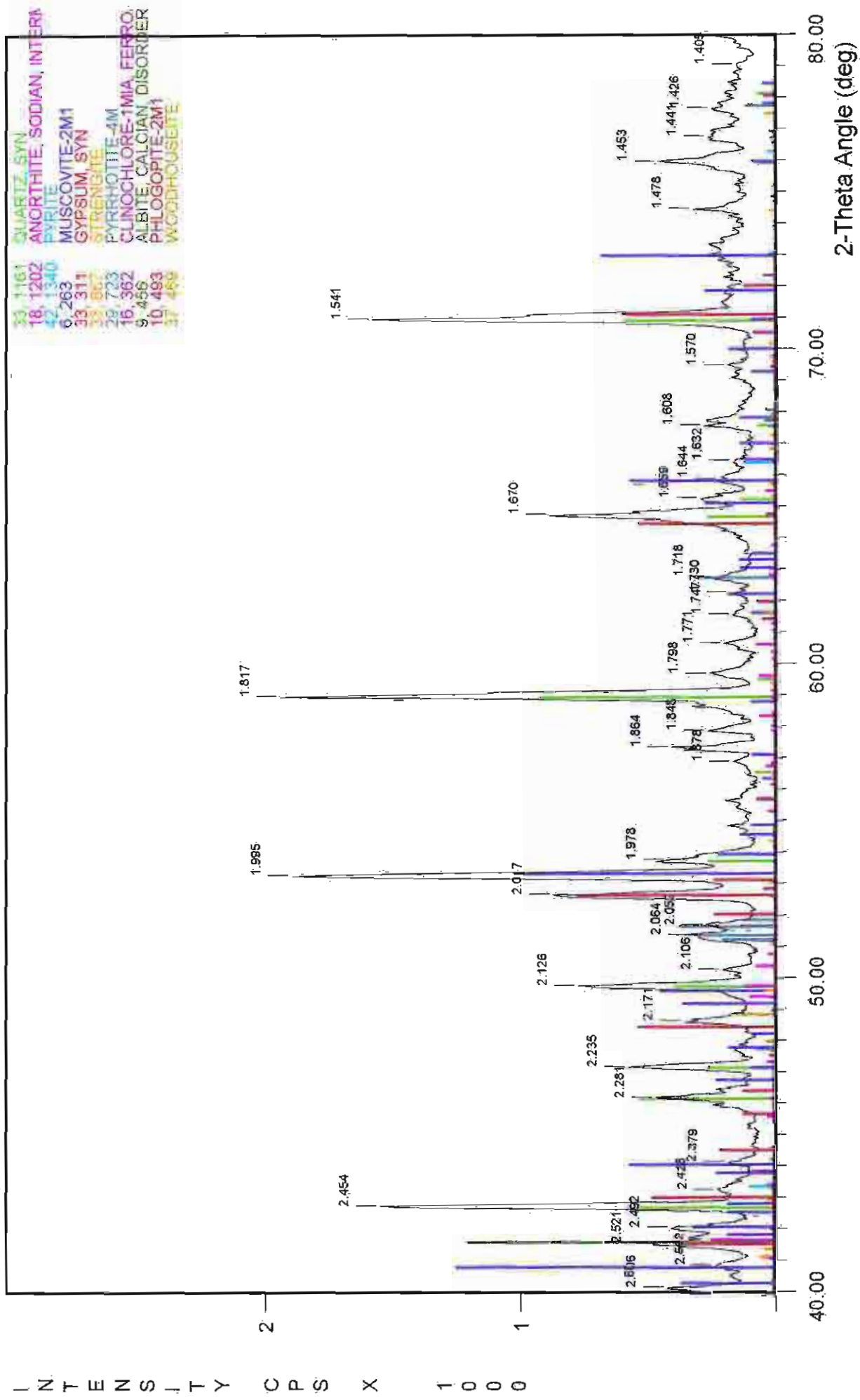
File Name: A:\1-495M

153cm top of grey medium sand region



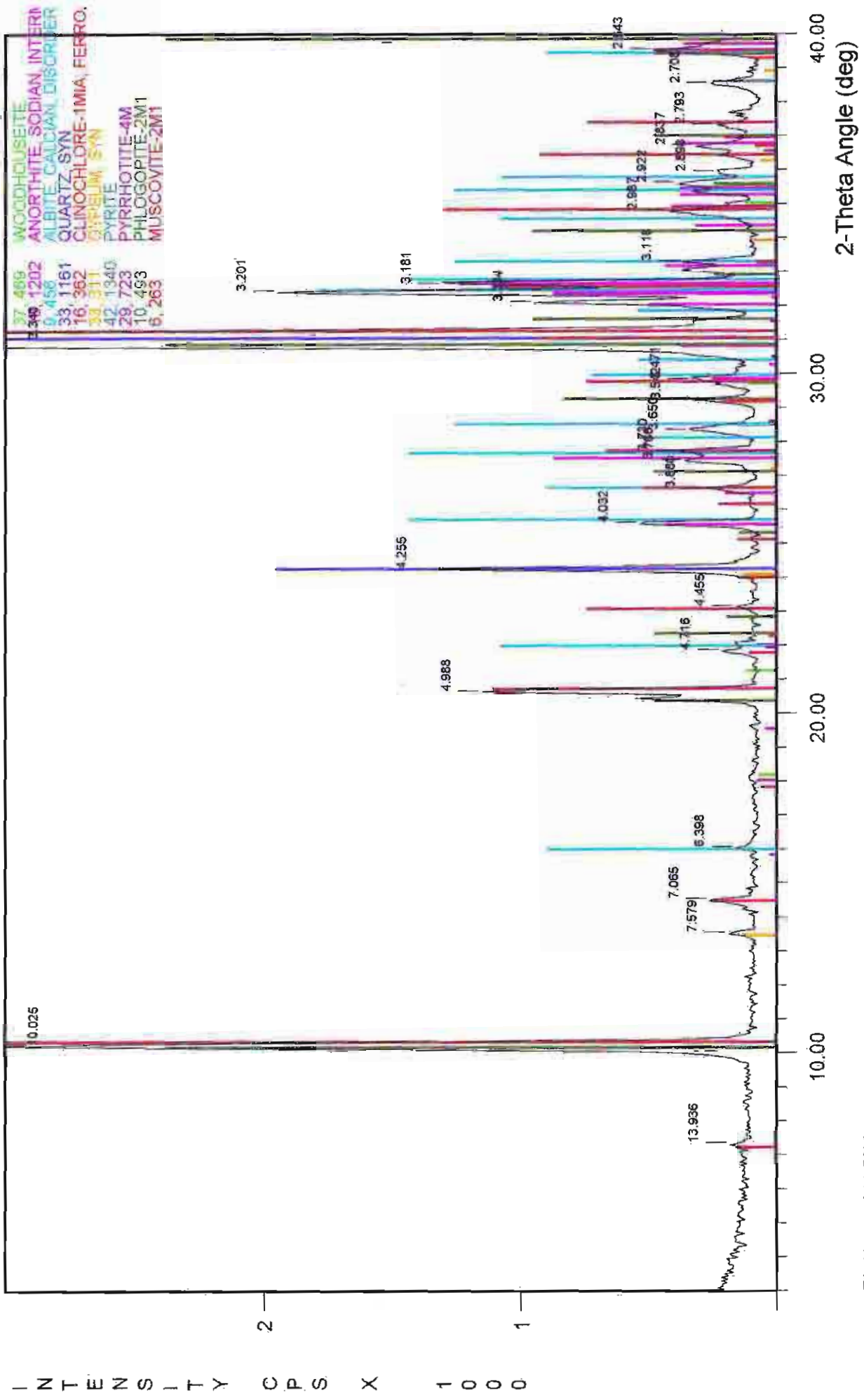
File Name: A:\1-53M

153cm top of grey medium sand region

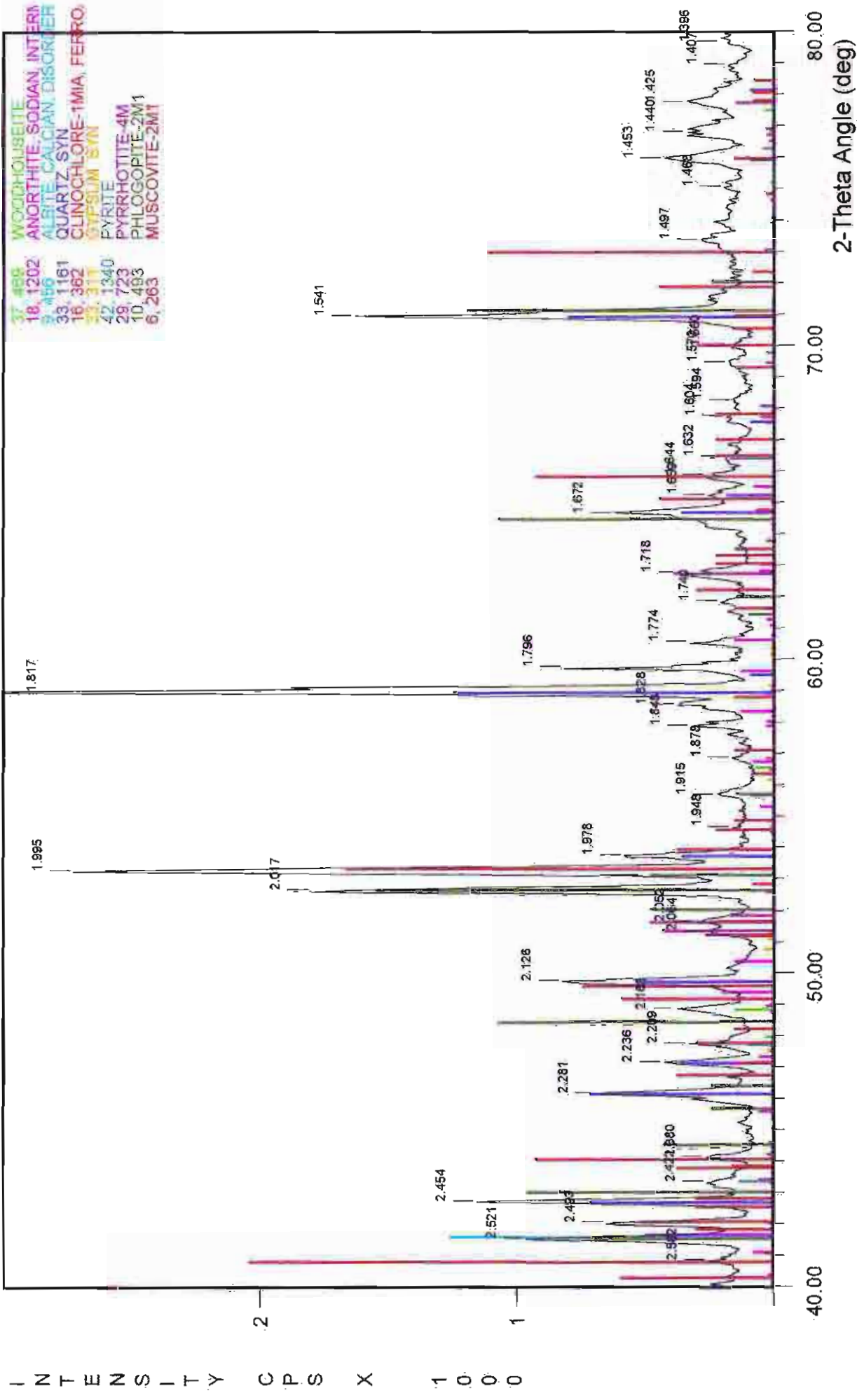


File Name: A:\11-53M

158cm base of grey medium sand region

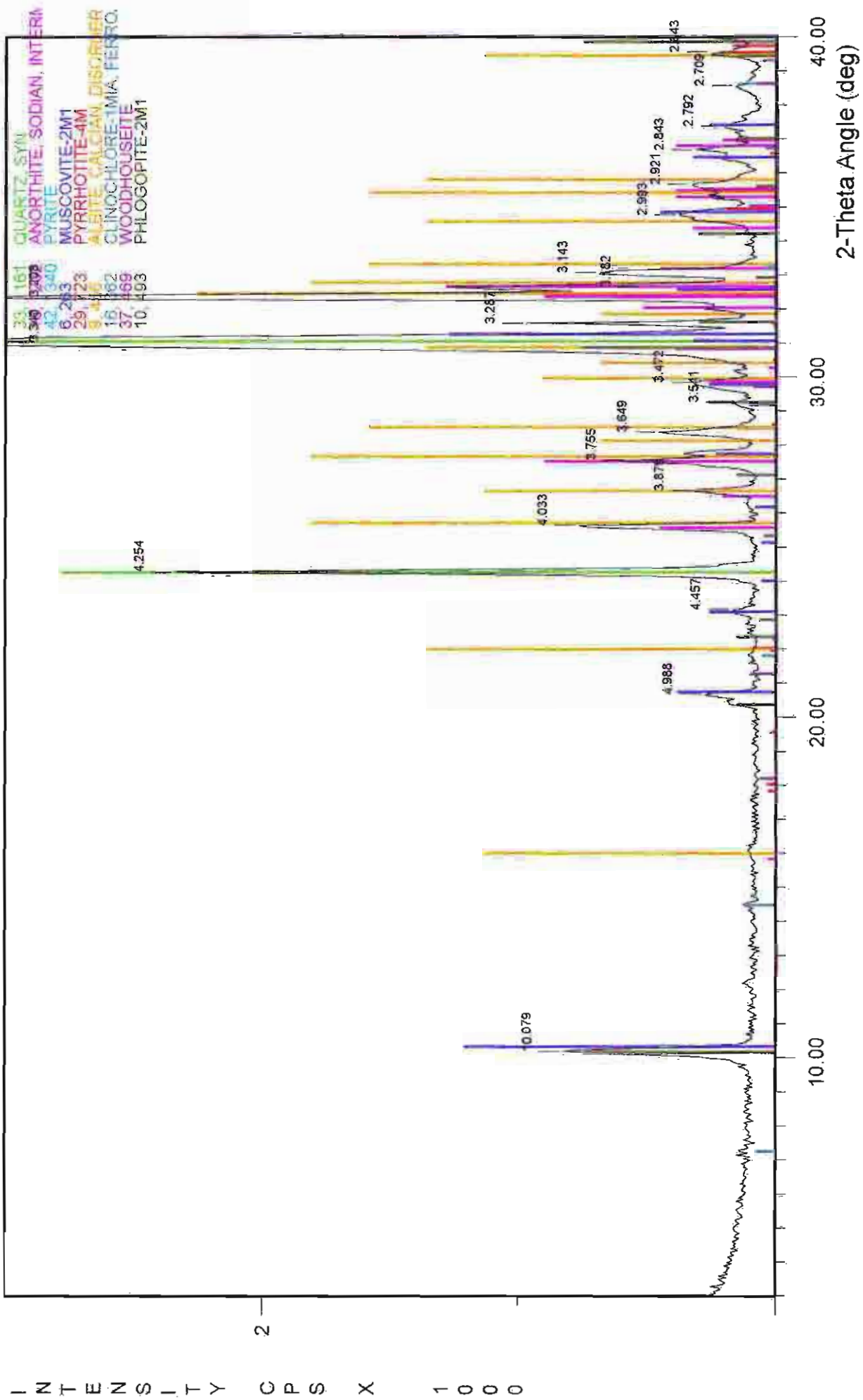


158cm base of grey medium sand region



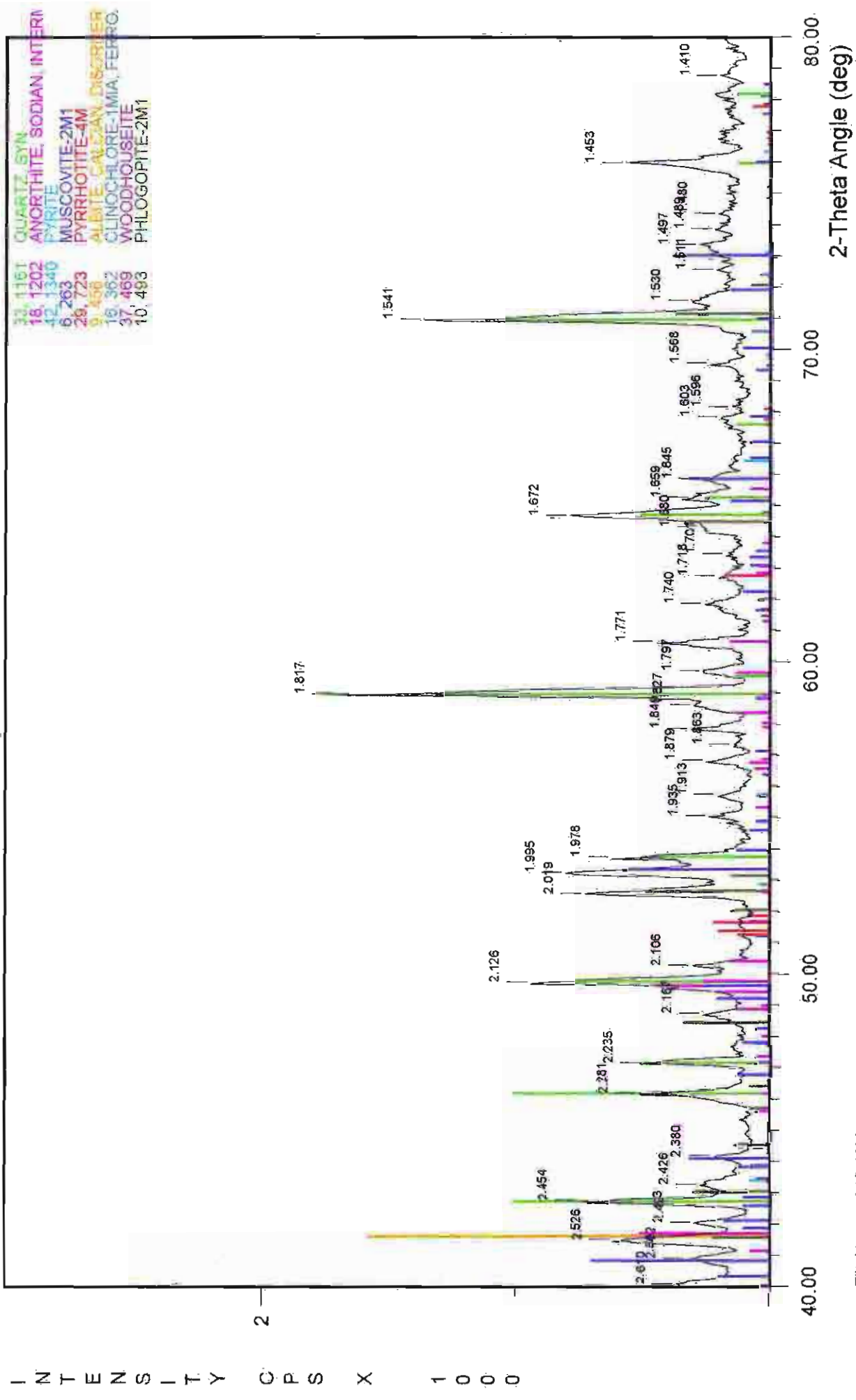
File Name: A:\1-58M

2.08-2.17m grey loamy medium-fine sand



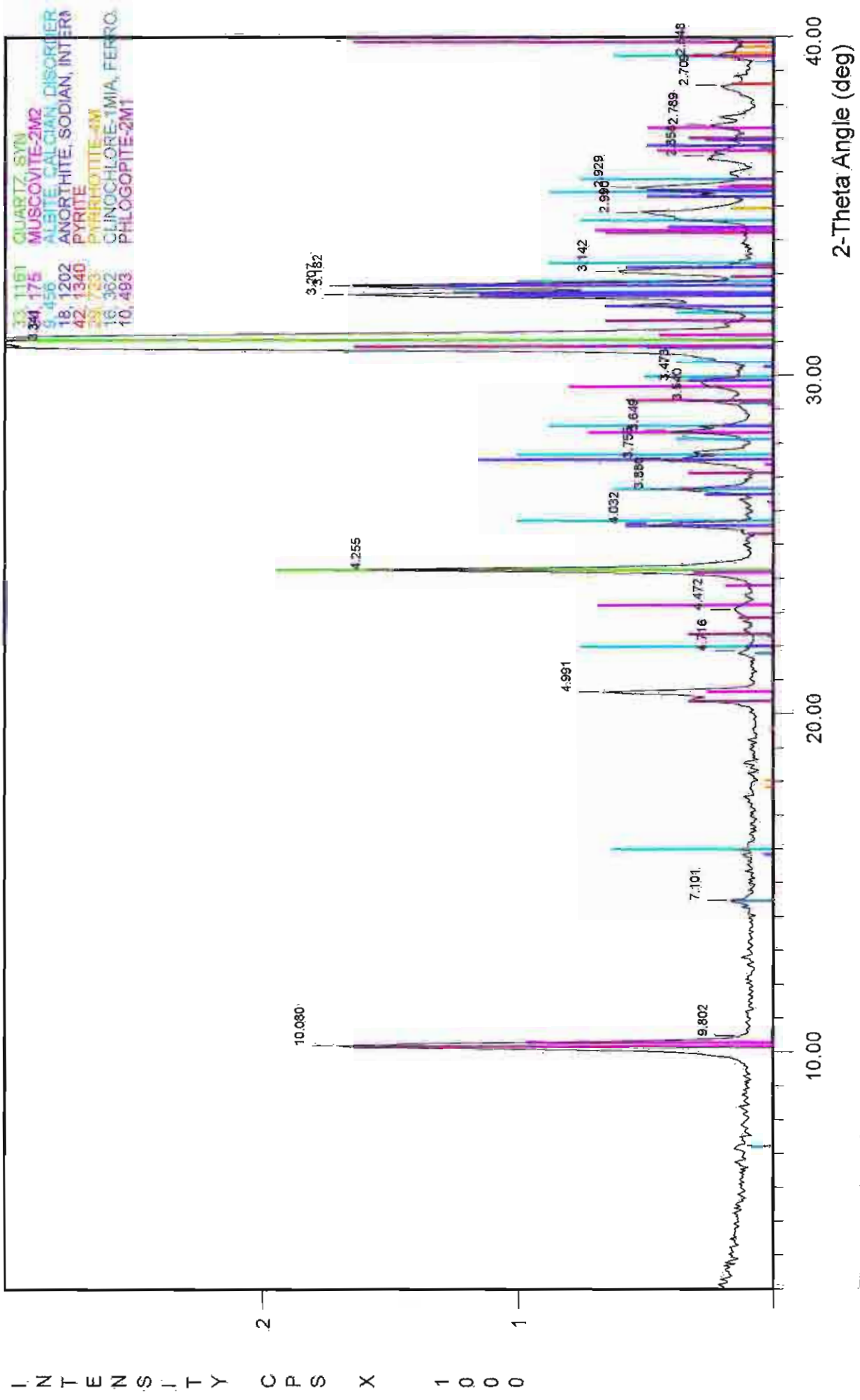
File Name: A:\2-13M

2.08-2.17m grey loamy medium-fine sand



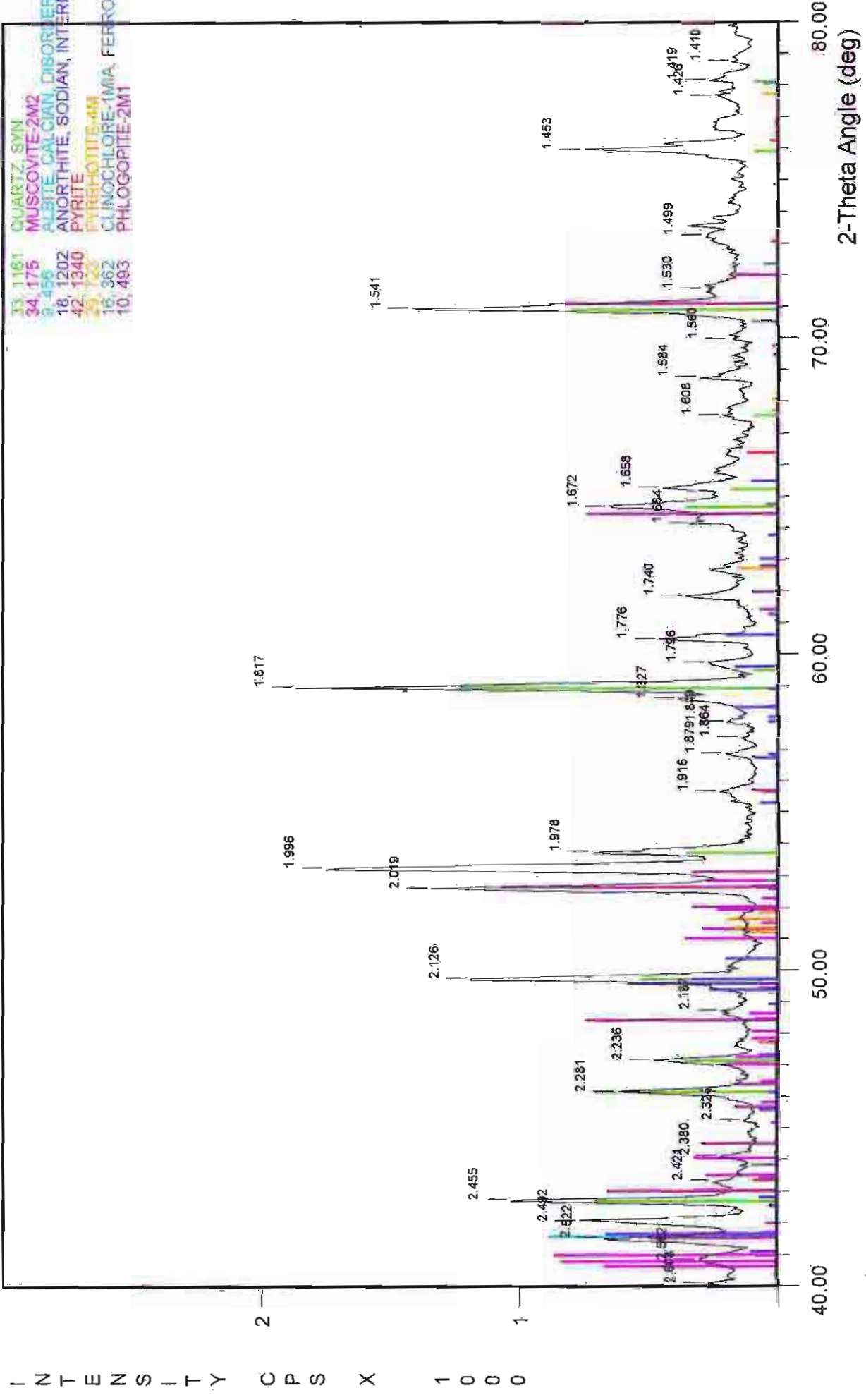
File Name: A:\2-13M

2.48-2.55m yellow-grey loamy medium-fine sand



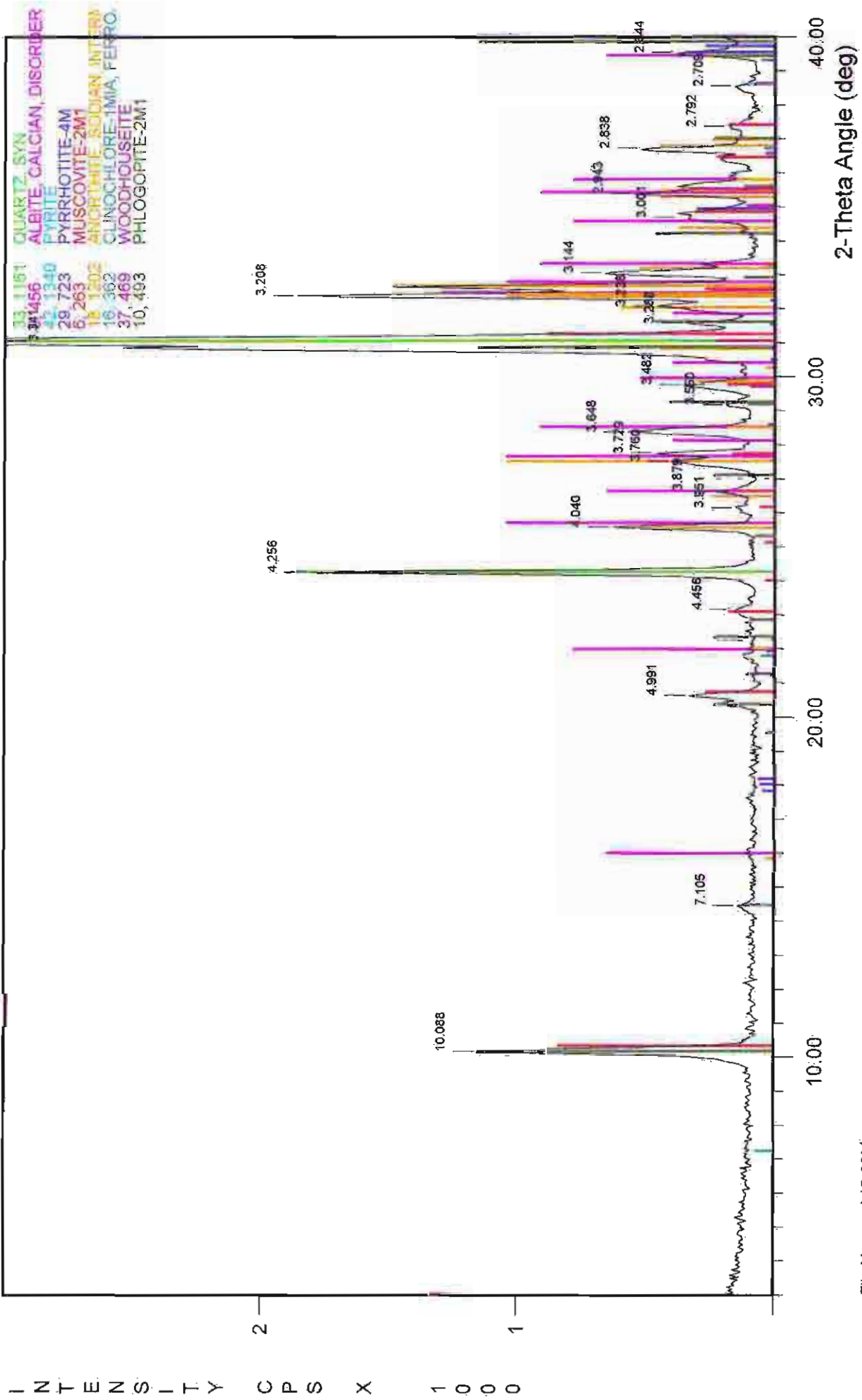
File Name: A\2-52M

2.48-2.55m yellow-grey loamy medium-fine sand



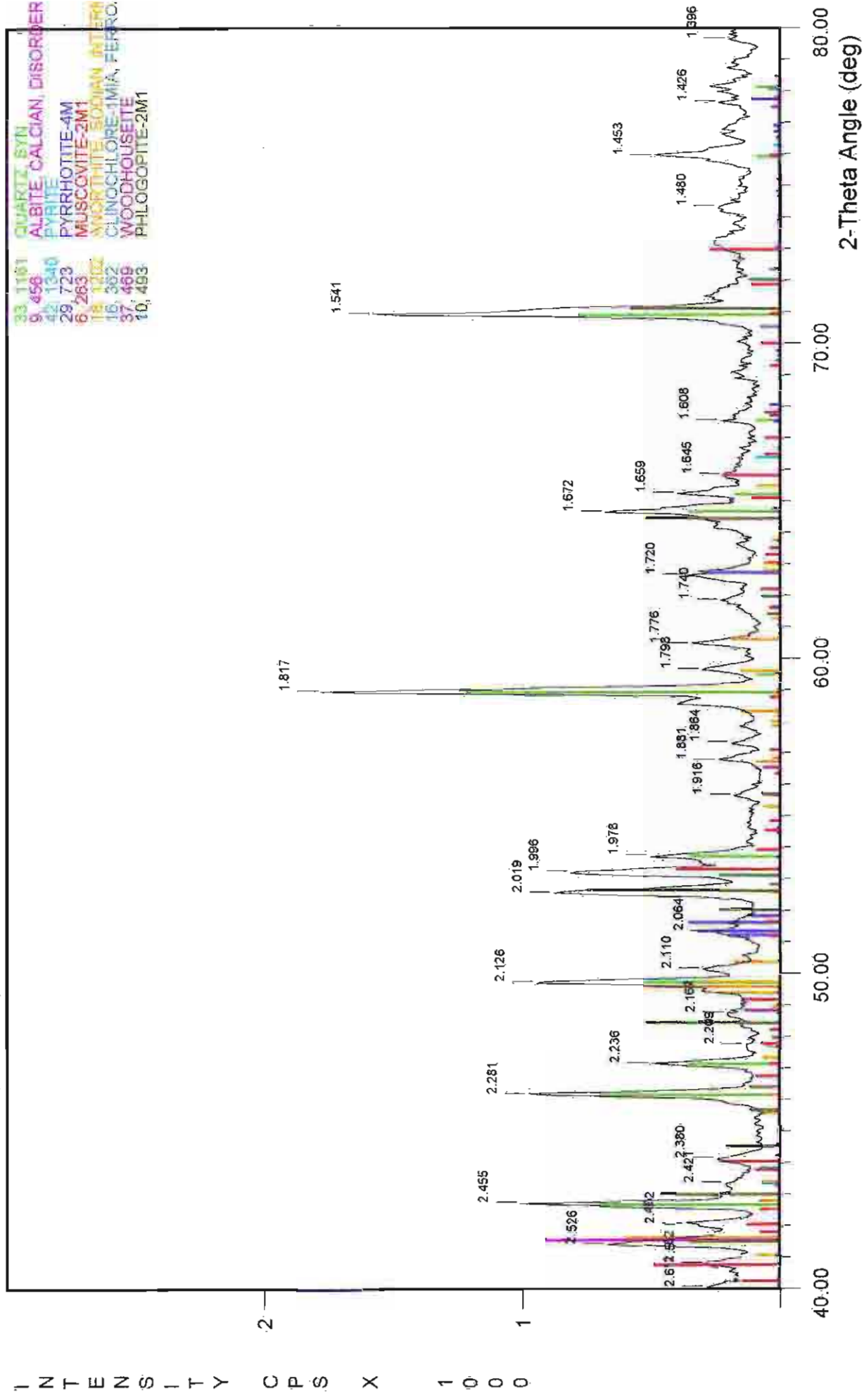
File Name: A\2-52M

2.76-2.85m olive grey loamy fine sand



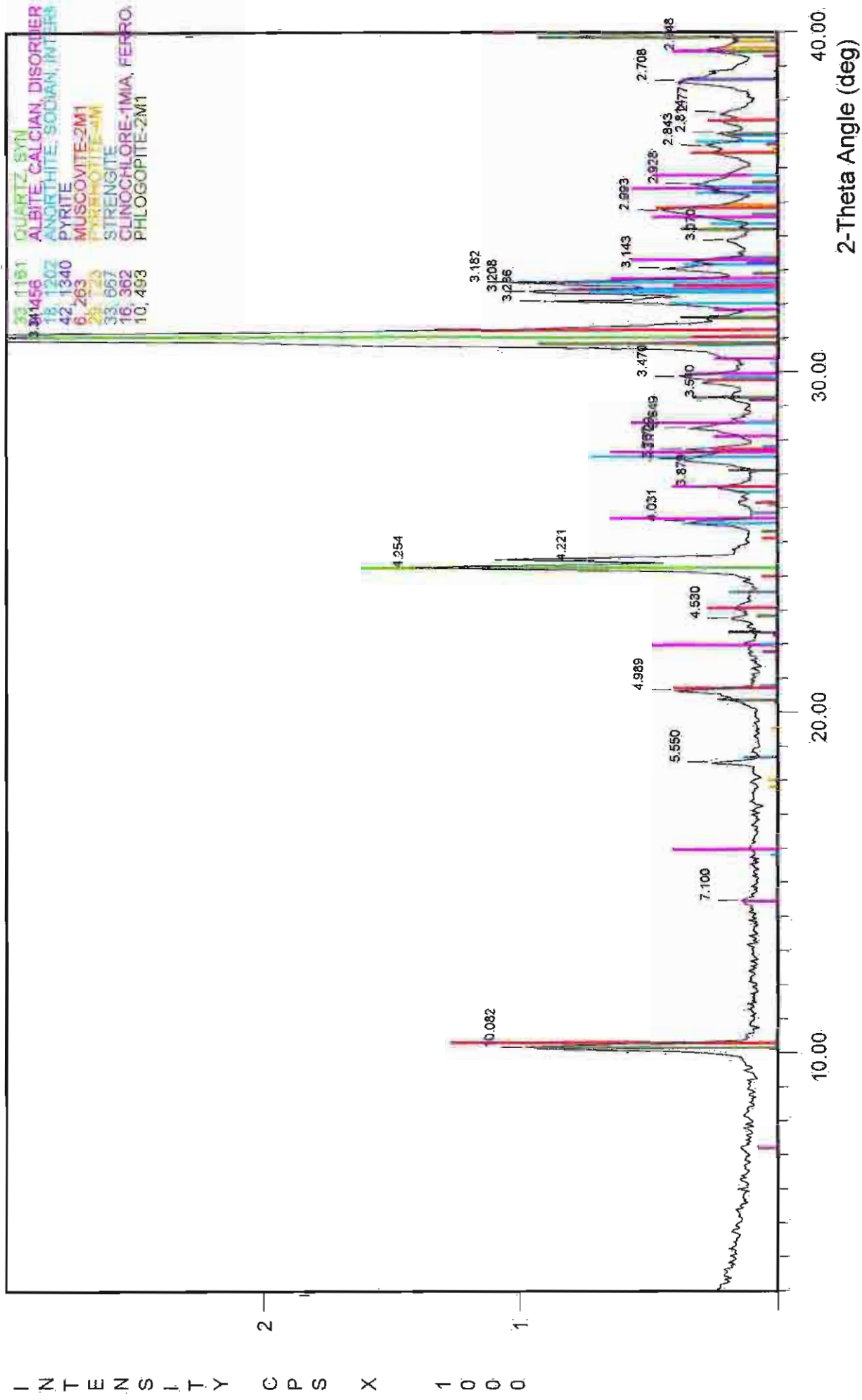
File Name: A:\2.80M

2.76-2.85m olive grey loamy fine sand



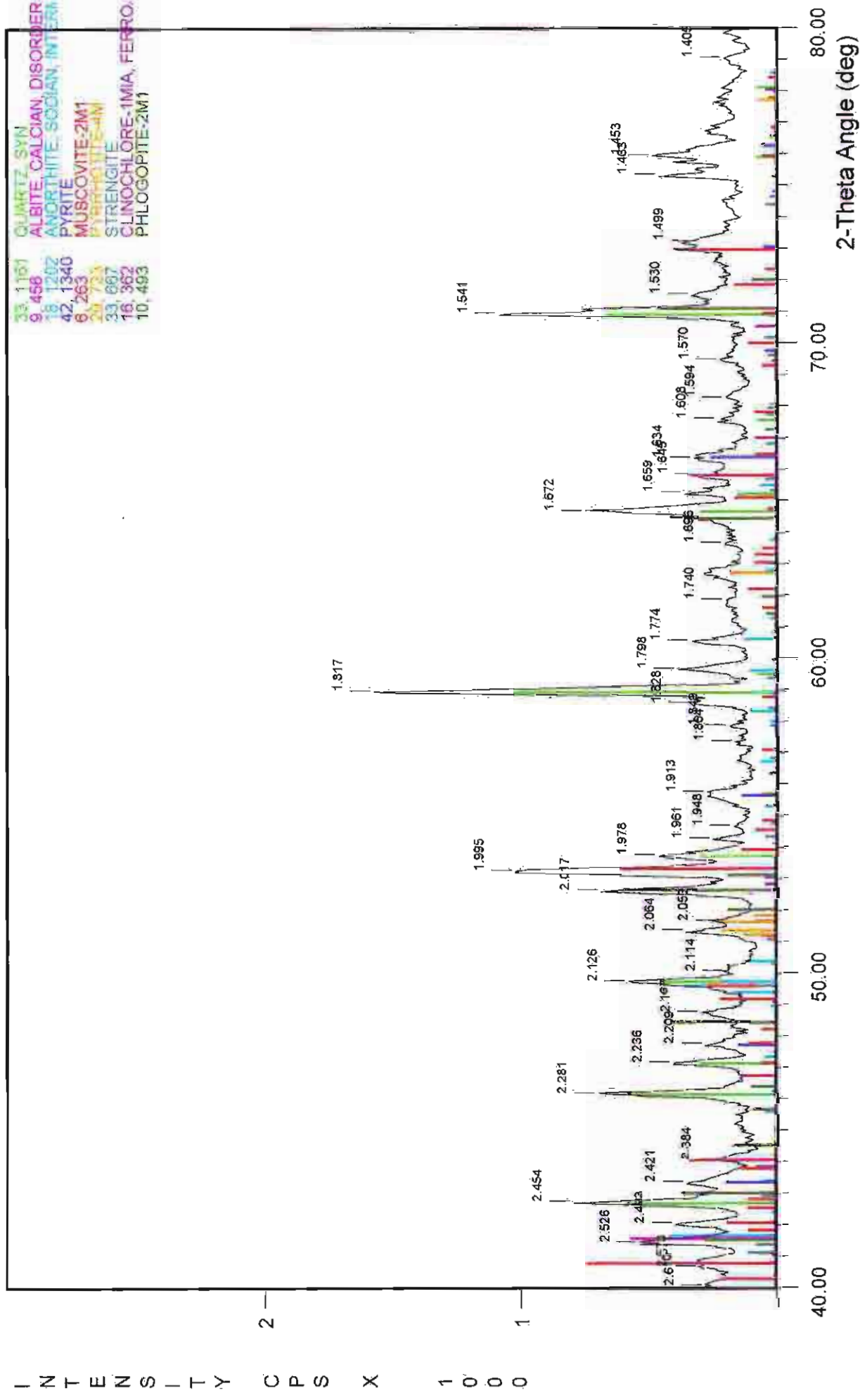
File Name: A:\2.80M

3.69-3.76m dark grey loamy medium sand



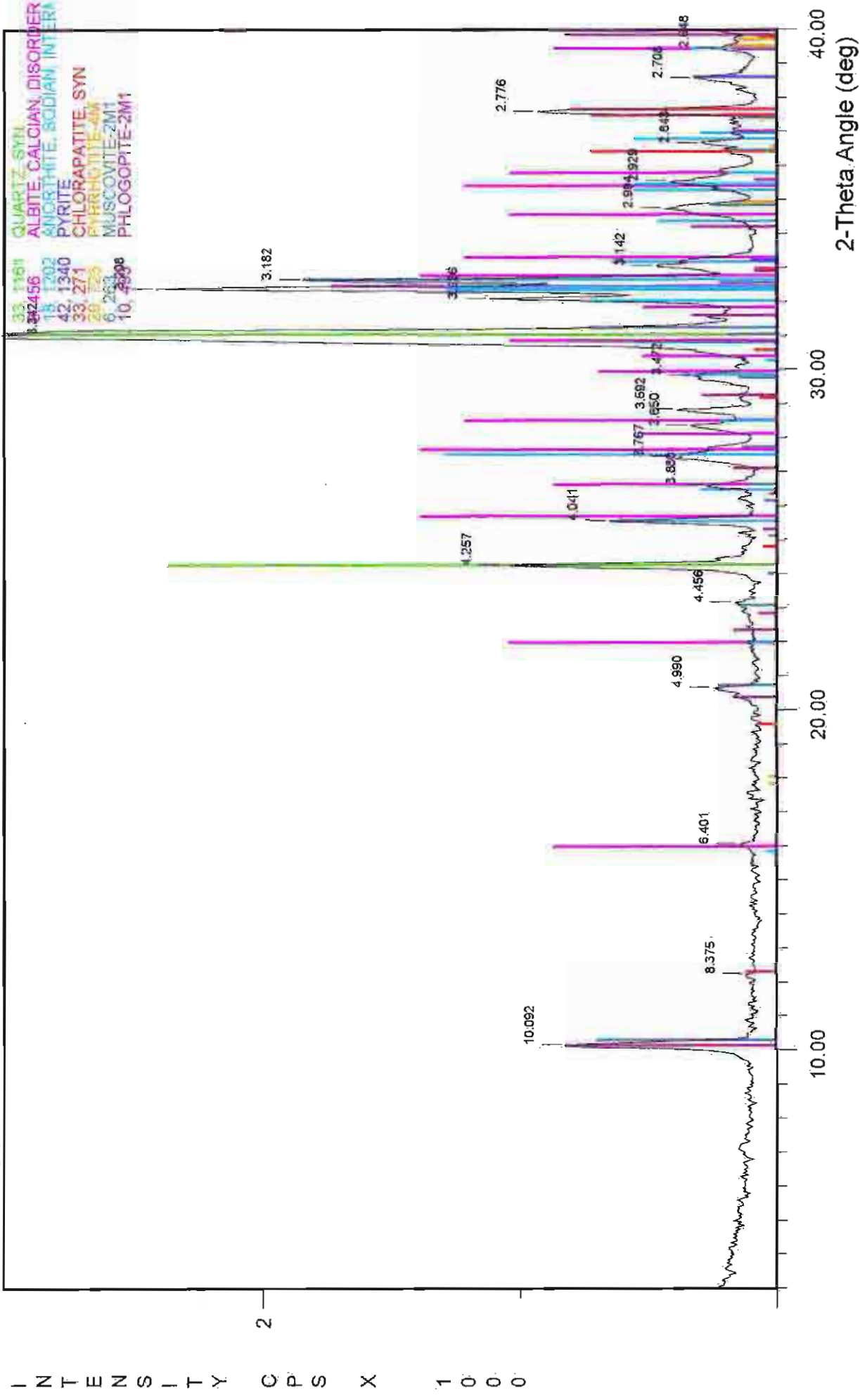
File Name: A\13-72M

3.69-3.76m dark grey loamy medium sand



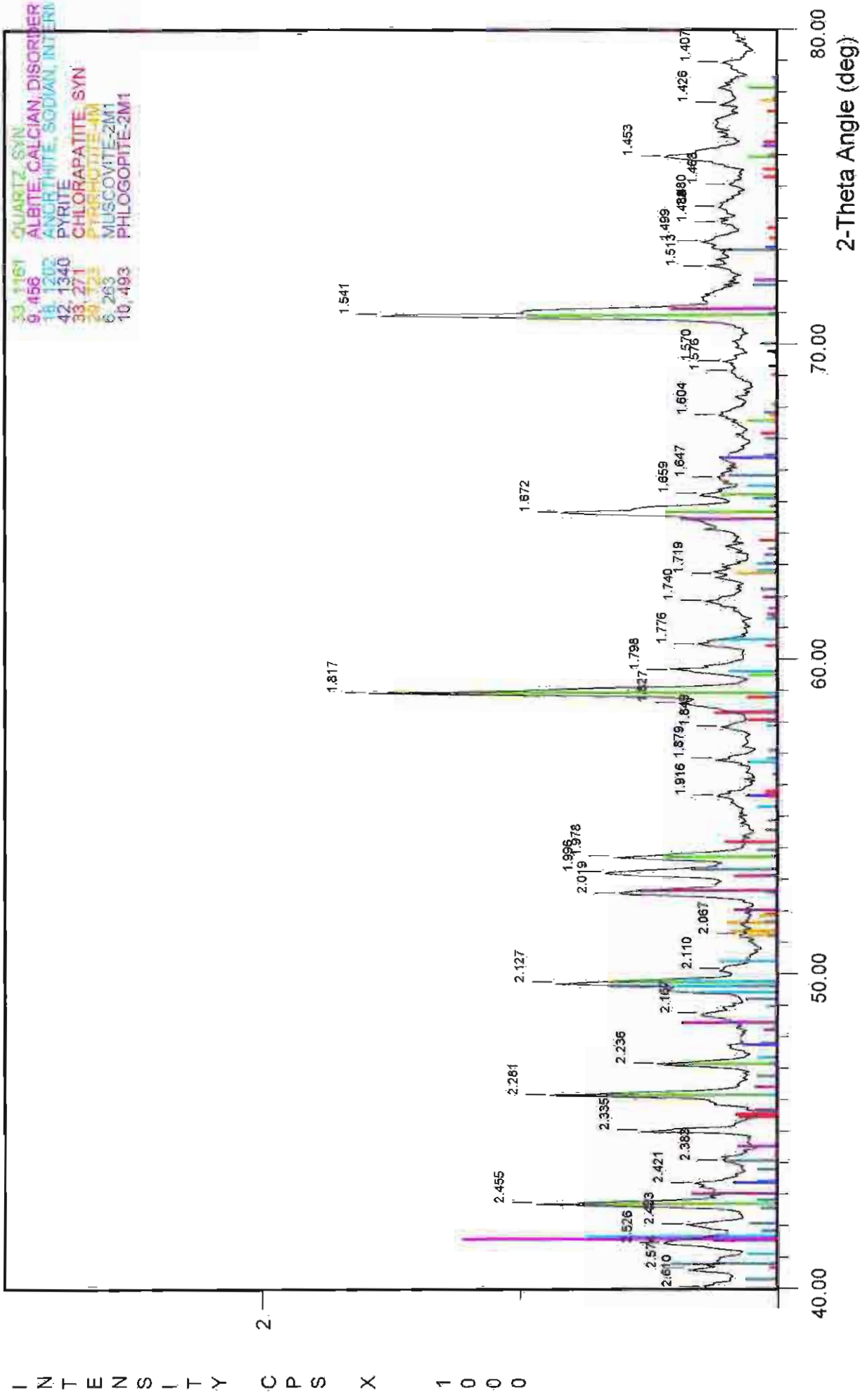
File Name: A13-72M

4.33-4.41m olive loamy fine sand



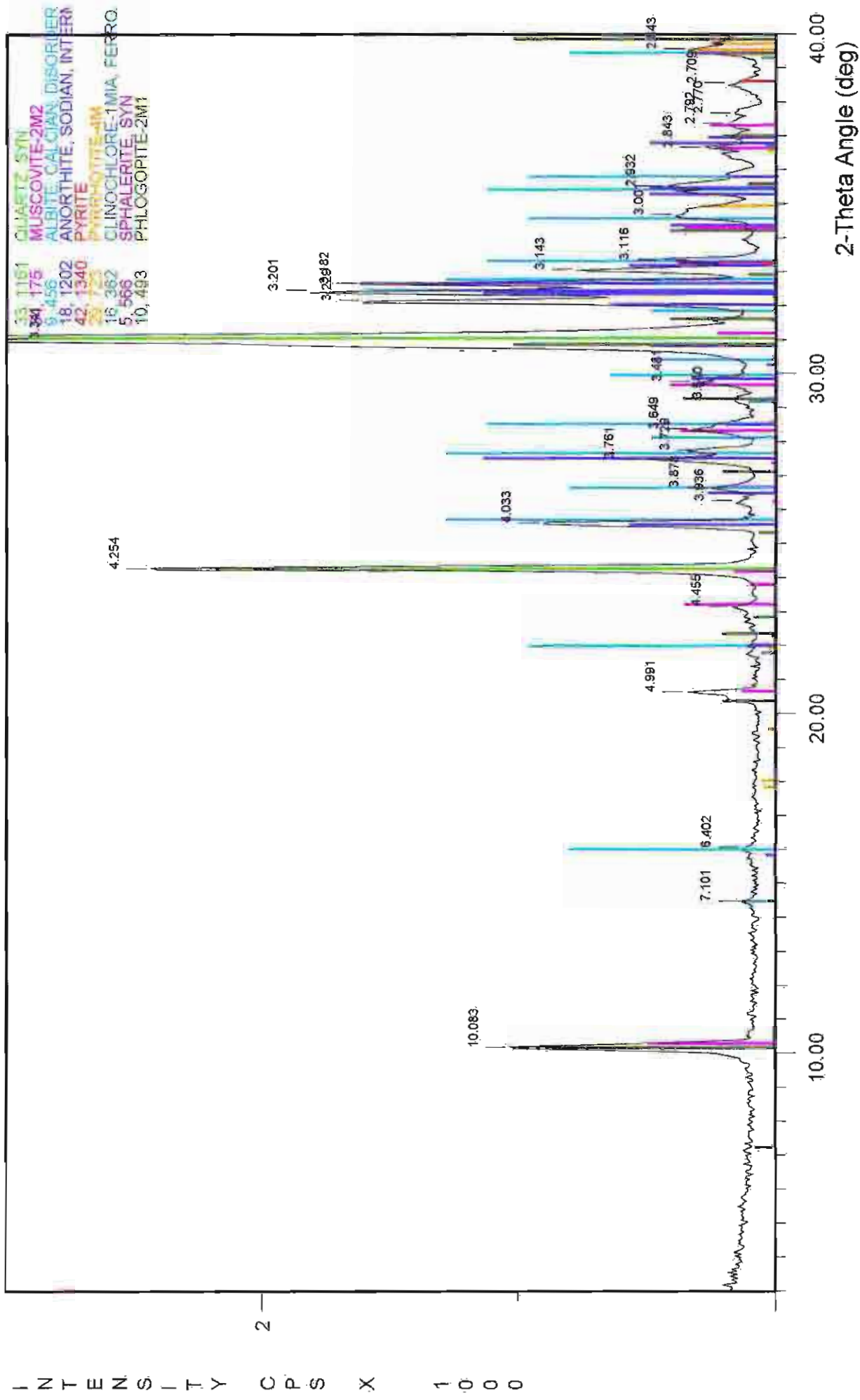
File Name: A:\4-37M

4.33-4.41m olive loamy fine sand

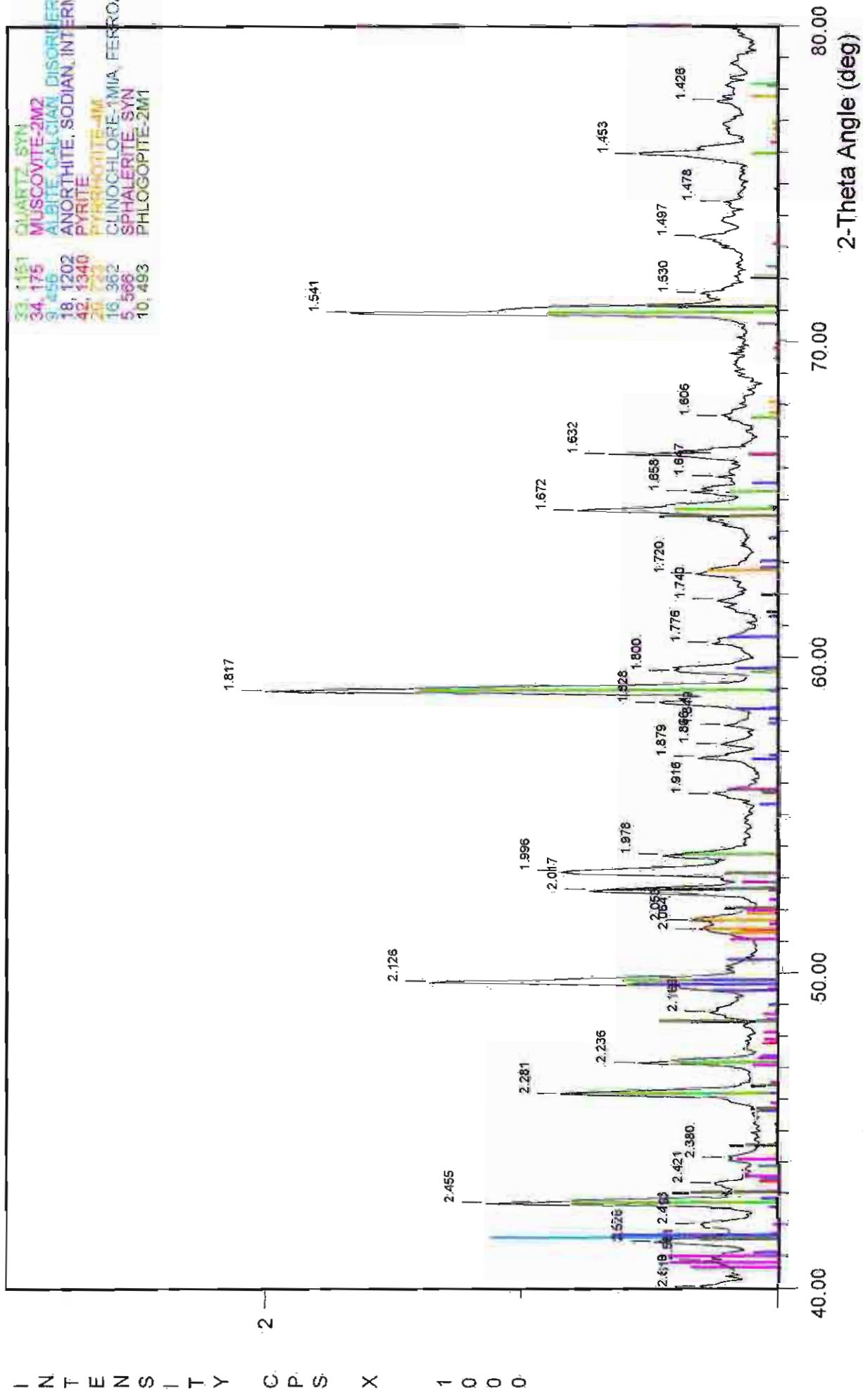


File Name: A:\4-37M

4.9-5m dark olive grey medium sand

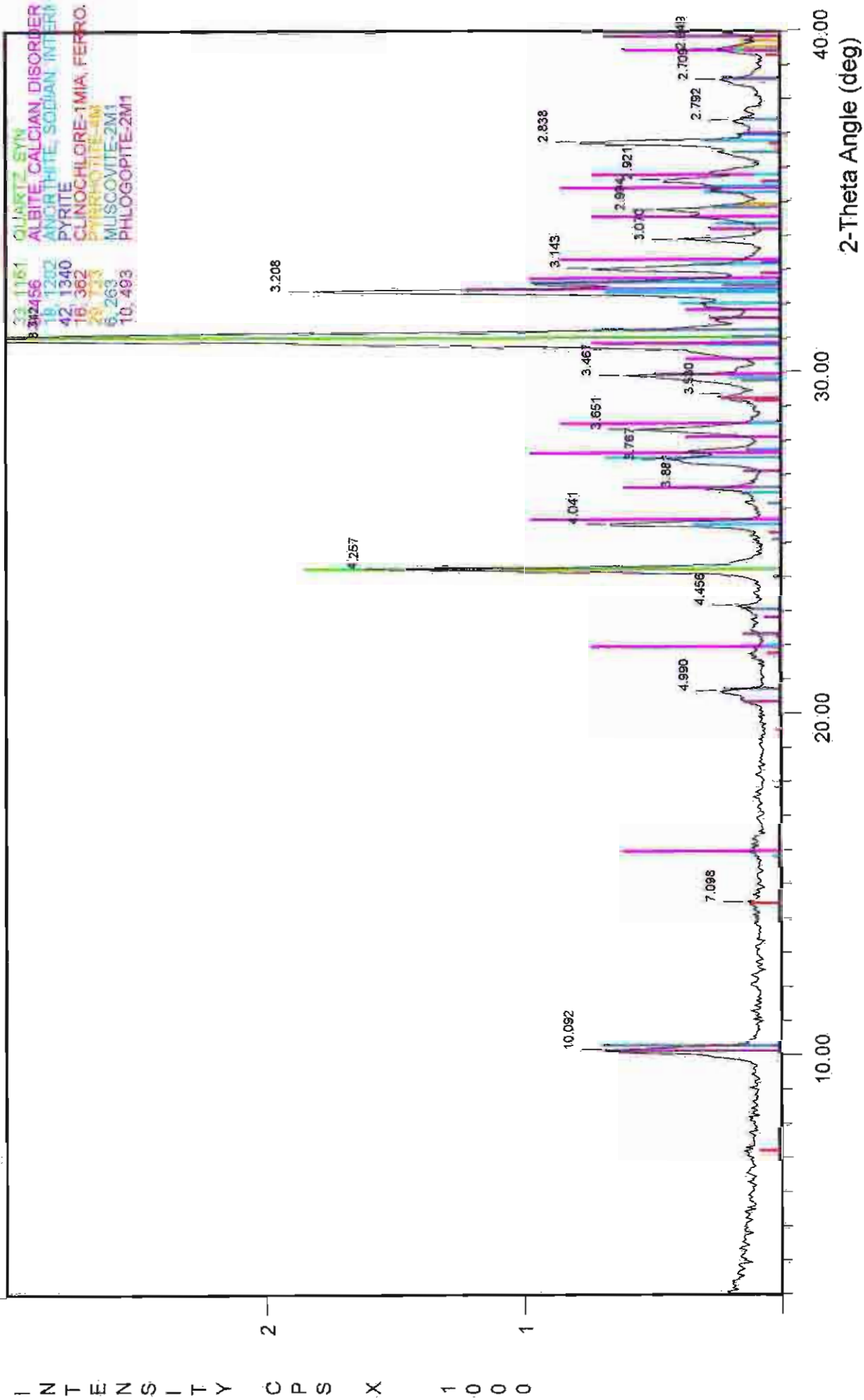


4.9-5m dark olive grey medium sand



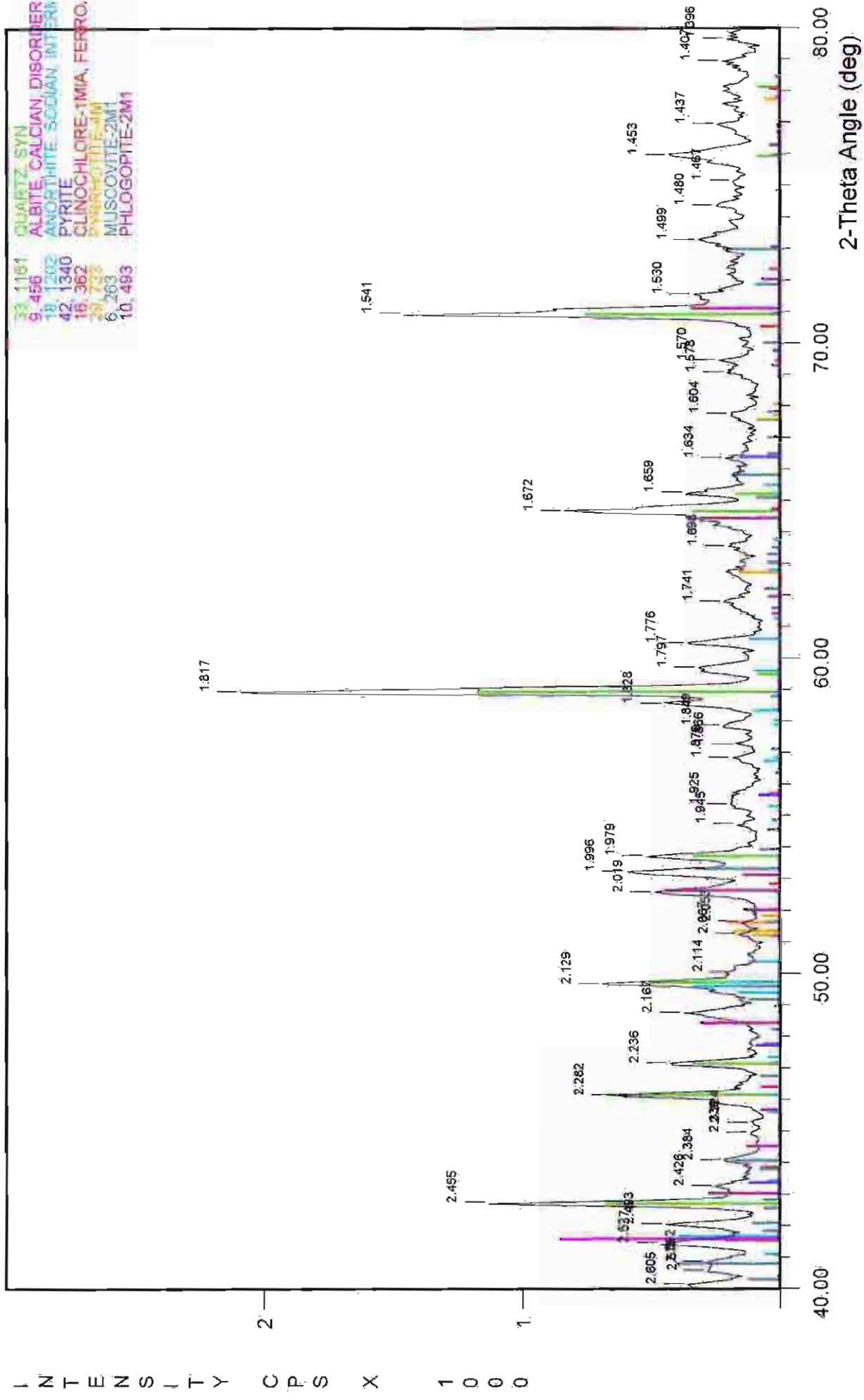
File Name: A:\4-95M

6.49-6.59m grey to light olive brown loamy fine sand



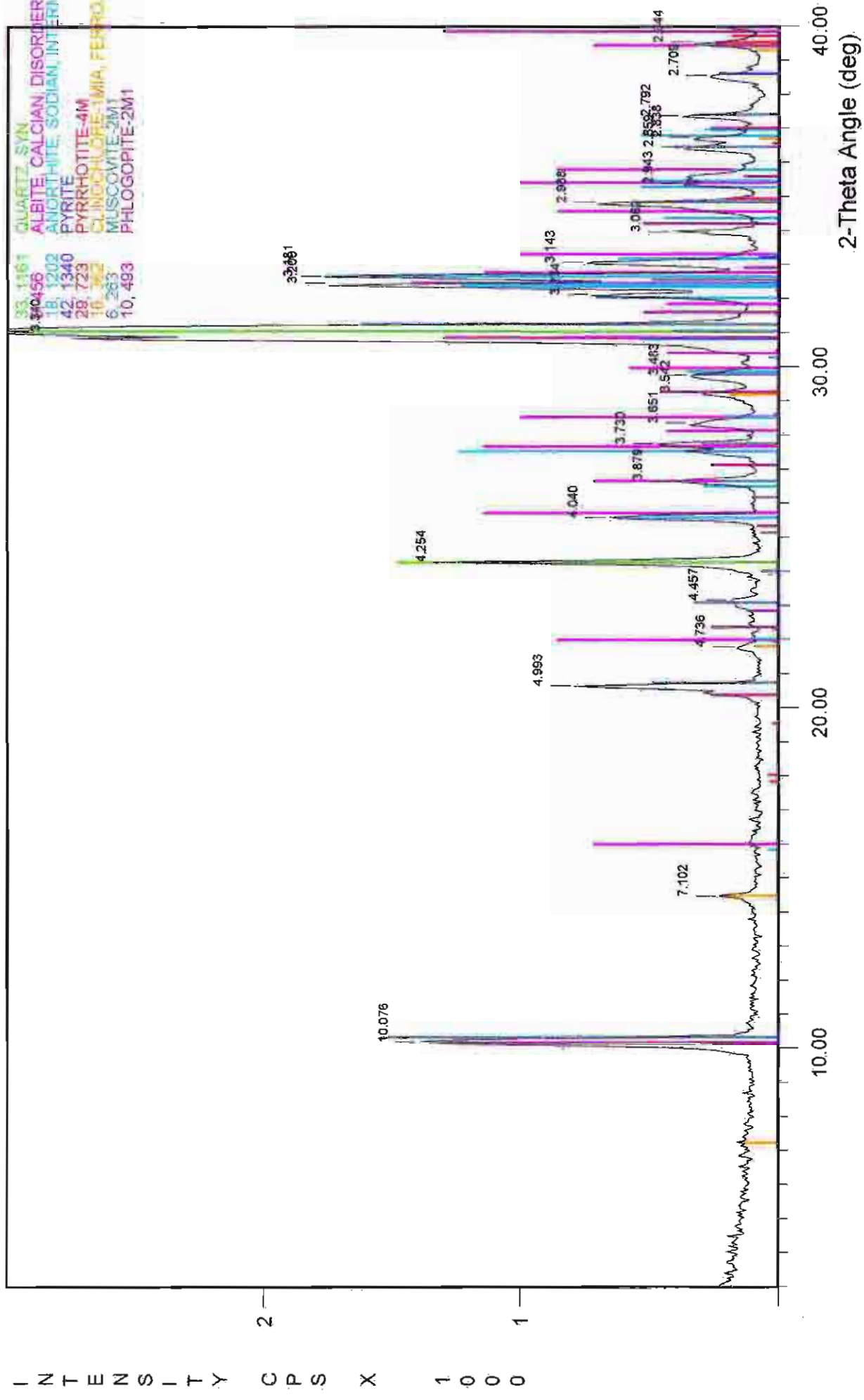
File Name: A\16-54M

6.49-6.59m grey to light olive brown loamy fine sand



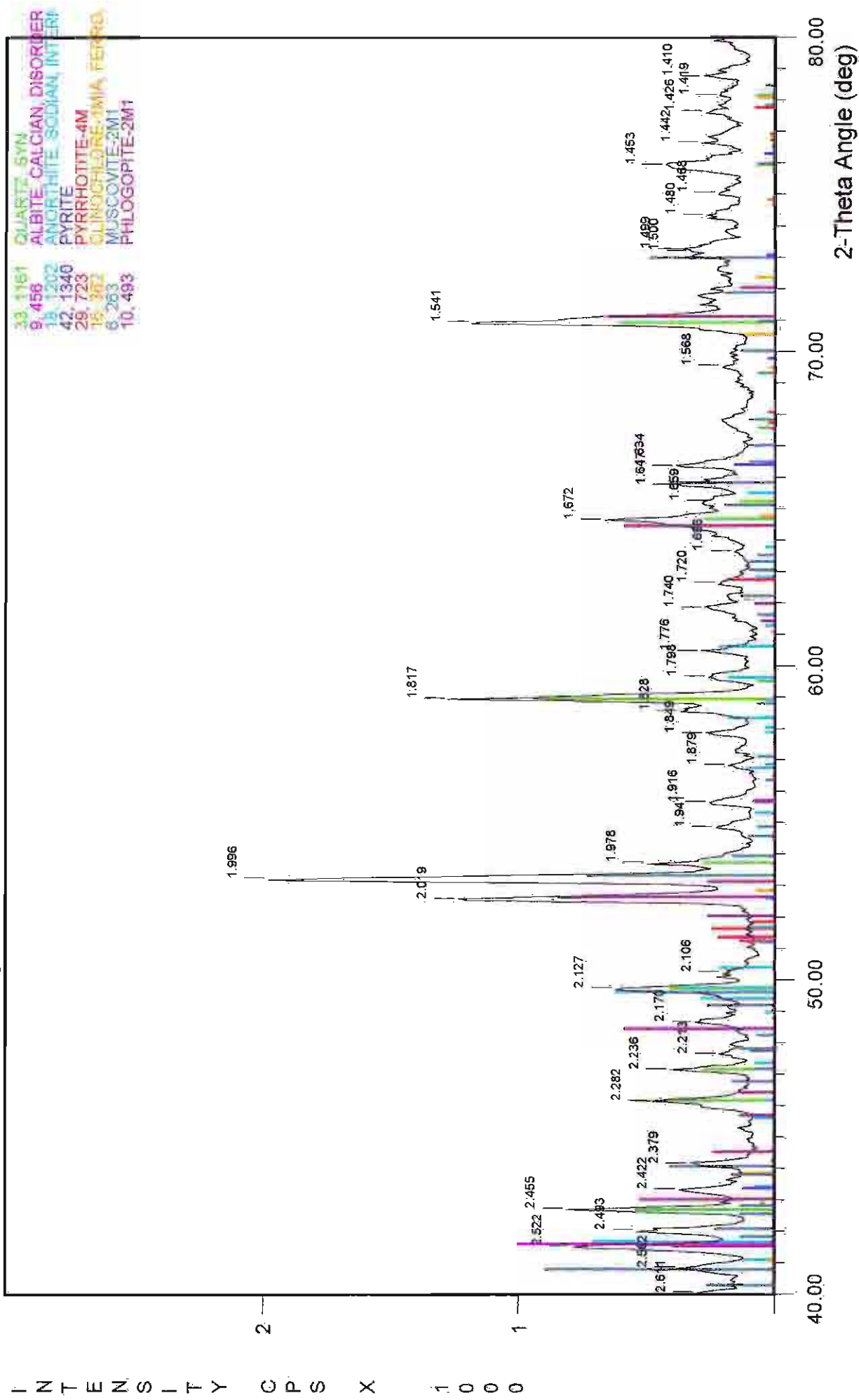
File Name: A:\6-54M

7.04m grey fine loamy sand



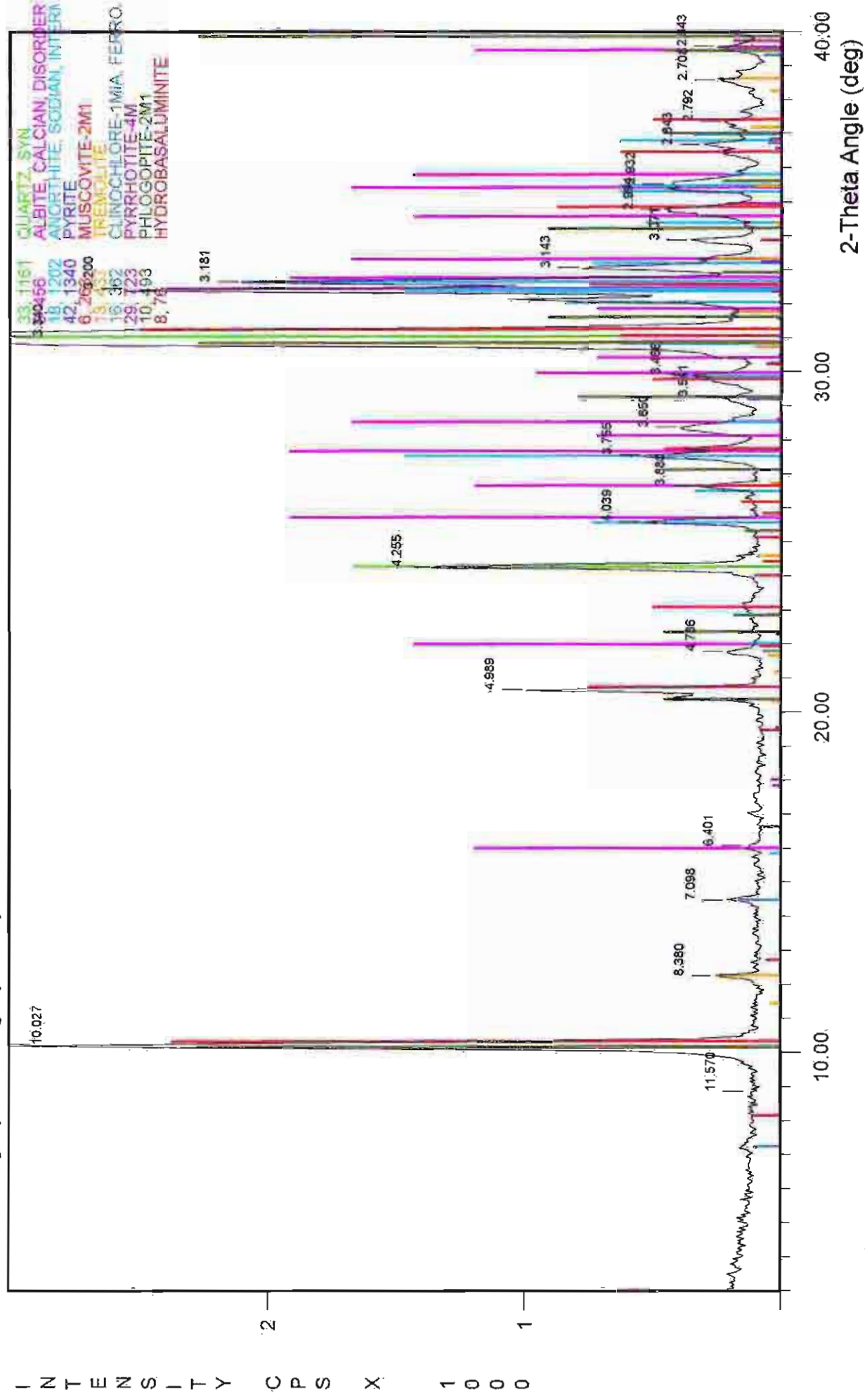
File Name: A\17-04M

7.04m grey fine loamy sand



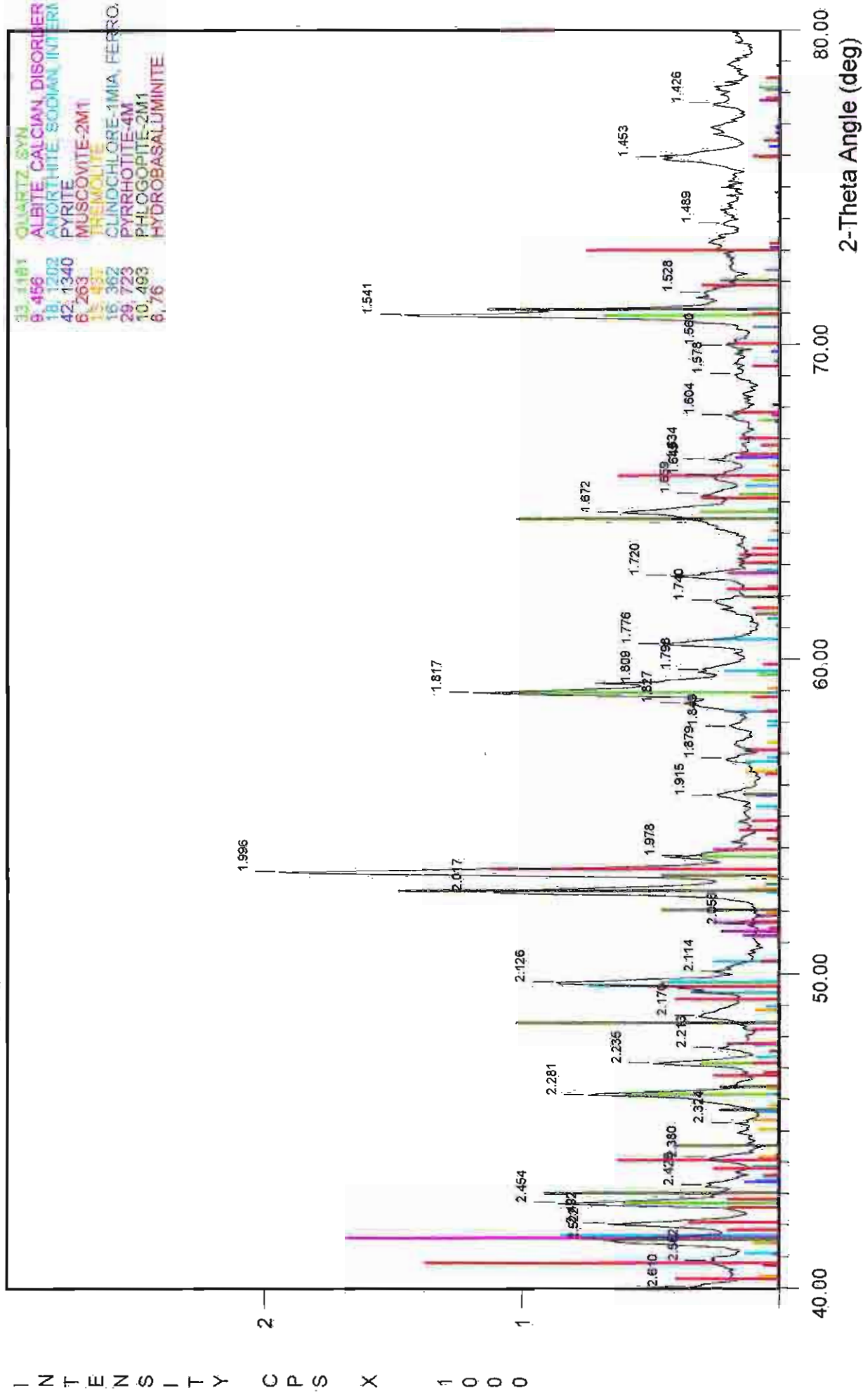
File Name: A:\7-04M

7.27-7.34m grey to dark grey loamy fine sand



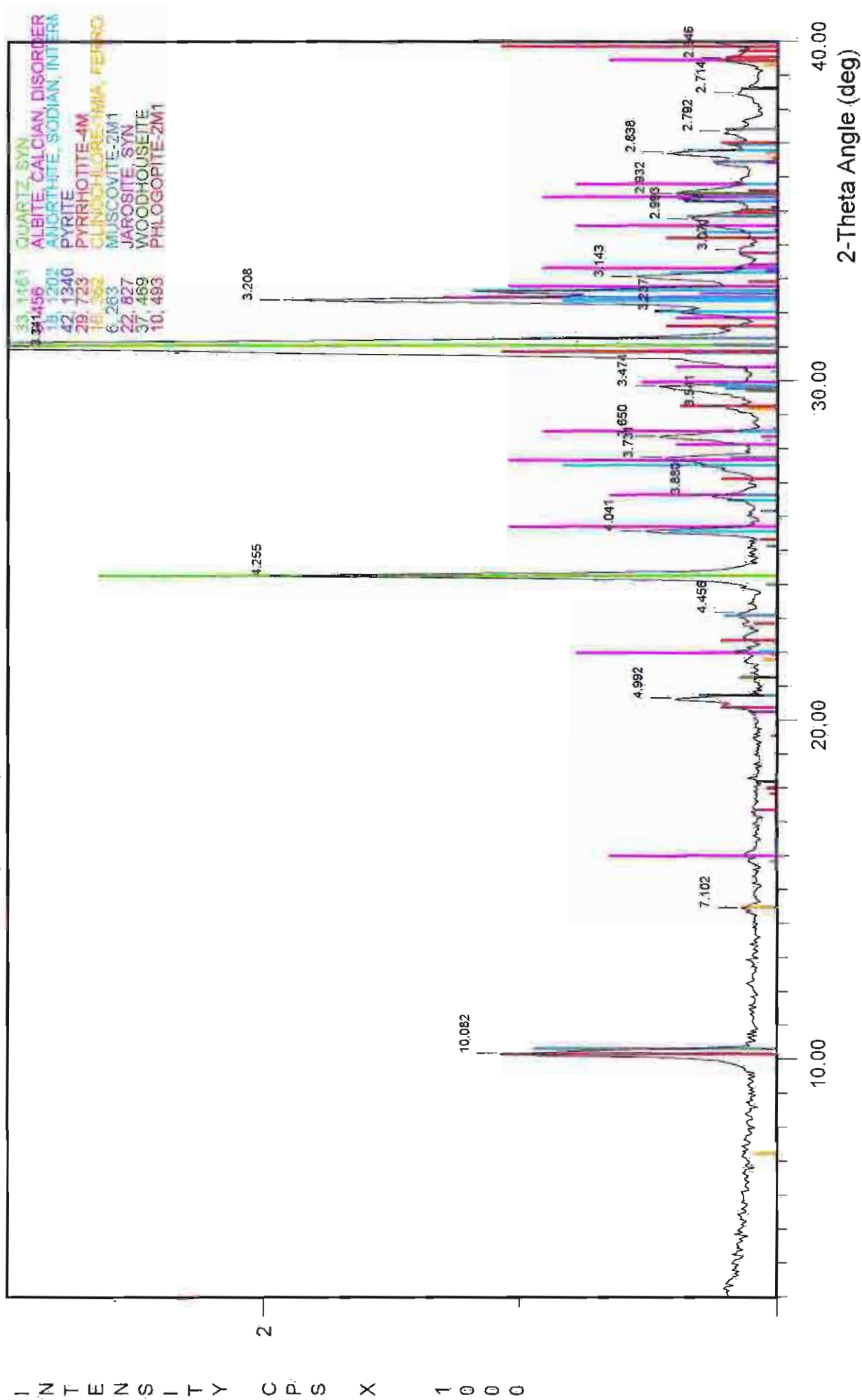
File Name: A:\7-31M

7.27-7.34m grey to dark grey loamy fine sand



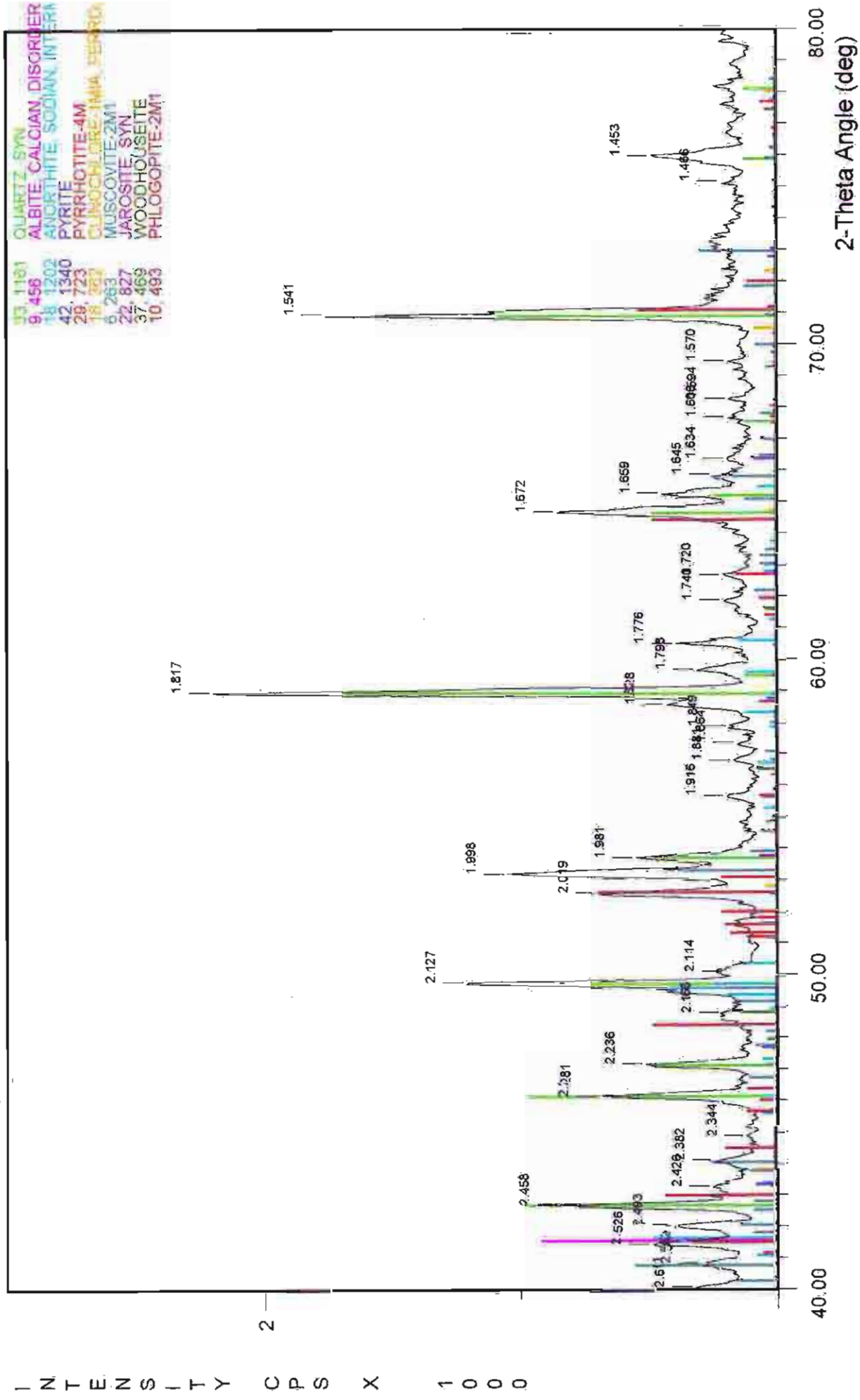
File Name: A:\7-31M

7.97-8.05m olive yellow - olive brown layer, loamy fine sand



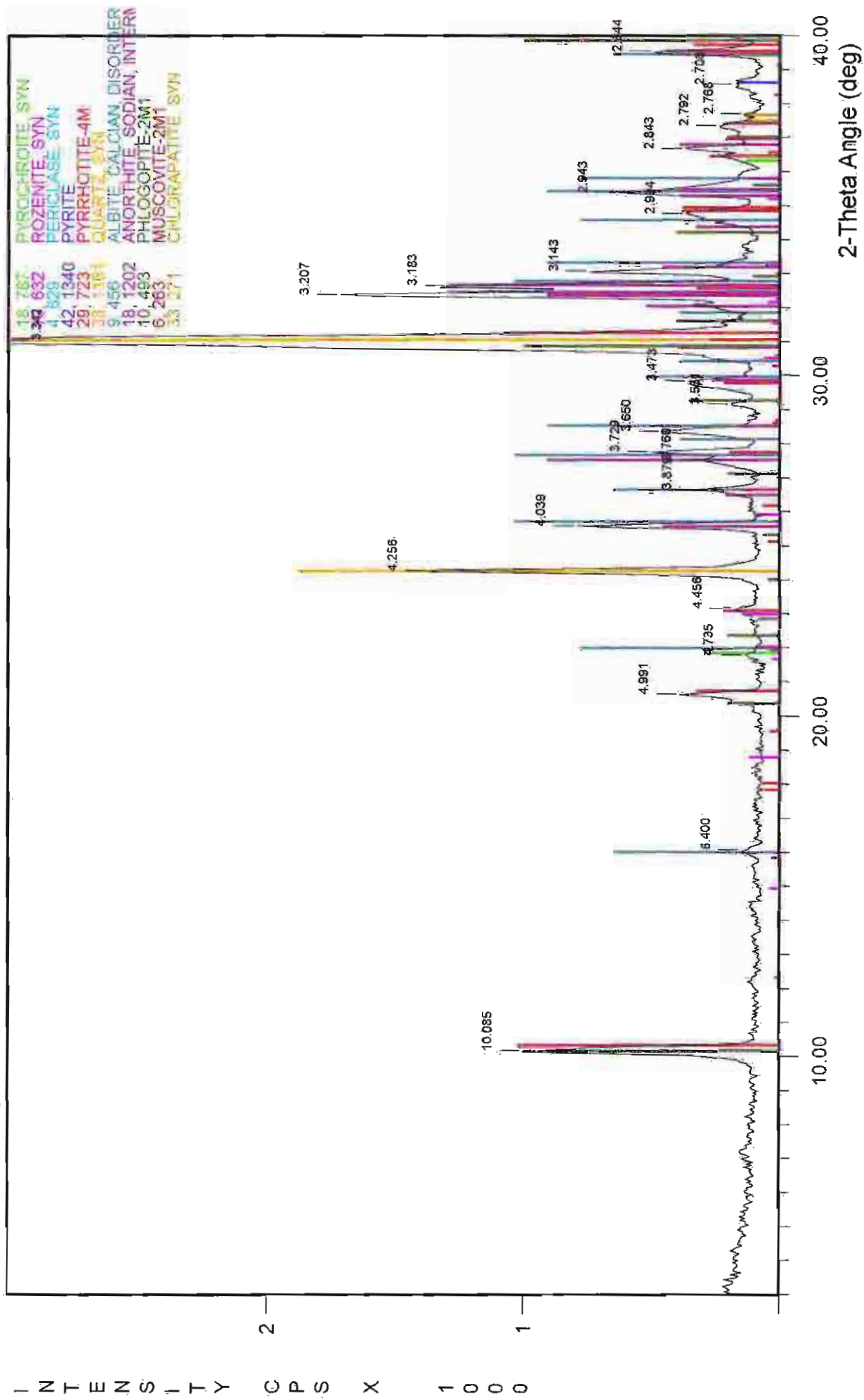
File Name: A\B-01M

7.97-8.05m olive yellow - olive brown layer loamy fine sand



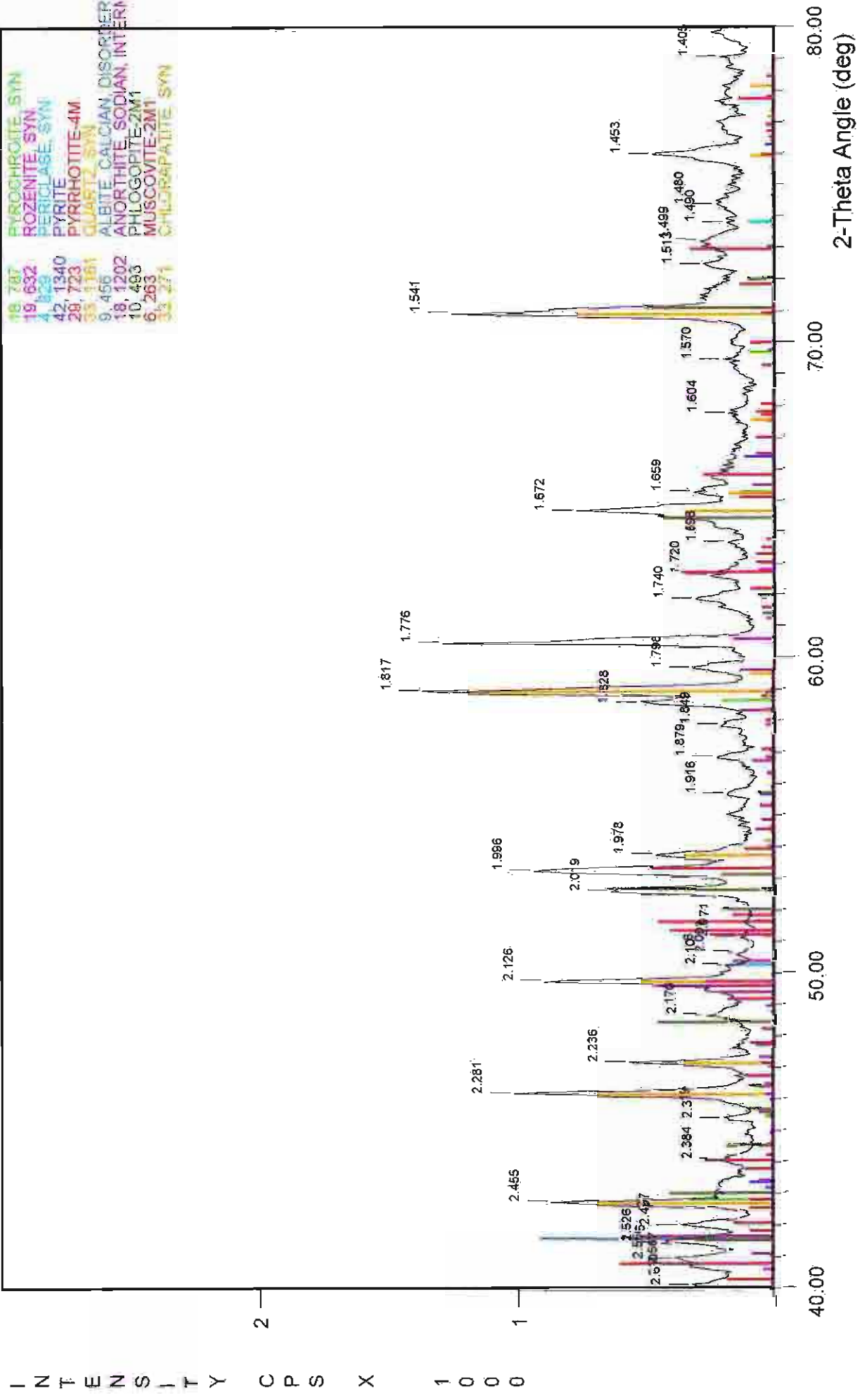
File Name: A\8-01M

9.68-9.77m dark grey silt



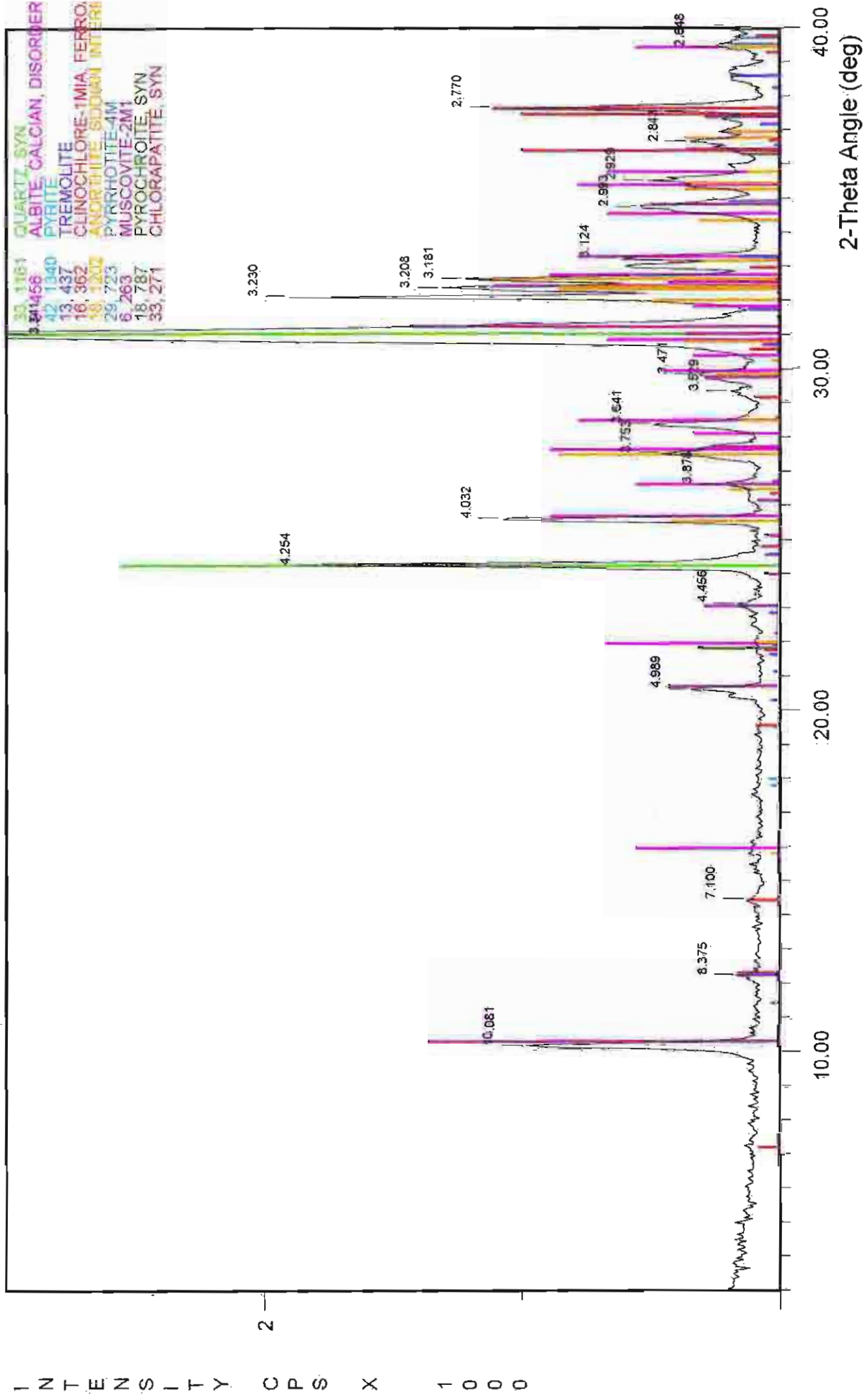
File Name: A:\9-72M

9.68-9.77m dark grey silt



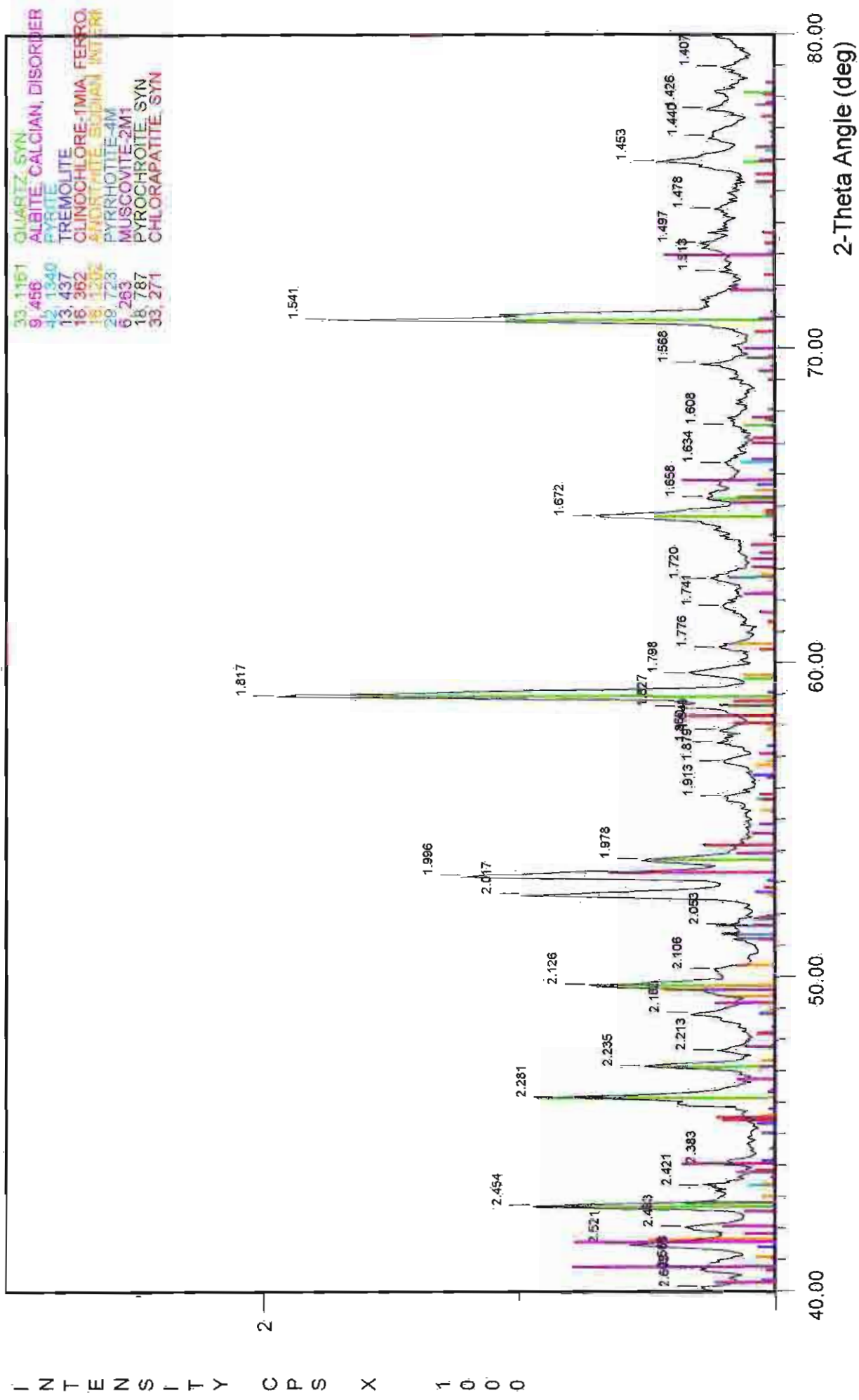
File Name: A:\9-72M

10.45-10.52m dark olive grey fine sand



File Name: A:\10-49M

10.45-10.52m dark olive grey fine sand

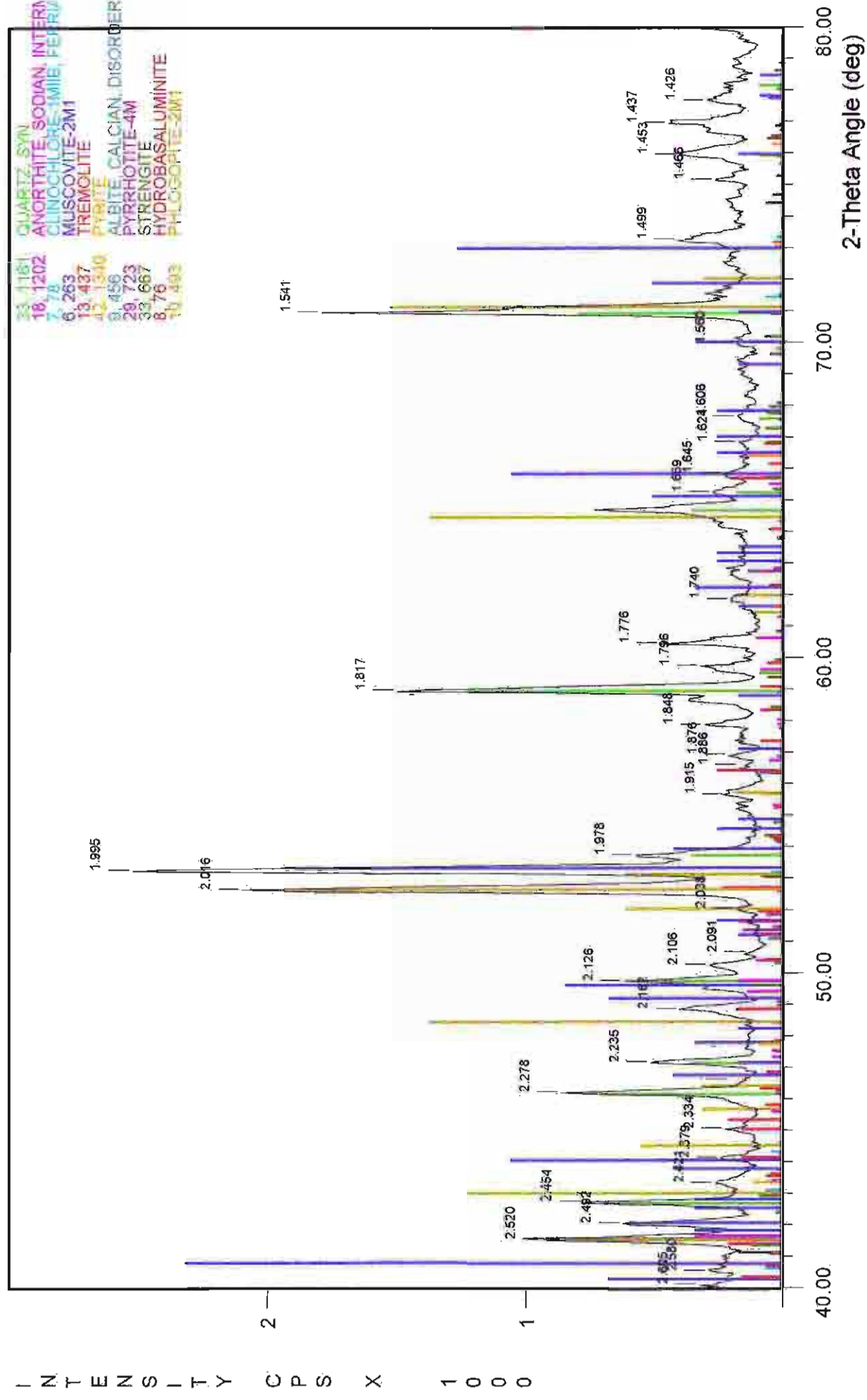


File Name: A:\10-49M

[illegible]

File Name: A:\10-94M

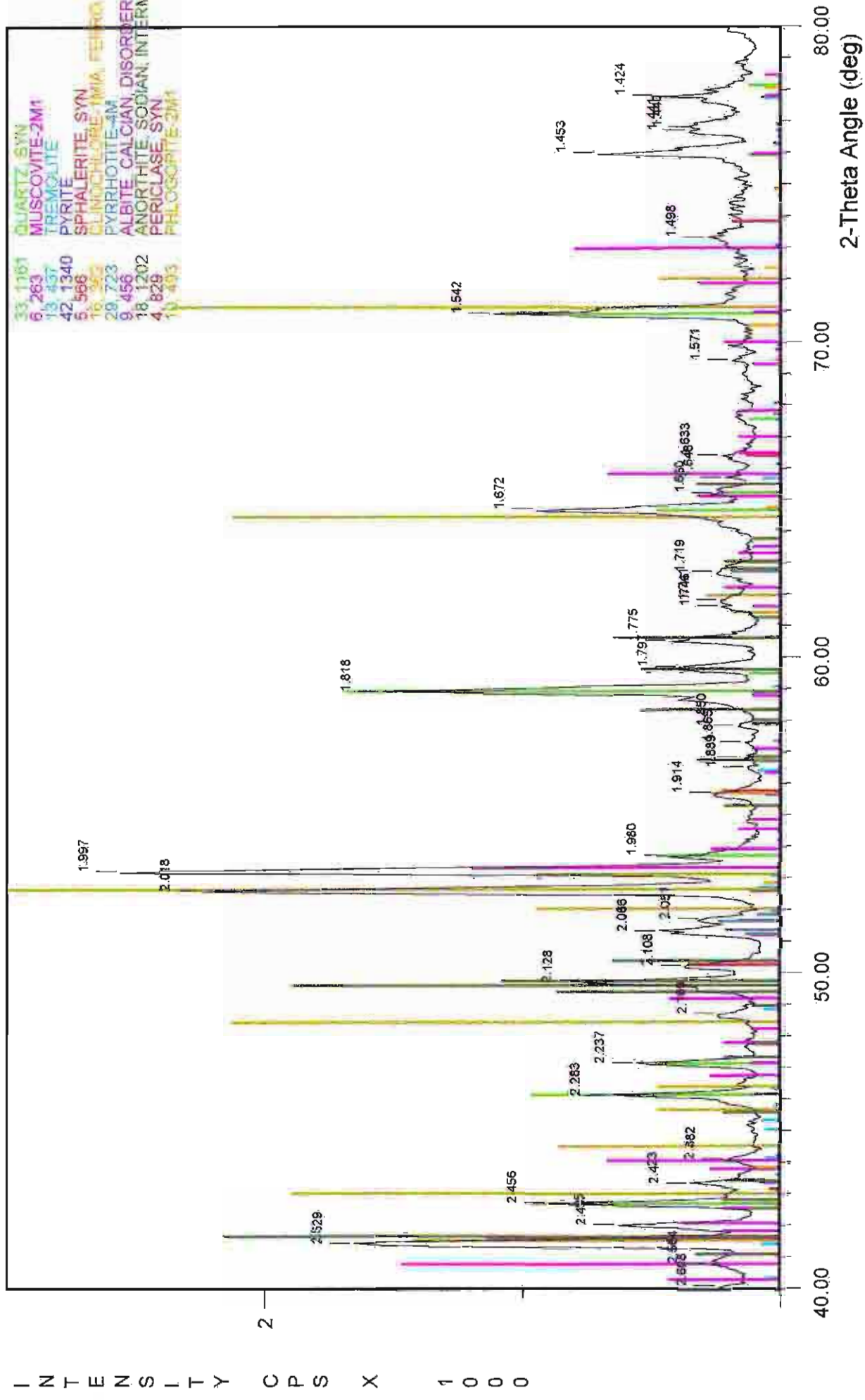
10.94m brown silt



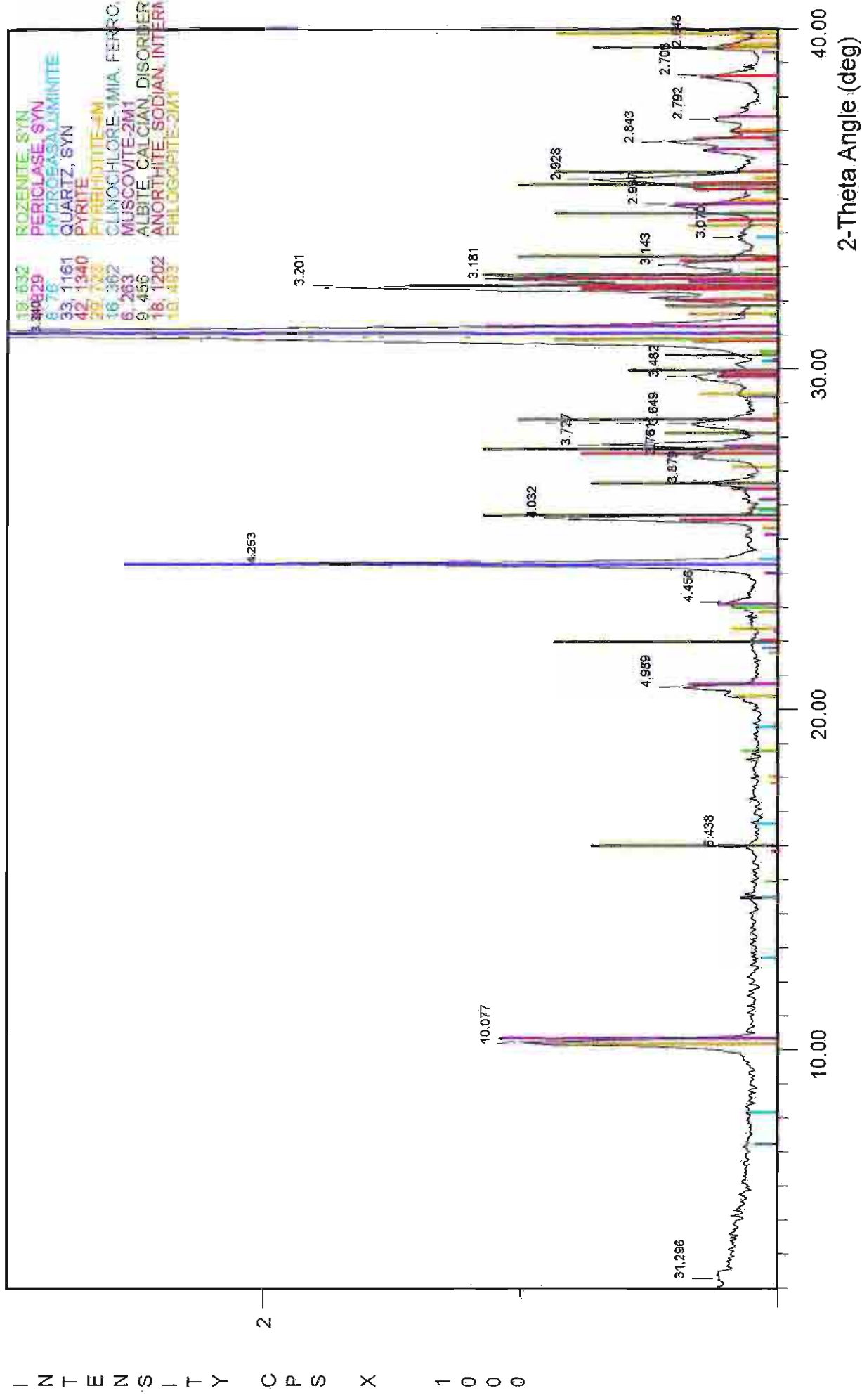
File Name: A:\10-94M

5

11.10m dark grey medium sand



11.65-11.75m grey loamy fine sand

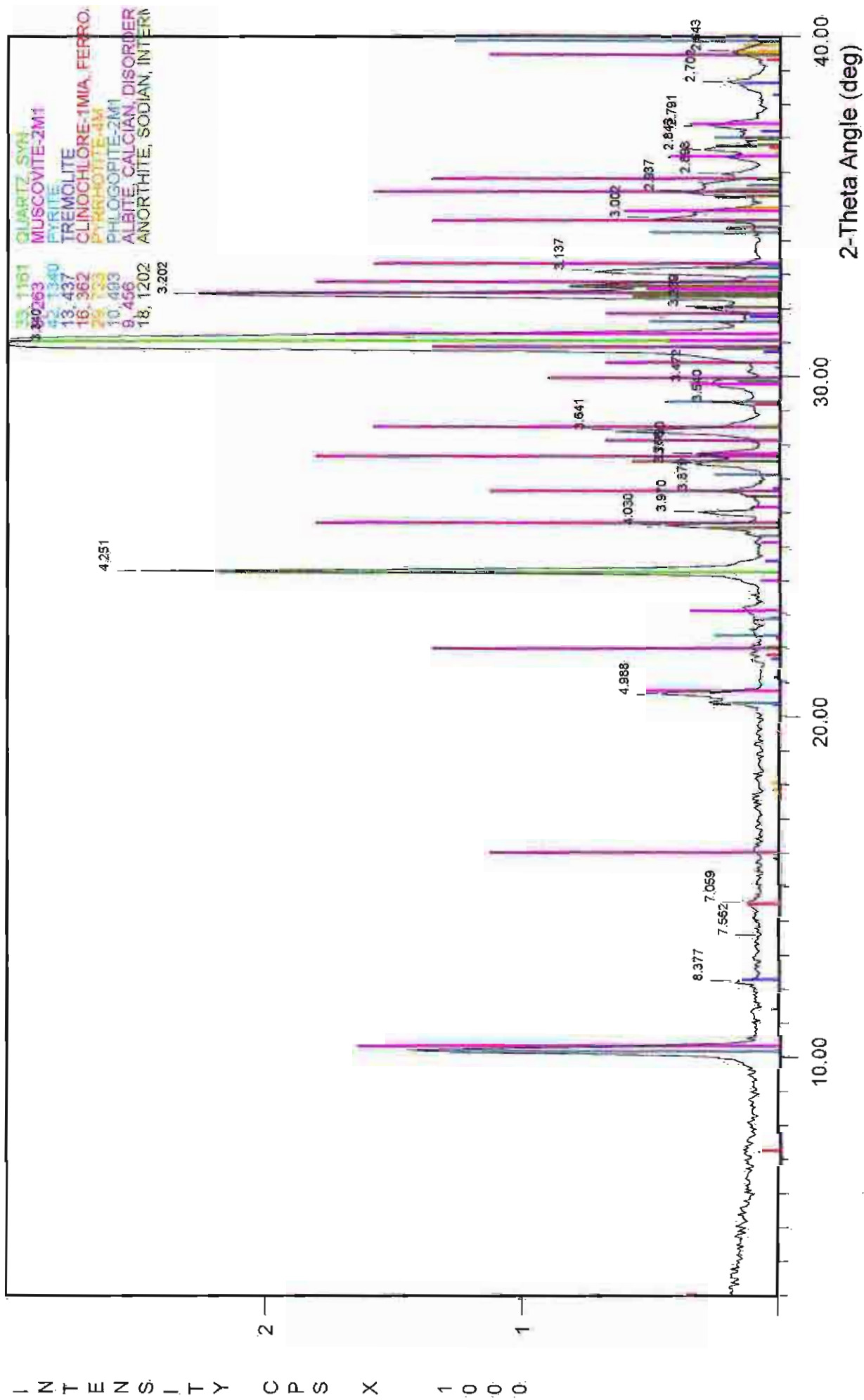


File Name: A:\11-70M

INTERNATIONAL OPS X 1000

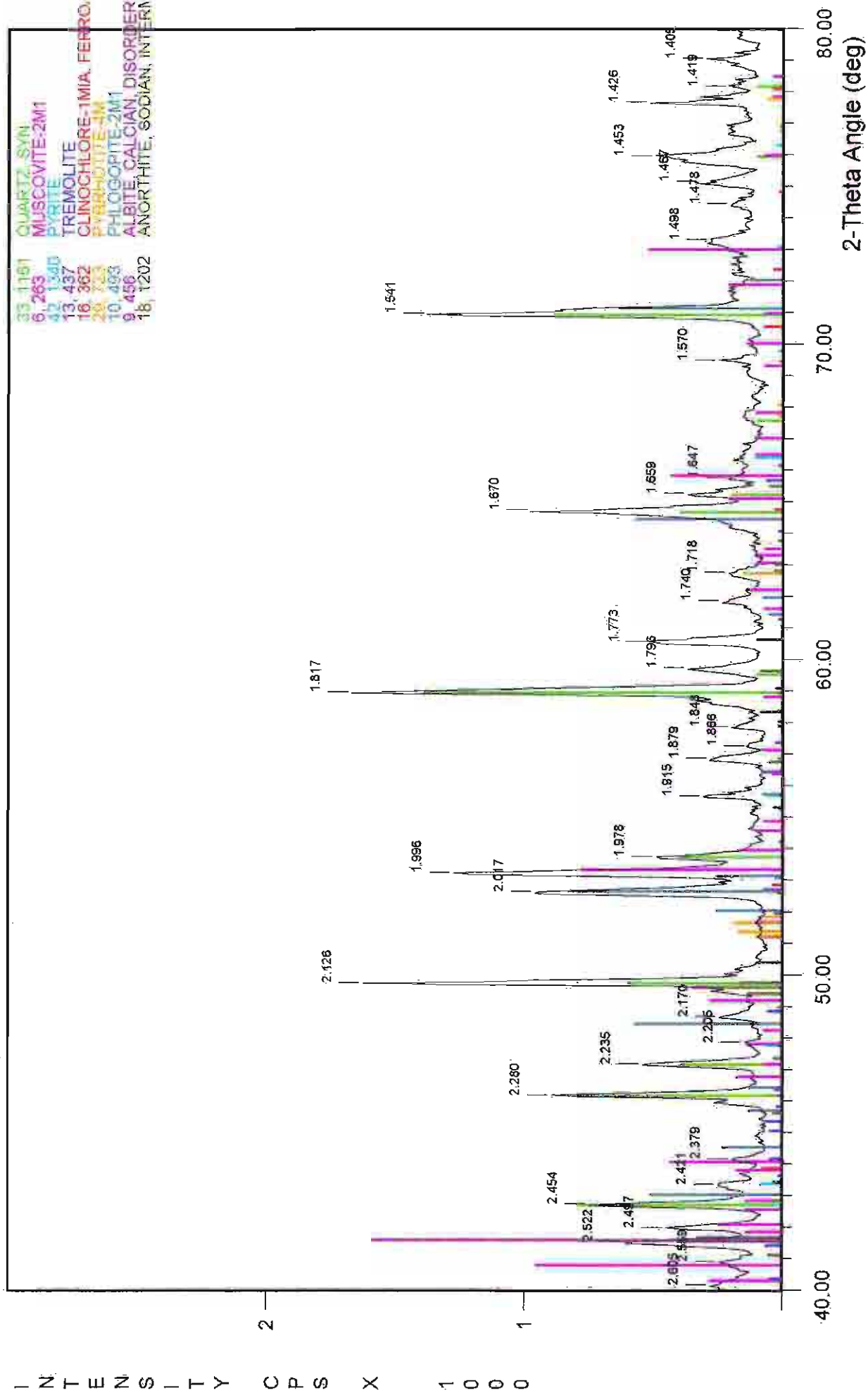


12.05m very dark grey - brown silt



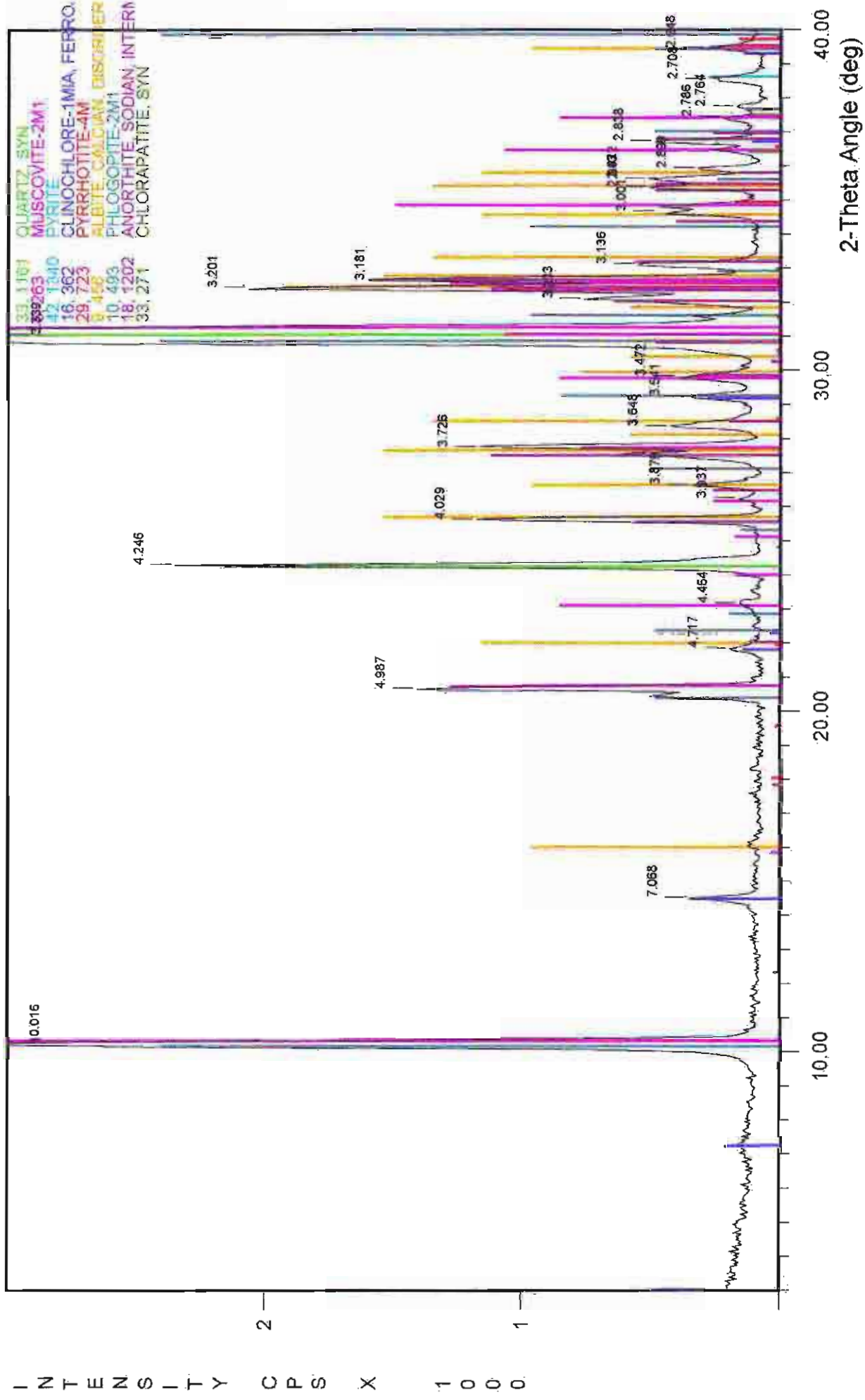
File Name: A:\12-05M

12.05m very dark grey - brown silt

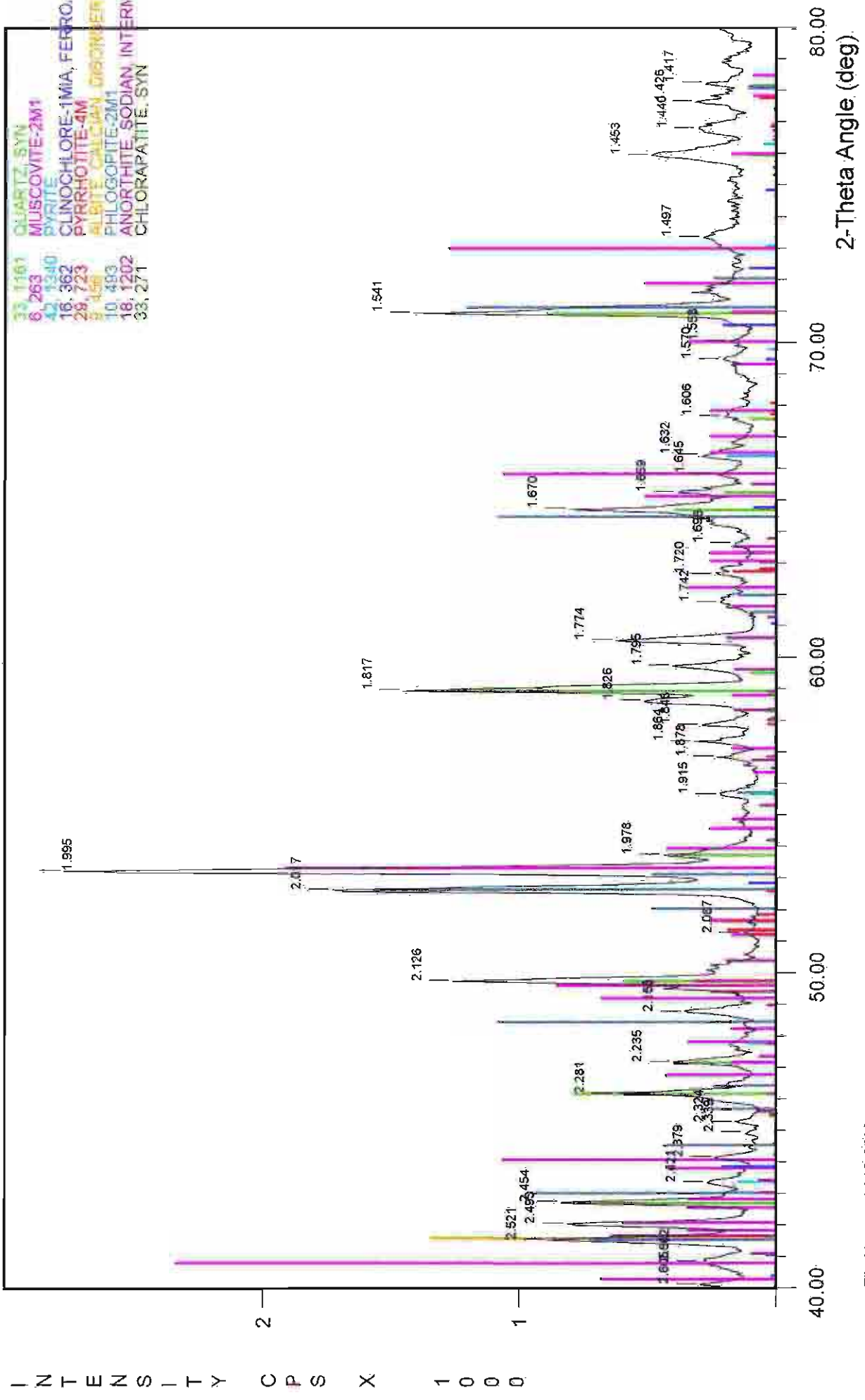


File Name: A:\12-05M

12.09m dark grey loamy fine sand

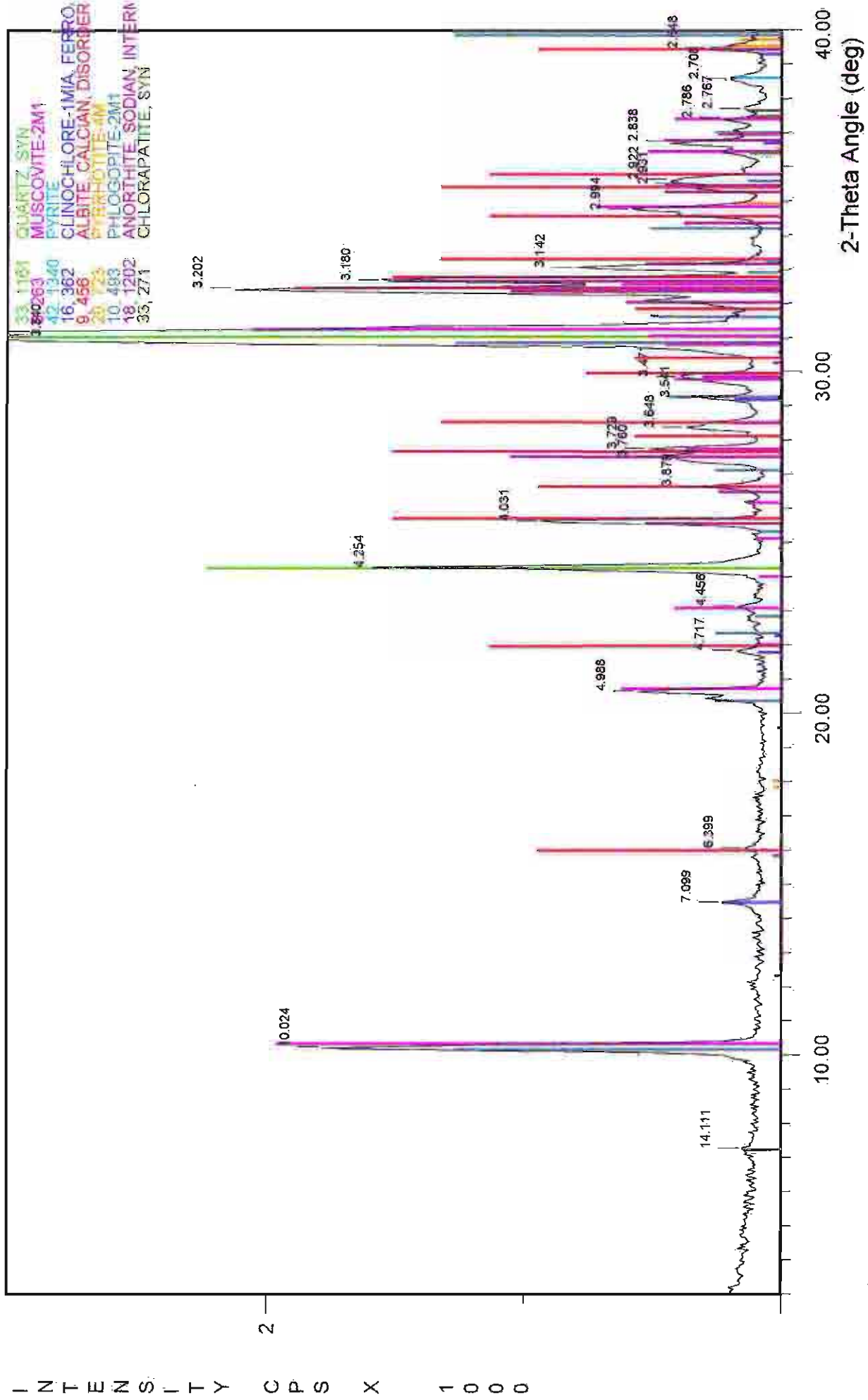


12.09m dark grey loamy fine sand



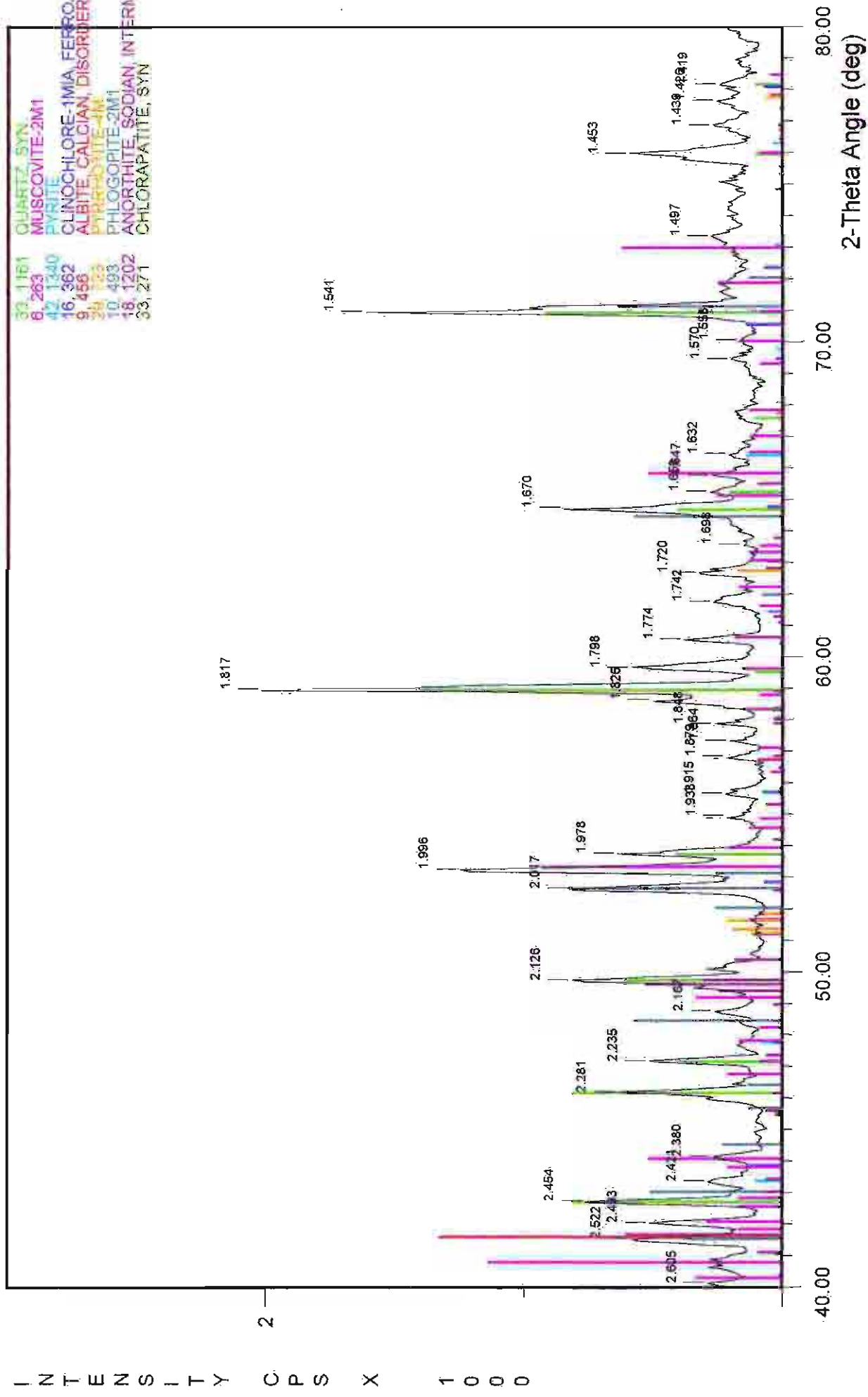
File Name: A:\12-09M

12.15m dark olive grey loamy fine sand.



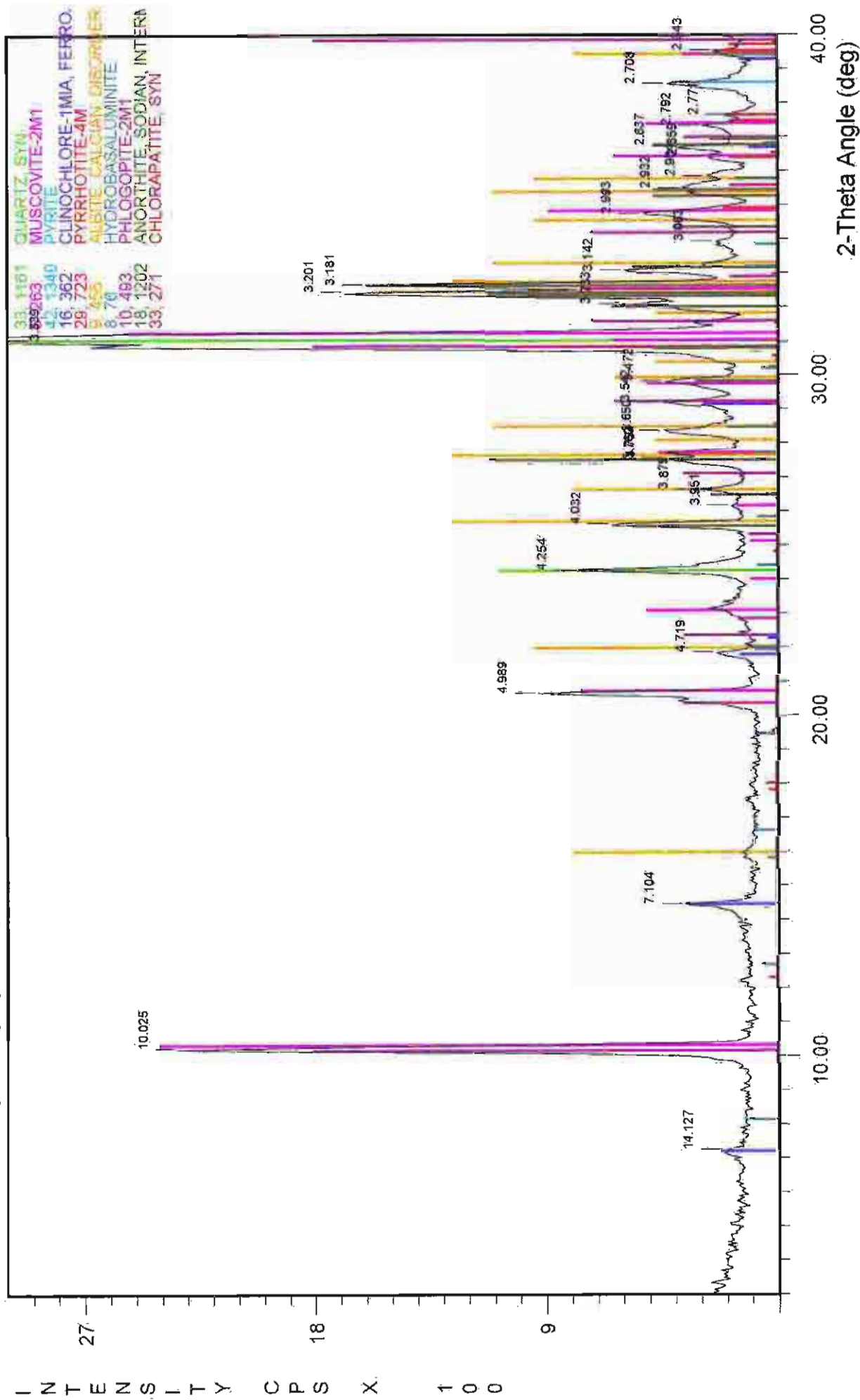
File Name: A:\12-15M

12.15m dark olive grey loamy fine sand

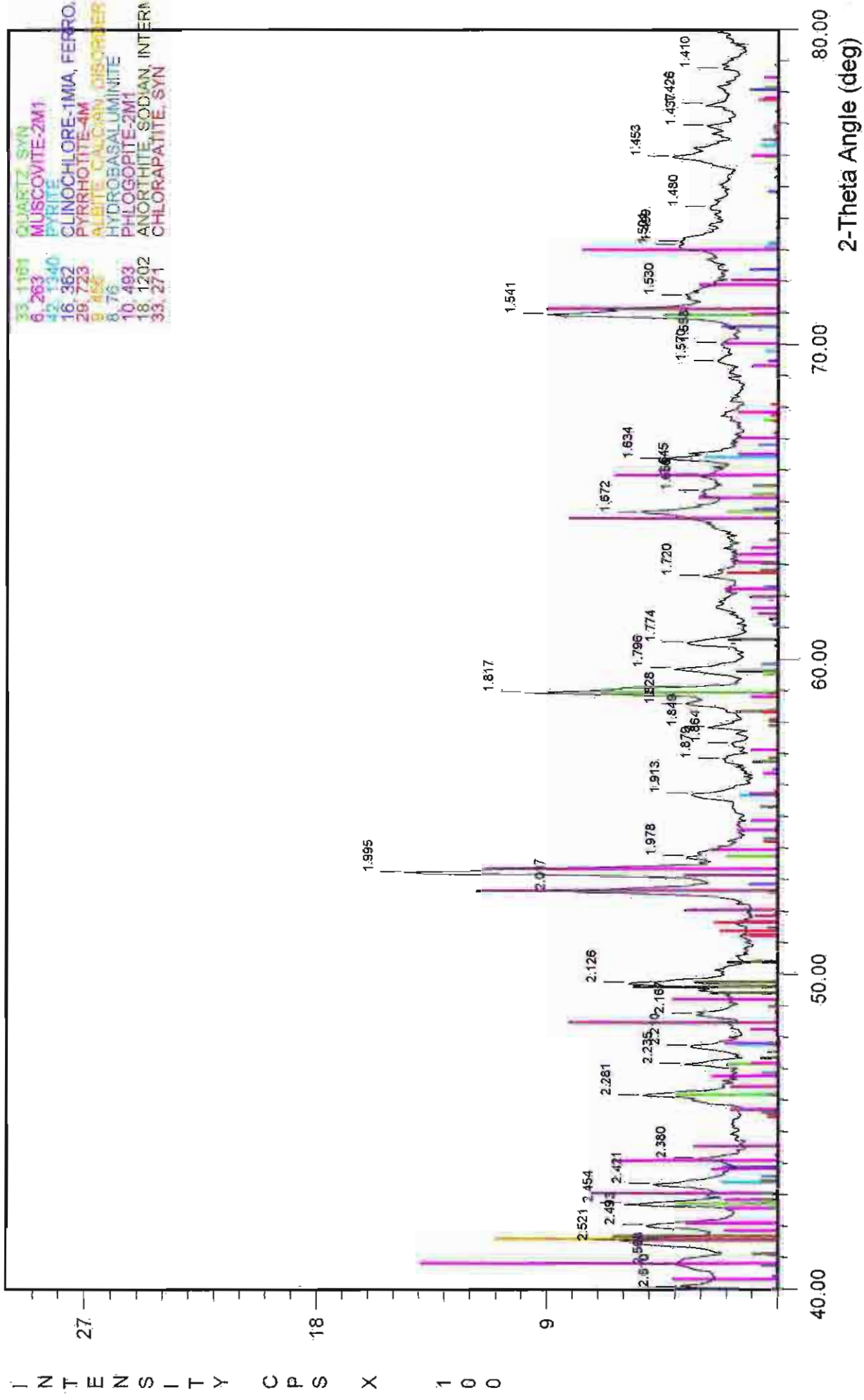


File Name: A:\12-15M

12.21m dark - very dark grey loamy fine sand

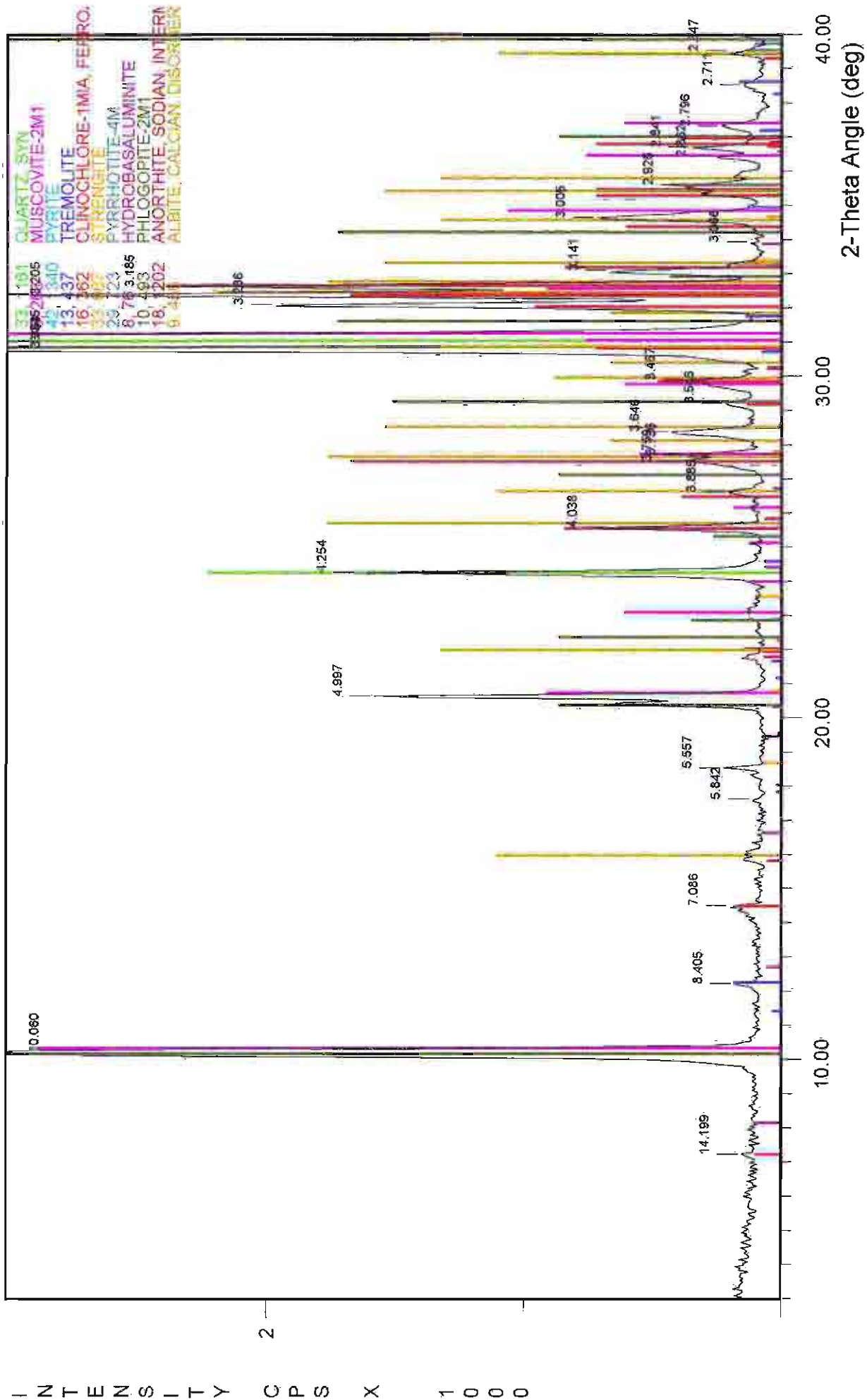


12.21m dark - very dark grey loamy fine sand



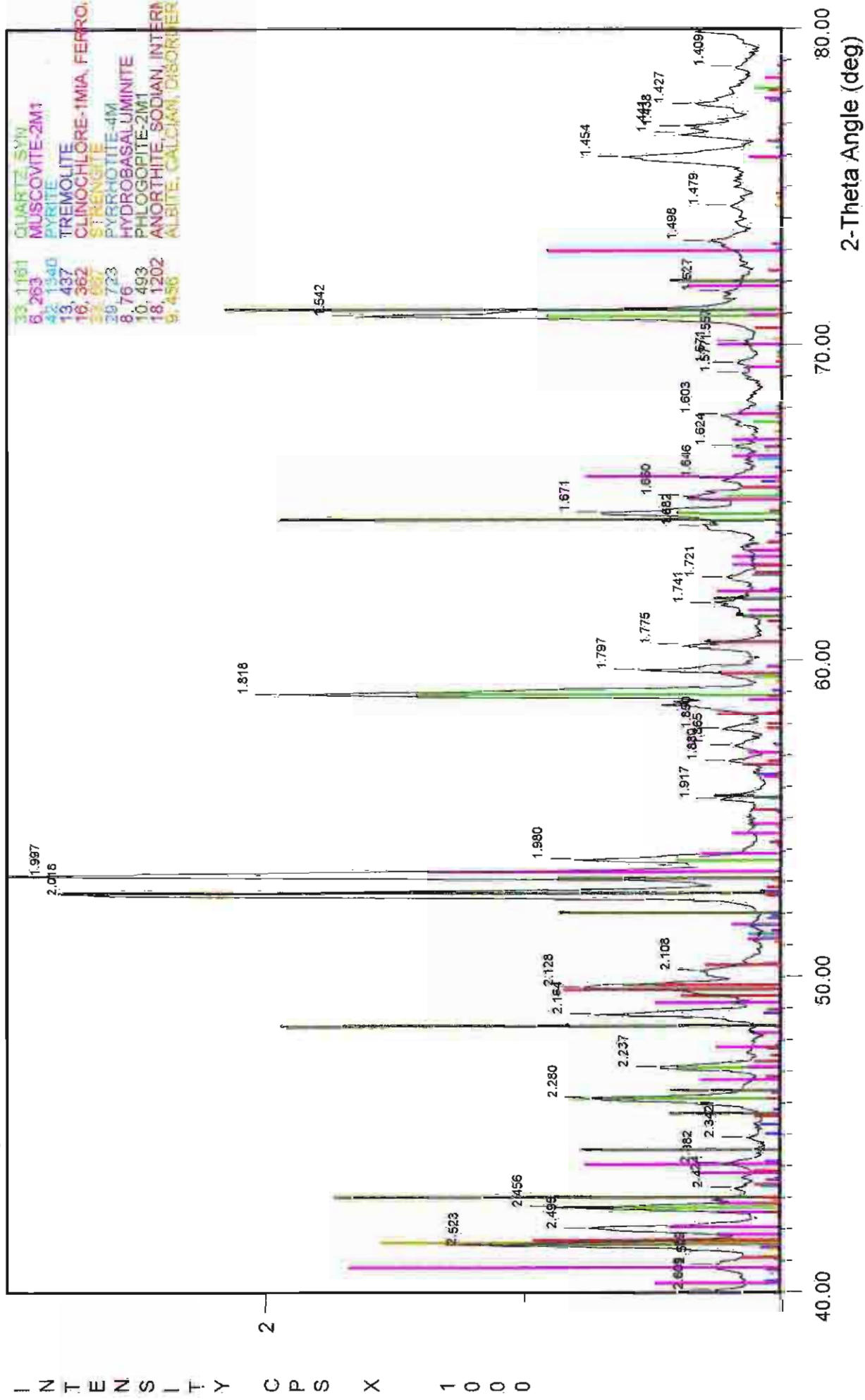
File Name: A:\12-21M

12.54m dark grey medium sand

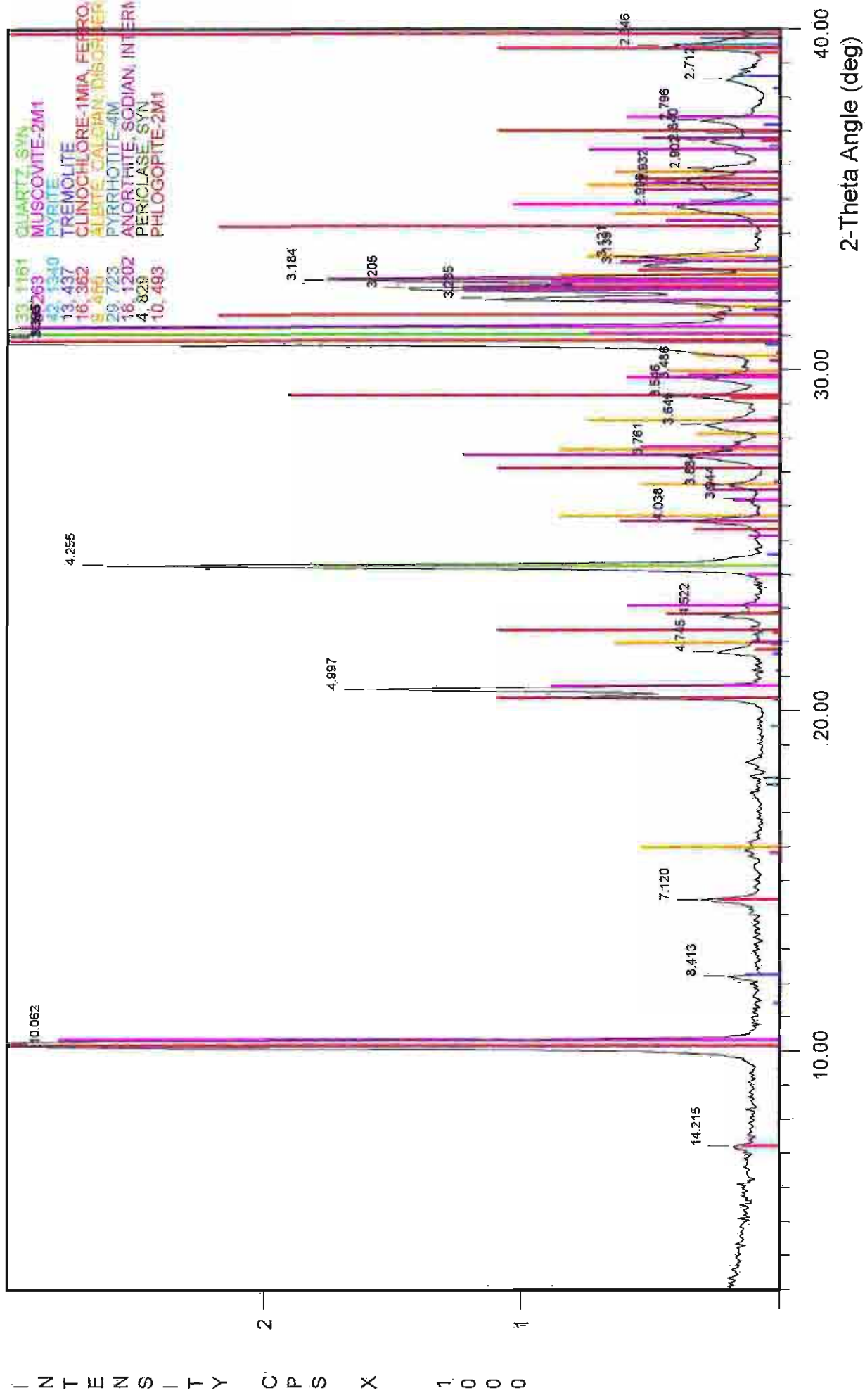


File Name: A:\12-54M

12.54m dark grey medium sand

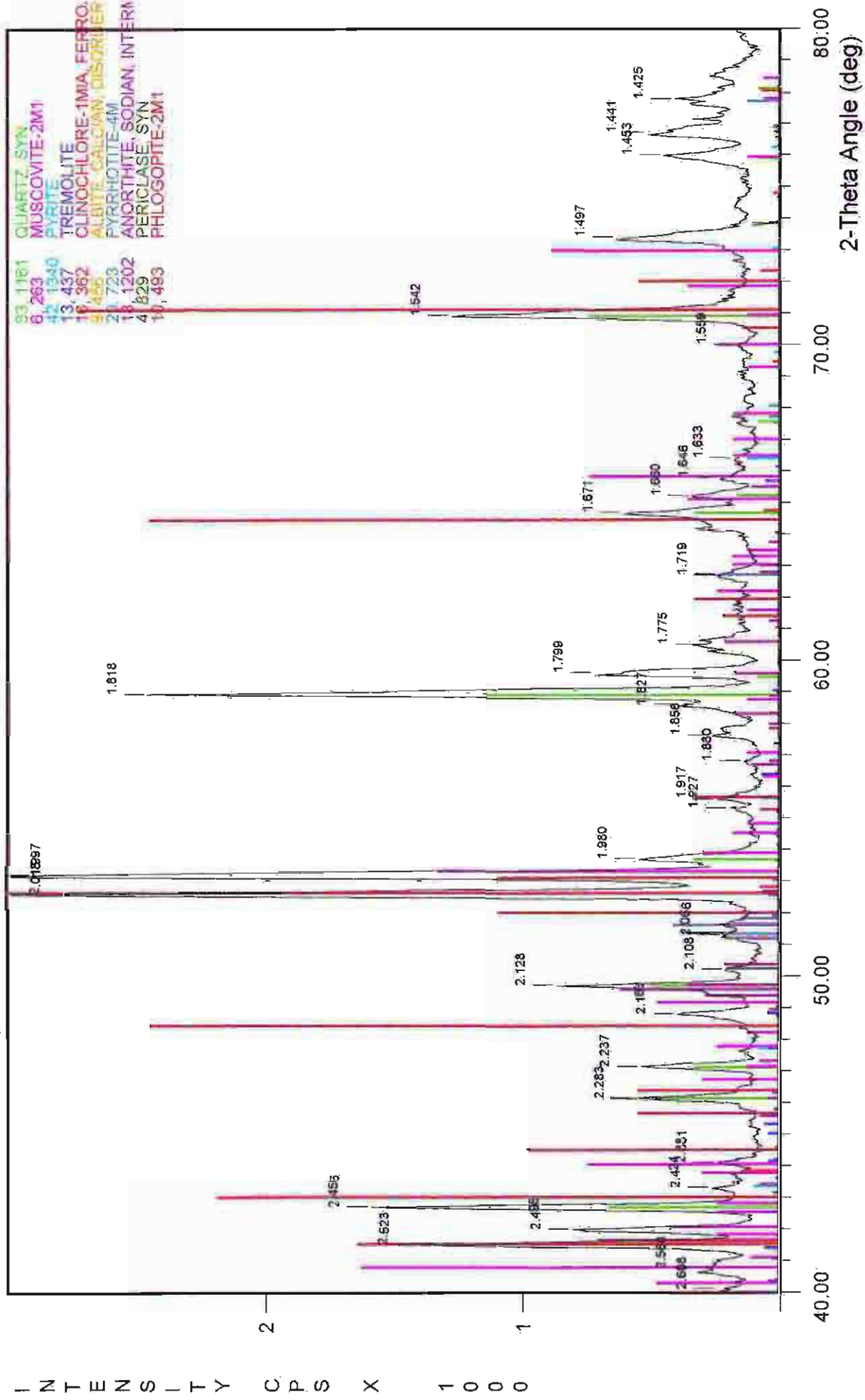


12.77m interbedded grey sand and silt

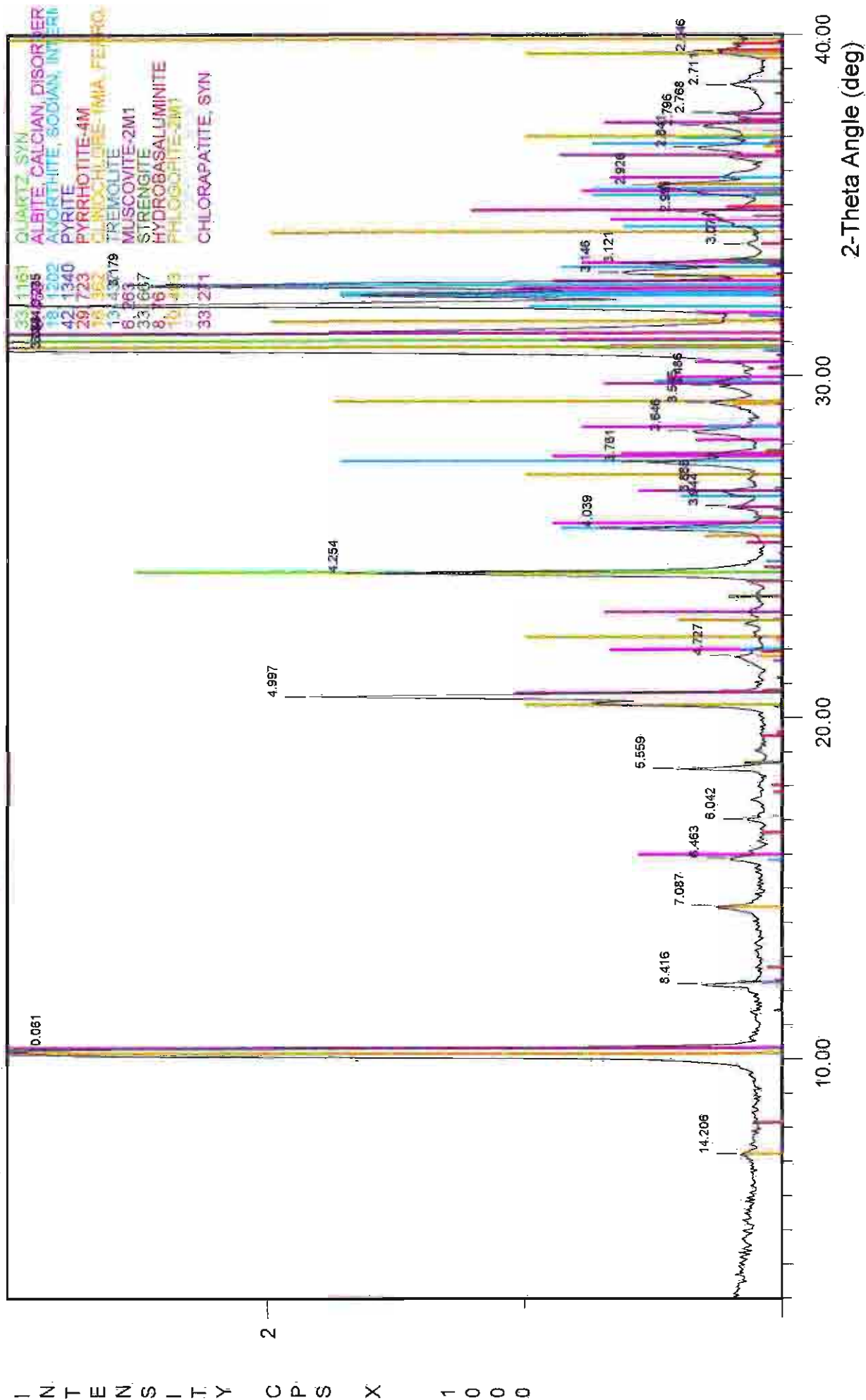


File Name: A:\12-77M

12.77m interbedded grey sand and silt

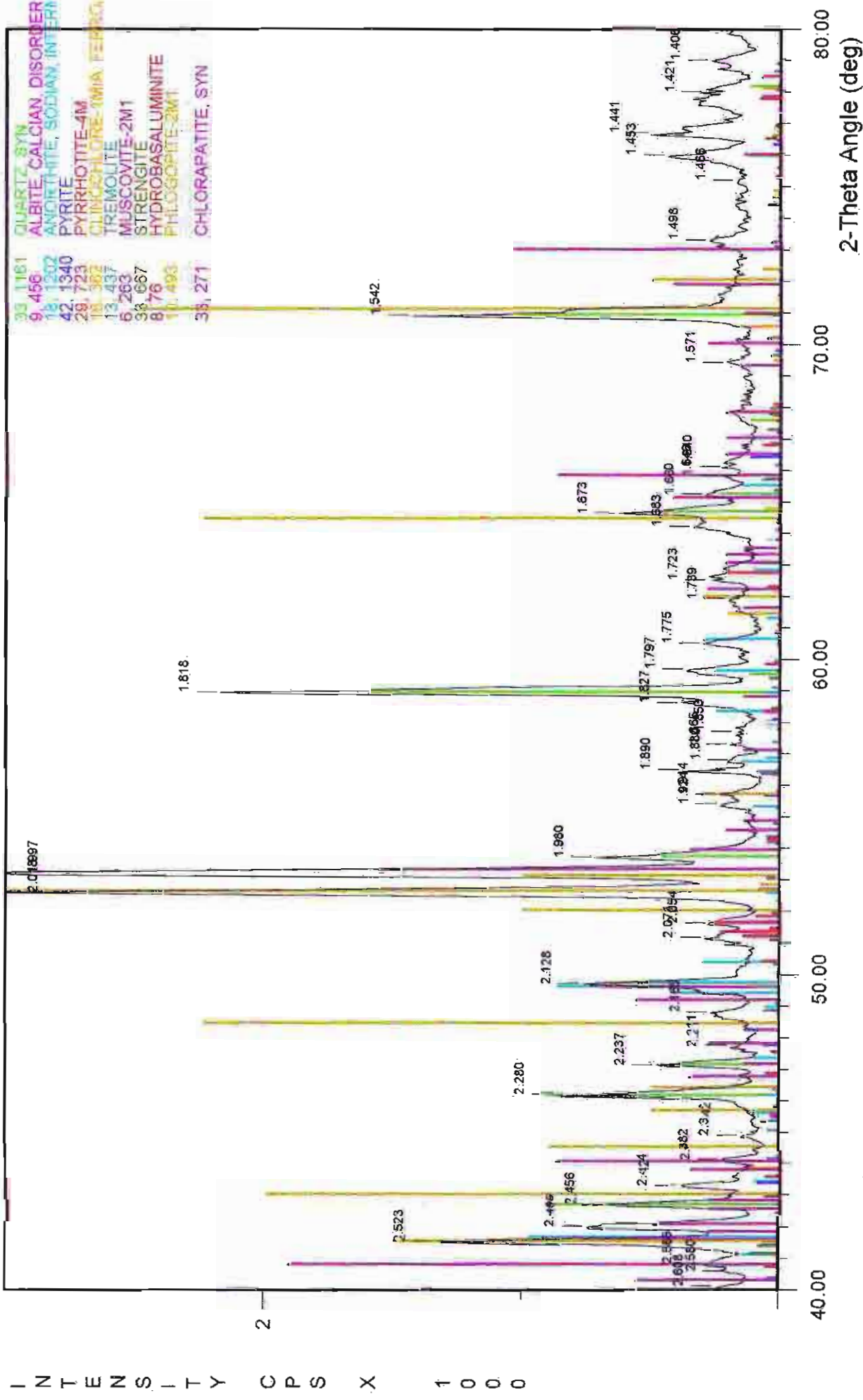


14.25m grey to light grey loamy fine sand



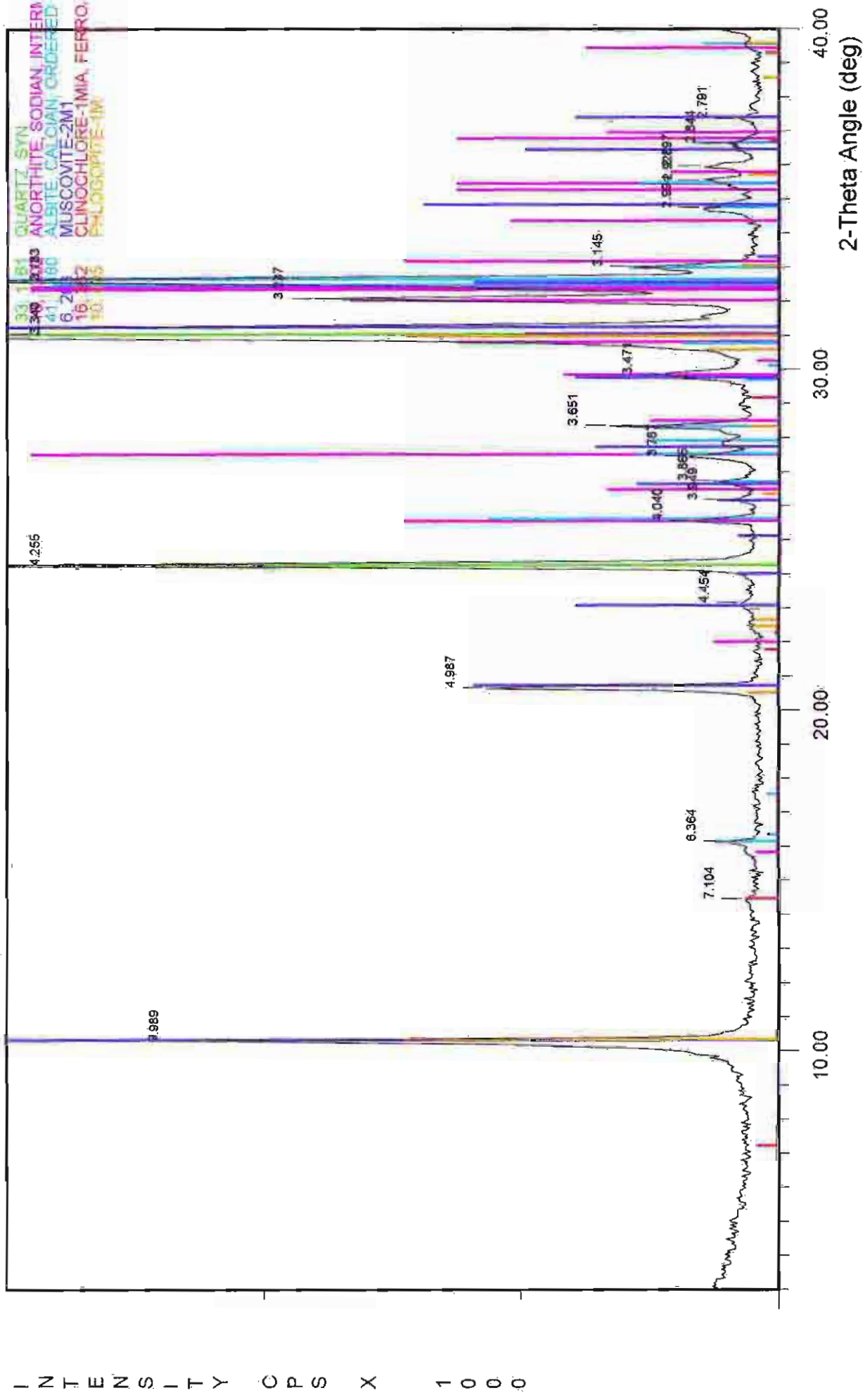
File Name: A:\14-25M

14.25m grey to light grey loamy fine sand



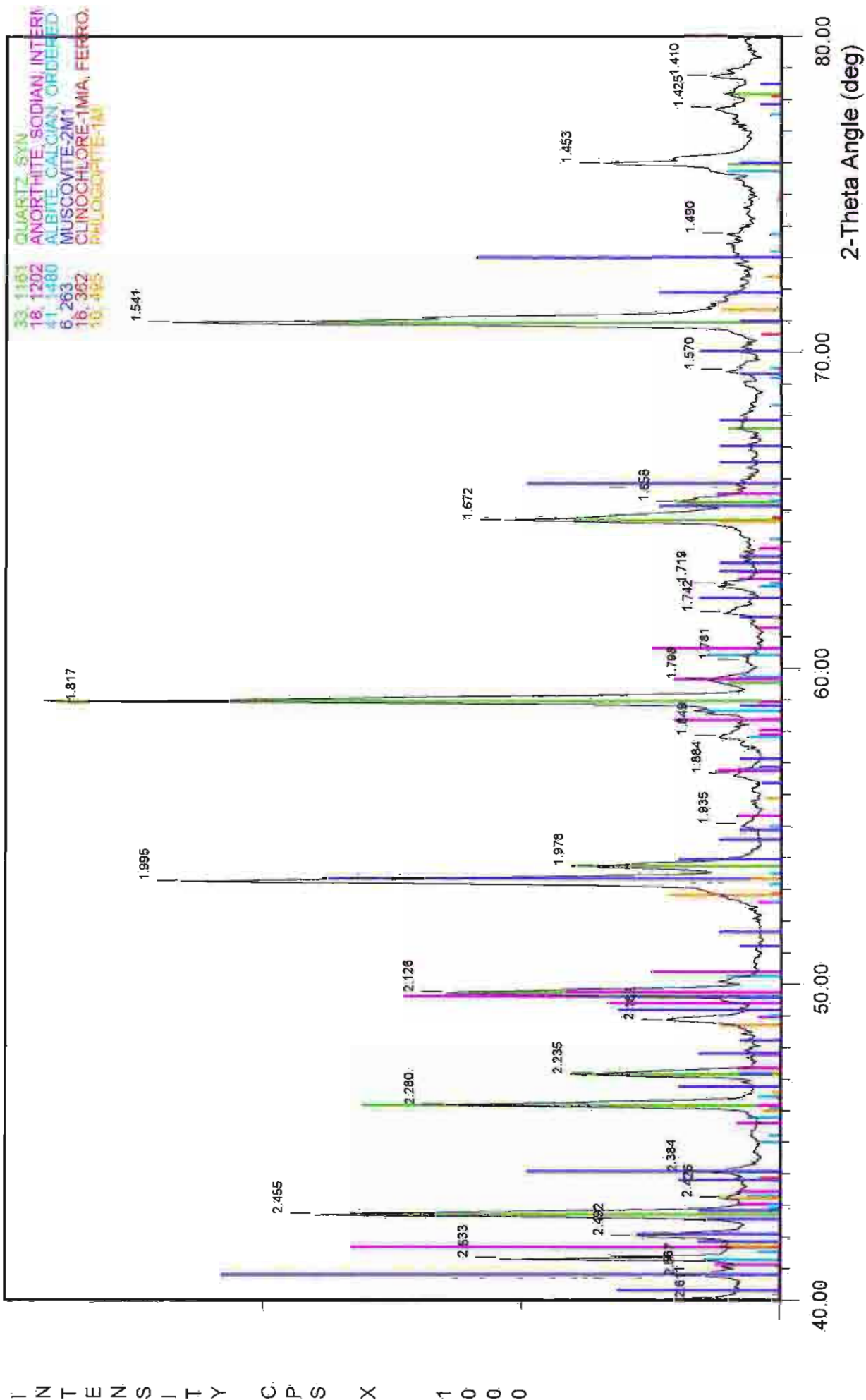
File Name: A:\14-25M

17.52m tailings base grey loamy fine sand



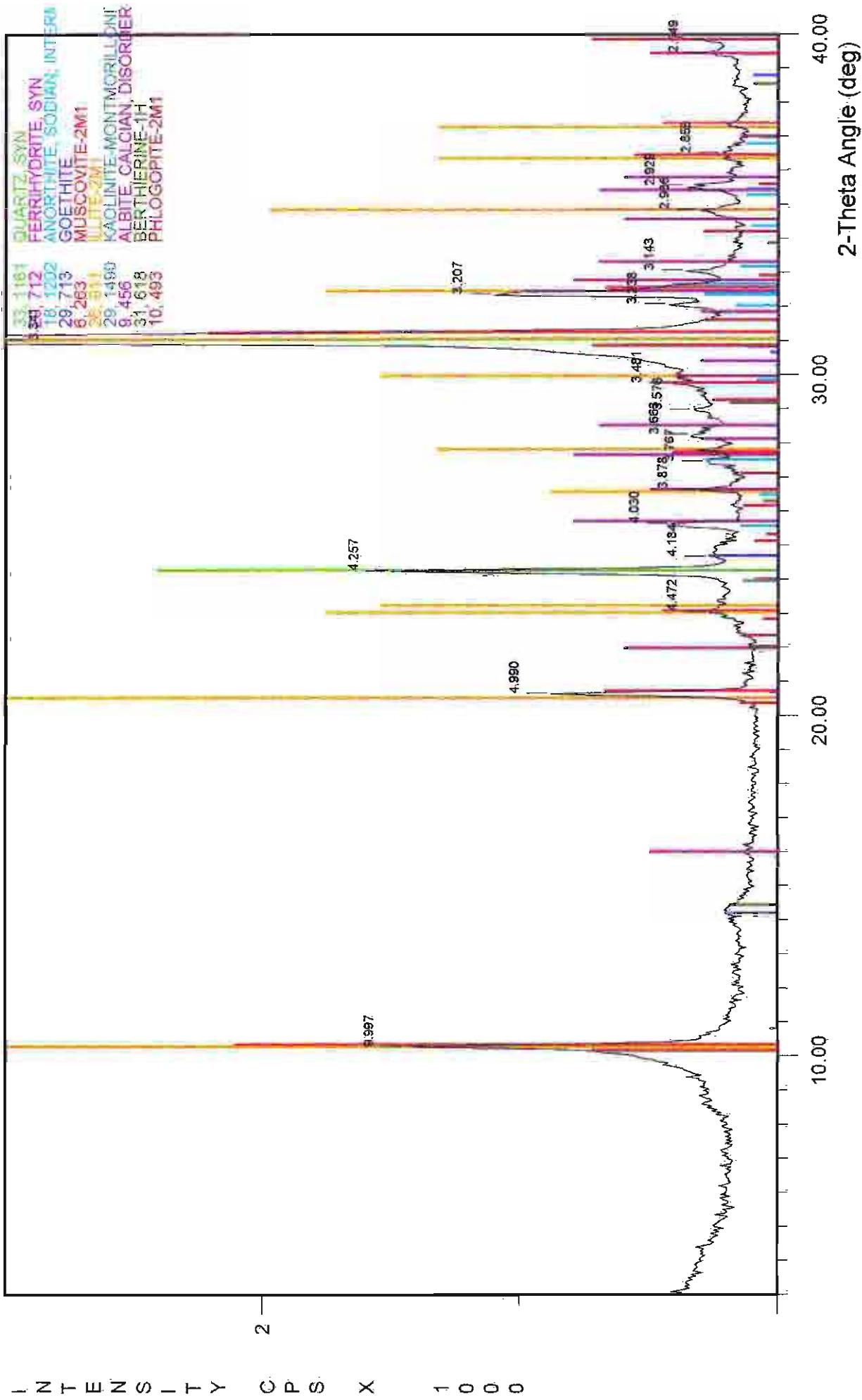
File Name: A:\17-52M

17.52m tailings base grey loamy fine sand



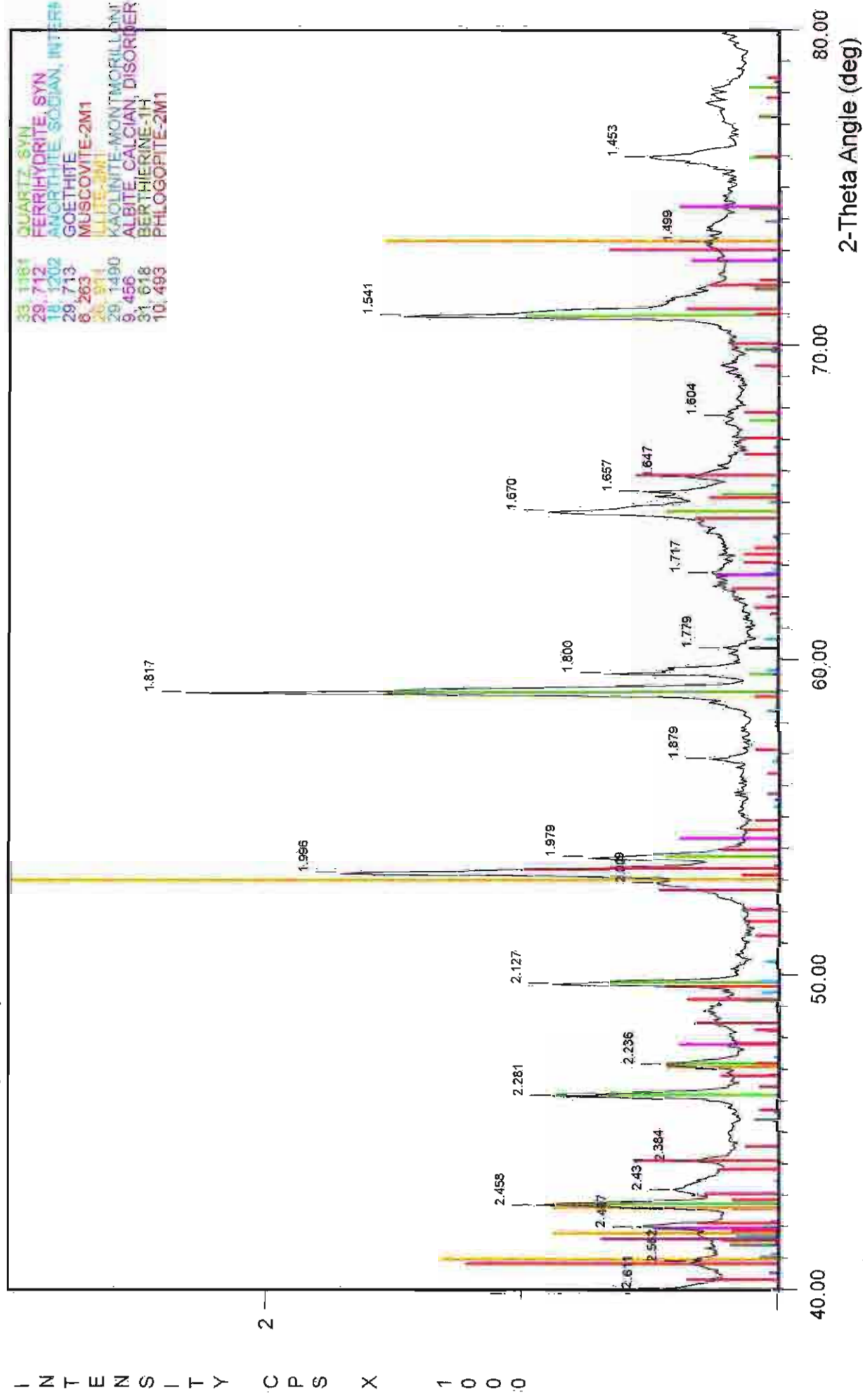
File Name: A:\17-52M

17.73m Redoximorphic depletion zone



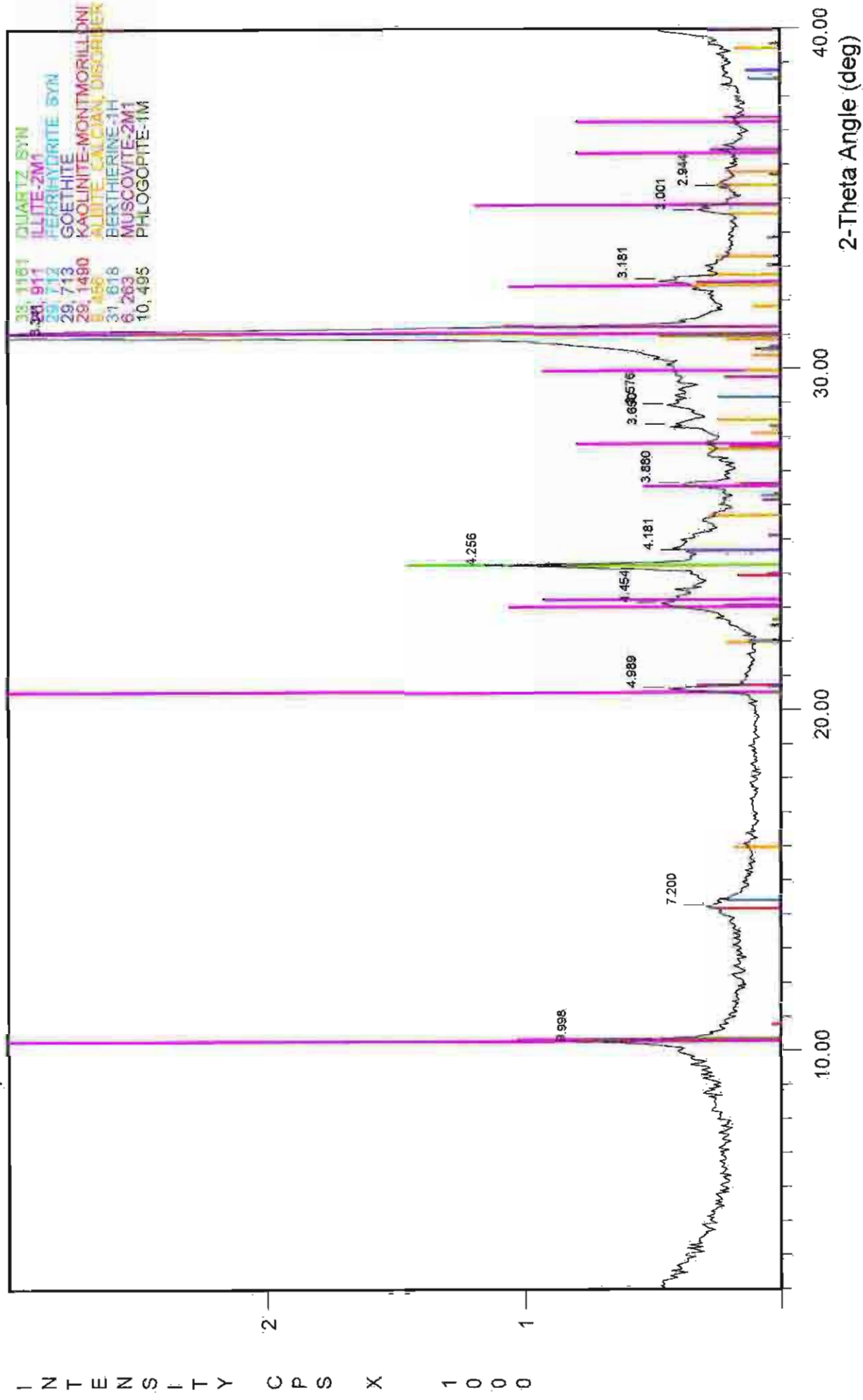
File Name: A:\17-73M

17.73m Redoximorphic depletion zone



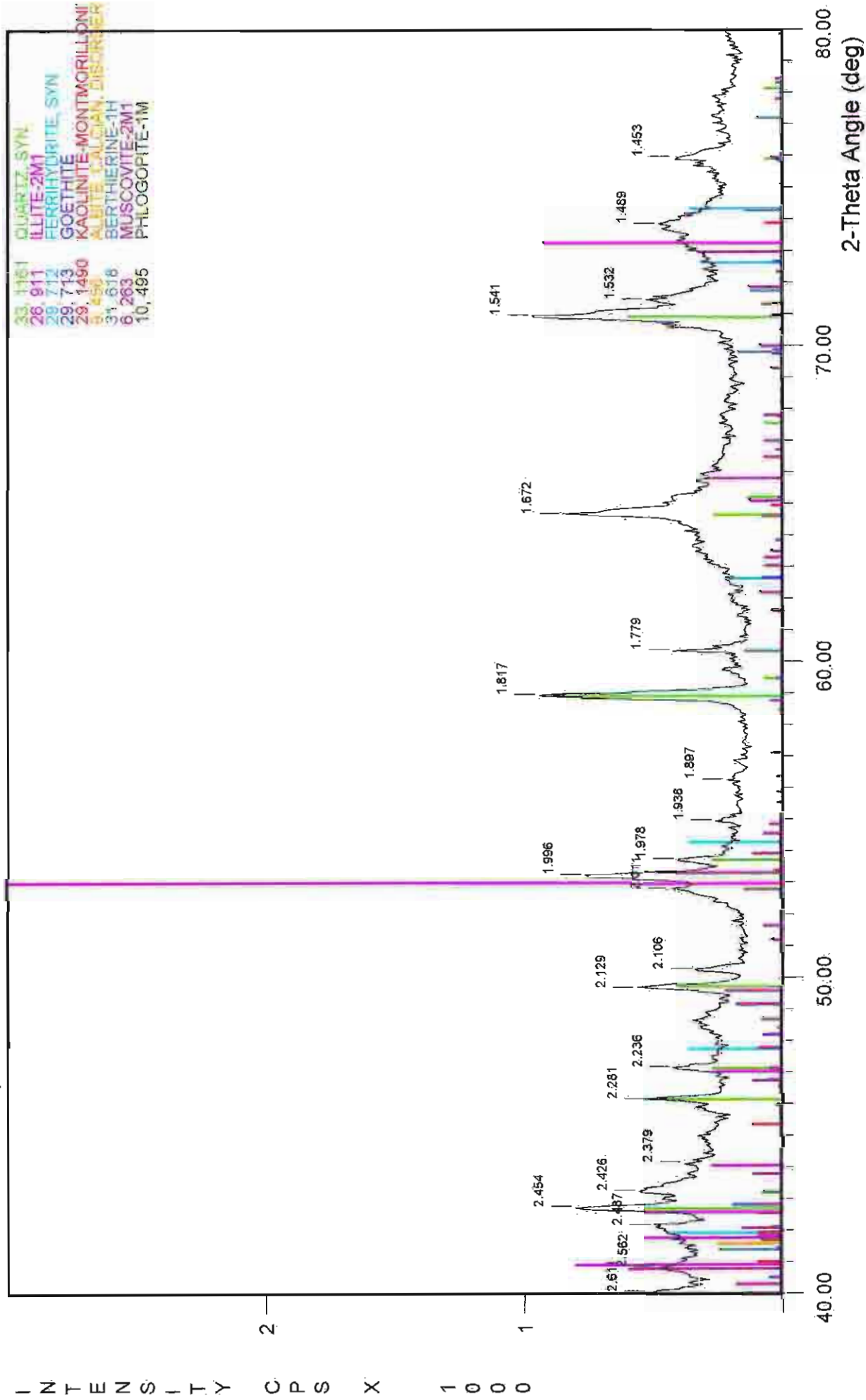
File Name: A:\17-73M

17.85m Redoximorphic accumulation zone



File Name: A:\17.85M

17.85m Redoximorphic accumulation zone



File Name: A:\17.85M

APPENDIX D

THE BACTERIAL INFLUENCE

It is important to recognise the role played by bacteria in the oxidation and reduction of iron and sulfur in order to understand the dynamics of mineral transformations associated with the generation and amelioration of acid mine drainage. Chemical reactions can be catalysed by microorganisms such as bacteria (Brierley, 1978; Brock and Brock, 1973; Brock, 1979 - cited in Ritchie, 1989). Within the tailings, bacterial activity has occurred at varying depths and certain reactions are still active today.

Iron Oxidising Bacteria

One type of micro-organism present are acidophilic bacteria, genus *Thiobacillus*, the common species are *Thiobacillus thiooxidans* and *Thiobacillus ferrooxidans*. The presence of the bacteria in the surface region is assumed, because the direct oxidation of Fe sulfides by air is too slow to generate the amount of acidity observed (Singer and Stumm, 1970). Thus it is suggested that *Thiobacillus ferrooxidans* act as catalysts in this situation by oxidizing aqueous Fe^{2+} whenever the pH of interstitial waters drop below 4.5. Singer and Stumm (1970) showed that at an acidic pH, the rate of oxidation was one million times faster in the presence of *T. ferrooxidans* compared to the chemical reaction rate.

Bigham *et al* (1992) explained the importance of rapid conversion of Fe^{2+} to Fe^{3+} . They illustrated that under strongly acid conditions the activity of Fe^{3+} in solution becomes significant and as a result, Fe^{3+} replaces oxygen as the primary oxidant of pyrite.

In the presence of bacteria and oxygen, the equations for the reaction are as follows (Smith, 1974- cited in Ritchie 1989):

a) pyrite conversion to ferrous sulfate

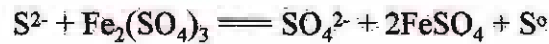


b) in the presence of *T. ferrooxidans*, ferrous sulfate is oxidised to ferric sulfate

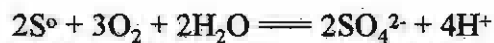
c) The Fe^{3+} then oxidises pyrite as rapidly as it is formed



d) The sulfide is then oxidised by ferric ion



or by oxygen and the S^0 produced in (c) is converted to SO_4 by *T. thiooxidans* and *T. ferrooxidans*



e) The Fe^{2+} produced is then subjected to further microbial action by *T. ferrooxidans* as in (b). A cycle is thus formed in which Fe^{3+} formed by microbial action reacts with pyrite



Thus, pyrite dissolution and acid generation are accelerated at low pH, by bacterial oxidation of Fe^{2+} which is the rate-limiting step in the overall process (Singer and Stumm 1970). However, there seem to be little physiological control by the organism over the type of minerals produced. The mineralisation process is extracellular and geochemical parameters for example pH, Fe and SO_4 concentration determine the mineralogical fate of iron once it is oxidized by either biotic or abiotic mechanisms (Bigham *et al*, 1992).

Therefore the activities in which acidophilic bacteria are involved can be characterized as "biologically induced mineralisation". Thus they are regarded as being catalysts of the pyrite oxidation rather than the producers of a particular mineralised by-product.

Sulfate Reducing Bacteria

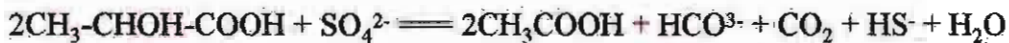
Lower in the profile different bacterial activities occur. The presence of Sulfate reducing bacteria (SRB) was hypothesised for levels below the water table, their existence was verified using the "Rapid Chek II SRB Detection System" (appendix F).

Results	Location	SRB quantity
	12m depth (top of water table)	10^3
	14.25m depth	0
	17.75m depth (soil below tailings)	10^4

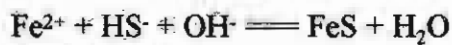
Appendix D The Bacterial Influence

The anaerobic sulfate reducing bacteria *Desulfovibrio* and *Desulfotomaculum* are heterotrophic (ie they grow utilising organic matter for energy, in the absence of oxygen) and produce H_2S from sulfate (Ritchie, 1989). The bacteria live in the water-saturated anaerobic environment, reduce sulfate to sulfide by using it as an electron sink during oxidation of organic matter, from which they derive their energy (Ivarson *et al*, 1982).

f) The following reaction (Rickard, 1973) shows an organic compound, lactate, being oxidised while sulfate is reduced, such reactions are carried out by SRB

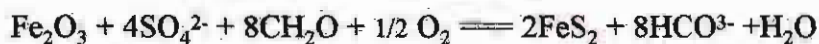


g) Then the sulfide as HS^- may react with Fe^{2+}



The FeS may at first be present as mackinawite, further reactions may produce griegite (Fe_3S_4) and pyrite (FeS_2) from mackinawite. Alternatively, pyrite may form directly, without mackinawite and griegite as intermediate steps (Pons *et al*, 1982).

h) Pons *et al* (1982) presented the following reactions to show pyrite (FeS_2) formation, using CH_2O to represent organic matter



where oxygen would be present in small amounts due to rainfall and groundwater flushing.

SRB's present at the top of the water table would use organic compounds leached from the surface as their energy source. Organic compounds may be in the form of partially degraded vegetation or flotation agents (secondary butyl xanthate and cresylic acid), added during processing.

Organic C% was determined for samples down the profile, the results are as follows:

DEPTH	%C
0.6m	0.07
3.7m	0.23
8.3m	0.19
11.7m (above water table)	0.06
12.5m (below water table)	0.15
17.8m (subsoil)	0.47

SRB are not active at lower depths (14.25m) as sulfate leached from the surface or organic C present in the profile is utilized at the top of the water table and thus is unavailable at depth. ICP data shows a decrease in the sulfate available at depth, additionally experimental sulfate determination through HCl and HNO₃ support this.

Redoximorphic Accumulation and Depletion Zones

The bacterial activity within the subsoil below the tailings has resulted in the formation redoximorphic accumulation and depletion zones. These are simply regions of iron oxides and oxyhydroxides concentration or removal. Prior to deposition of the tailings, the soils would have been oxidised resulting in the development of goethite and ferrihydrite accumulations identified through XRD as a redoximorphic accumulation zone. During the subsequent deposition of the tailings and the prevailing anaerobic conditions SRB have become active. The SRB present utilised the SO₄²⁻ present in the soil, forming sulfides, and the Fe³⁺ from iron oxides and oxyhydroxides are utilized in the formation of iron sulfides (eq h). The use of the iron oxides and oxyhydroxides in upper portions of the redoximorphic accumulation has caused the development of a redoximorphic reduction zone. Even though SRB were identified within the subsoil, large quantities of sulfides were not observed. This may be attributed to a number of different factors. Rabenhorst and James, (1992) explain that, for optimal growth rates, obligate anaerobes such as *Desulfovibrio* and *Desulfatovaculum* require virtual absence of oxygen, and they also prefer a pH near neutral (6-9), but, they have been isolated from areas of AMD with pH 3-4 where it appears they exist within microsites where pH in the immediate regions are more hospitable .

It seems that conditions are within the range for growth of bacteria and thus the production of sulfides, however, the low organic carbon levels would be the limiting factor, causing low sulfide levels within the soil.

In summary, sulfate-reducing bacteria require specific environmental conditions for optimal growth, they persist and grow over a wide range of conditions. While the bacteria are necessary catalysts for sulfate reduction, they are generally not the limiting factor. Carbon source availability, low redox potential and presence of Fe³⁺ and sulfate are however, keys to predicting minerals formation via sulfidisation. So, similar to the activities of acidophilic bacteria, the SRB act as a catalyst and do not mediate production of certain sulfides.

Secondary Sulfide Formation through bacterial activities

High levels of sulfide have been noted at 3.69-3.76m depth, an increase of approximately 1.5% S(wt) and a corresponding increases of Fe, along with increases in Cu and Zn compared to samples taken above and below this level. It was suggested that this is due to variations in ore processing at this time. It has also been hypothesized that this increase may be due to SRB activity during a 5 year interval when the tailings dam was water logged prior to the completion of deposition. The water table is thought to have been at approximately 1.3-1.4m depth.

Jorgensen B.B (1978) indicated the specific rate of reduction calculated for surface sediments is in the order of $50 \text{ nmol SO}_4^{2-} \text{ colony}^{-1} \text{ day}^{-1}$, thus approximately 50 nmol/cm^3 of sulfide produced per day. It should be noted that this rate has been determined for marine sediments, and rates vary between $1 - 10,000 \text{ nmol cm}^{-3} \text{ day}^{-1}$ have been recorded. A literature review of this subject suggests that sulfate reducing rates have not been measured on tailings dams and thus a assumption of $50 \text{ nmol SO}_4^{2-} \text{ colony}^{-1} \text{ day}^{-1}$ has been used. Over a period of 5 years this calculates to be 91250 nmol/cm^3 of S^{2-} . This corresponds to potential formation of 0.012g FeS/g or $1.2\% \text{ FeS}$. Thus providing there is enough sulfate being produced through oxidation at the surface and enough organic matter is supplied from the flotation products added to the tailings, it is not unreasonable to suggest SRB maybe responsible for this increase of sulfide at 3.69-3.76m depth.

Calculations

Assuming $50 \text{ nmol SO}_4^{2-} \text{ cm}^{-3} \text{ day}^{-1}$ can be reduced by SRB, over a 5 yr period when the dam was predominantly water saturated and active, the total amount of sulfate reduced is equal to:

$$5 \times 365 \times 50 = 91250 \text{ nmol cm}^{-3}$$

Assuming 1:1 ratio of sulfate reduction to sulfide formation from equation (f) then 91.25 umol of sulfide may be produced per cm^3

This can then be converted to g cm^{-3} using the molecular weight of sulfur

$$91.25 \times 10^{-6} \text{ mol} \times 32 = 2920.0 \times 10^{-6} \text{ g cm}^{-3}$$

$$= 2.9 \text{ mg cm}^{-3} \text{ as } \text{S}^{2-}$$

assuming that all the sulfide formed reacts with iron to form iron sulfide (eq g).

Appendix D The Bacterial Influence

To determine how much iron sulfide this represents:

$$\frac{S + Fe}{S} = \frac{32 + 56}{32} = 2.75$$

$$\begin{aligned} 2.9 \times 2.75 &= 7.975 \text{ mg cm}^{-3} \text{ as FeS} \\ &= 0.008 \text{ gcm}^{-3} \text{ as FeS} \end{aligned}$$

To convert mass to volume allowing comparison to previous results, using density of material previously determined as 1.5 g cm^{-3}

$$\begin{aligned} 7.975 \text{ gcm}^{-3} \times 1.5 \text{ gcm}^{-3} &= 11.96 \text{ mg/g as FeS} \\ &= 0.012 \text{ g/g} \\ &= 1.2 \% \end{aligned}$$

The increase observed at 3.69 - 3.76m depth of 1.5% sulfide, is therefore within the bounds of formations through sulfate reducing bacterial activities.

Sulfur Isotope Investigations

Sulfur isotope analysis was undertaken on samples from this depth range and compared to the ore body and other tailings samples. It was hypothesised that if the sulfides were formed by bacteria they would have a lighter isotopic value. Results obtained are as follows:

<u>DESCRIPTION</u>	<u>ISOTOPIC VALUE</u>
Ore body	-18.8
Base Tailings (10.68-10.77m depth)	-18.3
Secondary Pyrite Tailings- coarse (3.69-3.76m)	-16.0
Secondary Pyrite Tailings - fine (3.69-3.76m)	-15.9

A review of the sulfur isotope values determined by Seccombe *et al* (1985) indicated the pyrite deposit showed variations between -12 to -19, as a result of the ore's biogenic origin. Since the isotopic results of sulfides at 3.69-3.76m depth are within this range, it is difficult to positively determine if the sulfides were produced through secondary biogenic actions within the tailings. The results in this case are therefore inconclusive.

APPENDIX E

METHODS

1. SAMPLE COLLECTION

Core samples were removed from the tailings dam using a soft sediment piston core sampler and rig. Core were obtained with a simple jacking device, which forces the sampling tube gently into the sediment, thereby minimizing sample disturbance.

The rig was fastened to the sediment with screw anchors. When appropriately anchored, the jacking device was attached and activated. Core removal through this method allowed cores to be removed from desired depths without needing to remove sediments located above. A combination of thin walled UPVC plastic core tubes and stainless steel core tubes for firm sediments were used.

Immediately after sampling the cores were sealed for transport to the laboratory. The seals holds the cores firmly in place and therefore reduced sample disturbance and reaction with air.

Sediment stratigraphy was determine by extrusion of the cored samples. Cores contained in plastic tubes were sub-sampled with the aid of a pipe cutter while confined in a glove box of argon. Stainless steel samples were extruded through an arm hole in the glove box with minimal argon loss.

2. pH, ELECTRICAL CONDUCTIVITY AND REDOX POTENTIAL DETERMINATIONS

Samples were initially prepared for pH, EC and ICP measurements using the standard 1:5 sample : water dilution, and agitated for 1hr.

pH

A Radiometer-Copenhagen TTA80 assembly was used to achieve measurements of pH which were displayed on PHM Ion meter. Method A was selected for acidic samples. The electrode was stabilized using previously used pH 7 buffer solution, then calibrated using new pH 7 and pH 4 buffers. Results of pH were then obtained, these values are dependent on the salt content in solution. Consequently, it is a common practice in soil science to evaluate pH in a standard salt solution of sufficient concentration to negate the effect of native salt contained in the sample. Thus, pH was also measured in 0.01M calcium chloride suspensions (1ml 0.5M CaCl_2 added to the 50ml reverse osmosis water already present in the sample forming a 0.01M solution).

Electrical Conductivity

A Radiometer-Copenhagen CDM 83 Conductivity Meter was used for EC measurements. The analysis equipment consists of 3 platinum electrodes which were initially stabilized using previously used KCl solution. The cell constant was changed to achieve required calibration.

Redox Potential

Redox Potential (Eh) was measured with an IONODE combined platinum/silver - silver chloride electrode connected to a HANNA HI 8521 and used in an argon filled chamber (oxygen excluded). All readings were adjusted so that they refer to the standard Hydrogen electrode.

3. ELECTROMAGNETIC SURVEY

A Geonics EM31 instrument was used in the vertical dipole mode, with the transmitter/receiver being about 1m above ground level. Readings were made at approximately 10m intervals, as determined by pacing, along 9 transects.

Survey control was obtained by photocopying an aerial photograph on to graph paper and hence the locations of the EM transverses are not precise. Similarly the vegetation and pond boundaries could be improved by working from an original photograph or survey plan.

4 CLASSIFICATION OF MATERIALS

Samples were assessed for texture and wet colour (McDonald *et al*, 1985). Colour was recorded as hue, value and chroma using Munsell colour charts. Samples were analysed in 1:5 soil:water suspension for electrical conductivity, pH in water and pH in 0.1 M CaCl₂ (Rayment and Higginson 1992).

The 132 samples which were collected were classified using a hierarchical classification routine (FUSE) in the PATN (Version 3.3) in PATN. The quality of the grouping was assessed by displaying the classification in the three dimensions produced by a multidimensional scaling (MMS) ordination routine in PATN. The three dimensional display routine ACROSPIN (Version 2.0) was used to do this (Parker 1989).

5 INDUCTIVELY COUPLED PLASMA ATOMIC EMISSION SPECTROMETRY

As mentioned previously ICP analysis was undertaken in conjunction with pH and EC measurements using a standard 1:5 dilution of tailings to water. In the laboratory samples were removed from the main source for analysis to ensure contamination from pH and EC testing did not occur. Elemental analysis by inductively coupled plasma atomic emission spectrometry (ICPAES) against standards of an appropriate matrix was performed.

6. NET ACID PRODUCTION : (NAP) METHOD

Followed procedure of Miller et al (1994) with minor alterations, after reviewing the original procedures given in Coastech Manual (1991) and that by O'Shay *et al* (1990).

Objectives

The NAP test provides information on the risk of acid formation by mine waste materials; the relative reactivity of the contained sulfides; and is a measure of the amount of acid a material can generate. This information can then be used for planning and implementing waste rock and tailings disposal operations.

Equipment

600ml conical flasks
watch glasses
hot plate
250ml calibrated beaker
burette
pH meter

Reagents

15% hydrogen peroxide
NaOH pellets
potassium hydrogen phthalate
distilled water

Procedure

1. Pulverise the sample using the tungsten mill until uniform silt size obtained. From subsequent SEM examinations, most of the particles were below silt size (20 μ m) and all were less than the 75 μ m (200mesh, Tyler) recommended by Coastech Manual (1991).
2. Add 250ml of 15% hydrogen peroxide, (30% Merck reagent diluted 1:1 with deionised water) to 2.5g \pm 0.01g samples in 600ml conical glass beakers covered with watch glasses. Samples are kept in a fume hood during the test. The oxidation reaction results in the production of heat in some samples. Samples are considered to have finished reacting when:
 - 1) the sample solution boiled and then cooled
 - 2) after at least 24 hours has elapsedAny excess hydrogen peroxide left in the sample solution is broken down by heating the NAP solutions on a hot plate at approximately 100°C for about 30 minutes, until all effervescence ceases and the solution boils.
3. After the solutions cool, measure the pH values and determine acidity by pH titration of a 10ml sub sample of each solution with standardised NaOH in a microburette, to an endpoint of pH 7.0.

Appendix E Methods

Standardisation of NaOH

1. Prepare a 0.1N NaOH solution by dissolving 1.15g NaOH pellets in water, in a 250ml calibrated polythene beaker, then diluting it to the 250ml mark on beaker.
2. Titrate the solution against a solution containing an accurately weighted amount (approximately .2g) of potassium hydrogen phthalate, using phenolphthalein to determine the end point

Calculations

Normality of NaOH solution calculated using

$$N = \frac{1000 \times \text{wt. of phthalate}}{t \times 204.23} \quad \text{where } t = \text{average volume of three titrations}$$

NAP determined using Coastech manual scheme

$$\text{Net AP} = \frac{1250 \text{ ab}}{c} = 51 \text{ b (for 0.102N NaOH)}$$

where

NAP = Net acid potential in kg CaCO₃ equivalent per tonne

a = normality of NaOH

b = volume of NaOH added to 10ml aliquot to achieve a pH of 7.0

c = weight of sample

7 B.C RESEARCH INITIAL TEST

Modified from Coastech Manual (1991).

Objectives

To determine the balance between acid producing and acid consuming components of a mine waste by:

- 1) determining the neutralization capacity of sample
- 2) calculating the acid producing potential of sample

Comparison of the two values allows classification of the sample as potentially acid - consuming or -producing . If acid producing > acid consuming then the sample is classified as a potential acid producer.

Equipment

10ml beakers
50ml beakers
pH meter

Reagents

Distilled water
Certified grade .25N sulphuric acid

Procedure

1. Pulverise samples using tungsten mill until a uniform silt size is obtained. Subsequent SEM investigations indicated most of the particles are below silt size (20 μ m) and all are less than the 75 μ m (200 mesh, Tyler) recommended by Coastech Manual (1991).
2. Submitted subsamples of the test material for total sulphur analysis by LECO furnace method.
3. Weigh 4g of samples into 10ml beakers, add approximately 2ml of water to produce a paste and determine pH.
4. Transfer paste samples quantitatively into 50ml beakers, add distilled water to make total volume of 40mls. Determine pH.
5. While stirring sample slurry, titrated potentiometrically with standard .25N sulphuric acid to an end point of pH 3.5. Acid is continually added until the acid addition over a 24hr period is 0.1ml or less. Total volume of acid added is recorded.

Standardisation of H₂SO₄

Molarity of the acid solution is determined via titration with NaOH solution of known molarity. The end point is determined through addition of methyl red indicator, and titrant recorded.

Appendix E Methods

Calculations

Normality of H_2SO_4 solution calculated using

$$N_1 V_1 = N_2 V_2 \quad \text{where } N_1 = \text{normality of known solution}$$
$$V_1 = \text{volume of known solution}$$
$$N_2 = \text{unknown normality of solution}$$
$$V_2 = \text{average volume of three titrations}$$

Normality was found to be 0.249

Acid consumption in kg H_2SO_4 per tonnes of material is given by

$$\text{Acid consumption} = \frac{(\text{ml } 0.25\text{N } \text{H}_2\text{SO}_4 / 4) \times 0.049 \times 1000}{\text{wt sample in gm}}$$

Acid producing potential in kg H_2SO_4 per tonne of material

$$\text{Acid Production} = \% \text{ total S} \times 30.6$$

The factor of 30.6 is derived from chemical equations which show that 4 moles of H^+ are produced from each mole of pyrite (FeS_2). The use of % total S assumes that all the sulfur in the sample is present as pyrite. In subsequent tests a HCl and HNO_3 extraction was completed on the same material. A comparison of the acid production using the % total S and the % sulfide S can be observed in the text.

Net Neutralization potential, (Net NP), in kg H_2SO_4 per tonne of material is given by

$$\text{Net NP} = \text{NP} - \text{AP}$$

To allow comparison with the NAP method of estimating acid generating potential, NNP values are converted to kg CaCO_3 equivalent per tonne of material by multiplying by the factor 1.0214. The more negative the NNP value is, then the higher the acid generating potential.

8. SULFUR FORMS DETERMINATION BY HCl - HNO₃ EXTRACTION

Modified from M.S Burns (1969)

Objective

To determine the sulfide and sulfate quantities within a sample, thus obtaining a better understanding of the oxidation condition and acid mine drainage potential of the material. A similar method has been used for many years in the U.S as a standard procedure.

Equipment

250ml conical flasks
Hot plate
No 54 filter paper
funnels
100ml beakers
ICP tubes

Reagents

5N HCl
2N HNO₃
distilled water

Procedure

1. Pulverise samples using a tungsten mill until a uniform silt size is obtained. From subsequent SEM examination, most of the particles were are below silt size (20µm) and all were less than the 75µm (200 mesh, Tyler) recommended by Coatest Manual (1991).
2. Select approximately 1g of sample for total sulfur analysis by LECO furnace method.
3. Weigh 2g of each sample into 250ml conical flasks and add 50ml 5N HCl (492ml conc HCl added to 508 ml water). Bring samples to the boil on hot plate at approximately 150°C and boil for 15 minutes.
4. Filter samples whilst hot through No 54 filter paper. Retain approximately 10-12mls of sample for ICP analysis. Transfer the residue solids to filter papers using minimal water. Wash samples twice with 2ml 5N HCl each time. Then washed 6 times using distilled water. Allow samples to air-dry overnight. Retain approximately half of the solid for total sulfur analysis.
5. Transfer residue to 250ml conical flasks, add 50ml 2N HNO₃ (125ml conc HNO₃ added to 875ml distilled water). Bring samples to the boiled on the hot plate for 30 minutes and then filtered as in 4), retaining 10mls for ICP, then washed well. Air-dry residue and submit for total sulfur analysis.

9. SULFUR ISOTOPE DETERMINATION

Sample Preparation:

Samples of sulfides were directly selected from rock samples and removed from tailings samples using magnetic separation processes. An estimation of the purity was then ascertained using the microscope which determined the quantity of mineral sulfide to be analysed, eg. for pure pyrite - 10mg sample required. Samples are weighed into boats with 150mg Cu_2O as a source of oxygen, and placed in a furnace. The temperature of the furnace is increased to approximately 1050°C, where sulfur and oxygen combine to produce sulfur dioxide. Purification of sample is achieved through the use of cooling bars, and gas pressures are used as an indication of gas volumes obtained. Gas obtained are collected in glass tubes.

Gas Analysis

Gas samples are analysed using a Mass Spectrometer which allows determination of atomic and molecular masses of the sample, by comparison with a reference gas.

10. X-RAY FLUORESCENCE MAJOR AND TRACE ELEMENTAL ANALYSIS

The 'grab' weight method was employed in the preparation of the samples for major and trace element analysis. This involved accurately weighing approximately 1g of each of the finely ground oven dried (105°C) powders into glass vials with approximately 0.3g NaNO_3 . The mixture was transferred to a Pt-Au and preoxidised in an oven set to 750°C for 15 minutes. The preoxidised material was then fused into a homogeneous glass crucible over an oxy-propane flame at a temperature of approximately 1050°C and the molten material was poured into a 32 mm diameter Pt-Au mould heated to a similar temperature. The melt was then cooled by air jets for approximately 30 seconds. The resulting glass disks were analysed on a Philips PW1480 XRF system using a control program developed by Philips and algorithms developed by K. Norrish and P.G Fazey.

Appendix E Methods

Error Determination for fusion Analysis

The errors quoted below for each component are the standard deviations based on standard rock compositions. Trace element errors are quoted for < 200 ppm and > 200 ppm.

Component	<200 ppm	>200 ppm	Component	<200 ppm	>200 ppm
SiO ₂ (%)	-	0.24	Ni (ppm)	5.00	6.00
Al ₂ O ₃ (%)	-	0.15	Rb (ppm)	4.00	5.00
Fe ₂ O ₃ (%)	-	0.07	Ba (ppm)	14.00	40.0
MgO (%)	-	0.07	V (ppm)	4.00	7.00
CaO (%)	-	0.06	Cr (ppm)	7.00	10.0
Na ₂ O (%)	-	0.06	La (ppm)	18.00	21.0
K ₂ O (%)	-	0.03	Ce (ppm)	9.00	17.0
TiO ₂ (%)	-	0.02	Pb (ppm)	6.00	6.00
P ₂ O ₅ (%)	-	0.004	Y (ppm)	3.00	4.00
MnO (%)	-	0.005	Co (ppm)	3.00	3.00
Zn (ppm)	6.00	7.00	Ga (ppm)	3.00	3.00
Cu (ppm)	11.0	11.0	U (ppm)	5.00	7.00
Sr (ppm)	3.00	7.00	Th (ppm)	5.00	7.00
Zr (ppm)	9.00	11.0			

11. MINERALOGICAL ANALYSIS BY X-RAY DIFFUSION

Finely ground powders of samples were lightly pressed into aluminium sample holders to achieve random orientation of the mineral particles for XRD analysis. Measurements were made using a Philips PW1800 microprocessor-controlled diffractometer with Co K alpha radiation, variable divergence slit, and a graphite monochromator. The diffraction patterns were acquired in steps of 0.05° 2θ with a 1 second count time per step. Data were logged to permanent files on an ABM PC/XT (Self 1988) and subsequently analysed using a software package XPLOT developed by Raven (1990).

12. MICROSCOPIC EXAMINATIONS

Fragments of unground tailings and rock samples were inspected by reflected light in a Wild Makroskop M420 microscope. Selected small fragments were carbon-coated and examined in a Cambridge Stereoscan 250 Scanning Electron Microscope (SEM) operating at 20 kV. The elemental composition of particles located in the SEM was determined with Link energy-dispersive X-ray (EDX) microanalyser attachment. Rock thin sections were also made. Some of the rocks were impregnated with resin prior to slide making because of their friable nature. Initially the slides were observed under the reflected light microscope and specific regions identified for SEM analysis. Thus some selected slides were also carbon-coated and examined in the Cambridge SEM.

13. SULFATE REDUCING BACTERIA DETERMINATION

The "Rapid Chek II SRB Detection System" was used for the detection of Bacteria. This is a Immunoassay Test kit for the detection of Sulfate-reducing Bacteria. The Rapid chek II SRB test employs purified antibodies to detect the enzyme adenosine-s'-phosphosulfate (APS) reductase which is common to all strains of SRB.

The antibodies are attached to small particles that selectively capture the APS reductase enzyme. These particles and the captured enzymes are then isolated on a porous membrane, forming a reactive layer. This layer becomes blue when reacted a chromogen, indicating the presence of the APS reductase enzyme. Darker shades of blue indicate higher concentrations of the APS reductase enzyme thus higher numbers of SRB's. Each batch of reagents is calibrated to match known SRB quantities with distinct shades of this blue colour.

1. Mix hydration solution with lysing reagent and set aside.
2. In separate bottle mix sample, water and powder, and invert for 15 sec. Then using filter cap, squeeze bottle to expel fluid, making sure sample remains in filter cap.
3. Remove bottle and replace filter cap on an additional bottle containing 2ml of wash buffer and expel fluid once again through filter cap.
4. Remove cap and place on bottle with mixture formed in step 1. Mix well and leave for 2 minutes.
5. Replace lid with snap dropper filter tip and squeeze liquid into a vial containing immunoreagent. Let stand for 2 minutes.
6. Pour contents into a funnel device containing a membrane. Wait until fluid has drained through and wash with a wash solution.
7. Once wash fluid has drained through the membrane, place chromogen liquid on the membrane and leave for 10 minutes.
8. After 10 minutes, compare colour of device membrane to colour card to determine SRB concentration.